A Sheffield Hallam University thesis

ProQuest Number: 10697399

ProQuest 10697399

Hybrid Sol-Gel/Polyaniline Coating for the Corrosion Protection of AA2024

Mohamed Mostafa

A thesis submitted in partial fulfilment of the requirements of Sheffield Hallam University of the degree of Doctor of Philosophy

May 2009

Abstract

It is widely accepted that Cr(VI)-containing coatings will not be an acceptable component of any future coatings system due to the adverse health & safety aspects of Cr^{6+}. Conductive polymers, such as polyaniline and polypyrrole, have been proposed as potential suitable replacements for chromate containing coatings. However, whilst Polyaniline (PANI) has unique electrical and optical properties; is relatively cheap, easy to synthesise and very stable under a wide variety of experimental conditions, it has not been used widely as a coating due to a lack of adhesion to substrates and poor mechanical properties.

Sol-gel technology is finding increasing applications, for example, as hydrophobic self-cleaning and decorative colour coatings, formation of low-temperature cure high purity optical components and biomedical applications. The basic advantage of the sol-gel process is its ability to form inorganic structures and hybrid organic and inorganic network structures at relatively low temperatures using conventional coating techniques such as dip-, spin- or spraying.

In this study a novel anti-corrosion coating based upon the combination of a silica hybrid sol-gel system and polyaniline is presented. Chemically prepared PANI and a silica based sol were combined and applied to an Al alloy, AA2024-T3 substrate, to form a protective coating. The corrosion performance of these coated samples was evaluated by Electrochemical Impedance Spectroscopy (EIS). EIS test showed the impedance of the PANI/sol-gel coating remained stable for up to 24 months immersion in 3.5%NaCl solution. A Salt Spray Test (SST) study showed that the PANI/sol-gel coating can pass 500 hrs without showing any sign of corrosion nor delamination.

The "self healing" property was also investigated using Scanning Vibrating Electrode Technique (SVET) and scratch test. The corrosion properties of the AA were studied in acidic, alkaline and neutral 3.5% NaCl solutions respectively. The PANI/sol-gel coating showed different mechanisms of corrosion protection according to the solution pH.

The surface morphology was characterised by Scanning Electron Microscopy (SEM) which revealed that increasing PANI content increased the coating porosity. Mechanical properties of these coatings, notably adhesion, were

i

studied using Pull Off and Cross Cut techniques. The sol-gel coating exhibited excellent adhesion; however, increasing the PANI content had an adverse effect on coating adhesion.

Differential Scanning Calorimetry (DSC) was used to investigate the curing temperature of PANI/sol-gel coating. The technique showed that the coating was completely cured after drying for 5 hrs at 70°C.

The chemical characteristics of the coatings were evaluated using X-Ray Photoelectron Spectroscopy (XPS) and Fourier Transformation Infrared (FTIR) Spectroscopy.

The corrosion protection of AA2024 using the PANI/sol-gel coating was attributed to the formation of a complex compound containing the (Al-O-N) group that was produced from an interaction between PANI and the Al substrate. Transmission Electron Microscopy (TEM) was used to assess the interfacial interaction of the coating and metal substrate.

Acknowledgments

Foremost, I would like to express my most sincere appreciation and gratitude to my supervisor Prof. R. Akid to whom I am deeply indebted. I offer my special thanks to Dr H. Wang for his support and cooperation. I would also like to thank Dr. D. Greenfield for his invaluable advice, discussions with him always brought up interesting ideas and possible interpretations of the observed data.

I am highly obliged and indebted to Prof. T. English and D. Hammond, Corus Group, Rotherham, for their help and advice concerning the XPS analysis. I would also like to acknowledge Dr. D. Morgan, Cardiff University, for his help in conducting the XPS experiments. Special thanks are due to E. Smith, Nottingham University, for her continuous cooperation and advices in the XPS analysis. I furthermore wish to extend my appreciation to M. Ward and A. Walton at the University of Leeds for their help and hospitality during support with TEM and XPS analysis.

I wish to express my sincere feelings to my laboratory and Office mates for their help at various stages of my work and for keeping a congenial atmosphere during my stay in the department.

Above all, I wish to acknowledge from the depth of my heart the untiring sacrifices made by my parents to allow me to achieve the highest degree in the field of education. I fall short of words in expressing my abounding feelings for my sister and brothers for support. I warmly acknowledge the love and blessings showered by my relatives and friends.

My special thanks go to my wife Shaimaa and children, Nada and Omar, for their love, patience, support and encouragement.

Last, but not least, Egyptian Armament Authority is acknowledged for sponsoring me to join the Sheffield Hallam University.

Table of content

List of Abbreviations

AA	Aluminium Alloy
IMP	Intermetallic particles
EIS	Electrochemical Impedance Spectroscopy
SST	Salt Spray Test
SVET	Scanning Vibrating Electrode Technique
SEM	Scanning Electron Microscopy
XPS	X-Ray Photoelectron Spectroscopy
FTIR	Fourier Transformation Infrared Spectroscopy
TEM	Transmission Electron Microscopy
DSC	Differential Scanning Calorimetry
PANI	Polyaniline
EB	Polyaniline in Emeraldine Base form
ES	Polyaniline in Emeraldine Salt form
LE	Polyaniline in Leucoemeraldine form
NMP	N-methylpyrrolidinone
PANI/sol-gel	Mixture of Polyaniline and Sol gel
PANI/sol8	Mixture of PANI and sol-gel in 1:8 volume concentration
PANI/sol4	Mixture of PANI and sol-gel in 1:4 volume concentration
PANI/sol1	Mixture of PANI and sol-gel in 1:1 volume concentration
PANI/sol0.25	Mixture of PANI and sol-gel in 4:1 volume concentration
R_s	Solution resistance
C_c	Coating Capacitance
R_p	Pore resistance
C_{dl}	Double layer Capacitance
R_{ct}	Charge transfer resistance
E_{corr}	Corrosion potential
i_{corr}	Corrosion current
Q	Quinone
B	Benzene

Chapter1

Introduction

1.1 MOTIVATION

Corrosion has always been a problem that affects our life. Corrosion causes loss of valuable products which affects operational safety, product reliability and may cause plant shutdown resulting in costs to the UK economy of between 3-4% of Gross National Product.

Aluminium is the most widely used non-ferrous metal being used in cars, aircraft, construction, engineering structures and many other industrial applications. Pure aluminium metal does not have suitable strength for most applications and some alloying elements, such as copper and magnesium are required to improve the metal strength. An example of this is found in the 2000 series alloys where the main alloying element is copper. These alloys are very important in the aerospace industry. Unfortunately these alloys are not sufficiently corrosion-resistant to be used without protection in humid or aggressive media such as marine environments.

Chromate based coatings have historically been used to protect aluminium alloys. When this coating comes in contact with an aluminium substrate, chromium (III) is formed providing excellent corrosion protection. This coating also contains chromium (VI) which has been recognised as providing a "self healing" property. However, these types of coating may soon be banned due to their toxicity and adverse environmental impact and numerous have identified that chromium (VI) is a carcinogen causing kidney and liver damage, and even death.

As environmental legislation imposes greater restrictions on the use of these substances the demand for alternatives coating replacements increases.

Conductive polymers, such as polyaniline, are potential suitable replacements for chromate containing coatings. Polyaniline (PANI) has unique electrical and

optical properties and moreover, is relatively cheap, easy to synthesise and very stable under a wide variety of experimental conditions.

Further motivation is the potential opportunity to exploit other properties of the conductive polymers notably that conductive polymers such as polyaniline have the ability to adsorb electromagnetic waves.

A final motivation, there is a need to increase the lifetime of the coating systems with decreasing of overall cost of corrosion protection. Since early reports that polyaniline can provide corrosion protection to stainless steel, there have been numerous investigations of using polyaniline as an additive in corrosion protection systems. Most of this research interest in using polyaniline has been for the corrosion protection of ferrous alloys. However, a few studies have been reported for the use of polyaniline in the corrosion protection of aluminium for example polyaniline has been used with epoxy and acrylic binders in the corrosion protection of metals.

In the present study, polyaniline is combined with a silica sol-gel to combine the corrosion property of polyaniline with the mechanical properties of silica sol-gel. Sol-gel coatings have the ability to produce a thin bond-coating with excellent adhesion between the metallic substrates and subsequent top coats.

1.2 AIMS AND OBJECTIVES

Recently, conductive polymers and sol-gel have many interesting individual applications due to the ongoing demand for the replacement of chromate as an environmentally benign alternative. Although organic conductive polymeric coatings have been explored with good results, the mechanical properties of the conductive polymers are still poor.

The potential advantages of using PANI/sol-gel combination are to improve the mechanical properties of PANI and to adjust the conductivity of sol-gel. These new features of PANI/sol-gel will have diverse commercial applications.

The aim of this work is therefore to investigate;

1) The applicability of different combination of PANI/sol-gel system to be applied to 2024-T3 AA substrates.

2) The optimum relative concentration of PANI and sol-gel from corrosion point of view.

3) The mechanical properties of the PANI/ sol-gel coating.

4) The mechanism of corrosion protection of PANI/sol-gel coated 2024AA.

1.3 RESEARCH APPROACH

This study is divided into three sections in order to cover the aims of study giving above; the first part is to investigate the most effective way to combine PANI and sol-gel. In this section PANI and sol-gel were used individually as a top coat or as combination to form one coat and then applied to 2024-T3 substrate. The coated metal sample substrates were immersed in 3.5% NaCl solution and electrochemical impedance spectroscopy (EIS) was used to investigate the corrosion resistant of the coated sample to identify the optimum combination of these materials. The Scanning Electron Microscope (SEM) was used to study the surface morphology, the effect of coating thickness and effect of corrosive solution on both bare and coated metal.

In the second section, the mechanical properties of the coating were investigated using selected techniques such as micro-hardness and adhesion.

Finally the mechanism of protection of the aluminium alloy was studied in the third section. Fourier transform Infrared (FTIR), X-ray photoelectron spectroscopy (XPS) Transition Electron Microscopy (TEM) were used to study the chemical changes in the coating and the coating/metal interface.

1.4 STRUCTURE OF THE THESIS

Chapter 1 provides a review of the literature, which is divided into five subsections. Section 1.1 gives a brief introduction to the corrosion cost and the general introduction to the corrosion protection measures. Section 1.2 introduces the aluminium 2024 alloy and its mechanism of corrosion. Section 1.3 gives a general introduction to conductive polymers and their application while section 1.4 focuses specifically on polyaniline (PANI) as one of the selected conductive polymers. Section 1.5 provides an introduction to silica sol-gel preparation, applications, advantages, disadvantages and corrosion protection application for aluminium alloys.

Chapter 2 describes the techniques used in this study. Section 2.1 presents the techniques used in the corrosion performance measurements namely;

Electrochemical Impedance Spectroscopy and Salt Spray Testing. Section 2.2 gives a brief introduction to the characterisation techniques used in this study notably, Scanning Electron Microscopy, X-Ray Photoelectron Spectroscopy, Transmission Electron Microscopy and Fourier Transform Infrared Spectroscopy. Section 2.3 present the techniques used to investigate the mechanical properties of the coating.

Chapter 3 presents the experimental work which illustrates polyaniline preparation, coating preparation, samples preparation with the results from these experiments being given in Chapter 4. A discussion of these results is presented in chapter 5 and the conclusions and future work are given in chapter 6.

CHAPTER 2

LITERATURE REVIEW

2.1 CORROSION

Corrosion is an electrochemical process based on the universal laws of nature. It is the destruction or deterioration or surface wastage of metals or alloys due to oxidation and reduction reactions resulting in the formation of corrosion products [1][2][3]. Corrosion does not include wear or other mechanical effects [2]. All metallic structures can corrode. It is just a question of "at what rate" they will corrode.

2.1.1 Aspects of Corrosion Damage

The detrimental and economic consequences of corrosion can be briefly summarised by the following main aspects [1];
1. Poor appearance of rusted objects.
2. Loss of valuable products.
3. Effects on operational safety.
4. Effects on products reliability.
5. Environmental impact.

2.1.2 Cost of Corrosion:

The degradation by corrosion of structural and functional components is a huge cost to modern industrialized economies. The cost is not simply the replacement value of a corroded component but also the indirect costs including any product and production loss, maintenance etc. The original [4] cost of corrosion survey estimated that the cost to the UK economy is between 3-4% of Gross National Product (GNP) per year. Although more limited in scope this concluded that the cost is still of the order to 2-3% of NGP per year. On a more

5

personal note, the corrosion costs around £600 per capita per year; it is equivalent to around 1-2p/£ for each tax-payer.

Similar surveys undertaken in the USA and Japan also arrived at a similar annual cost, with the total annual estimated direct cost of corrosion in the USA amounting to a staggering $276 billion; approximately 3.1% of the GNP. This suggests that, although corrosion management has improved over several decades, industry must find more and better ways to encourage, support, and implement optimal corrosion control practices [5].

2.1.3 Forms of Corrosion

Corrosion may be classified into several forms. The basis for this classification is the appearance of the corroded metal surface. Each form can often be identified by mere visual observation. These forms include:

1. Uniform or general corrosion attack.
2. Localised corrosion.
3. Galvanic or bimetallic metals corrosion.
4. Crevice corrosion.
5. Pitting corrosion.
6. Selective corrosion.
7. Flow-Induced Erosion–Corrosion.
8. Stress corrosion synergy, e.g., stress corrosion cracking, corrosion fatigue, and hydrogen embrittlement [6].

This arbitrary listing covers practically all corrosion failures and problems. The forms are not listed in any order of importance.

2.1.4 Corrosion Control

The job of a corrosion engineer is to minimise or mitigate this process. A number of measures can be applied to reduce the corrosion rate. The three key aspects of corrosion protection are material selection, design, and control of the environment. These measures can be treated as follows: material selection, design, control of the environment, cathodic and anodic protection and coating.

2.1.4.1 Coatings

Protective coatings are probably the most widely used approach adopted for corrosion control. Coatings can be classified as:

1. Metallic coatings.
2. Non-metallic coatings.
3. Conversion coatings

The polyaniline and sol-gel coatings will be reviewed in detail later in this chapter.

2.2 ALUMINIUM

Aluminium [7] is the most used non-ferrous metal. Aluminium has many advantages, lightweight, thermally and electrically conductive, ease of recycle, easily recycled, variety of alloys ...etc.

One of the most important properties of aluminium and its oxide (naturally produced when it is in contact with air) is that it is non-toxic material. This property allows aluminium to be used in food industry

Aluminium [6] is the lightest metal with exception of magnesium, with the highest strength to weight ratio. This ratio makes aluminium to be the most suitable metal in the aircraft industry.

Pure aluminium has good corrosion resistance properties; however, it has bad strength and ductility. Alloying elements are added to pure aluminium to improve its mechanical properties and to meet the technical demands of different applications.

About 15 [6] alloying elements are used with aluminium; usually less than 10 weight percent of the alloy, both can change the material properties.

Aluminium alloys are classified into two types: wrought alloys, need work to shape, and cast alloys which poured in a molten condition into a mould or ingot that gives their shape.

2.2.1 Aluminium 2024

Aluminium 2024 (AA 2024) is perhaps [6] the best known of the aerospace alloys and most widely used alloy in aircraft.

AA 2024 has copper as its main alloying element being added at normally 3.8 - 4.9 % levels. It is used in aircraft industry because of its high strength to weight ratio, and its good fatigue resistance.

Normally 2024 AA has a composition showed in Table 2- 1

Table 2- 1 2024-T3 composition

Cu	Mg	Mn	Fe	Si	Zn	Ti	Cr	Others	Al
3.8-4.9	1.2-1.8	0.3-0.9	0.5	0.5	0.2	0.15	0.1	0.15	rest

The most common alloy is the AA 2024-T3 grade, where T3 refers to the heat treatment applied to the alloy, in this case AA 2024-T3 has a solution treatment at 495 °C for 48 hours (hot work) to dissolve the alloying elements into a single solid solution phase. Quenching in water results in a supersaturated solid solution (SSSS) of alloying elements in the aluminium. Finally, ageing at room temperature is carried out to control the decomposition of the SSSS to form finely dispersed precipitates. The dispersion of precipitation controls the mechanical properties of the alloy. Full details of these processes and the resulting microstructures are outside the scope of this study.

All SSSS particles are showed in Table 2-2 with their area percentage in the alloy matrix.

Table 2-2 SSSS Particles and area percentage

Intermetallic particals type	Volume %
Al_2CuMg	2.69
$Al_6(Cu.Fe.Mn)$	0.85
Al_2Cu_2Fe	0.17
$(AlCu)_6Mn$	0.37

Whilst the high strength of AA 2024-T3 is a consequence of the presence of these fine particles, the alloying elements significantly decrease the corrosion resistance compared to that of pure aluminium. Moreover, the inhomogeneous

distribution of Cu combined with the presence of these IMP originate local galvanic cells [8].

The presence of IMPs form galvanic sites in the alloy matrix for example, copper rich Al_2-Cu-Mg particles act as anodic then cathodic site with respect to aluminium matrix. These galvanic sites make 2024 AA susceptible to localised corrosion notably pitting corrosion.

2.2.2 Corrosion of Aluminium

Due to its highly electronegative standard electrode potential ($\approx$ -1600 mV versus SHE), aluminium is naturally oxidising, in air and water, forming a stable uniform passive oxide film covering a few nanometres on the surface of the metal;

$$2Al + 3/2O_2 \rightarrow Al_2O_3 \qquad\qquad (2-1)$$

This passive oxide film prevents the corrosion of the underlying metal by reforming when the metal is scratched or damaged.

The formation and stability of different Al species can be seen from the Pourbaix diagram which represents the relationship between the metal electrode potential and pH. It is clear from Pourbaix diagram that aluminium is passive in pH range of 4-8.3 while outside this pH range it is corroded under acidic and alkaline conditions. These regions are shown in Figure 2-1 and include;

a) Immunity region: here the metal is considered to be totally immune from corrosion attack.

b) Passive region; Here the metal is covered with an oxide that protects the metal from the environment.

c) Corrosion region: Here the metal is susceptible to corrosion attack.

The data taken from the Pourbaix diagram is significant however, many factors need to be taken in consideration for example; nature of medium, temperature, and the alloying elements. Furthermore, the diagrams are for equilibrium conditions and do not provide any information on the rate of corrosion.
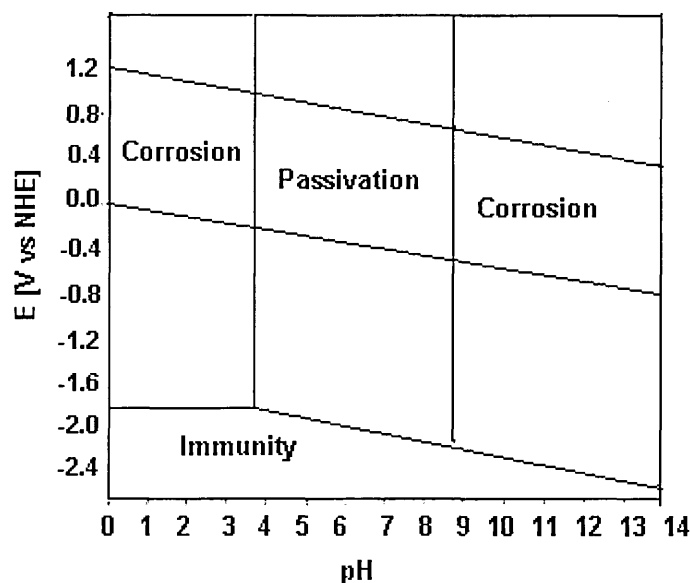
Figure 2-1 Pourbaix Diagram of aluminium at 25°C[7]

Aluminium alloys [7] are usually susceptible to localised corrosion (pitting corrosion) caused by a breakdown of the passive film. Whilst the mechanism of pitting is often complicated, it generally consists of two stages; initiation and propagation.

A pit can initiate following absorption of chloride ions into the passive film. This generally occurs at a weak point in the film, for example at an intermetallic particle (IMP). Whether the pit will stop growing (metastable pit) or continue to grow (stable pit) will depend upon the alloy and electrolyte compositions. If the pit remains active, it will propagate according to the oxidation of Al;

$$2Al \rightarrow 2Al^{+3} + 6e^- \qquad\qquad (2-2)$$

And oxygen or/and hydrogen reduction depending upon the electrode potential of the metal and the pH of the solution;

$$O_2 + 2H_2O + 4e^- \rightarrow 4OH^- \qquad\qquad (2-3)$$

$$O_2 + 4H^+ + 4e^- \rightarrow 2H_2O \qquad\qquad (2-4)$$

$$2H^+ + 2e^- \rightarrow H_2 \qquad\qquad (2-5)$$

$$H_2O + 2e^- \rightarrow 2OH^- + H_2 \qquad\qquad (2-6)$$

For the neutral and alkaline solutions, reduction of dissolved oxygen and hydrogen formation will take place (equation 2-3). However, within an acidic solution, the reduction reaction is represented by hydrogen ion reduction (equations 2-4 and 2-5).

In case of absence of oxygen and hydrogen ions, water reduction will take place (equation 2-6).

The creation of Al^{3+} ions within the pit, via dissolution of Al, leads to ion migration of Cl⁻ ions (charge attraction) into the pit leading to the formation of chloride complexes, for example, $AlCl_4^+$.

Hydrolysis of aluminium ions will lead to the formation of H^+ ions (acidification), which will lower the pH of the pit (ca. < 3).

$$Al^{+3} + 3H_2O \rightarrow Al(OH)_3 + 3H^+ \qquad\qquad (2-7)$$

In this case, the solution inside the pit becomes more aggressive causing further Al dissolution and auto-catalytic propagation of pitting. Figure 2-2 is a general schematic of the pitting corrosion mechanism of aluminium.

11

In AA2024, pitting corrosion after initiates at the location of the intermetallics, which cover about 3% of the surface area of the alloy. The majority (60%) of intermetallic sites are S-phase, composed of Al_2MgCu [8], which are electrochemically active (anodes) with respect to the alloy matrix. The chemical and electrochemical dissolution of magnesium and aluminium from Al_2MgCu particles occurs at the initial stages of the corrosion process leading to enrichment of copper at those sites [8][9][10]. The intermetallic precipitates lead to separation of anode and cathode sites causing deep dealloying (pits). Pits containing copper inside which redeposit as a thin film around the pits due to the chemical dissolution of copper. The redeposition of copper has an important role in the development of localised corrosion as this causing an increase in the cathodic area thereby supporting an increased anodic current density in the pit [11]. Figure 2- 3 shows a schematic of the corrosion AA containing IMPs.
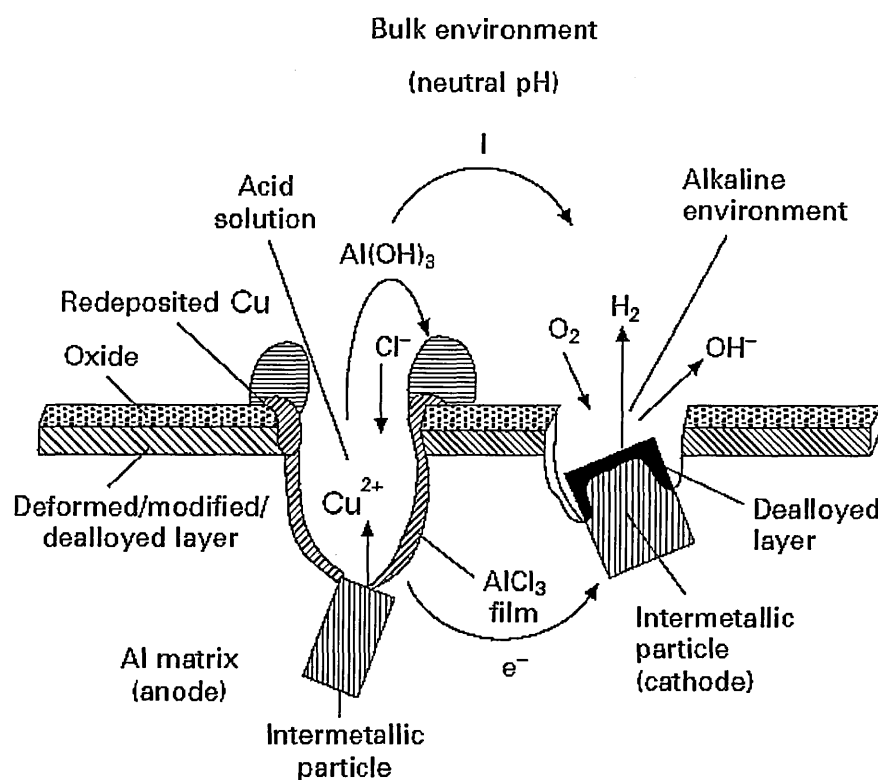

Figure 2- 3 Mechanism of pitting corrosion of aluminium 2024 [11].

Thus, the suppression of S-phase dealloying and copper redeposition can be an effective strategy of inhibition of localized corrosion on AA2024. Organic

compounds that are able to form insoluble complex compounds with components of the S-phase are potential candidates to provide strong inhibiting action

For some applications AA2024 can be clad with a thin layer of pure aluminium to improve its corrosion properties. However, this thin layer affects the alloy strength and can be damaged.

Chromate conversion coatings have historically been used in protection of clad 2024-T3. The corrosion protection mechanism of the conversion process is considered to involve the reduction of Cr (VI) by electrons released during anodic dissolution of Al. A protective hydrated of chromium (III) film forms as shown in equations 2-8 and 2-9 [12].

$$2Al \rightarrow 2Al^{+3} + 6e^- \qquad\qquad (2-8)$$

$$Cr_2O_7^{2-} + 8H^+ + 6e^- \rightarrow 2Cr(OH)_3 + H_2O \qquad (2-9)$$
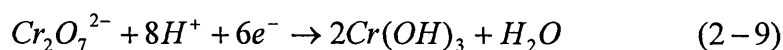
Once Cr (III) is formed, it is irreversibly adsorbed onto the metal surface forming a near-monolayer film. This film is nonconductive and inhibits (blocks) the adsorption of oxygen on the surface. Moreover, it inhibits further Cr(VI) reduction [13]. However despite this effective corrosion protection, the personnel exposure limit for hexavalent chromates has been reduced to a level ($1\mu g/m^3$ according to National Institute for Occupational Safety and Health, USA) [14] such that industry finds compliance difficult. Due to its toxic and carcinogenic effects of these materials, Cr(VI) based systems are facing a world-wide ban.

Hence the new trend in corrosion protection technology is to replace these kinds of coatings with "environmentally friendly" coatings. In this respect conductive polymeric and sol-gel coatings are potential replacement of chromate coating.

2.3 CONDUCTING POLYMERS

Conducting polymers are a prospective class of new materials that combine processability and flexibility of polymers with electrical and optical properties of metals and semiconductors. There are many examples of organic conductive polymers, such as polyaniline, polypyrrole, polythiophene and polyacetylene.

The first cited information regarding polyaniline dates back to 1862 by H. Letheby, while its four oxidation states were not discovered until the beginning of the 20th century. The first synthesis of conductive polyacetylene was by Shirakawa, MacDiarmid and Heeger in 1977 [15]. They found that a thin film of polyacetylene could be oxidised with iodine vapour, increasing its electrical conductivity by a factor of 10^9. The importance of this discovery was highlighted in 2000 by awarding the Nobel Prize in chemistry to the authors of this achievement [16].

Interest in the study of conductive polymers has increased dramatically over the last 25 years as a result of the advantages of using conductive polymers, notably that they are light, inexpensive and easily processed. The electrical conductivity of these polymers is considered to be intermediate between insulators and metals; with a specific conductivity of range 10^{-9}-10^6 S/cm. Figure 2-4 shows the specific conductivities of conductive polymers with respect to metals and insulators.
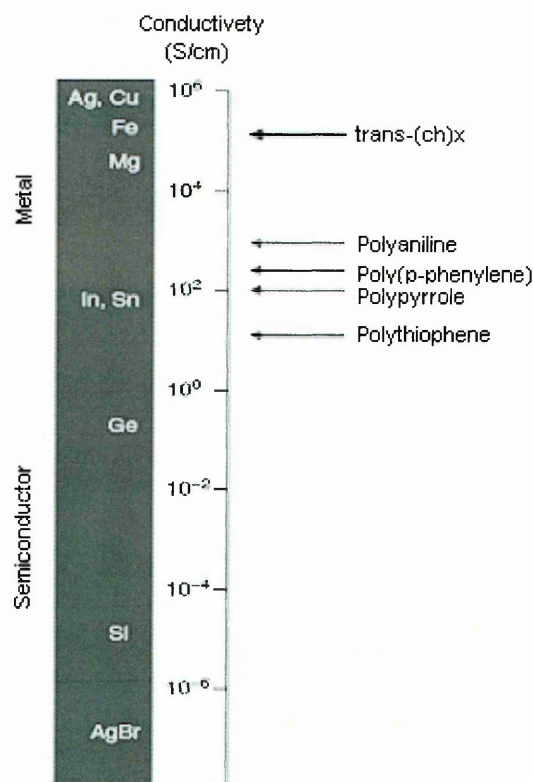
Figure 2-4 Specific conductivity of conductive polymer with respect to metals and insulators [17]

Electrically conductive polymers have attracted great attention because of their unique electrical and optical properties that can be useful in numerous applications for example consumer electronics and antistatic textiles. Among the most exciting applications is the use of conducting polymers in light-emitting devices (LEDs), replacing silicon as the traditional substrate material for clock radios, audio equipment, televisions, cellular telephones, automotive dashboard displays [18].

Current examples of these applications include conductive polymers as both cathodic and solid electrolyte of batteries [19] [20]. Potential advantages of polymeric batteries include high reliability, light weight, non-leakage of electrolyte solution, thin film form, flexibility and high energy display. Currently, their conductivity is being explored in conducting adhesives, artificial muscles [21]. Other applications include electronic shielding [22] [23] [24], integrated circuit device sealed against moisture, radiation and ion contamination and conductive adhesives [25].

Wide commercial utilization required further increase in intrinsic conductivity and improvements in the chemical properties and processability of these conductive polymers [26].

2.3.1 Conductivity of conductive polymers

Material electrical properties can be determined by its electronic structure. According to band theory, the Highest Occupied Molecular Orbital (HOMO) represents the valence band and the Lowest Unoccupied Molecular Orbital (LUMO) represents the conduction band. The difference between these two bands is called the band gap. The electrical properties of a material depend upon the width of the band gap. When electrons from the valence band are excited into the conduction band, electronic conduction occurs.

When the energy gap between the valence band and the conduction band is of the order of several electron volts, the material remains an insulator. However, if this gap is below 1 eV, material is considered as a semiconductor and when there is an overlap between the two bands, the martial would be conductive as shown in Figure 2-5.

Figure 2-5 Energy band in solids.

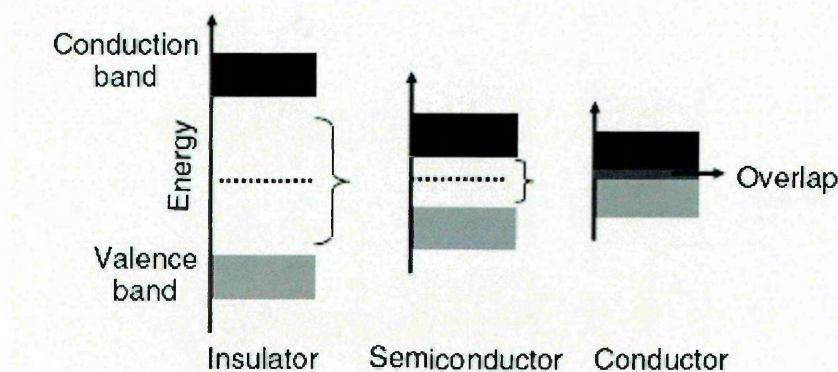For polymers, Carbon atom has 6 electrons outside the nucleus, 4 of them are the valance electrons. Carbon atom can have sp3 hybridization, one s orbital and 3 p orbital forming saturation compound.

In saturated polymers, carbon atoms are bonded to 4 neighbouring atom to saturate the valance orbital such as polyethylene $(CH_2)n$ which has a big band gap of 8.8 eV[17] and so is insulator.

16

The main electronic feature of conducting polymers is the π-conjugated system which can consequently undergo sp2 hybridization, one s orbital and 2 p orbital, to form unsaturated compounds. In this hybridization, one p orbital, P_z, is left without any effect and overlaps with the neighbour carbon atom forming π bond. The π-conjugation of the polymer chain generates high energy occupied and low energy unoccupied molecular orbital leading to a system that can be readily oxidized or reduced [27]. Most organic conjugated polymers have a band gap greater than 1.5 eV, which means these polymers are intrinsically insulating, however, doping organic polymers increases the conductivity [27]. Removal of a charge from the valance band generates a radical cation whose energy lies in the band gap, this cation is called polaron. It stabilizes itself by polarizing the medium around it and hence its name.

When a second electron is removed from the system, it creates another polaron or bipolaron.

The formation of a polaron or bipolaron accompanied by distortion of lattice or structural deformation, leads to an upward shift of the valance band and a downward shift of conduction band and presence of two localized electronic states in the gap as shown in Figure 2-6 [27].
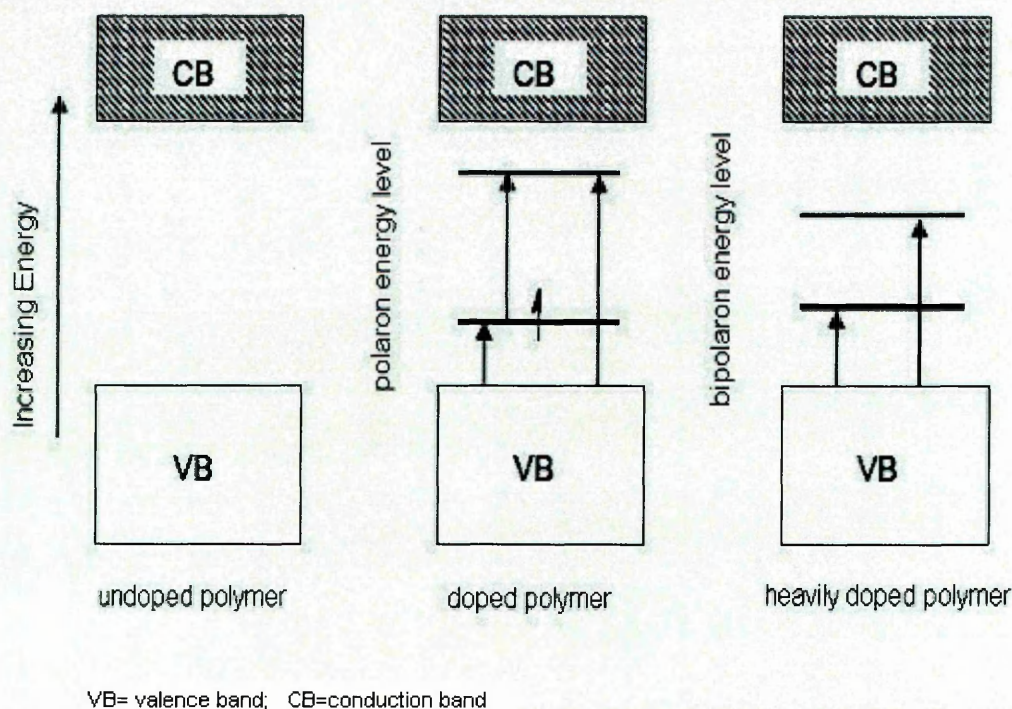

VB= valence band; CB=conduction band

Figure 2-6 Illustration of energy levels and allowed transition of polaron and bipolaron

This leads to a new, smaller band gap, therefore increasing conductivity by decreasing the ionization energy required for an electron to move from the valance band to the conduction band.

2.3.2 Corrosion Protection using conductive polymers:

The materials being used for corrosion protection are coming under increasing scrutiny by environmental organisations. The use of chromium and cadmium for corrosion protection will soon be banned. Barrier coatings, such as epoxy, are employed extensively; however, they are not very durable/robust once a defect in the coating has been formed. The corrosive species then attack the underlying metal and, thereby, increase the exposed surface, accelerating the corrosion process.

The corrosion inhibiting properties of conducting polymers were suggested by MacDiarmed in 1985 [28]. The initial study on the protection of metal against corrosion by conducting polymers was reported in the same year by DeBerry Polypyrrole has been used for the protection of various metals. Previous studies utilizing polypyrrole as a corrosion protection coating shows that it works quite well [29] [30]. Much work on corrosion protection has focused on PANI [31] [32] [33] [34]; however studies have extended to other types of conducting polymers [35] [36].

There are several proposed mechanisms for corrosion protection of conductive polymers. These include, simple galvanic coupling by which the polymer has a lower oxidation potential than the metal it is protecting [37]; an alternative mechanism is by the formation of an oxide protective layer [38], alternatively the polymer may cause a shift of the electrochemical interface from metal solution interface to the polymer/ solution interface [39].

2.4 POLYANILINE

Polyaniline is one of the oldest known synthetic organic conductive polymers. In 1862 Letheby obtained a partly conductive material which was polyaniline by anodic oxidation of aniline in sulphuric acid, [16]. There was little interest until the late 1970's when a sudden resurgence in polyaniline research occurred as a

result of its unique electrical and optical properties. The continuously growing interest in the study of PANI may be illustrated by the number of publications published in this area as shown in Table 2-3.

Table 2-3 Publications relating to PANI released over the last 20 years

Publication year	No. of publication
2008	1245
2007	1140
2006	1014
2005	968
2004	825
2003	776
2002	702
2001	700
2000	555
1997-1999	1682
1986-1989	948

This interest is caused by the unique properties of PANI; notably that it is relatively cheap, easy to synthesise and very stable under a wide variety of experimental conditions. PANI exists in three oxidation states, as shown in Figure 2-7 , changing from the completely reduced leucoemeraldine, all nitrogen atoms are amine, through the emeraldine base, half of the nitrogen atoms are amine where other half is imine, up to the completely oxidized pernigraniline, all nitrogen atoms are imine [18].
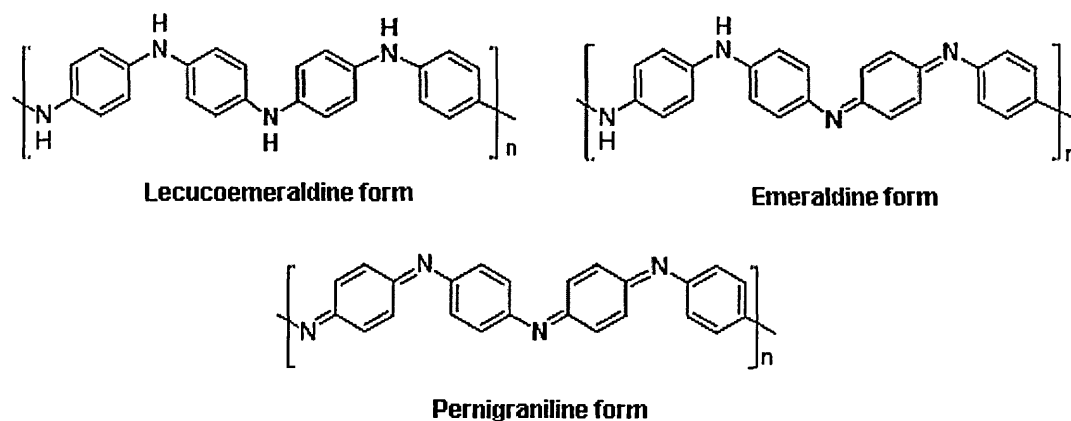
Figure 2-7 The oxidation states of PANI [18].

The electrical and optical behaviour of these forms are strongly dependant on pH and dopant effects [40].

All these forms of PANI are insulating; however, electrically conducting emeraldine can be obtained by doping the emeraldine base (EB) in acidic medium forming the emeraldine salt (ES), as shown in Figure 2-8. Emeraldine is the most environmentally stable form of PANI. The conductivity of emeraldine salt depends upon the nature of the dopant [18].
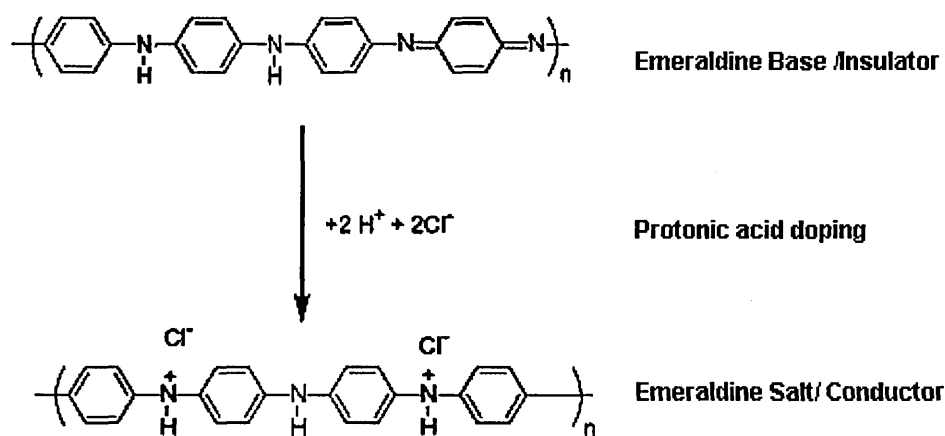
Figure 2-8 Formation of ES from EB [18]

The emeraldine base is a stable polymer with thermal stability to temperatures in excess of 420 °C. The doped polymers are significantly less stable, and their thermal stability varies with the dopant [41].

Polyaniline has been used in many applications; including rechargeable batteries, electrochromic display devices, intelligent windows, transparent electrode, electromagnetic impulse shielding, sensors, gas separation membranes, solar cells, fuel cells, corrosion protection, printed, circuit board and transparent conductive coatings[42] [43] [19] [24].

2.4.1 Polyaniline Preparation

Polyaniline can be easily prepared by oxidative polymerisation of the aniline monomer in the presence of various acids. This can be achieved chemically using an appropriate chemical oxidant or by electrochemical oxidation on different electrode materials.

A great deal of research [44] [45] [46] [47] has been carried out in this area due to the different properties of the (e.g. conductivity and solubility). These properties depend upon the preparation technique used and synthesis condition.

2.4.1.1 Chemical preparation

Chemical synthesis is the major commercial method of producing polyaniline. The chemical polymerisation of distilled aniline is carried out by its oxidation with an oxidant, for example, ammonium persulphate [48], ferric chloride [49], benzoyl peroxide [50] or potassium dichromate [51] in acidic medium. Different acids can be used to prepare polyaniline; such as sulphuric acid [48] or hydrochloric acid [52]. The acidic solution of the dissolved monomer is stirred and the oxidant solution is added dropwise to the monomer solution. The solution is kept stirring overnight to complete the polymerization. The polyaniline precipitate is then collected by filtration and washed with deionised water to ensure the removal of any un-polymerised monomer. The polymer powder is dried at 60°C for 48 hours. The material obtained by this method was identified as the emeraldine salt [48] of the acid used.

The emeraldine salt was completely converted to the emeraldine base by deprotonation with strong alkaline solution, usually ammonium hydroxide

Due to the poor solubility of polyaniline in common solvents, numerous studies have been carried out to identify the optimum method for dissolving the polyaniline. These approaches include substitution of alkyl chains to the nitrogen atom [53] or benzene ring [54]. However, substituted soluble polyaniline is less conductive than the unsubstituted polymer [55]. Another successful approach used for producing soluble polyaniline is to employ an organic acid, in particular sulphonic acid, as a dopant for the polymer. Such acids include dodecylbenzene sulphonic acid [56] [57] and Camphorsulphonic acid [58]. Furthermore, the copolymerization and blend with other polymer were conducted to improve the processablity of polyaniline [59] [60].

2.4.1.2 Electrochemical preparation

The electrochemical technique is often used to prepare polyaniline in order to overcome the processablity problems associated with the polymer. Electrochemical synthesis provides a homogeneous film deposited on the surface of the working electrode. A wide range of working electrodes has been used in the electrochemical preparation of polyaniline.

Preparation may be carried out using a potentiostat-galvanostat system. A three electrode system is used where the working and counter electrodes are separated from each other by a porous glass disk. Typically the counter electrode is a platinum plate and a silver chloride Ag/AgCl wire is used as the reference electrode. A cyclic voltammogram (CV) technique is used to follow the electrochemical oxidation of aniline in acidic medium [61]. Figure 2-9 shows an example of the cyclic voltammogram of a PANI film in which H_2SO_4 was used as the acidic medium.
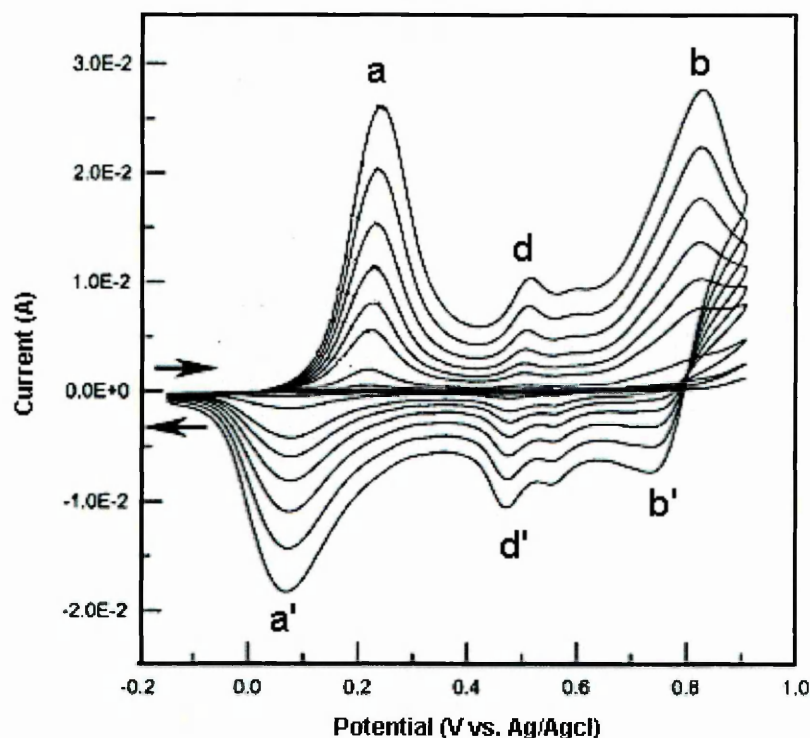
Figure 2-9 Cyclic voltammetry for PANI film, 1 M H_2SO_4, 50 mV/s.[61].

Two main redox pairs were observed in the voltammogram. The first redox pair (peaks a and a') are attributed to the leucoemeraldine –emeraldine transition, whereas the second (peaks b and b') are attributed to the emeraldine– pernigraniline transition. However, during the second voltammetric cycle, two intermediate peaks of relatively low intensity were observed between 0.6 and 0.9 V (peaks d and d'). These peaks have been associated with the degradation of PANI at potentials around 0.9 V when benzoquinone and a range of insoluble products are produced [62].

The electrochemical activity of PANI depends mainly on the pH of the medium; in neutral and alkaline media PANI loses its electrochemical activity [18].

2.4.2 Mechanism of Oxidative Polymerization of Aniline

The most generalized mechanism of aniline is based mainly on the kinetic studies of the electrochemical polymerization of aniline as shown in Figure 2-10.
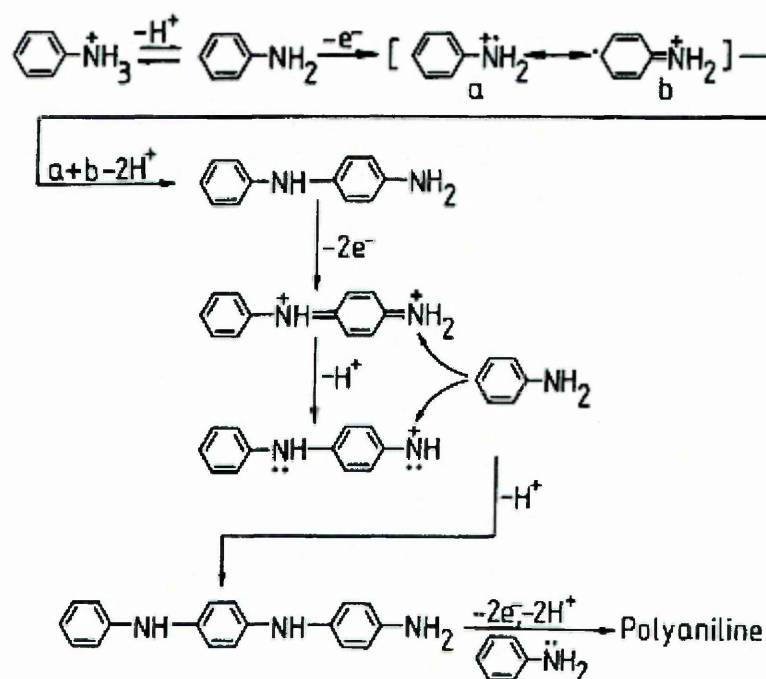
Figure 2-10 Mechanism of the polymerization of aniline [18]

The slowest step in the polymerization of aniline is the oxidation of the aniline monomer to form dimeric species. The dimers are immediately oxidized and then react with an aniline monomer via an electrophilic aromatic substitution, followed by further oxidation and deprotonation to afford the trimers. This process is repeated, leading eventually to the formation of PANI [18].

2.4.3 Conductivity Range

The electrical conductivity of Polyaniline can be controlled over a wide range. Polyaniline conductivity depends on the oxidation state and the type of dopant. The full range of conductivity ranges from 10^{-9} for undoped polyaniline to 11.9 S/cm for the hydrochloric acid emeraldine salt as shown in Table 2-4. This wide

range of conductivities of polyaniline allows polyaniline to be used in numerous applications one of these application is conductive coating.

Table 2-4 Conductivity of PANI using different dopants. [63], [64]

Acid	Conductivity (S cm^{-1})
Hydrochloric	11.9
Sulphuric	10.1
Methanesulfonic	9.7
Nitric	7.7
Phosphoric	4.8
Hydrobromic	4.7
Dodecylbenzenesulfonicc	4.4
Camphorsulfonic	3.1
Hydrofluoric	1.4
Succinic	0.28
Formic	0.21
Tartaric	5.5 x10^{-2}
Acetic	4.2 x10^{-2}
Dedoped	3.9 x10^{-9}

2.4.4 PANI-Based Corrosion Resistant Coating

Conductive polymers have three main problems with respect to corrosion protection: Firstly: the dopant may itself activate substrate corrosion. A dopant is necessary to balance the electrical charge but it may interact with the electrolyte. In NaCl solution anionic dopants will facilitate the penetration of Cl$^-$ ions by an ion exchange mechanism. Therefore, conductive polymers can weaken the barrier properties of resins within a paint. Even if the coating is in contact with salt free water, the dopant can induce an osmotic pressure which may lead to the delamination of the coating. Secondly: the polymeric backbone is difficult to dissolve or disperse in common solvents finally: the dopants in

aqueous environments, at pH values above 4, leach from the conductive polymer into the solution [62].

DeBerry was the first to report the corrosion inhibition effect of PANI [28] . He electrodeposited PANI on stainless steel (SS) 410 and 430 using cyclic voltametery (CV) The CV was carried out in a solution containing aniline and perchloric acid by cycling the potential of the working electrode from -0.2 to 1.0 V versus a saturated calomel electrode (SCE). The coated SS samples subsequently remained passive for a period of 50 days, in 0.1 M H_2SO_4 acidic solution. In the presence of chloride ions (0.15M Na_2SO_4 +0.05M H_2SO_4+0.1M NaCl) PANI coated samples showed no evidence of pitting corrosion for more than 30 days. Moreover, when PANI was removed by scratching the electrode to expose the substrate to the corrosive medium, the open circuit potential (OCP) went down and rose again. This result suggested that the PAIN "healed" the 'damaged' passive layer of the SS and has the potential to be used as an anti-corrosion coating.

Since the publication of this report a great deal of interest in the corrosion properties of PANI has been taken place. Most of the PANI corrosion research has been focussed on the corrosion application of ferrous based materials. At the time, little studies on the corrosion protection of Al alloys using polyaniline had been carried out.

10 years later, in 1995 Racicot et al [65] found a way to overcome the adhesion problem of PANI by combining PANI with other polymers. The authors formed a new co-polymer consisting of PANI and polyvinyl, containing carboxylic acid to facilitate processing and adhesion performance. The new co-polymer was applied on AA 7075 and the following two types of corrosion tests were carried out;

1) Polarization in 0.5 N NaCl. This test showed that the new co-polymer reduced the corrosion current by two orders of magnitude below that of the uncoated sample and the corrosion potential increased by 50 mV above than that of the bare sample. Moreover, the sample was polarized anodically to +700mV and no pitting appeared. The polarization curve of the coated sample was compared with a sample that anodized in 1N H_2SO_4. Both of samples

have similar corrosion behaviour. These results suggested that a passive layer was formed.

2) Coated samples were scratched and immersed in 0.5 N NaCl. The scratched samples showed no pitting or undercutting of coating after seven days of immersion. The authors suggested that the formation of a protective layer by oxidation of the Al surface was due to galvanic coupling with the electroactive polymer. The mechanism implied the capability of the coating to 'self-heal' by forming a passive layer

Racicot and co-workers, [66] continued their work with PANI and prepared a double strand complex of unknown polyanione molecule, serving as a dopant, and PANI. This complex showed the characteristics of a conductive polymer, moreover, it could be dispersed in a suitable solvent and the dopant contributed to good adhesion with the metal substrate.

A thin film of the double strand coating was applied on AA 7075 and then immersed in 0.5M NaCl (pH=3.6) solution. After three months, the coated sample showed less pitting than the bare sample. An electrochemical impedance spectroscopy study in 0.5M NaCl (pH=3.6) showed that the impedance of the double strand coated sample remained high (10^6 ohm) for three weeks. However, Alodine$^©$, a commercial chromate coating, coated sample was far less resistant to corrosion in this acidic salt environment and the impedance of the Alodine decreased by one order during the first three days.

In a further test, both samples were scratched and subject to salt spray testing, for 200 hours. Results showed that the scratch in the double strand coated remained sharp, however, the Alodine coated sample showed undercutting. The authors suggested that the double strand coating provided protection through the formation of an oxide film or oxide-like interfacial layer between the polymer and the metal surface. The authors postulated that if this layer remained stable against the corrosive anions, it would reduce the corrosion current.

Epstein et al [67] used PANI as an anti-corrosion for aluminium 2xxx and 3xxx series, where samples were coated (ca. 20 μm) with emeraldine base (EB) PANI and sulphonated PANI and then tested in 0.1M NaCl solution for 10 or 66 hours. The potentiodynamic studies showed that the corrosion potential of EB

coated samples were higher than that of sulphonated PANI coated samples. However, both potentials were more positive than that of uncoated samples. The corrosion current of coated samples were reduced tenfold from that of uncoated samples. An X-ray Photoeletron Spectroscopy (XPS) study revealed less corrosion for coated samples compared with uncoated samples. A sample of AA 3003 was coated by EB and then exposed to 0.1M HCl at 80 °C for 2 hours. Another sample in which an aluminium film was evaporated on EB (on a glass slide) and exposed to HCl vapour. XPS was used to study the PANI/Al interface of both samples using depth profiling from the Al side. Reduced oxidation of the aluminium for both samples was seen as evidence of corrosion protection. The XPS study of the coated 2024 sample also showed a decrease or absence of copper in the top several hundred nanometres of the coated surface. The author suggested that the PANI coating played a role of dissolving the copper containing corrosion products which eliminated the galvanic coupling between the copper containing precipitates and aluminium matrix; thereby causing dramatic decrease in corrosion rate.

Several researchers [37], [68], [69] have attributed the corrosion prevention mechanism of a PANI coating to a shift in the corrosion potential to the passive region. Table 2-5 showed that polyaniline has a higher OCP than that of most active metals, including aluminium, zinc and magnesium.

Table 2-5 Reduction potentials for a variety some active metals, chromate and conducting polymers

Redox couple	Reduction potential (vs. SHE at pH 7)
Mg/Mg^{+2}	-2.36
Al/Al_2O_3	-1.66
Zn/Zn^{+2}	-0.76
Fe/Fe^{+2}	-0.44
CrO_4^{2-}/Cr_2O_3	0.42
Polypyrrole	-0.1 to +0.3*
Polyaniline	0.4 to +1.0*
Polythiophene	+0.8 to 1.2*

*Dependent on the dopant, electrolyte and doping level, moreover, further range modification can be done by substitution.

However, the electrochemical mechanism of moving the mixed potential of the PANI/Al couple into the passive range of a metal (e.g. Fe) cannot operate for aluminium in the same way since the OCP of PANI at near neutral pH is greater than the pitting potential of aluminium.

In order to understand the corrosion prevention mechanism of PANI on aluminium, Cogan et al [70] coupled PANI, doped with camphor sulfonic acid (PANI-CSA), on Indium Tin Oxide (ITO) to AA in the corrosive solution.

The coupling of PANI on ITO with AA 2024-T3 in neutral 3.5 wt% NaCl in both saturated argon and oxygen solutions showed that the colour of PANI-CSA changed from green to blue colour in both solutions. The authors suggested that the corrosion mechanism of the PANI-CSA coated sample may be attributed to the reduction of the conductive form of PANI (ES) to the non-conductive form (LB) which acted as a barrier. However, PANI "healed" the corrosion defects; thus, the mechanism may be due to the residuals of solvent and/or oligomers and/or monomer from the polymerization process acting as inhibitors. In particular, the presence of residual monomer in the polymer

obtained by electrochemical or chemical polymerization has been previously noted by Gospodinova et al [26].

Continuing their work, Racicot and his co-workers [71] prepared what they called "double strand PANI/polyacrylic acid" which was cast onto AA 7075 and AA 2024 substrates. A series of EIS measurements of the double strand sample was carried out in 0.5N NaCl solution with different pH values. It was found that PANI lost its ability to protect the aluminium substrate at pH=11 when its conductivity decreased.

The authors suggested that the protection may come from chemical transformation of the aluminium surface notably the oxidation power of the conductive form of PANI. They further concluded that the aluminium passive layer is a non-oxide passive layer and the conductive PANI form is not working as a barrier coating for ions and electrons. However, its ability to transfer charges at the polymer/metal interface is important for passivation of the metal surface within the corrosive environment.

Until this time, none of the above authors had addressed the question "How can PANI protect the aluminium alloys from corrosion?", or that is "what is the mechanism of protection?" Tallman et al [72] studied the interaction between PANI and aluminium alloys.
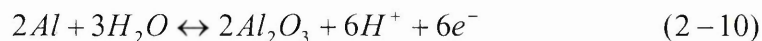
The corrosion performance of PANI coated AA 2024 and AA 7075 in dilute Harrison's solution was evaluated using EIS and electrochemical noise method (ENM). PANI was doped with dinonylphthalene sulfonic acid and the coating thickness was 40 μm. During the first few days of immersion the impedance increased, about one order of magnitude. The ENM indicated strong interactions between the metal substrate and the polymer during this period. These interactions were accompanied by a decrease in solution pH. With an epoxy top coat (90-100 μm) PANI coated samples showed better corrosion resistance than that of the epoxy coat alone; however, PANI coated samples were not as good as Alodine coated samples.

PANI coated samples exhibited two interesting types of behaviour during immersion in dilute Harrison's solution; 1) in the first ten days of immersion, PANI coated samples exhibited one order of magnitude decrease in impedance

compared with that of an epoxy-only sample despite a higher coating thickness suggesting that PANI does not inhibit the charge transfer at the metal surface.

2) With prolonged immersion time, the impedance began to increase, which may be attributed to an interaction between the metal and polymer which in turn may be activated if sufficient electrolyte is present at the metal/polymer interface. The above results suggested the following mechanism:

$$2Al + 3H_2O \leftrightarrow 2Al_2O_3 + 6H^+ + 6e^- \qquad\qquad (2-10)$$

$$3ES + 6H^+ + 6e^- \leftrightarrow 3LB \qquad\qquad (2-11)$$

Then

$$3LB \leftrightarrow 3EB + 6H^+ \qquad\qquad (2-12)$$

The increase in impedance may be attributed to the growth of an insulating oxide film at the metal/polymer interface.

The authors gave some suggestions; however, they did not provide any proof of what happened at the coating metal interface.

Later in 2002 [73], an XPS study on AA 5005 was carried out by Fujita et al to evaluate the changes at the PANI (EB)/AA5005 interfacial area. The AA5005 samples were pre-treated with different pre-treatments;

 1) Abraded only.

 2) Etching in a sulphuric acid, sodium dichromate and cupper sulphate solution (68 °C for 10 min.).

 3) Cleaning with a commercial borate cleaner (40-50(C).

The samples were then coated with PANI (EB) and placed in a humidity chamber. XPS analysis showed that the PANI (EB) is reduced in different ratios depending on the pre-treatment process; the abraded sample showed a higher reduction, while, the chromate pre-treatment showing the least reduction.

At the same time the aluminium is oxidized to hydroxide or oxy-hydroxide rather than aluminium oxide Al2O3.

Conroy et al [74] deposited PANI electrochemically on high purity aluminium (99.99%) at constant potential of 1.25V (SCE) in tosylic acid solution. The corrosion potential of the PANI coated sample was 450mV nobler that uncoated

sample, however, the corrosion current of the coated sample was higher that uncoated one.

Kunal et al [75] deposited PANI electrochemically on AA 2024-T3 substrates from an oxalic acid solution containing the aniline monomer. Oxalic acid reacted with the aluminium forming a passive aluminium oxalate layer. As the reaction preceded the aluminium oxalate film was covered by PANI. The minimum potential for PANI preparation was found to be 3.0 V versus SCE. A potentiodynamic study in 3.5 wt% NaCl solution showed that the corrosion rate of the PANI coated sample was lower than that of the uncoated samples. Moreover, the corrosion current and corrosion potential were found to be dependant on preparation conditions, e.g., preparation current density and time.

Huerta et al [76] obtained the same results as Kunal [75]. Huerta et al prepared a very adherent PANI film electrochemically on AA 2024-T3 from an oxalic acid solution containing the aniline monomer. It was prepared by applying an anodic current density of 1mA/cm^2 for 500 s. The open circuit potential, in 3.5 wt% NaCl solution, was shifted positively only 65mV from that of the uncoated metal. However, the corrosion current of the coated sample was higher than that of the uncoated one. The authors suggested that may be due to the corrosion current of the coated sample included the oxidation of PANI and that the active area of the electrode was unknown. The EIS study showed that the impedance of the PANI coated sample initially increased and then began decreasing after 5 days in the solution. Furthermore, a new time constant appeared after 24 hours immersion in the solution. The change in phase angle was attributed to the formation of Al_2O_3. For long term immersion, the PANI coated sample did not show severe corrosion when immersed in 0.1 M NaCl solution for 2.5 months. The authors suggested that the corrosion prevention of AA2024-T3 may be attributed to the formation of a compound with the re-deposited copper on the surface thereby, avoiding Al-Cu galvanic coupling.

When aqueous aniline monomer [77] and polyacrylic acid solutions are mixed, aniline binds to the polyacrylic acid backbone due to intermolecular forces including hydrogen bonding and electrostatic attraction. After the mixture is acidified, aniline is polymerized by an oxidant such as sodium persulphate. The

prepared double strand PANI is stable in its conductive form over a range of pH values from 0 to 9. The prepared double strand was dispersed in a commercial water-bone epoxy paint and applied to the surfaces of 2024, 7075 and 6061 aluminium alloys giving a coating thickness of about 20 μm.

An EIS study showed that the impedance values of coated samples dropped by three orders of magnitude when PANI converted from the conductive to non-conductive form. This result suggests that the corrosion protection of PANI coated samples is related to its conductivity.

Salt spray tests for scratched samples (1000 hours) showed that the double strand PANI exhibited neither undercut nor blistering although accumulation of white aluminium oxide at the scratch line was obtained. However, the control "epoxy containing PANI" coated sample showed blistering of the coating near the scratch.

Immersion in sea water (pH =8) for 40 days revealed blistering of the epoxy control sample, however, the double strand PANI containing sample showed substantial resistance to blistering and subsequent corrosion.

For testing the resistance of samples to filiform corrosion, samples were scratched and then dipped in HCl solution for two minutes followed by air-drying, then placed in 85% humidity chamber for 6 days, this cycle was repeated for 8 weeks. The PANI double strand sample showed less filiform corrosion than that of an epoxy control sample.

Huerta et al [78] electrochemically prepared a conductive co-polymer of polyaniline and polypyrrole (PPY) on both carbon steel and AA2024-T3. The polymerising solution contained oxalic acid and different relative monomer concentrations.

The corrosion performance of the coated samples was influenced significantly by the electrochemical deposition parameters.

The DC polarisation study of PANI and PANI/PPY coated AA2024 showed that the copolymer offered a better corrosion performance than single polymer coated sample; the corrosion current being decreased by two orders of magnitude and the corrosion potential increased by about 600mV.

Huerta et al [79] had continued preparing PANI electrochemically. This time PANI was prepared electrochemically on AA1050, using anodic activation of the

substrate in nitric acid containing aniline. The anodic pre-treatment made the aluminium surface porous and resulting pits were filled with PANI. This pre-treatment improved the corrosion resistance in 0.1M NaCl; the current density of the pre-treated sample was about two orders of magnitude less than that of the bare sample. Since the electrochemical technique is not practical, Huerta et al [80] tried to improve the processability of PANI by chemical co-polymerisation. A PANI co-polymer with O-anisidine was chemically synthesised. The co-polymer was applied by both chemical and electrochemical methods on stainless steel, SS304, and AA6061. The copolymer offered better corrosion protection for both substrates. The corrosion potential of SS304 was markedly ennobled; however, the change in corrosion potential of AA6061 was improved but less than that of the SS. The solubility in common solvents remained a challenge

The effect of sulphonic acids, as dopants for PANI, for the corrosion prevention of AA3003 was investigated by Ogurtsov et al [81]. PANI was doped by p-toluene-sulfonic, camphorsulfonic and dodecylbenzenesulfonic acids and applied on the metal surface. The corrosion resistance of PANI with artificially created defects (hole) was evaluated by EIS in aqueous 3.5% NaCl and 0.1 N HCl solutions. The results were compared with undoped PANI and bare metal. The undoped PANI showed the highest corrosion resistance, however, PANI doped with camphorsulfonic and dodecylbenzenesulfonic acids showed less corrosion protection than bare metal in both corrosive solutions. The undoped PANI showed better corrosion inhibition in neutral solution than in the acidic solution.

Kendig et al [82], [83] used PANI not only as a corrosion prevention material but also as a film that can be tailored to release corrosion inhibitors on demand. PANI was doped with 1- pyrrolidine dithiocarbamate; an oxygen reduction reaction inhibitor (ORR) and applied on the AA2024-T3. When PANI was reduced the dopant would be released causing a two fold effect on inhibition of corrosion. A rotating disk electrode was used to measure the cathodic current density and a UV technique was used to detect the released inhibitor. A salt fog test using a scratched sample showed only slight tarnishing in the scratch after

48 hours of exposure. This result demonstrates the effectiveness of incorporation of an ORR inhibitor in the protective coating based on PANI for AA2024.

Seegmiller et al [84] improved the mechanical properties of PANI by mixing it with a nonconductive polymer. PANI doped with camphorsulphonic acid (PANI-CSA) in m-cresol was mixed with polymethylmethacrylate (PMMA) and applied on AA 2024-T3 substrate. PMMA improves the mechanical properties of PANI and it is miscible with the PANI-CSA solution. The coating thickness was 10 μm. The OCP measurement in 10 mM H_2SO_4 (pH=2) showed that the PANI/PMMA coated sample has higher OCP than that of the bare and PMMA samples. The OCP of the PANI/PMMA coated sample was -0.12 V (vs. Ag/AgCl) suggesting the oxygen reduction reaction is not likely to be significant. A Raman ex situ study showed that the PANI was partially reduced by the aluminium substrate after immersion in the solution for 15 hours. A scanning electrochemical microscope combined with Raman microscope was used to study scratched samples. This study showed that a PANI blend can inhibit corrosion in the damage site. While the absence of PANI led to hydrogen evolution taking place. Raman microscopy revealed that PANI is reduced near the scratch and this reduction decreased away from the scratch. The authors suggested that the mechanism of protection of AA2024-T3 is a combination of growth of protective oxide film and a shift in the metal OCP to a higher potential which suppresses both hydrogen evolution and oxygen reduction. The later would inhibit OH^- production, thereby preventing damage of the alloy surface by dissolution of its protective oxide film.

Yang et al [62] related the anti-corrosion properties of PANI to its oxidation power. Typical PANI contains about 1000 repeating monomer units. The doped form may have about 100 positive charges carried on a polymeric chain $(PANI)^{+100}$ which means $(PANI)^{+100}$ is an oxidant with oxidation potential E=0 (vs. SCE) when it is in equilibrium with air. In this case, $(PANI)^{+100}$ can oxidize aluminium as follows

$$(PANI)^{+100} + Al + 3/2\ H_2O \longrightarrow 1/2\ Al_2O_3 + 3H^+ + (PANI)^{+97} \quad (2\text{-}13)$$
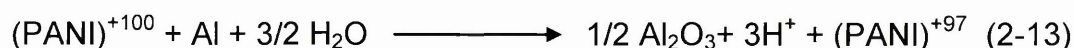
The oxide produced is not necessarily adherent and passive but it is possible that it is formed at an appropriate rate to prevent the initiation of any pitting corrosion.

In support of this, charging/ discharging of PANI electrochromic windows can undergo 10^5 cycles, moreover, $(PANI)^0$ spontaneously changes in air to $(PANI)^{+100}$. PANI was prepared using the backbone of polyacrylic acid to form double strand PANI. Salt spray and filiform corrosion tests showed that double strand PANI had better performance than PANI alone.

Cecchetto et al [85] studied the corrosion resistance of AA 5182 coated by PANI (EB) using a spin coating technique. The potentiodynamic study in 0.1N NaCl (pH=6) oxygen free solution of samples with different EB thicknesses showed that a significant increase in corrosion potential values and decrease in corrosion current values resulted as a function of EB thickness. The study showed that the cathodic branch was controlled by a diffusion limited reaction.

Another potentiodynamic study using a rotating disk working electrode in 0.1N Na_2SO_4 in both oxygenated and oxygen free solutions showed no change in the cathodic branch with increasing rotation speed of the working electrode. Consequently, the current was independent of oxygen reduction. For a better understanding of the electrochemical activity of the EB coatings in neutral environments, electrochemical and IR studies were carried out on an indium tin oxide (ITO) coated substrate in oxygen free 0.1 M Na_2SO_4 electrolyte at pH 3.8 and 7.2.

The result showed that EB was electrochemically activated in both environments being related to the presence of the doped polymer emeraldine salt (ES) inside the film. The authors revealed that the diffusion-limited current observed under cathodic polarization of EB-coated aluminium samples could be related to the reduction of the doped fraction of the polymer and was limited by the diffusion of the anions involved in the electrochemical reaction inside the coating.

The authors concluded that EB is able to provide an ennobling effect of the metal substrate, mediated by the formation of ES, which, in turn, is reduced to LB as shown in Figure 2-11. ES could be generated by the doped water in EB in the solution and/or by acid-base interaction of EB with the hydrated substrate.

This weak EB electrochemical activity combined with its low ion permeability and its low electronic conductivity provides a decrease of the hydrogen and oxygen reduction rates, and improves corrosion resistance of aluminium substrates in a neutral environment.
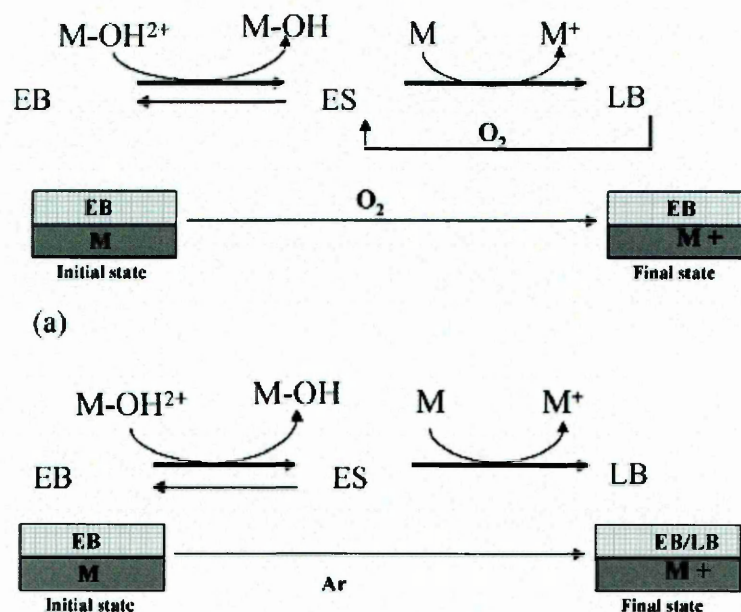

Figure 2-11 The reaction of PANI oxidation states to protect metal substrate

Cecchetto et al continued studying the effect of PANI on the corrosion resistance of aluminium AA5182 [86]. The samples were coated by thin films of EB obtained from a 5% solution in N-methylpyrrolidinone. The coating thickness was 2-3µm and tested in de-aerated 0.1N NaCl (pH=6) solution. When a cathodic current was applied on the uncoated metal, grooves around the iron–manganese rich intermetallic particles due to the dissolution of the surrounding matrix were observed by SEM. However, a single anodic sweep to 0.6 V vs. OCP was not enough to create significant damage to the coated surface. In contrast, when a potential of 0.6 V vs. OCP was applied for 5 min, it caused localized breakdown of the EB film

Salt spray tests on coated AA5182 samples revealed that EB provided good corrosion protection on aluminium alloys. The layer remained adhered to the substrate and no pits were observed after 50 hours in the salt spray chamber.

The SEM study of an AA5182 EB coated sample after 500 hours in the salt spray chamber showed localized pits.

Additionally, blistering and break down of the coating took place at some pit sites and the blue colour of PANI changed to a blueish-green colour around the site of breakdown. The author attributed the change of colour to the conversion of EB to the ES state by the acid solution formed inside the pits.

The authors suggested that the breakdown is caused mainly by hydrogen bubbles produced during pit formation. The acid solution generated at the pit sites contributed to detachment of PANI at these sites.

An electrochemical study in an argon saturated electrolyte of bare and EB coated AA5182 substrate showed that the corrosion potential of the coated substrate is 400 mV nobler than that of bare sample, furthermore, the corrosion current is more than 1 order of magnitude lower than that of the bare metal.

EB can slow down the rate of local acidification on aluminium substrates at the pit sites by a self healing process (EB converted to ES consuming H^+).

PANI was electrochemically prepared on both sheet and wire beam electrode (WBE) of AA1100 from tosylic acid [87],[88]. The study showed that the pre-treatment, cathodic polarisation of the working electrode, affected the homogeneity of the prepared layer. The polarization of coated sheet in 0.5 M NaCl showed an increase in the corrosion potential of the coated sample, about 150 mV, and a shift in the pitting potential by +135mV. Notwithstanding, the corrosion potential showed an increase in the coated sample with respect to the bare one, PANI deposits behaved as cathodes over the WBE surface whereas the areas with less PANI deposits behave as the anodes. Furthermore, the anodic current values decreased with the extension of electrode exposure. On the basis of these results, the authors concluded that aluminium electrode with PANI deposit decreased the localized corrosion; however, it increased the general corrosion.

NiZn ferrite/PANI particles were added to the precursors of a silica sol-gel forming 10, 20 and 30 % hybrid coatings [89],[90]. The coatings were applied to both AA2024 and AA6061 samples. The polarization measurements showed that these coating have nobler corrosion potential, about 100mV above the bare

sample; moreover, they have two orders of magnitude less corrosion current than that of the bare sample. Salt spray testing for 168 hrs showed no signs of corrosion for the coated samples. The authors suggested that the corrosion protection related to the good barrier properties of these coatings.

Chemically prepared [91] PANI doped with phosphoric acid was added as a pigment in both acrylic and epoxy binders and applied to AA2024 T3 as a primer. The primer thickness was 55-60μm and a polyurethane topcoat was applied to make the total thickness of 100μm. The EIS study, in 0.5% NaCl solution, showed that both of the coating systems have exhibited high impedance, above $1x10^6$ Ohm.cm^2, during 50-days exposure.

The authors refer the corrosion protection to the formation of an oxide layer that growth with immersion time in addition to the passivation ability of the PANI which shift the OCP in noble direction with time of exposure.

Zubillaga et al [92] prepared PANI electrochemically incorporation with inorganic filler, TiO_2 nanoparticles. Anodizing was carried out at a constant voltage of 8 V in aqueous oxalic acid solution containing aniline monomer and TiO_2 nanoparticles under a nitrogen atmosphere. The coating was prepared on AA3105 forming an oxide porous film of 2-3μm with outer layer of PANI/TiO_2 of several nanometers thickness. PANI only coated sample showed pits after 168 hrs in salt spray test, on the other hand, PANI/TiO_2 coated sample did not showed any sign of corrosion over 1000 hrs salt spray test. Furthermore, EIS results showed that the PANI/TiO_2 sample had stable higher impedance, $1x10^6$ Ohm.cm^2, than that of both bare and PANI only coated samples. The improved protection of PANI coating with TiO_2 filler referred to that TiO_2 acts as a blocking barrier layer for the anodic porous aluminium oxide.

2.5 SOL-GEL TECHNOLOGY

The sol–gel process is a chemical synthesis method that has been used for the preparation of inorganic materials such as glasses and ceramics. Ebelmen first reported the synthesis of silica from silicon alkoxide in 1844 [93].

Although first discovered in the 1800s a new interest emerged in the early 1970s when monolithic inorganic gels were formed at low temperatures and

converted to glasses without a high temperature melting process. Through this process, homogeneous inorganic oxide materials with desirable properties of hardness, optical transparency, chemical durability, tailored porosity and thermal resistance, can be produced at low temperatures, as opposed to the much higher melting temperatures required in the production of conventional inorganic glasses [94].
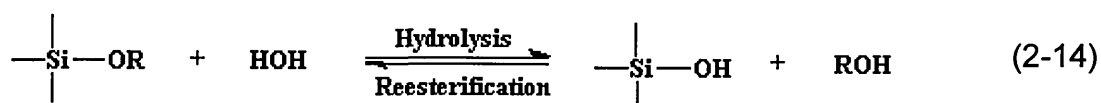
In the 1990s, a new approach appeared with the homogeneous combination of organic and inorganic precursors to form a hybrid structure. This approach offers a huge number of possibilities in the field of organic-inorganic hybrid sol-gel materials [93].

Generally, the sol-gel process, as the name implies, involves the evolution of inorganic networks through the formation of a colloidal suspension (sol) and gelation of the sol to form a network in a continuous liquid phase (gel) [94].

In a typical sol-gel process, the precursor is subjected to a series of hydrolysis and polymerization reactions to form a sol. Then the sol is subjected to another series of condensation reactions to form gel. With further drying, the gel is converted into dense ceramic or glass particles [95].

A gel can be considered as a giant molecule, which has been formed as a consequence of the growth by condensation of polymers or aggregation of particles. The coherent solid 3-D network inside the fluid phase is known as a "gel". The solid phase particles range in size from several nanometres to hundreds of nanometres [93]. The precursors for synthesizing these colloids consist of a metal or metalloid element surrounded by various reactive ligands. Metal alkoxides are most popular because they react readily with water. The most widely used metal alkoxides are the alkoxysilanes, such as tetramethoxysilane (TMOS) and tetraethoxysilane (TEOS). However, other alkoxides such as aluminates, titanates, and borates are also used in the sol-gel process.

Three reactions are generally used to describe the sol-gel process: hydrolysis, alcohol condensation, and water condensation.

$$\equiv Si-OR + HOH \xrightleftharpoons[\text{Reesterification}]{\text{Hydrolysis}} \equiv Si-OH + ROH \qquad (2\text{-}14)$$

$$—\overset{|}{\underset{|}{Si}}—OH \quad + \quad —\overset{|}{\underset{|}{Si}}—OH \quad \underset{\text{Hydrolysis}}{\overset{\text{water Condensation}}{\rightleftharpoons}} \quad —\overset{|}{\underset{|}{Si}}—O—\overset{|}{\underset{|}{Si}}— \quad + \quad HOH \quad (2\text{-}15)$$

$$—\overset{|}{\underset{|}{Si}}—OH \quad + \quad —\overset{|}{\underset{|}{Si}}—OR \quad \underset{\text{Alcoholysis}}{\overset{\text{Alcohol Condensation}}{\rightleftharpoons}} \quad —\overset{|}{\underset{|}{Si}}—O—\overset{|}{\underset{|}{Si}}— \quad + \quad ROH \quad (2\text{-}16)$$

The overall reaction;

$$[\equiv Si-O-Si\equiv]_n \xrightarrow{\text{polymrization}} \qquad (2\text{-}17)$$
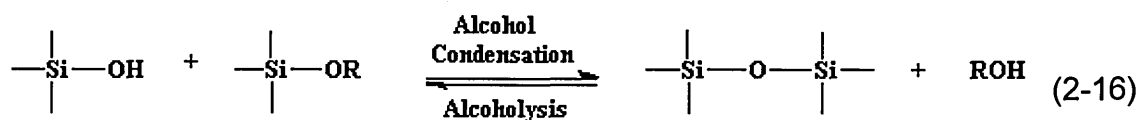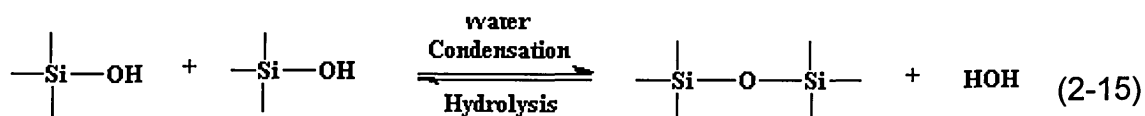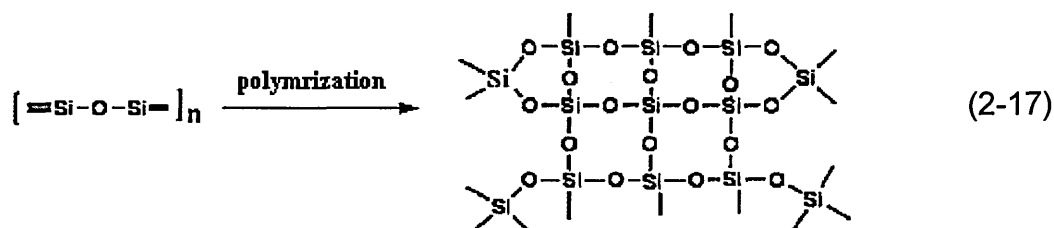
Generally, the hydrolysis reaction (Eq. 2-14), through the addition of water, replaces alkoxide groups (OR) with hydroxyl groups (OH). Subsequent condensation reactions (Eqs.2-15 and 2-16) involving the silanol groups (Si-OH) produce siloxane bonds (Si-O-Si) plus the by-products water or alcohol.

The characteristics and properties of a particular sol-gel depend on a number of factors that affect the rate of hydrolysis and condensation reactions, such as, pH, temperature and time of reaction, reagent concentrations, catalyst nature and concentration, H_2O/Si molar ratio, aging temperature and time, and drying. Thus, by controlling these factors, it is possible to vary the structure and properties of the sol-gel-derived network over a wide range [94].

Many specific applications of sol-gel include optics, protective and porous films, window insulators, dielectric and electronic coatings, high temperature superconductors, reinforcement fibres, fillers, and catalysts.

2.5.1 Hybrid inorganic /organic sol-gel

Organic polymers and inorganic materials have their own advantages and disadvantages. Organic polymers are easily processed; they are light weight, flexible and easily shaped. However they are normally soft and have low strength at high temperature. Inorganic materials usually have good mechanical and thermal properties; however, they are brittle and heavy.

A hybrid organic/inorganic sol-gel employs both materials in a homogeneous combination, gaining the advantages of both organic and inorganic materials. Using hybrid sol-gel technology it is possible to control the mechanical and optical properties for different applications.

Sol-gel technology has some advantages to synthesize organic/inorganic hybrid materials such as low temperature processing. Low temperature processing allows for both inorganic and organic materials to be homogeneously mixed without affecting the properties of the organic material. Hybrid organic/inorganic sol-gel usually produced by involved organic group into the inorganic precursors e.g. organoalkoxysilanes which contains (an) organic group(s) (R') as shown in Figure 2-12 [96].

$$
\begin{array}{ccc}
\overset{\cdot}{R} & & R^{\cdot} \\
| & & | \\
-\!\!\!-\!\!Si\!\!-\!\!OR & R\,O\!\!-\!\!\!-\!\!Si\!\!-\!\!OR \\
| & & |
\end{array}
$$

Figure 2-12 Shapes of alkoxysilane

2.5.2 Sol-gel Process

Several steps are involved in the sol-gel process in order to obtain the final material, namely: mixing, gelation, aging, drying and curing. Figure 2-13 shows the diagram of sol-gel processes, where, at each step there are numerous physical and chemical factors that affect the properties of final sol-gel.

42
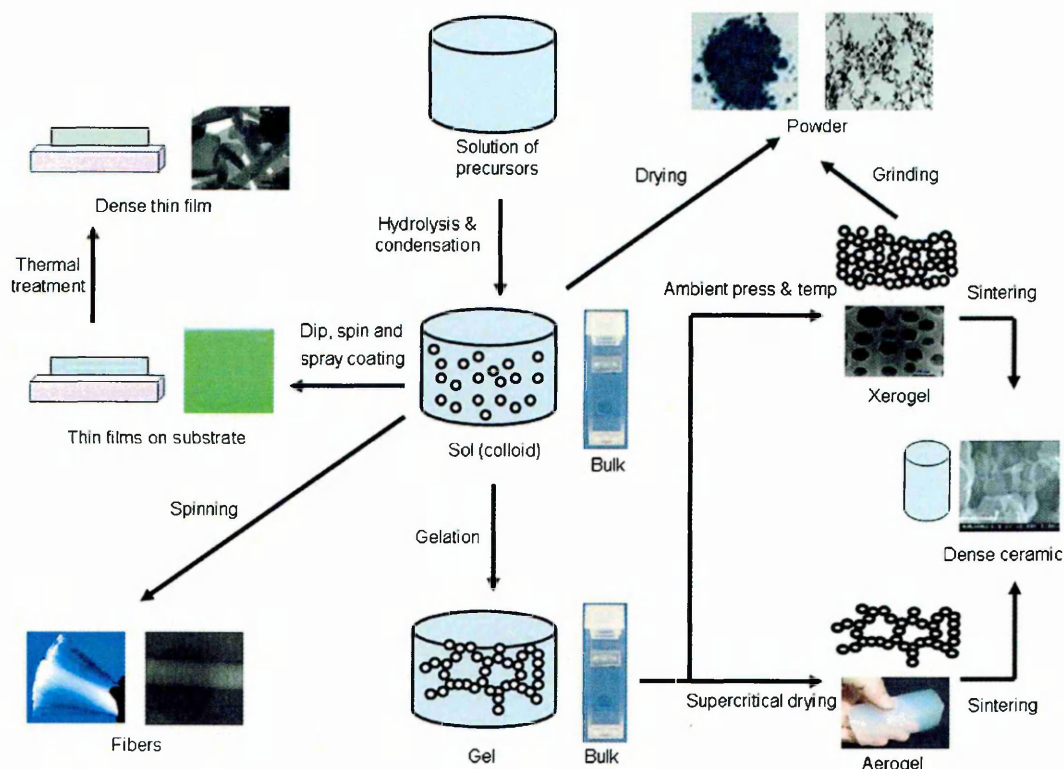
Figure 2-13 The process of sol-gel production [97]

An alkoxide precursor such as $Si(OR)_4$ is hydrolyzed by mixing with water. The hydrolysis and polycondensation reactions initiate at numerous sites within the $Si(OR)_4$ + H_2O solution as mixing occurs [98] in the presence of a common solvent (normally alcohol) [93]. When sufficient interconnected Si-O-Si bonds are formed in a region, they respond cooperatively as colloidal particles or a sol. The final result is a colloidal dispersion of extremely small nano particles that finally form a 3-D entangled network [93]. The size of the sol particles and the cross-linking within the particles depend upon the pH and *R* ratio *(R =* $[H_2O]/[Si(OR)_4]$ [98] .

With time polycondensation of silicon alkoxide produces colloidal particles that link together to become a 3-D network. In this process the catalyst plays an important role due to the ionic charge of the silica particles, with a direct influence on the polycondensation rate. At low pH, the silica particles have very little ionic charge and thus can collide and aggregate into chains forming a polymeric gel. This effect is produced around pH=2 where the surface charge is zero [93].

Conversely, at high pH, where the rate of dissolution and solubility of silica is higher (maximum at pH 7), the particles grow in average size and diminish in number as the smaller ones dissolve and the silica is deposited upon the larger ones [93]. The molecular configurations of the acid and base catalysed sol-gel are shown in Figure 2-14. The dramatic change in the rheological behaviour of the sol is used to identify the gel point.

• Acid-catalyzed

— Yield primarily linear or randomly branched polymer

• Base-catalyzed

— Yield highly branched clusters

Figure 2-14 The shape of sol-gel with acidic and alkaline catalyst [94].

At this stage of sol-gel preparation, the sol can be applied to a substrate to form a thin film coating. Additionally, the sol can be spun to form a fibre or dried to form a powder as shown in Figure 2-13.

Alternatively, with time, gelation of the solid network immersed in the pore liquor continues to evolve. This aging process occurs via three steps, polymerisation, syneresis and coarsening. Polymerization of unreacted hydroxyl groups increase the connectivity of the gel network, this process runs parallel with some shrinkage followed by a spontaneous and irreversible shrinkage of the gel network resulting in expulsion of pore liquid, the driving forces of the liquid produce compressive stresses that draw the solid network into the liquid.

During drying the liquid is removed from the interconnected pore network. Large capillary stresses can develop during drying when the pores are small (20 nm) which can cause the gels to crack [98].

The drying process may take weeks, even months, to form a monolithic dried gel at room temperature (xerogel). One alternative to accelerate drying is to add drying control chemical additives such as formamide and oxalic acid that modify the surface tension of the interstitial liquids, allowing fast elimination of the unwanted residues. Either way, the most efficient way of neutralizing the undesired effects of surface tension is to suppress the liquid-vapour interface. This is achieved by treating the gel in an autoclave. The resulting product is a gel with its pores filled with air called an 'aerogel' [93].

Heating the porous gel at high temperature causes densification to occur. Solid networks move by viscous flow or diffusion to eliminate porosity. The densification temperature depends on the dimensions of the pore network, the connectivity of the pores, and surface area [98]. In gels with high pore surface areas the driving forces are great enough to produce sintering at exceptionally low temperatures, where the transport processes are relatively slow.

A great deal of research is now taking place to improve and modify the process and deal with those factors affecting the final product allowing the sol-gel to be tailored according to a specific application.

2.5.3 Advantages and Disadvantages of the Sol-Gel Technique

The basic advantage of the sol-gel process is its ability not only to form inorganic structures (semiconductors, ceramics and glasses) but also to form hybrid organic and inorganic network structures at relatively low temperatures. Furthermore, the coating process is very similar to conventional coating techniques such as dip-, spin- or spray coating and does not require any vacuum processes, and is therefore a cost-effective way to produce homogeneous films on large scales [99]. Moreover, it can either produce a thin bond-coating to provide excellent adhesion between the metallic substrates and subsequent top coats or produce a thick coating to offer corrosion protection to metals. It can also easily shape materials into complex geometries in a gel state and produce high purity products because the organo-metallic precursors of the

desired ceramic oxides can be mixed, dissolved in a specified solvent and hydrolyzed into a sol, and subsequently a gel. The composition of the sol-gel materials can be highly controllable. The sol-gel formed materials can be cured from room temperature to high temperature according to the desired formulation and required properties [100].

However, the sol-gel method has some potential disadvantages such as; relatively high cost raw materials, large shrinkage during processing, residual fine pores and stresses leading to cracking [101].

2.4.3 Sol-gel Applications

The specific uses of sol-gel produced glasses or ceramics are derived from the various material shapes generated in the gel state, i.e., monoliths, films, fibres, and monosized powders [94].

Films and coatings represent the earliest commercial application of sol-gel materials. Thin films, of the order of nanometres, formed by dipping or spinning may be processed without the formation of cracks. Optical coatings are one example of the sol-gel coating which change the optical properties of the substrate e.g. reflectance, transmission or absorbance. Hydrophobic, self-cleaning decorating colour coatings [102], anti-corrosion coating [103] and abrasion resistance coatings [104] are other examples of sol-gel films. Monoliths which are defined as bulk gels cast to shape and processed without cracking, are another form of application. The principle advantage of monoliths appears in the formation of high purity optical components without melting or polishing [105]. They can be processed at room temperature. Applications of monoliths include fibre optics, lenses, graded reflective index glasses and transparent foams. Ultra-fine and uniform ceramic powders can be formed by the sol-gel technique [106]. These powders of single- and multicomponent compositions can be used for dental and biomedical applications [107]. However, the important application of sol-gel processing is to carry out zeolite synthesis [108] [109]. Also powder abrasives, used in a variety of polishing operations, are made using the sol-gel process.

Finally, ceramic membranes for filtration, reverse osmosis [110], chromatography [111] and photocatalysis [112] can be produced by this technique [101].

One of the most important recent applications of sol-gel technology is corrosion protection [97], [103], [113]. Sol-gel technologies excel in the production of thin film inorganic or hybrid coatings and a number of studies have been conducted on the development and characterization for corrosion protection using sol-gel coatings.

Using conventional inorganic sol-gel protective coatings for example SiO_2, TiO_2, Al_2O_3, ZrO_2, CeO_2, and binary or mixed oxides were tested for corrosion control [114]. In all these cases, the films were prepared by a spin or dip coating then aged followed by a high-temperature densification process.

The main drawbacks of inorganic sol-gel films include [114];

(a) Sol-gel films are porous therefore; water and oxygen can diffuse to the metal surface.

(b) During drying and densification, shrinkage occurs and usually leading to formation of cracks.

(c) The difference in thermal expansion coefficients of the metal and the protective film often cause film failure by debonding between substrate and coating during temperature fluctuations.

(d) Spin- or dip-coating techniques can not offer thick sol-gel coatings.

A more realistic approach for producing defect free film formation is being taken by combining the various metal oxides with organic segments i.e. organic-inorganic hybrid system. These may be synthesised using organic functionalised metal alkoxides that promote reaction between an organic group and the inorganic alkoxide. This system is a potential replacement for chromates due to the ability to tailor the systems to the specific needs of the user [115]. The inorganic components contribute to an increase in scratch resistance, durability and adhesion to the metal substrate. The organic component increases density, flexibility, and functional compatibility with organic paint systems. Other advantages of the organically modified sol–gel systems are the possibility to prepare thick, crack-free coatings and a low

temperature curing process compared with the production of conventional inorganic sol-gel films [113].

2.5.4 Corrosion protection of aluminium by silica sol-gel

Sol–gel coatings are one of the new alternatives to chromate conversion treatments proposed for corrosion protection of aluminium alloys. The advantages of the sol–gel technique over conventional coating methods are; easier preparation of crack-free films with control of composition forming an inorganic oxide matrix at lower temperature with respect to ceramic methods [116].

Silica sol–gel coatings can form Van der Waals bonds with the metallic surface which can be transformed to stable covalent Me–O–Si bond during drying process. Applying silica sol-gel coatings can protect metals from corrosion due to the formation of silica rich Al-oxide film which blocks the pores of Al oxide film to form a high corrosion-resistant layer. This layer acts as an inert barrier for the oxygen diffusion to the metal surface thereby impeding but not preventing the metal from corrosion [116].

Since a coating contains micropores, cracks, and areas of low cross-link density they provide a path for diffusion of corrosive species such as water, oxygen and chloride ions to the coating/metal interface [113], [117]. Indeed, addition of organic components, such as epoxy or vinyl, can increase the resistance to corrosion and improve the barrier property of the sol-gel film [118] [119].

However, the main drawback of these coatings is the lack of active corrosion protection and self-healing ability. This property can be significantly improved by incorporation of inorganic or organic inhibitors into the sol–gel films [103].

Addition of cerium, vanadates and molybdenum compounds was found to have an inhibiting action on corrosion processes of different metallic substrates [103] [113] [120].

However, cerium oxide, vanadates and molybdenum compounds are expensive materials, which could increase the total cost of the coating.

Some of the most effective and environmentally friendly inhibitors are derived from cerium salts. Use of cerium dopant into sol–gel coatings can be an alternative to chromate pretreatments of aluminium alloys [121] [103] [122].

However, cerium salts are highly soluble in aqueous solution which affects the corrosion performance in long time application [120]. The capsulation of cerium salts in the sol-gel matrix reduces its solubility in aqueous solutions and improves the corrosion performance [103] [123].

It could be concluded that hybrid silica sol–gel barrier coatings are able to improve the chemical and mechanical properties of the coated substrate, such as resistance to corrosion, wear, due to its lesser sensitivity to chemical attack. However, silica sol-gel coatings require additives to provide an active corrosion inhibition offering self healing properties.

REFERENCES

[1]   M.   Fontana, N. Greene, 1986, "Corrosion Engineering " Mcgraw-Hill Education, Berkshire, UK, .

[2]   K. Othamer, 1977, "Encyclopaedia of Chemical Technology, " John Wiley, Hoboken, NJ, USA, .

[3]   L. Shreir, R. Jarman and T. Burstein, 1994, "Corrosion," Butterworth Heinemann, UK, .

[4]   S. Lyon, R. Akid, 2006, "Cost of Corrosion," 2007(24 April) .

[5]   M. Brongers, 2004, "Cost of Corrosion Study," 2007(25 April) .

[6]   R. Akid, 2004, "The Handbook of Advanced Materials: Enabling New Designs,"John Wiley & Sons, Inc., Hoboken, New Jersey, USA, pp. 487-540.

[7]   C. Vargel, M. Jacques, and D.M.P. Schmidt, 2004, "Corrosion of Aluminium,"Elsevier, Amsterdam, pp. 81-109.

[8]   R. Buchheit, R. Grant, B. Mckenzie, G. Zender, 1997, "Local Dissolution Phenomena Associated with S Phase (Al2CuMg) Particles in Aluminum Alloy 2024-T3," Journal of the Electrochemical Society, 144pp. 2621-2628.

[9]   N. Birbilis, R. BuchheitJ., 2005, "Electrochemical Characteritics of Intermetallic Phases in Aluminium Alloys: An Experimental Survey and Discussion," Journal of the Electrochemical Society, 152(4) pp. B140-B151.

[10] P. Leblanc and G. Frankel, 2002, "A Study of Corrosion and Pitting Initiation of AA2024-T3 using Atomic Force Microscopy," Journal of the Electrochemical Society, 149(6) pp. B239-B247.

[11] S. Lamaka, M. Zheludkevich, K. Yasakau, 2007, "High Effective Organic Corrosion Inhibitors for 2024 Aluminium Alloy," Electrochimica Acta, 52(25) pp. 7231-7247.

[12] M. Kendig, A. Davenport, and H. Isaacs, 1993, "The Mechanism of Corrosion Inhibition by Chromate Conversion Coatings from x-Ray Absorption Near Edge Spectroscopy (Xanes)" Corrosion Science, 34(1) pp. 41-49.

[13] J. William and R. McCreery, 2002, "2002Inhibition of Corrosion-Related Reduction Processes Via Chromium Monolayer Formation," Journal of the Electrochemical Society, 149(9) pp. B379-B386.

[14] National Institute for Occupational Safety and Health, USA, "Chromium(Vi) Oxide," (Jan. 2009) pp. 2.

[15] H Shirakawa, E Louis, A Macdiarmid, Ck Chiang, A Heeger, 1977, "Synthesis Of Electrically Conducting Organic Polymers - Halogen Derivatives Of Polyacetylene, (Ch)X," Journal Of The Chemical Society-Chemical Communications, 16pp. 578--580.

[16] E. Krutmeijer, , 2008, "Conductive Polymer," 2007(15 July) .

[17] S. Freund and B. A. Deore, 2007, "Self-Doped Conducting Polymers," John Wiley & Sons Ltd, , The Atrium, Southern Gate, Chichester, West Sussex PO19 8SQ, England, pp. 326.

[18] D. Pesiri, 2006, "Conductive Polymers," 2007(24 April) .

[19] P. Novák, K. Müller, K. Santhanam, and O. Haas, 1997, "Electrochemically Active Polymers for Rechargeable Batteries," Chemical Review, 97(1) pp. 207- 282.

[20] JK Kim , G Cheruvally, J Choi , J Ahn , SH Lee , D Choi , C Song, 2007, "Effect of Radical Polymer Cathode Thickness on the Electrochemical Performance of Organic Radical Battery," Solid State Ionics, 178(27-28) pp. 1546-1551.

[21] R. Baughman., 1996, "Conducting Polymer Artificial Muscles," Synthetic Metals, 78(3) pp. 339-353.

[22] S. Koul, R. Chandra, and S. Dhawan, 2000, "Conducting Polyaniline Composite for ESD and EMI at 101 GHz," Polymer, 41(26) pp. 9305-9310.

[23] J. Pomposo., J. Rodríguez, and H. Grande, 1999, "Polypyrrole-Based Conducting Hot Melt Adhesives for EMI Shielding Applications," Synthetic Metals, 104(2) pp. 107-111.

[24] E Hakansson, A Amiet, A Kaynak, 2006, "Electromagnetic Shielding Properties of polypyrrole/polyester Composites in the 1-18 GHz Frequency Range," Synthetic Metals, 156(14-15) pp. 917-925.

[25] T Hino, S Taniguchi, and N Kuramoto, 2006, "Syntheses of Conductive Adhesives Based on Epoxy Resin and Polyanilines by using N-Tert-Butyl-5-Methylisoxazolium Perchlorate as a Thermally Latent Curing Reagent," Journal Of Polymer Science Part A-Polymer Chemistry, 44(2) pp. 718--726.

[26] N. Gospodinova, and L Terlemezyan, 1998/12, "Conducting Polymers Prepared by Oxidative Polymerization: Polyaniline," Progress in Polymer Science, 23(8) pp. 1443-1484.

[27] J.. Bredas and G. Street, 1985, "Polarons, Bipolarons, and Solitons in Conducting Polymers ," Accounts of Chemical Research, 18(10) pp. 309-315.

[28] D. DeBerry, 1985, "Modification of the Electrochemical and Corrosion Behavior of Stainless Steels with an Electroactive Coating," Journal of the Electrochemical Society, 132(5) pp. 1022-1026.

[29] V.Gelling., M. Wiest, D Tallman, 2001/11, "Electroactive-Conducting Polymers for Corrosion Control: 4. Studies of Poly(3-Octyl Pyrrole) and Poly(3-Octadecyl Pyrrole) on Aluminum 2024-T3 Alloy," Progress in Organic Coatings, 43(1-3) pp. 149-157.

[30] C. Ferreira, S.Aeiyach, J. Aaron, 1996/0, "Electrosynthesis of Strongly Adherent Polypyrrole Coatings on Iron and Mild Steel in Aqueous Media," Electrochimica Acta, 41(11-12) pp. 1801-1809.

[31] J. Camalet., J. Lacroix, S. Aeiyach, 1998, "Electrosynthesis of Adherent Polyaniline Films on Iron and Mild Steel in Aqueous Oxalic Acid Medium," Synthetic Metals, 93(2) pp. 133-142.

[32] S Sathiyanarayanan, S Muthukrishnan, G Venkatachari, 2006, "Performance of Polyaniline Pigmented Vinyl Acrylic Coating on Steel in Aqueous Solutions," Progress In Organic Coatings, 55(1) pp. 5-10.

[33] C. Jeyaprabha, S. Sathiyanarayanan, G. Venkatachari, 2006, "Polyaniline as Corrosion Inhibitor for Iron in Acid Solutions," Journal of Applied Polymer Science, 101(4) pp. 2144-2153.

[34] A. Özyılmaz, M. Erbil, and B. Yazıcı, 2006, "The Electrochemical Synthesis of Polyaniline on Stainless Steel and its Corrosion Performance," Current Applied Physics, 6(1) pp. 1-9.

[35] P. Pawar, A Gaikwad,. and P. Patil, 2007, "Corrosion Protection Aspects of Electrochemically Synthesized Poly(o-Anisidine-Co-o-Toluidine) Coatings on Copper" Electrochimica Acta, 52(19) pp. 5958-5967.

[36] G. Kousik, S Pitchumani, and N Renganathan, 2001, "Electrochemical Characterization of Polythiophene-Coated Steel," Progress in Organic Coatings, 43(4) pp. 286-291.

[37] N. Ahmad, and A MacDiarmid., 1996, "Inhibition of Corrosion of Steels with the Exploitation of Conducting Polymers," Synthetic Metals, 78(2) pp. 103-110.

[38] G Spinks , A Dominis, G Wallace, D Tallman, 2002, "Electroactive Conducting Polymers for Corrosion Control - Part 2. Ferrous Metals," Journal Of Solid State Electrochemistry, 6(2) pp. 85-100.

[39] J Lacroix , J Camalet , S Aeiyach, K Chane-Ching, J Petitjean, E Chauveau, P Lacaze, 2000, "Aniline Electropolymerization on Mild Steel and Zinc in a Two-Step Process," Journal Of Electroanalytical Chemistry, 481(1) pp. 76-81.

[40] W. Focke, G. Wnek, and Y. Wei, 1987, "Influence of Oxidation State, pH, and Counterion on the Conductivity of Polyaniline," Journal of Physical Chemistry, 91(22) pp. 5813- 5818.

[41] V. Kulkarni, L Campbell., and W. Mathew., 1989/6, "Thermal Stability of Polyaniline," Synthetic Metals, 30(3) pp. 321-325.

[42] B. Wessling, and J. Posdorfer, 1999, "Corrosion Prevention with an Organic Metal (Polyaniline): Corrosion Test Results," Electrochimica Acta, 44(12) pp. 2139-2147.

[43] P. Kinlen, D Silverman, and C Jeffreys, 1997, "Corrosion Protection using Polyaniline Coating Formulations," Synthetic Metals, 85(1-3) pp. 1327-1332.

[44] M. Mikhael, A. Padias, and H. Hall Jr., 1997, "N-Alkylation and N-Acylation of Polyaniline and its Effect on Solubility and Electrical Conductivity," Journal of Polymer Science, Part A: Polymer Chemistry, 35(9) pp. 1673-1679.

[45] A. Andreatta, A. Heeger, and P.Smith, 1991, "Polyaniline. Solubility in Sulfuric Acid, Solution Properties and Processing" Synthetic Metals, 41(3) pp. 1063-1068.

[46] Y. Cao, J. Qiu, , and P. Smith, 1995, "Effect of Solvents and Co-Solvents on the Processibility of Polyaniline: Solubility and Conductivity Studies," Synthetic Metals, 69(1-3) pp. 187-190.

[47] M. Lu, Y. Wu, H. Jiang, 1998, "High Conducting Polyaniline," Gongneng Cailiao/Journal of Functional Materials, 29(5) pp. 483-485.

[48] J. Chiang, and A. MacDiarmid, 1986/1, "'Polyaniline': Protonic Acid Doping of the Emeraldine Form to the Metallic Regime," Synthetic Metals, 13(1-3) pp. 193-205.

[49] L Zhang, M Wan , Y Wei, 2006, "Nanoscaled Polyaniline Fibers Prepared by Ferric Chloride as an Oxidant," Macromolecular Rapid Communications, 27(5) pp. 366-371.

[50] P. Swapna Rao, D. Sathyanarayana, S. Palaniappan, 2002, "Polymerization of Aniline in an Organic Peroxide System by the Inverted Emulsion Process ," Macromolecules, 35(13) pp. 4988--4996.

[51] X. Zeng, and T Ko, 1998, "Structures and Properties of Chemically Reduced Polyanilines," Polymer, 39(5) pp. 1187-1195.

[52] G. Morales, M. Llusa, M. Miras, 1997, "Effects of High Hydrochloric Acid Concentration on Aniline Chemical Polymerization," Polymer, 38(20) pp. 5247-5250.

[53] J Yano, 1991, "The Transformation of Electroinactive Polymers Derived from Aniline Derivatives into Electroactive and Functional Polymers .2. Making Poly(n,n-Di-n-Butylaniline) Films have Anion Exchangeability and Selective Potential Response to Dissolved Iodide-Ions," Journal Of The Electrochemical Society, 138(2) pp. 455--459.

[54] Y. Wei,' R. Hariharan, and A. Sandeep, 1990, "Chemical and Electrochemical Copolymerization of Aniline with Alkyl Ring-Substituted Anilines," Macromolecules, 23(3) pp. 758- 764.

[55] A. Bhattacharya, 1999, "Conducting Polymers in Solution - Progress Toward Processibility," Journal Of Macromolecular Science-Reviews In Macromolecular Chemistry And Physics, C39(1) Pp. 17-56.

[56] W. Yin, and E. Ruckenstein, 2000, "Soluble Polyaniline Co-Doped with Dodecyl Benzene Sulfonic Acid and Hydrochloric Acid," Synthetic Metals, 108(1) pp. 39-46.

[57] Y Cao, P. Smith and A. Heeger, 1992, "Counter-Ion Induced Processibility of Conducting Polyaniline and of Conducting Polyblends of Polyaniline in Bulk Polymers," Synthetic Metals, 48(1) pp. 91-97.

[58] Y Xia, A Macdiarmid, A Epstein, 1994, "Camphorsulfonic Acid Fully Doped Polyaniline Emeraldine Salt - in-Situ Observation of Electronic and Conformational-Changes Induced by Organic Vapors by an Ultraviolet-Visible Near-Infrared Spectroscopic Method," Macromolecules, 27(24) pp. 7212--7214.

[59] L Xin-Gui , M.Huang , L Feng , W. Cai , Z. Jin , Y. Yu-Liang, 2000, "Oxidative Copolymerization of 2-Pyridylamine and Aniline ," Journal Of Polymer Science Part A-Polymer Chemistry, 38(24) pp. 4407-4418.

[60] C. Yang, Y. Cao, P Smith, 1993, "Morphology of Conductive, Solution-Processed Blends of Polyaniline and Poly(Methyl Methacrylate)," Synthetic Metals, 53(3) pp. 293-301.

[61] B. Sarı, , and M. Talu, , 1998, "Electrochemical Copolymerization of Pyrrole and Aniline," Synthetic Metals, 94(2) pp. 221-227.

[62] Y Sze, R. Brown and J. Sinko, 2005, "Designing Conductive Polymers for Improved Metal Protection , 11 48 (2005)," European Coating Journal, 11pp. 48-54.

[63] J. Stejskal, J. Hlavatá, D. Holler, P.Trchová, M. Prokes, J. Sapurina, Irina, 2004, "Polyaniline Prepared in the Presence of various Acids: A Conductivity Study," Polymer International, 53(3) pp. 294.

[64] J. Prokes, and J Stejskal, 2004/10, "Polyaniline Prepared in the Presence of various Acids: 2. Thermal Stability of Conductivity," Polymer Degradation and Stability, 86(1) pp. 187-195.

[65] R. Racicot, H. Clark, .C. Yang, M. Alias and R. Brown, 1995, "Thin Film Conductive Polymers on Aluminum Surfaces: Interfacial Charge Transfer and Anti-corrosion Aspects," SPIE, Anonymous pp. 2528.

[66] R Racicot, R. Brown, and S Yang, 1997, "Corrosion Protection of Aluminium Alloys by Double-Strand Polyaniline," Synthetic Metals, 85(1-3) pp. 1263-1264.

[67] A. Epstein, J. Smallfield, H. Guan, 1999/6, "Corrosion Protection of Aluminium and Aluminium Alloys by Polyanilines: A Potentiodynamic and Photoelectron Spectroscopy Study," Synthetic Metals, 102(1-3) pp. 1374-1376.

[68] A. Mirmohseni, and A.Oladegaragoze, 2000, "Anti-Corrosive Properties of Polyaniline Coating on Iron," Synthetic Metals, 114(2) pp. 105-108.

[69] B Wessling 1994, "Passivation Of Metals By Coating With Polyaniline - Corrosion Potential Shift And Morphological-Changes," Advanced Materials, 6(3) Pp. 226-228.

[70] S Cogan, M Gilbert, G. Holleck, J Ehrlich and M Jillson, 2000, "Galvanic Coupling of Doped Poly-Aniline and Aluminium Alloy 2024-T3 " Journal Of The Electrochemical Society, 147(6) Pp. 2143--2147.

[71] R. Racicot, C. Sze and R. Brown, 2000, "Electrochemical Impedance Spectroscopy Studies of a Double Strand Polyaniline Coating on Aluminium Alloys in Acidic Environments," Proceedings of Corrosion / 2000, Research Topical Symposium, Surface Conversions of Aluminium and Ferrous Alloys for Corrosion Resistance, Anonymous pp. 113--128.

[72] D. Tallman, Y. Pae, G. Bierwagen, 2000, "Conducting Polymers and Corrosion: Part 2 - Polyaniline on Aluminum Alloys " Corrosion, 56(4) pp. 401-410.

[73] J. Fujita, M. Hyland, 2003, "Polyaniline Coatings for Aluminium: Preliminary Study of Bond and Anti-Corrosion," International Journal of Modern Physics, 17(8-9) pp. 1164-1169.

[74] K. Conroy, and C. Breslin, 2003, "The Electrochemical Deposition of Polyaniline at Pure Aluminium: Electrochemical Activity and Corrosion Protection Properties," Electrochimica Acta, 48(6) pp. 721-732.

[75] G. Shah - A. Gouri , S. Jude, 2002, "Polyaniline Coated on Aluminium (Al-2024-T3): Characterization and Electrochemical Studies," Journal of Applied Polymer Science, 85pp. 1669-1675.

[76] D. Huerta-Vilca, S. Moraes, and A. Motheo, 2003, "Electrosynthesized Polyaniline for the Corrosion Protection of Aluminium Alloy 2024-T3". Vol.14 no.1 São Paulo Jan./Feb. 2003," Journal of Barazilian Chemical Society, 14(1) pp. 52--58.

[77] S. Yang, R. Brown, R. Racicot, Y. Lin, F. McClarnon, 2003, "Electroactive polymer for corrosion inhibition of aluminum alloys," ACS Symposium, Electroactive Polymers for Corrosion Control, Anonymous pp. 196-206.

[78] J. Iroh, Y. Zhu, K. Shah, 2003/9, "Electrochemical Synthesis: A Novel Technique for Processing Multi-Functional Coatings," Progress in Organic Coatings, 47(3-4) pp. 365-375.

[79] D. Huerta-Vilca, S. Moraes, and d. Motheo, A., 2004/1/6, "Anodic Treatment of Aluminium in Nitric Acid Containing Aniline, Previous to Deposition of Polyaniline and its Role on Corrosion," Synthetic Metals, 140(1) pp. 23-27.

[80] D. Huerta-Vilca, S. Moraes, M. Pantoja, A. MotheoJ, 2004, "PANI as Prospective Replacement of Chromium Conversion Coating in the Protection of Steels and Aluminium Alloys," Molecular Crystals And Liquid Crystals, 415pp. 229--238.

[81] N. Ogurtsov, A. Pud, P. Kamarchik, 2004/5/7, "Corrosion Inhibition of Aluminium Alloy in Chloride Mediums by Undoped and Doped Forms of Polyaniline," Synthetic Metals, 143(1) pp. 43-47.

[82] M Kendig, 2004, "Environmentally Triggered Release of Oxygen-Reduction Inhibitors from Inherently Conducting Polymers," CORROSION, 60(11) pp. 1024-1030.

[83] M. Kendig, M. Hon, and L. Warren, 2003, "'Smart' Corrosion Inhibiting Coatings," Progress in Organic Coatings, 47(3-4) pp. 183-189.

[84] J Seegmiller, J da Silva, D Buttry, S. Torresi IC, R Torresi, 2005, "Mechanism of Action of Corrosion Protection Coating for AA2024-T3 Based on Poly(Aniline)-Poly(Methylmethacrylate) Blend " Journal Of The Electrochemical Society, 152(2) pp. B45-B53.

[85] L. Cecchetto, , D. Delabouglise, and J. Petit, "On the Mechanism of the Anodic Protection of Aluminium Alloy AA5182 by Emeraldine Base Coatings: Evidences of a Galvanic Coupling," Electrochimica Acta, 52(11) pp. 3485-3492.

[86] L. Cecchetto, R. Ambat, A. Davenport, 2007/2, "Emeraldine Base as Corrosion Protective Layer on Aluminium Alloy AA5182, Effect of the Surface Microstructure," Corrosion Science, 49(2) pp. 818-829.

[87] T. Wang, and Y. Tan, 2006, "Understanding Electrodeposition of Polyaniline Coatings for Corrosion Prevention Applications using the Wire Beam Electrode Method," Corrosion Science, 48(8) pp. 2274-2290.

[88] T. Wang, and Y. Tan, 2006, "Electrodeposition of Polyaniline on Aluminium Alloys for Corrosion prevention—A Study using the Wire Beam Electrode (WBE)," Materials Science and Engineering: B, 132(1-2) pp. 48-53.

[89] K. Wu, C Chao, C. Liu,., 2007, "Characterization and Corrosion Resistance of Organically Modified silicate–NiZn ferrite/polyaniline Hybrid Coatings on Aluminum Alloys," Corrosion Science, 49(7) pp. 3001-3014.

[90] K. Wu, P. Chen, C. Yang, 2008, "Infrared Stealth and Anticorrosion Performances of Organically Modified Silicate-NiZn ferrite/polyaniline Hybrid Coatings," Journal of Polymer Science, Part A, Polymer Chemistry, 46(3) pp. 926-935.

[91] S. Sathiyanarayanan, S. Azim, S. Venkatachari, 2008, "Performance Studies of Phosphate-Doped Polyaniline Containing Paint Coating for Corrosion Protection of Aluminium Alloy," Journal of Applied Polymer Science, 107(4) pp. 2224-2230.

[92] O. Zubillaga, F. Cano, I. Azkarate, 2008, "Corrosion Performance of Anodic Films Containing Polyaniline and TiO2 Nanoparticles on AA3105 Aluminium Alloy," Surface and Coatings Technology, 202(24) pp. 5936-5942.

[93] D. Rosa-Fox, N., Esquivias, L., and M. Piñero, 2003, American Scientific Publishers, pp. 241--270.

[94] K. Mauritz, 1999, "Sol-Gel Chemistry. Http://www.Psrc.Usm.edu/ mauritz/solgel.Htm." 1999(29/7) .

[95] C. Brinker and G. Scherer, 1990, "Sol-Gel science," Academic Press Inc.,

[96] G. Philipp, and H. Schmidt, 1984, "New Materials for Contact Lenses Prepared from Si- and Ti-Alkoxides by the Sol-Gel Process," Journal of Non-Crystalline Solids, 63(1-2) pp. 283-292.

[97] D. Wang, and G. Bierwagen, "Sol–gel Coatings on Metals for Corrosion Protection," Progress in Organic Coatings, In Press, Corrected Proof.

[98] L. Larry Hench and J. West, 1990, "the Sol-Gel Process," Chemical Review, 90(1) pp. 33-- 72.

[99] C. Bechinger, H. Muffler, C. Schäfle, 2000/5/1, "Submicron Metal Oxide Structures by a Sol-Gel Process on Patterned Substrates," Thin Solid Films, 366(1-2) pp. 135-138.

[100] T. Troczynski, 2004, "Www.Ceramics.Mmat.Ubc.Ca, the University of British Columbia, Introduction to Sol Gel," .

[101] C. Brinker and G. Sherer, 1990, "Sol-Gel Science," Academic Press, San Diego, .

[102] Y. Xiu, D. Hess, and C. Wong, 2008, "UV and Thermally Stable Superhydrophobic Coatings from sol–gel Processing," Journal of Colloid and Interface Science, 326(2) pp. 465-470.

[103] H Wang, and R. Akid, 2008, "Encapsulated Cerium Nitrate Inhibitors to Provide High-Performance Anti-Corrosion sol–gel Coatings on Mild Steel," Corrosion Science, 50(4) pp. 1142-1148.

[104] C. Li, K. Jordens, and G. Wilkes, 2000, "Abrasion-Resistant Coatings for Plastic and Soft Metallic Substrates by sol–gel Reactions of a Triethoxysilylated Diethylenetriamine and Tetramethoxysilane," Wear, 242(1-2) pp. 152-159.

[105] M. Toki, T. Takeuchi, S. Miyasita, S. Kanbe, 1992, "Fabrication of High-Purity Silica Glass through the Wspa Sol-Gel Process," Journal of Materials Science, 27(11) pp. 2857-2862.

[106] S. Lee, and B. Jun, 2005, "Preparation of Ultrafine PZT Powders by Ultrasonic Spray Combustion Synthesis (USCS)," Ceramics International, 31(1) pp. 53-56.

[107] A. Balamurugan, G. Sockalingum, J. Michel, 2006, "Synthesis and Characterisation of Sol Gel Derived Bioactive Glass for Biomedical Applications," Materials Letters, 60(29-30) pp. 3752-3757.

[108] M. Sathupunya, E. Gulari, and S. Wongkasemjit, 2003, "Na-A (LTA) Zeolite Synthesis Directly from Alumatrane and Silatrane by Sol-Gel Microwave Techniques," Journal of the European Ceramic Society, 23(8) pp. 1293-1303.

[109] P. Worathanakul, and P. Kongkachuichay, Summer 2008, "New SUZ-4 Zeolite Membrane from Sol-Gel Technique," International Journal of Chemical and Biomolecular Engineering, 1(3) pp. 131-135.

[110] T. Yazawa, H. Tanaka, H. Nakamichi, T. Yokoyama, 1991, "Preparation of Water and Alkali Durable Porous-Glass Membrane Coated on Porous

Alumina Tubing by Sol-Gel Method," Journal of Membrane Science, 60(2-3) pp. 307-317.

[111] R. Hodgson, Y. Chen, Z. Zhang, D. Tleugabulova, H. Long, X. Zhao, M. Organ, M. Brook, and D John., 2004, "Protein-Doped Monolithic Silica Columns for Capillary Liquid Chromatography Prepared by the Sol−Gel Method: Applications to Frontal Affinity Chromatography," Analytica Chimestry, 76(10) pp. 2780-2790.

[112] J. Yu, X. Zhao, and Q. Zhao, 2000, "Effect of Surface Structure on Photocatalytic Activity of TiO2 Thin Films Prepared by Sol-Gel Method," Thin Solid Films, 379(1-2) pp. 7-14.

[113] M. Zheludkevich, I. Salvado and M. Ferreira, 2005, "Sol–gel Coatings for Corrosion Protection of Metals," Material Chemistry, 15pp. 5099-- 5111.

[114] O. Lev, Z. Wu, S. Bharathi, V. Glezer, A. Modestov, J. Gun, L. Rabinovich, and S. Sampath, 1997, "Sol-Gel Materials in Electrochemistry," Chemical Material, 9(11) pp. 2354-- 2375.

[115] R. Twite, and G. Bierwagen, 1998, "Review of Alternatives to Chromate for Corrosion Protection of Aluminium Aerospace Alloys," Progress in Organic Coatings, 33(2) pp. 91-100.

[116] S. Hamdy, and P. Butt, 2006, "Environmentally Compliant Silica Conversion Coatings Prepared by sol–gel Method for Aluminium Alloys," Surface and Coatings Technology, 201(1-2) pp. 401-407.

[117] X. Yang, D. Tallman., V. Gelling, 2001/5/22, "Use of a sol–gel Conversion Coating for Aluminum Corrosion Protection," Surface and Coatings Technology, 140(1) pp. 44-50.

[118] N. Voevodin, C. Jeffcoate, L., Simon, 2001 "Characterization of Pitting Corrosion in Bare and sol–gel Coated Aluminum 2024-T3 Alloy", Surface and Coatings Technology, 140(1) pp. 29-34.

[119] A. S̆urca Vuk, M. Fir, R. Jes̆e, 2008, "Structural Studies of Sol-Gel urea/polydimethylsiloxane Barrier Coatings and Improvement of their Corrosion Inhibition by Addition of various Alkoxysilanes," Progress in Organic Coatings, 63(1) pp. 123-132.

[120] V. Moutarlier, B. Neveu, and M. Gigandet, 2008, "Evolution of Corrosion Protection for Sol-Gel Coatings Doped with Inorganic Inhibitors," Surface and Coatings Technology, 202(10) pp. 2052-2058.

[121] A. Pepe, M. Aparicio, S. Ceré, 2004, "Preparation and Characterization of Cerium Doped Silica sol–gel Coatings on Glass and Aluminium Substrates," Journal of Non-Crystalline Solids, 348pp. 162-171.

[122] N. Rosero-Navarro, A. Pellice, A. Durán, 2008, "Effects of Ce-Containing Sol-Gel Coatings Reinforced with SiO2 Nanoparticles on the Protection of AA2024," Corrosion Science, 50(5) pp. 1283-1291.

[123] H. Wang, and R. Akid, , 2007, "A Room Temperature Cured sol–gel Anticorrosion Pre-Treatment for Al 2024-T3 Alloys," Corrosion Science, 49(12) pp. 4491-4503.

CHAPTER 3

EXPERIMENTAL WORK

3.1 TEST TECHNIQUES

3.1.1 Corrosion Performance Technique

The rapid and accurate measurement of electrochemical phenomena is of considerable importance for a range of studies, not only for research, but also in practical applications. It is possible to measure effects such as corrosion rate by direct analytical methods, for example weight loss measurements or solution analysis by spectroscopy; however, these methods are often slow, time consuming and inefficient. Additionally, they are restricted to systems in which the products formed by the process do not form adherent layers.

Given that the processes under consideration are electrochemical, it is possible to evaluate them using electrical methods based on Faraday's law, which relates the change in mass per unit area to the current flow. The advantages of this approach are a relatively short measuring time, high accuracy and the possibility of monitoring the process continuously.

Naturally there are also disadvantages, namely the system under investigation has to be perturbed from its normal state by an external signal, which inevitably changes the properties of the system. The DC technique has been widely used for corrosion rate measurement, but the method generally requires a relatively large perturbation (or polarisation) signal and can, in fact, fail when the corrosion measurement required the use of a low conductivity medium. AC methods are finding increasing applications in electrochemical research, because only small perturbation signals (which do not disturb the electrode properties) can be used and low conductivity media can also be investigated [1].

3.1.1.1 Electrochemical Impedance Spectroscopy (EIS)

Electrochemical impedance spectroscopy (EIS) uses a range of low magnitude polarizing voltages, much like linear polarisation. However, EIS voltage cycles from peak anodic to cathodic magnitudes (and vice versa) using a spectrum of alternating current (AC) voltage frequencies [2].

If a potential is applied across an electrochemical cell, a current is caused to flow through the cell, with a value determined by the processes taking place at the electrode. If the applied potential is sinusoid ($\Delta E \sin(\omega t)$) then the subsequent current will also be sinusoidal, with a value ($\Delta I \sin(\omega t + \Phi)$) as shown in Figure 3-1 where Φ is the phase angle.
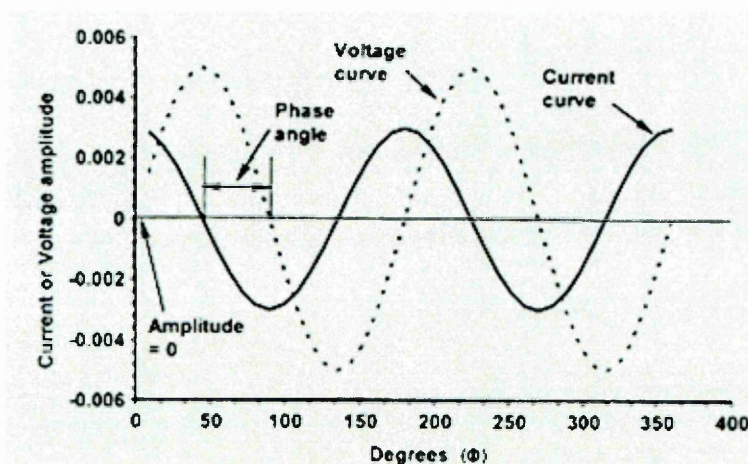
Figure 3-1 AC voltage-current phase angle [2].

The relationship between the applied potential and the current flow is known as the impedance. The impedance can be express in two ways;

(i) Cartesian co-ordinates (Nyquist plot)

Impedance	$Z = a - jb$
Resistive component of impedance	$a = r \cos \theta$
Capacitive component of impedance	$b = r \sin \theta$

(ii) Polar co-ordinates (Bodes plot)

Modulus of impedance	$r = |Z| = \sqrt{a^2 + b^2}$
Phase angle	$\theta = \tan^{-1}(-b/a)$

63

Resistance and capacitance values are obtained at each frequency, and these quantities can provide information on corrosion behaviour and rates, diffusion, and coating properties. Capacitive and resistance properties of an electrified interface produce time constants. Time constants produce a) semicircles in Nyquist plots b), inflections in Bode phase diagrams, and c) negative values for Bode magnitude plot slopes. There are a number of factors and processes that can produce multiple time constants on the same test electrode [1]. Here some simple EIS examples will be given to illustrate how the technique may be used.

Bare metal:

Every metal immersed in a solution has an electrical Double Layer (DL) interface with the solution. The corresponding electrical circuit of a DL consists of: solution resistance (R_s), charge transfer resistance (R_{ct}) and DL capacitive reactance (C_{dl}) as shown in Figure 3-2.
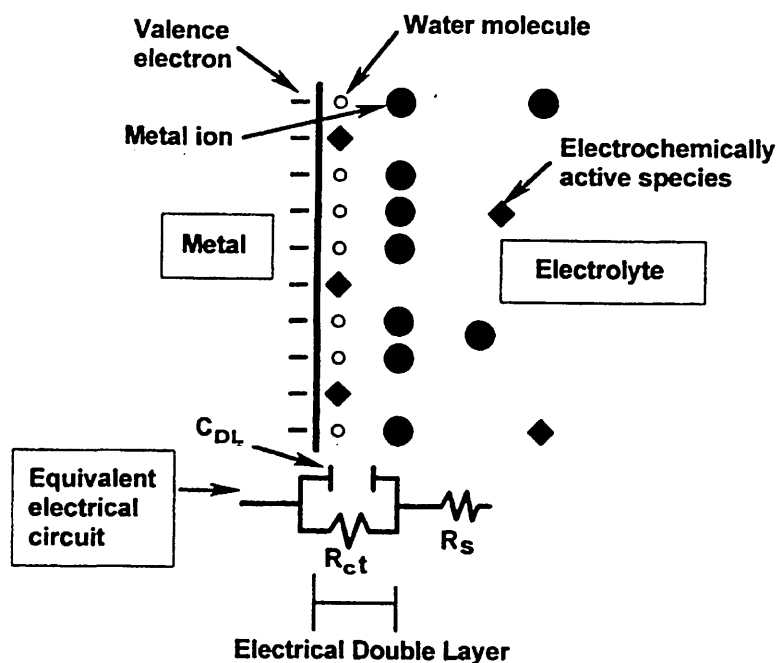
Figure 3-2 Electrical double layer and its equivalent circuit [2]

This circuit would be represented by one semi-circle on the Nyquist plot and its radius represents the charge transfer resistance, Figure 3-3. Bode plot, where a

single time constant and two resistances represent the bare metal as shown in Figure 3-4.
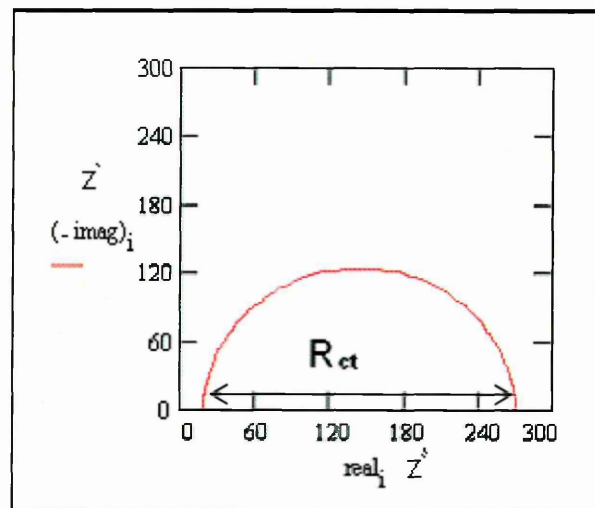
Figure 3-3 Nyquist plot of bare metal [3]
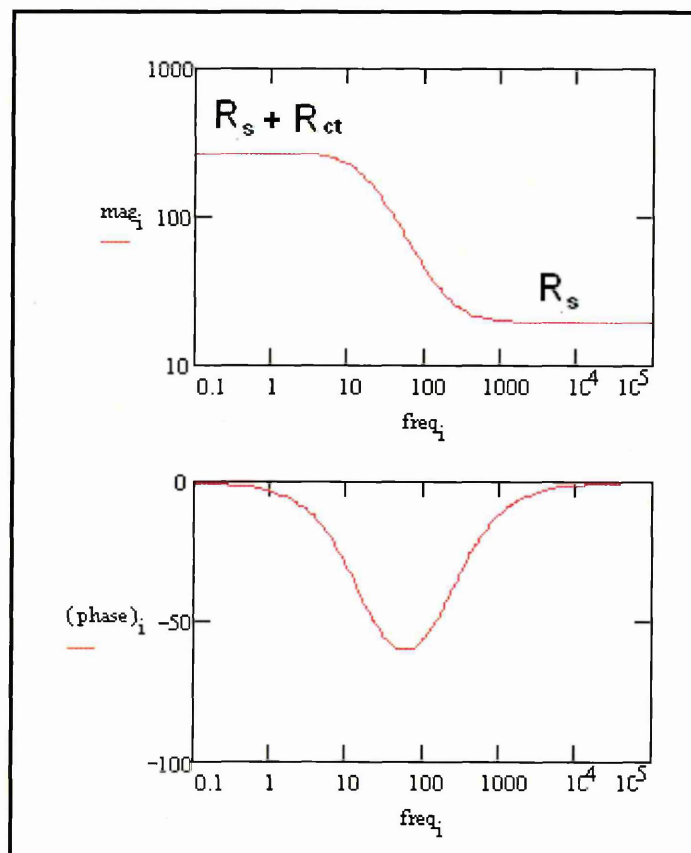
Figure 3-4 Bode plot of bare metal [3]

Coated metal:

A coated metal when represented through a simple equivalent circuit contains two capacitances and three resistances as shown in Figure 3-5.
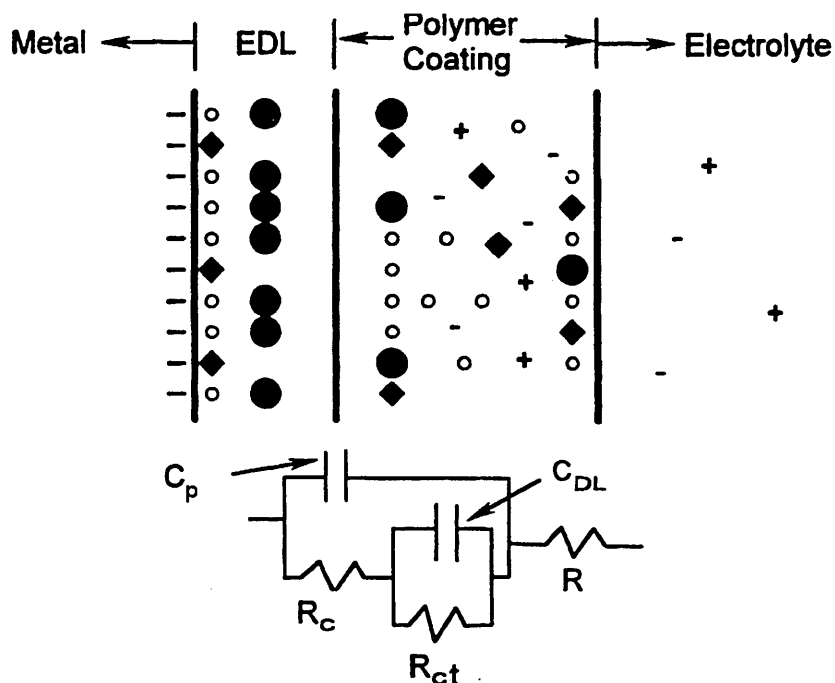
Figure 3-5 Electrified interface structure for a corroding coated metal [2].

This circuit will be represented by two semi-circles on the Nyquist plot; the radius of the first semi-circle represents the coating resistance, while the second semi-circle is related to the charge transfer resistance as shown in Figure 3-6. In the Bode plot, two time constants and three resistances represent a coated metal in solution. The resistance at high frequency, 10^5 Hz, represents the solution resistance where the resistance at the frequency range 10^4-10^3 Hz, represents the sum of the coating and solution resistances. Finally, the low frequency resistance, 10^{-1}-10^{-2} Hz, represents the sum of the solution, coating and charge transfer resistances as shown in and Figure 3-7
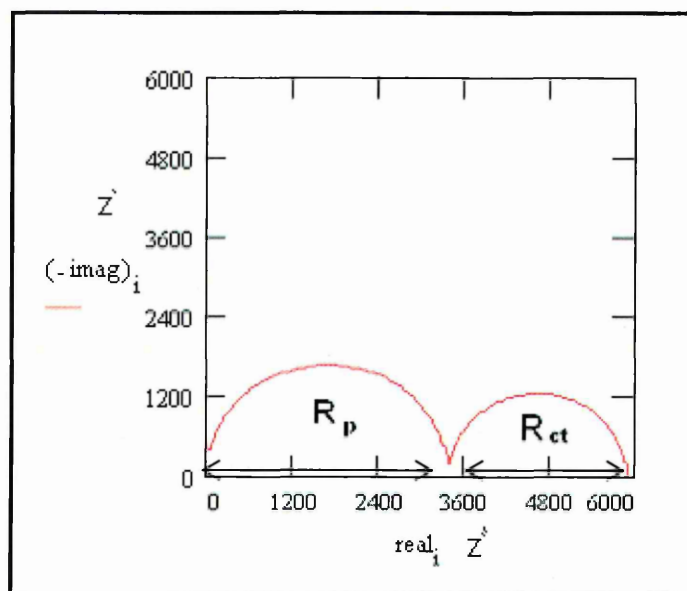
Figure 3-6 Nyquist plot of coated metal [3]
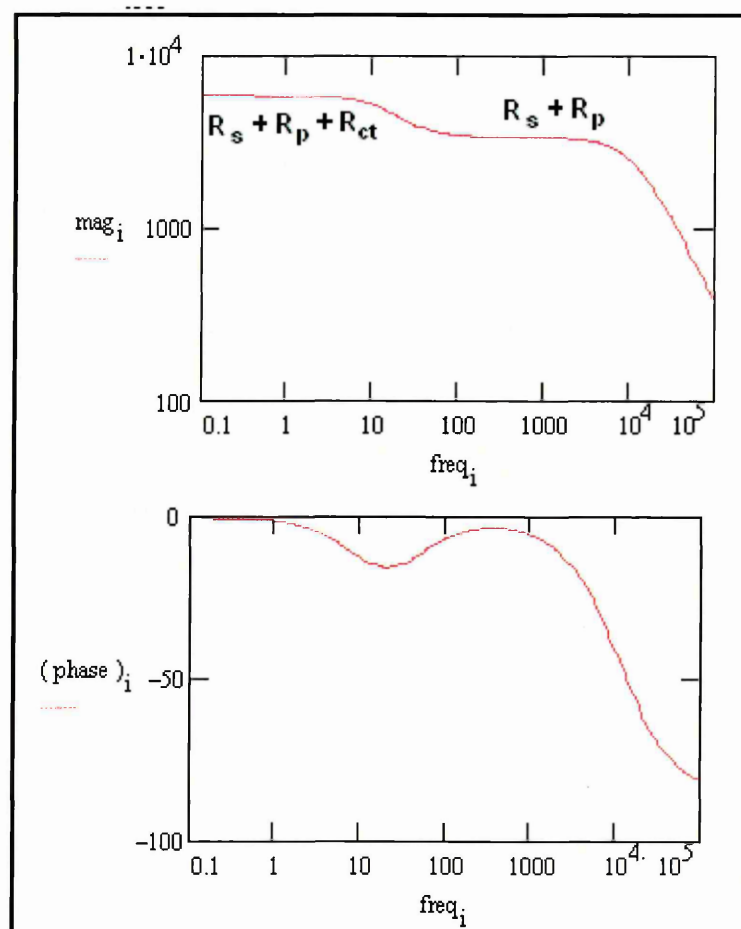
Figure 3-7 Bode plot of coated metal [3]

EIS data is generally analysed in terms of an equivalent circuit model as showed in the above examples. The type of electrical components in the model circuit and their interconnection control the shape of the impedance spectrum. These factors affect the degree to which the impedance spectrum of the model matches the experimentally measured spectrum. The choice of the model is applied to a given cell based upon knowledge of the cell's physical characteristics. By monitoring the change of each component in the equivalent circuit during the test, a mechanism of metal, coating and medium interaction can be investigated.

In this study, corrosion tests were carried out in a three electrode type cell using the sample (working electrode), a saturated calomel reference electrode and a platinum counter electrode. Electrochemical impedance measurements were obtained at measured E_{ocp} values applying ±10 mV perturbation, in the frequency range from $3x10^4$ Hz to 10 mHz. Electrochemical corrosion measurements were performed in 3.5 wt% NaCl (pH=6.8) solution at room temperature, in open air with an ACM instrument in 3.5 wt% NaCl solution which was renewed every ten days. Impedance curve fitting was carried out using ZSimpWin 3.10 software.

3.1.1.2 Salt Spray Test (SST)

The Salt Spray test, (or "Salt Fog") is the most popular and commercial test for evaluating protective coatings. Salt spray testing has been widely used in the industry for the evaluation of corrosion resistance of coatings for over 80 years (first edition of the ASTM B117 standard in 1939).

It is an accelerated corrosion test to predict the protection capability of a coating. Salt spray testing subjects a test sample to conditions that are considered more corrosive than field exposure. Evaluation is primarily based upon the appearance of corrosion products during or after a given test time.

One of the principal advantages of salt spray testing is its speed (8-3000hrs) compared to with field exposure where it may take years to obtain useful data.

The drawbacks of SST are: (1) salt spray testing time is shorter than the expected life of a coating. (2) SST conditions are stable; however, corrosion is a complicated process that can be influenced by many external factors.

In this study, neutral salt spray testing (according to ASTM B 117): was carried out for 500 hours. A 5% sodium chloride solution with a pH range of 6.5 to 7.2 was used. The temperature of the salt spray chamber was controlled at 35±1°C, within the exposure zone of the closed chamber. Furthermore, when the SST was finished, a sellotape test is carried out to check any undercut and delamination of the coating following the SST.

3.1.1.3 Scratch Test

Sample was immersed in the corrosive solution (3.5% NaCl) for 5 days before scratching. The scratch is performed using a razor blade and the scratch thickness is about 150 μm. The scratch penetrates down to the substrate. After scratching, the sample is reimmersed in a fresh solution and EIS measurements are carried out periodically.

3.1.1.4 Scanning Vibrating Electrode Technique (SVET)

SVET is a "non destructive" [4], in-situ technique used to study the localised micro-galvanic corrosion activity with high resolution by measuring the potential gradients emanating from a current source on a surface within an electrolyte. Measurement achieved by vibrating a fine tipped platinum electrode (at fixed amplitude) a few hundred microns above the sample surface in a perpendicular plane. The potential of the microelectrode is recorded at the highest and lowest probe position resulting in the generation of a sinusoidal AC signal. This signal is then measured using a lock-in amplifier. The resulting signal is converted to current density by a simple calibration procedure using a known point source of current density creating a spherical potential field. This field exhibits an equivalent potential drop along radii at equivalent distances from the current source. The probe 3D position and frequency are then adjusted to conduct the maximum signal from the point source. The measuring potential represents the current of the point source according to the following equation [5]

$$CF = \frac{i}{V_{out}}$$

Where

         CF   calibration factor

i current density

and V_{out} SVET output signal

In this study an EG&G instrument model SCV100 instrument, was used to investigate the "self healing" properties of the PANI/sol-gel coating.

3.1.2 Characterising Techniques

3.1.2.1 Scanning Electron Microscope (SEM)

The first, true scanning electron microscope (SEM) was developed and described in 1942 by Zworykin [6] and the first commercial SEM, the Cambridge Scientific Instruments Mark I, was available in 1965.

Scanning electron microscopy is the best known and most widely-used of the surface analytical techniques. SEM, accompanied by X-ray analysis, is considered a relatively rapid, inexpensive, and basically non-destructive approach to surface analysis. High resolution images of surface topography, with excellent depth of field are produced using a highly-focused, scanning (primary) electron beam [6].

In a typical SEM, an electron gun, usually tungsten filament, produces electrons and accelerates them at high energy towards an anode. Two or three condenser lenses demagnify the electron beam until a diameter of 1-5 nm is achieved. The beam passes through pairs of scanning coils in the objective lens over a rectangular area of the sample surface as shown in Figure 3-8.
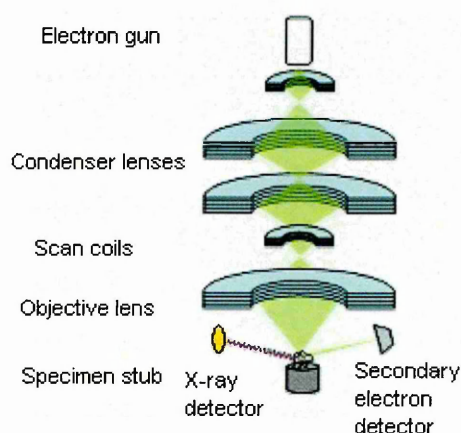
Figure 3-8 SEM components

When the primary electron beam interacts with the sample, the electrons lose energy by repeated scattering and absorption within a teardrop-shaped volume of the specimen known as the interaction volume, which extends from less than 100 nm to around 5 µm into the surface [7] as shown in Figure 3-9

.
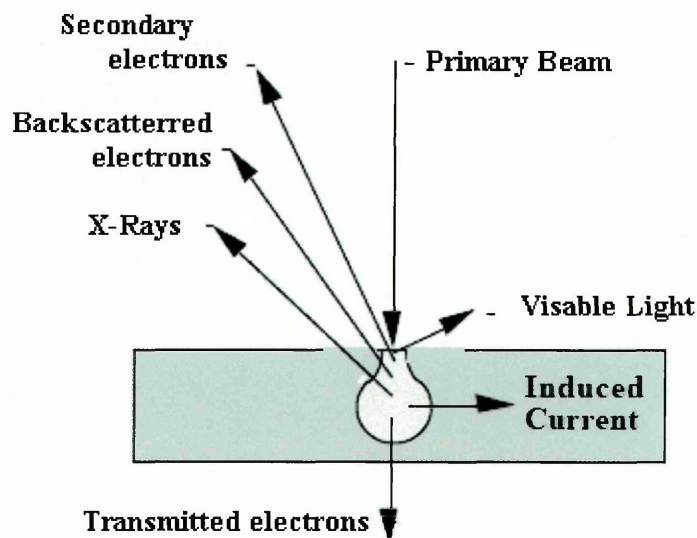
Figure 3-9 Teardrop-shape

The energy exchange between the electron beam and the sample results in the emission of electrons and electromagnetic radiation which can be detected to produce an image [8]. If the beam enters the sample perpendicular to the surface, then the activated region is uniform about the axis of the beam and a certain number of electrons escape from within the sample. As the angle of incidence increases, the escape distance of one side of the beam will decrease, and more secondary electrons will be emitted. Thus steep surfaces and edges tend to be brighter than flat surfaces, which results in images with a well-defined, three-dimensional appearance [7].

Backscattered electrons (BSE) consist of high-energy electrons originating in the electron beam that are reflected or back-scattered out of the specimen interaction volume. The BSE signal is proportional to the atomic number of the sample and can be used to create images reflecting the composition of the object under investigation [7]. BSE may be used to detect contrast between

areas with different chemical composition, especially when the average atomic number of the various regions is different, since the brightness of the BSE image tends to increase with the atomic number.

Energy-dispersive x-ray analysis (EDX) is the most common method used with scanning electron microscope. The process is fully automated with the emitted x-rays being collected simultaneously as a series of pulses. The pulses are amplified and sent to a multichannel analyser (MCA). This allocates each pulse to one of about 1000 channels, each represents particular x-ray energy. In this way the MCA creates a histogram of all the different energies of the x-rays detected.

The peak height indicates the number of pulses (intensity) of that particular energy. Each element produces a series of peaks in a unique pattern and the analyst then decides which peak of the series is going to be measured to quantify the amount of that element present. The most commonly used EDX detectors cannot measure elements lighter than oxygen. This technique gives compositional information on different areas of the same image and is very useful in the study of materials [8].

In this study, a fully computerised SEM, Philips XL 40 microscope, equipped with energy dispersive X-ray analysis, was used to study the microstructure and the chemical composition of the samples. The acceleration potential was varied from 12- 20 KV according to the nature of the sample. Non-conductive samples were coated with graphite to improve their conductivity.

3.1.2.2 X-Ray Photoelectron Spectroscopy (XPS)

XPS is a surface analysis technique that probes the first ten to twenty atomic layers. XPS is used to determine quantitative atomic and chemical composition. It is a surface technique with a sampling volume that extends from the surface to a depth of approximately 50-70 Angstroms. XPS is an elemental analysis technique that is unique in providing chemical state information of the detected elements.

In this technique [9], a photon is absorbed by an atom, leading to ionization and emission of an electron from the core levels as shown in Figure 3-10. The energy of the emitted photoelectrons is then analysed by the electron

spectrometer and the data presented as a graph of intensity versus electron energy. Photoelectron spectroscopy uses monochromatic sources of radiation. The process of photoionization can be considered in several ways: one way is to look at the overall process as follows:

Ejected K electron
(1s electron)

Vacuum

Valence band

L$_{2,3}$

L$_1$

Incident X-ray

K
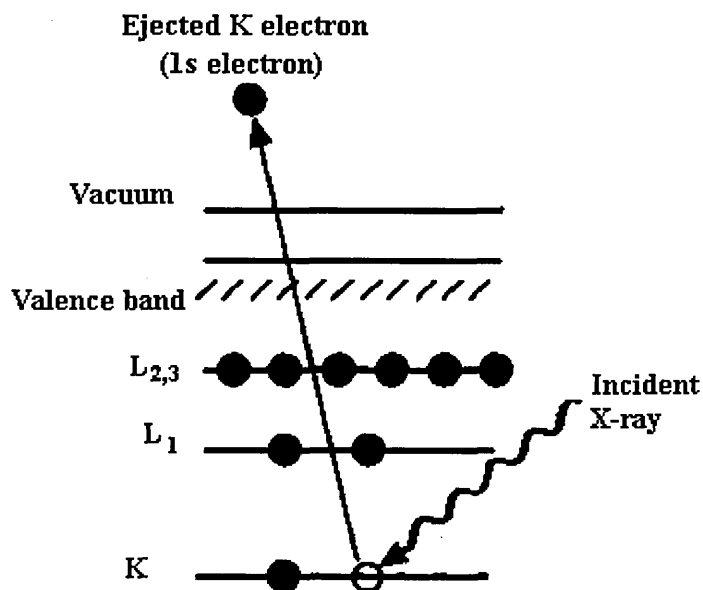
Figure 3-10 Incident photon and correspondence emission of electron

$$A + h\nu = A^+ + e^-$$

Where   h - Planck constant (6.62 x 10^{-34} J s)

ν - Frequency (Hz) of the radiation

A - Atom

A$^+$- Excited atom

Conservation of energy then requires that:

$$E(A) + h\nu = E(A^+) + E(e^-)$$

Since the electron's energy is present as kinetic energy (KE) this can be rearranged to give the following expression for the KE of the photoelectron:

$$KE = h\nu - (E(A^+) - E(A))$$

The final term in brackets represents the binding energy (BE) of the electron,

$$KE = h\nu - BE$$

73

For each element, there will be a characteristic binding energy associated with each atomic orbital, and the presence of peaks at particular energies indicates the presence of that element in the sample. Moreover, the area under the peaks represents the concentration of the element within the sample. Therefore, XPS technique provides qualitative and quantitative analysis of the sample surface.

In this study, XPS analysis is carried out at Cardiff University, University of Nottingham, Corus Company and University of Leeds under the same conditions.

Photoelectron spectroscopic analysis was performed using a mono-chromated Al kα X-ray source (1486.6eV) typically operated at 10mA emission current and 10kV anode potential – 100W.

The take off angle for the photoelectron analyser is 90 degrees and acceptance angle of 30 degrees. Data analysis was carried out using CASAXPS software to determine atomic % values from the peak areas.

A survey scan and high resolution scans were conducted on each sample. The high resolution scans were charge corrected to the main C 1s peak = 284.7 eV [10] and then quantified to compare the amounts of each element present. Components were fitted under the peaks to give chemical information. Survey scans were run for 10-20 minutes and high resolution scans were run for between 1 and 10 minutes depending on the signal. The analysis chamber pressure was better than 5 x 10^{-9} Torr.

During XPS study, all parameters (FWHM ±0.1eV, position of components in each element ±0.1eV), used in high resolution core level were fixed. Shirley background subtraction and Gaussian shaped were applied in XPS spectrum peak fitting procedure. During depth profile analysis, FWHM ±0.15eV and position of components in each element ±0.15eV were applied.

3.1.2.3 Transmission Electron Microscope (TEM)

The TEM technique has been particularly used in metallurgy for developing images of crystals and metals at the molecular level. It also allows metal structures to be studied, interactions and identifying defects.

TEM is capable of displaying magnified images of a thin specimen, typically with a magnification in the range 10^3 to 10^6.

Transmission Electron Microscope consists of electron gun, condenser lens, objective lens, intermediate lens, projective lens and apertures as shown in Figure 3-11.
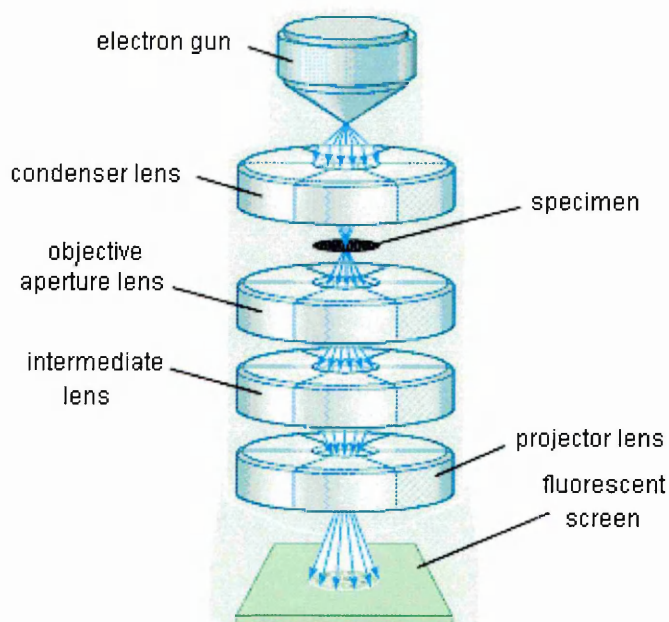
Figure 3-11 TEM instrument diagram

The electron gun, usually tungsten filament, produces a stream of monochromatic electrons. This stream is focused to a small, thin, coherent beam by the use of condenser lens which also control the sot size on the sample. The beam is governed by the condenser aperture by blocking high angle electrons. The beam strikes the specimen and parts of it are transmitted.

This transmitted part is focused by the objective lens into an image. Two apertures can restrict the beam; the objective aperture which enhances contrast by blocking out high-angle diffracted electrons and the selected area, optional, aperture which enables the user to examine the periodic diffraction of electrons by ordered arrangements of atoms in the sample.

The image is then passed down the column through the intermediate and projector lenses to be enlarged all the way

The image strikes the phosphor image screen and light is generated allowing the image to be observed. The darker areas of the image represent areas of the sample that are thicker or denser and vice versa.

The conventional method for preparing TEM sample consists of mechanically cutting sample (usually within dimension of 3 x 3 mm^2), thinning by mechanical polishing to 30-60 μm, gluing onto a copper grid, and finally low-angle ion milling. However, this method is time consuming and may cause a mechanical failure (damage) of sample.

An alternative method to TEM sample preparation consists of using a focused ion beam (FIB) etching technique. A FIB etches samples at high speeds and does not mechanically damage fragile samples. Using an FIB avoids damage of the sample which can occurs during conventional gluing process

In this study, TEM analysis was carried out (at the University of Leeds) on a Philips/FEI CM200 FEGTEM fitted with an Oxford Instruments UTW EDX detector and a Gatan GIF200 imaging filter. The FIB sectioning was carried out on an FEI Nova 200 NanoLab high resolution Field Emission Gun Scanning Electron Microscope (FEGSEM) with precise Focused Ion Beam(FIB) etching and (Pt) deposition capabilities for in-situ TEM sample preparation (Kleindieck nanomanipulator).

Sample preparation involved, Gallium focused ion beam milling of a thin section from the sample as shown in Figure 3-12. This was then removed using a manipulator (a fine tungsten needle), which was attached to the section using deposited platinum, Figure 3-13. Using the manipulator, the section was then removed to a standard copper TEM sample mount. The section was fixed to the mount using deposited platinum, and then the final thinning was performed, to a thickness of 100nm. The sample was then ready for TEM analysis as shown in Figure 3-14.
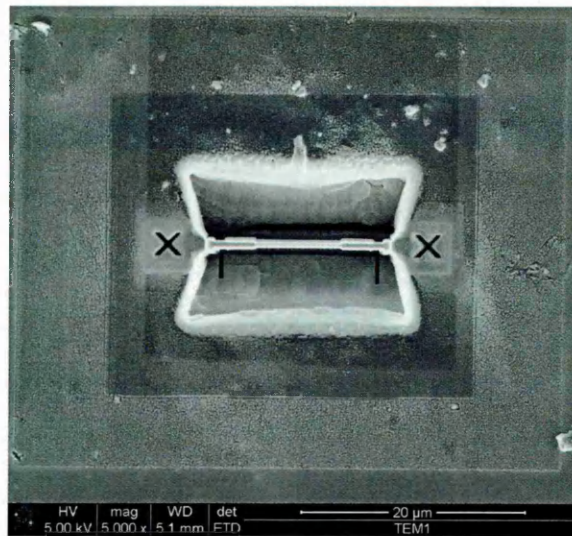
Figure 3-12 Milling out a thin section from sample using FIB
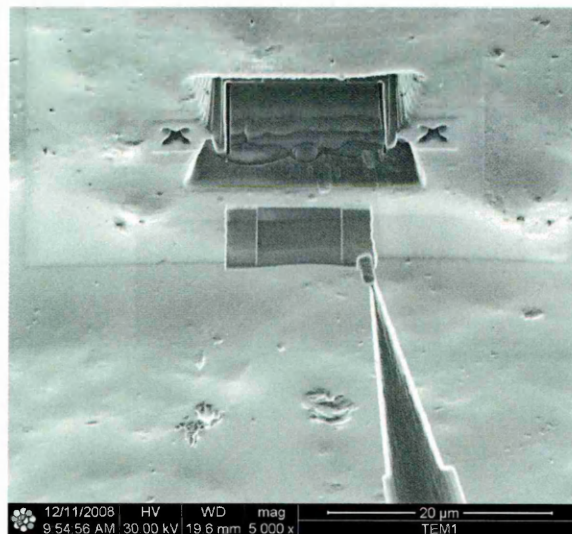
Figure 3-13 Removing the TEM sample from the bulk sample
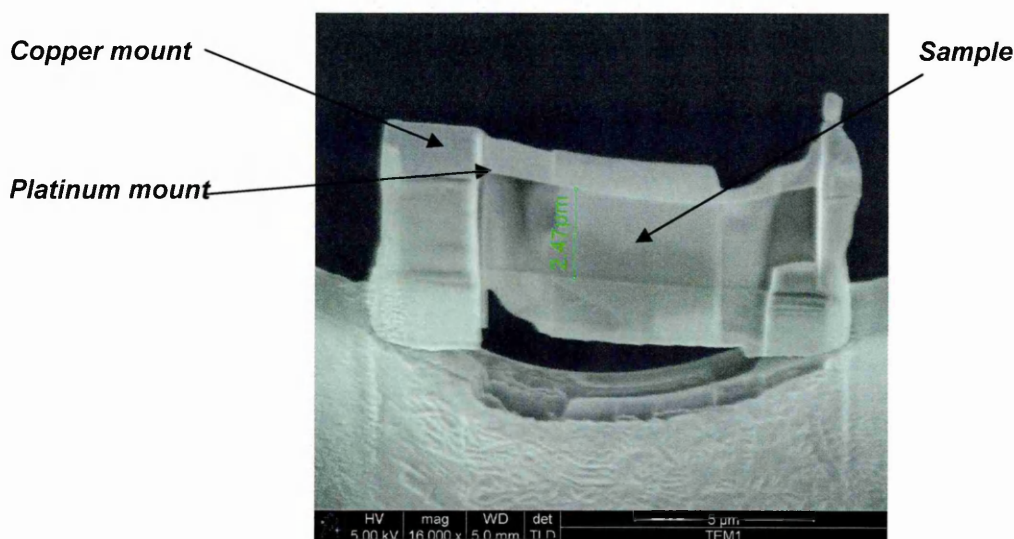
Figure 3-14 TEM sample

3.1.2.4 Fourier Transformation Infrared (FTIR) Spectroscopy

Infrared (IR) spectroscopy is one of the most common spectroscopic techniques used for analysis of both organic and inorganic chemicals. In any molecule, all atoms are vibrating continuously with respect to each other. The major types of molecular vibrations are stretching and bending. When the frequency of IR radiation equals the vibrational frequency of the atom on the molecule, the molecule absorbs the radiation [11]. The absorbed infrared radiation energy is converted into vibrations (stretching and/or bending). The resulting spectrum represents the molecular absorption and transmission, creating a specific spectrum for each molecular by determining the chemical functional groups in the sample. Moreover, the size of the peaks can provide information regarding the amount of material present.

IR spectroscopy can be performed using transmittance (T) or absorbance (*A*). Transmittance is the ratio of radiant power transmitted by the sample to the radiant power incident on the sample. Absorbance (*A*) is the (base 10) logarithm of the reciprocal of the transmittance (*T*).

The IR technique has many advantages; for example, it can analyse a wide range of sample types (gases, liquids, and solids); it can provide a fingerprint of a molecules, it is a non-destructive technique, it does not require external

calibration and it can work as a dynamic technique (collecting a scan every second).

Infrared radiation wavelengths range from 0.78 to 1000 μm being the range between the red end of the visible and the microwave regions respectively, however, Infrared is usually presented in wavenumbers (from 13,000 to 10 cm−1). Wavenumber is defined as the number of waves per unit length.

$$Wavenumber(v) = \frac{1}{\lambda(in\,\mu m)} \times 10^4$$

Where λ is the wavelength

There are three ranges of Infrared; near IR 13,000–4,000 cm^{-1}; mid IR 4,000–200 cm^{-1} and far IR 200–10 cm^{-1}.

Mid IR is the most commonly used range 4000 and 400 cm^{-1}

Fourier transform spectrometers have recently replaced dispersive instruments due to their superior speed. Instead of applying each IR frequency sequentially (in a dispersive IR spectrometer), all frequencies are applied simultaneously in Fourier transform infrared (FTIR) spectroscopy.

3.1.2.5 Contact Angle

Contact angle is the angle formed by the solid surface and the tangent line to the upper surface at the end point of a drop of liquid. Alternately, it is the angle made by the intersection of the liquid/solid interface and the liquid/air interface.

Contact angle is a parameter used for understanding the wetting between a liquid droplet and a substrate which is very important for many everyday applications such as detergency, adhesion, wetting, flotation, suspensions, solid emulsions, erosion, printing, pharmaceutical [12].

Contact angle measuring is used to determine the surface properties of solids and liquids using the sessile or pendant drop method. The sessile drop method is an optical contact angle technique used to estimate wetting properties of a localized region on a solid surface. The angle between the baseline of the drop and the tangent at the drop boundary is measured and the geometry of a drop can be analyzed optically in static or dynamic technique. Contact angle is sensitive to contamination and external factors such as temperature, humidity,

solid surface roughness, and static electricity therefore, these factors should be controlled.

A high contact angle indicates a low chemical affinity which is referred to as a low degree of wetting. A low contact angle indicates a high solid surface energy or chemical affinity, and a high or sometimes complete degree of wetting. For example, a contact angle of zero degrees will occur when the droplet has turned into a flat puddle which indicates complete wetting. Hydrophobic and hydrophilic properties of surfaces can be evaluated using contact angle measurements. When the solid surface is hydrophilic, the droplet will completely spread out on the solid surface and the contact angle will be close to 0°. Typically hydrophilic surfaces will exhibit contact angles between 0° to 30°. However, strongly hydrophobic surfaces will have a contact angle higher than 90°. If the surface is hydrophobic, the contact angle will be close to 90°. In contrast super hydrophobic surfaces have water contact angles as high as 150° and may up to 180°.

In this study, Contact angles were measured from sessile water drops using a goniometer and camera (Data Physics, shown in Figure 3-15) with SCA202 software. All measurements were made using drops with a total volume of 2 μm of deionised water with the needle of the syringe in the water drop and just above the solid surface. The contact angle was recorded after it has reached a relatively constant value at room temperature in ambient air as shown in Figure 3-16 . The measurements were carried out at different 12 point on the surface of each sample for each measurement and the average of these measurements was used value. The corroded sites were avoided for the samples that corroded before the end of the measurement, such as sol gel coated AA 2024.

Coated and bare samples were separately immersed in 3.5% NaCl solutions and the contact angles were measured before and after immersion.
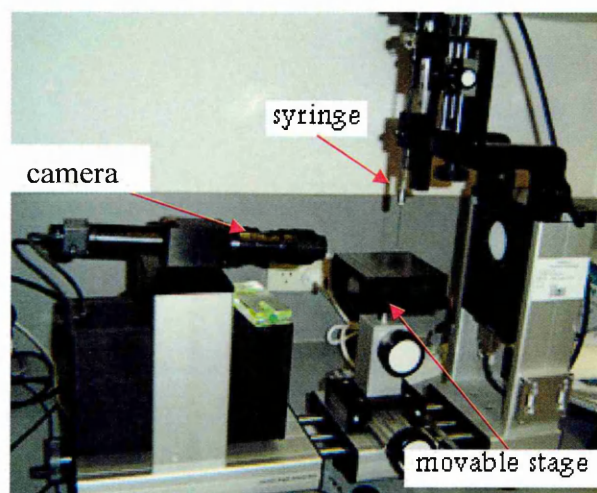
Figure 3-15 Contact angle measurement instrument
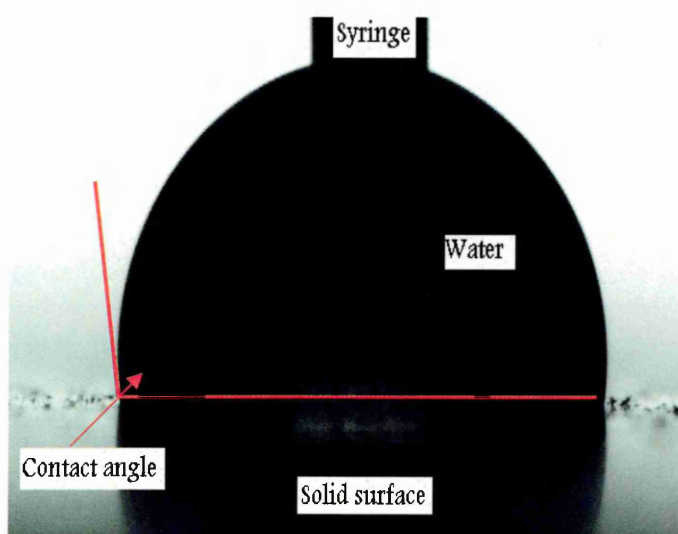
Figure 3-16 Shape of water drop in contact to solid surface and the syringe

3.1.2.6 Differential Scanning Calorimetry (DSC)

Differential scanning calorimetry [13] is one of the most widely used thermal analysis techniques for the characterization of materials. It enables the determination of glass transitions temperature, melting and boiling points, crystallisation time and temperature, percent crystallinity, oxidative/thermal stability, purity, reaction kinetics and rate and degree of curing. Generally, the sample temperature is increased linearly as a function of time. DSC directly measures heat changes in the sample that occur during changes in temperature, making it possible to study materials in their native state.

When the sample temperature is increased, the supply of thermal energy may induce physical or chemical processes in the sample, e.g. melting or decomposition, accompanied by a change in enthalpy, the latent heat of fusion, heat of reaction etc. Such enthalpy changes may be detected by DSC and related to the processes occurring in the sample.

In DSC, the measuring principle is to compare the rate of heat change of a sample to an inert material, which are heated at the same rate. Changes in the sample that are associated with absorption or evolution of heat cause a change in the differential heat flow which is then recorded as a change. The area under the peak is directly proportional to the enthalpic change and its direction indicates whether the thermal event is endothermic or exothermic

In this study, Mettler model DSC25 was used to assess the curing temperature and time at a temperature rate of 10 °C/min and 70 ml/min follow of air.

3.1.3 MECHANICAL PROPERTIES TECHNIQUES

3.1.3.1 Micro-Hardness

Hardness is a measure of the resistance of a material to deformation. During a hardness measurement, a tip is forced into the material being tested. The ratio between the total load and the projected area or depth of the permanent (plastic) indent provides a measure of hardness.

In this study, the micro-hardness was evaluated using the Vickers hardness test method.

The Vickers hardness test method evaluates the micro-hardness by indenting the test material with a diamond pyramid indenter. The diamond pyramid is a right pyramid with a square base and an angle of 136 degrees between opposite faces as shown in Figure 3-17.
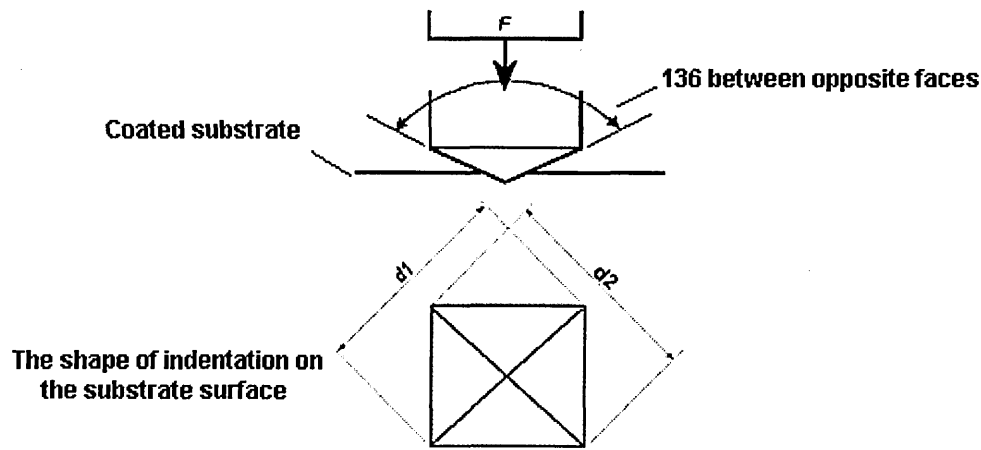
Figure 3-17 Vickers hardness indenter and shap of indented surface

The indenter is subjected to a specific load (in this study 10 g was used) for 10 seconds. To avoid substrate interference, the indentation depth was less than 50% of the coating thickness. The load is then gradually removed to allow the complete relaxation of the tested material. The two diagonals of the indentation left in the surface of the material after removal of the load are measured using a microscope. The area of the indentation is then calculated and the Vickers hardness is calculated according to the following equation;

$$HV = \frac{2F\sin(\frac{136}{2})}{d^2} \qquad HV = 1.854\frac{F}{d^2} \qquad approximately$$

Where:

F..... applied force.

d^2.... d1xd2

3.1.3.2 Adhesion Tester

Adhesion of coatings is generally considered one of the most significant properties in the evaluation of a coating's performance, reliability and durability for any application. The adhesive strength of a coating represents the strength of the bond between the substrate and coating.

A Pull off adhesion test determines the greatest perpendicular tension force that a surface area can bear before a plug of material is detached. Failure will occur

along the weakest plane within the system comprised of the test fixture, adhesive, coating system, and substrate, and will be exposed by the fracture surface.

Elcometer 108, a hydraulic pull off tester shown in Figure 3-18, was used in this study to measure the adhesion of the coating to the metal substrate according to ASTM D4541. Tests were made on clean flat surfaces as follows; the dolly is glued to the surface under test, making sure that the internal hole in the dolly is clear from adhesive (in this study commercial UHU™ super glue was used). The glue is left to cure for 24 hrs before completing the adhesion test. The instrument is then attached to the dolly glued to the coating surface. The instruments handle is then turned to increase the hydraulic pressure which forces the dolly away from the substrate. The value of the force is displayed and recorded on the dial.
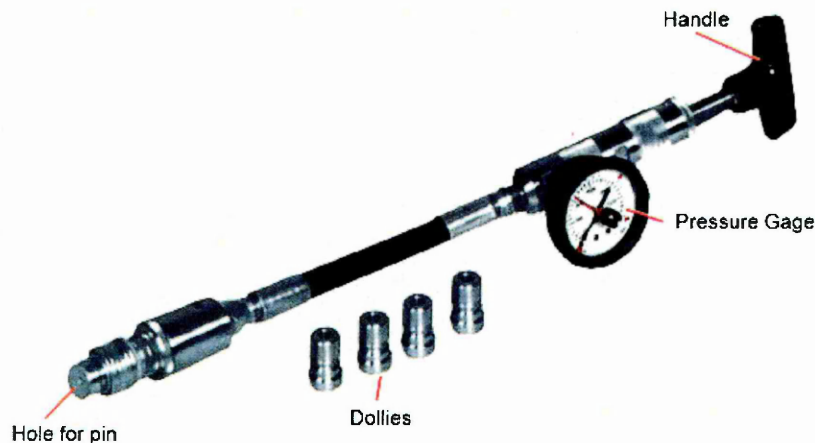
Figure 3-18 Hydraulic pull off tester

3.1.3.3 Cross Cut adhesion test

It is a test method for measuring the resistance of paint coatings to separation from substrates [14] when a right-angle lattice pattern is cut into the coating, penetrating through to the substrate. Various cutting tools can be used either manually or mechanically for this purpose. The test results are evaluated according to the scheme indicated in Figure 3-19. The classification is based on estimating the amount of paint flakes separated from the substrate. If in doubt

about the real percentage of detachment, one may brush off the loose parts or remove them by means of an adhesive tape.
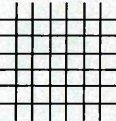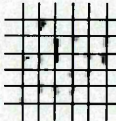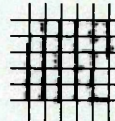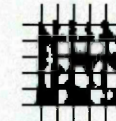
Figure 3-19 Principle of classifying paint film adhesion in the cross-cut test [14].

3.1.3.4 Sellotape Adhesion Test

A sellotape test is carried out as follows; the samples are sharply scratched using a razor to form a cross hatch. Sellotape tape is applied to the cross-hatch and fixed well before peeling it from the surface. The sellotape is examined for signs of any detached coating.

3.1.3.5 Bend Test for Coating

Bending test is performed to determine the flexibility, adhesion and elongation of organic coatings on substrates on a sheet by bending a coated substrate around a specified arc. A Mandrel bend tester is a frame that has a bending lever with a roller which pivots on a steel conical mandrel with a diameter from 3.2 to 38.1mm as shown in Figure 3-20.
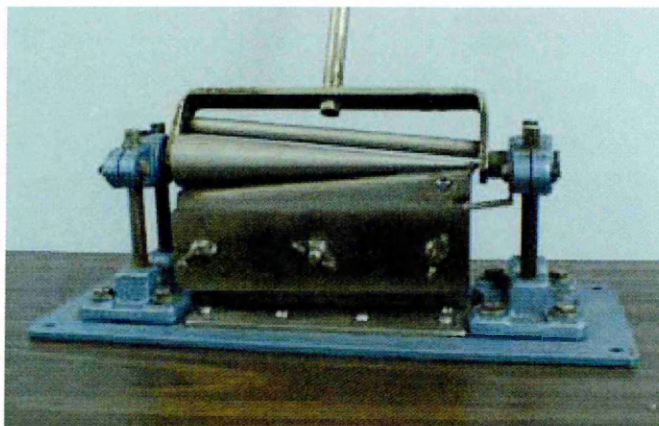
Figure 3-20 Mandrel bend tester

The coating materials under test should have uniform thickness. After drying or curing the coated panels are bent over a mandrel and the resistance to cracking

of the coating is determined. The specimen can be bent on part of, or along the entire length, of the mandrel. The test can terminate at a given angle of bend over a specified radius or continue until 180°. The results corresponding to different test diameters can be observed in a single operation using a magnifier glass.

In this study, an Elcometer 1510 Conical Mandrel Bend Tester was used according to ASTM D522 as follows;

Test panels were clamped so that the panel just touches the mandrel and the handle was left until the bending piece touched the test panel. The handle was then left over 180° in 1 to 2 seconds.

3.2 EXPERIMENTAL WORK

All experimental work has been carried out at room temperature, and glassware was thoroughly cleaned by acetone and then deionised water before use. Experiments were carried out under stagnant condition without removing the dissolved oxygen. The chemicals used in this work were of analytical grade.

3.2.1 Polyaniline Preparation:

Polyaniline was prepared chemically according to Yanhou et al [15] as illustrated in the following scheme

```
┌─────────────────────────────┐   ┌─────────────────────────────┐
│ (NH₄)₂S₂O₈ in  1M HCl        │   │ Aniline solution in 1M HCl  │
└─────────────────────────────┘   └─────────────────────────────┘
                │                             │
                └──────────────┬──────────────┘
                               ▼
              ┌─────────────────────────────────┐
              │ Mixing under vigorous stirring at │
              │ temp. of 0-5°C for 24 hrs         │
              └─────────────────────────────────┘
                               │
                               ▼
              ┌─────────────────────────────────┐
              │ Filtration and washing          │
              └─────────────────────────────────┘
                               │
                               ▼
              ┌─────────────────────────────────┐
              │ Drying (ES)                     │
              └─────────────────────────────────┘
                               │
                               ▼
              ┌─────────────────────────────────┐
              │ Mixing with 1M NH₄OH for 2      │
              │ Hrs                             │
              └─────────────────────────────────┘
                               │
                               ▼
              ┌─────────────────────────────────┐
              │ Filtration                      │
              └─────────────────────────────────┘
                               │
                               ▼
              ┌─────────────────────────────────┐
              │ Drying (EB)                     │
              └─────────────────────────────────┘
```
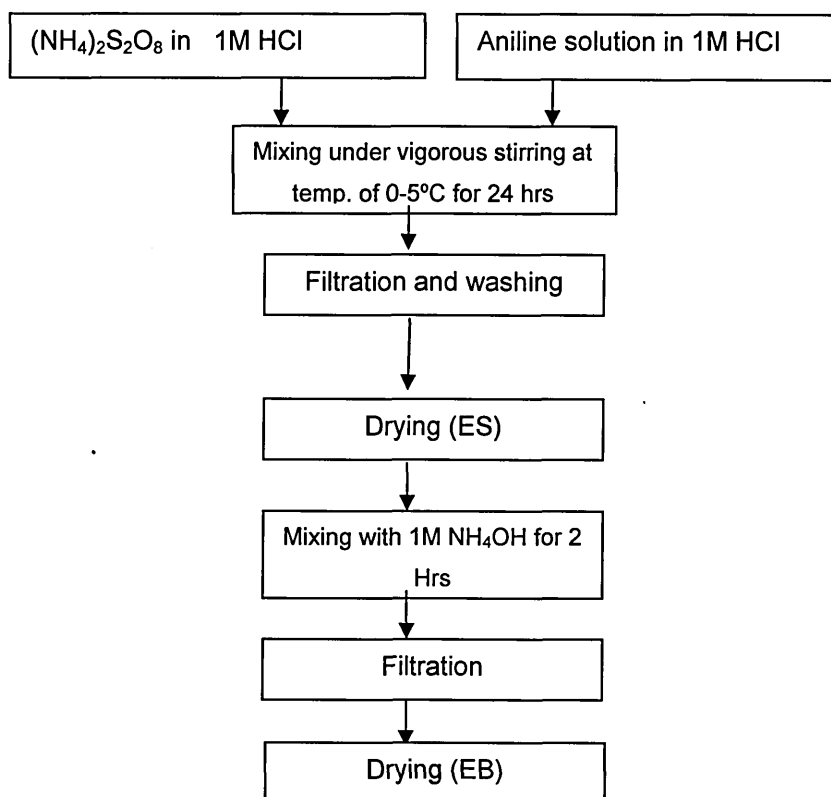
Figure 3-21 Schematic sketch of chemical synthesis and characterization of polyaniline

All solutions used in the preparation of polyaniline are consisted of acetone aqueous mixtures (water/acetone 60:40%). Acetone is used to improve the solubility and dispersibility of PANI in both N-methylpyrrolidinone and sol- gel. The chemical oxidation of aniline is performed by its oxidation with ammonium persulphate in 1M hydrochloric acid solution. Aniline 5.0 ml (0.107 M) is dissolved in 300 ml 1M HCl at 0-5°C and stirred for 1 hour. A solution of 5.6 g ammonium persulphate in 100 ml HCl is added dropwise to aniline solution over period of 15 min with vigorous stirring. The solution is kept stirring at this temperature for 6 hours. The precipitate is collected with a Buchner funnel and washed with four portions of 50 ml 1M HCl. The precipitate is dried at 60 °C for 24 hours, the HCl doped PANI (ES) is obtained as a green powder. The basic form of PANI (EB) is obtained by stirring the ES with 1M NH₄OH for 4 hours followed by filtration and drying.

The PANI sample is dissolved in N-methylpyrrolidinone (NMP) solvent to form 3.5 % solution.

3.2.2 Sample Preparation

Aluminium alloy 2024-T3 samples (obtained from Q-panel 2.54cm×10.16cm×0.156 cm) were cleaned with deionised water followed by ultrasonic cleaning in a commercial alkaline solution (Industrial KLEEN IKB 501). This was followed by washing with deionised water. The final cleaning stage is pickling in nitric acid 50% solution for 30 sec and then drying for 30 min at 70 °C before applying the coating.

For bend tests, a sample thickness of 0.5 mm was used.

For XPS and TEM analysis the metal sample (1cm x1cm x0.156cm) was subjected to the same cleaning procedure. Furthermore, these samples were ground to a mirror finish (1 μm) followed by washing with deionised water and drying at 70 °C for 30 min before applying the coating.

3.2.3 Preparation of the PANI/Sol-gel Coating

- For corrosion test; the base form of PANI (EB) is dissolved in NMP to make a 3.5 % PANI solution.

Organic-inorganic hybrid silica base sols catalysed by HNO_3 acid with a solution pH value of 1.5-2, prepared at Sheffield Hallam University by Dr H. Wang, were used in this study.

The PANI solution is added to the sol-gel liquid and stirred for 4 hours to form a homogeneous solution of PANI doped-sol. The PANI/sol-gel coating is prepared in different relative concentrations. The sol is applied to one side of the metal surface using a spray coating technique. The metal is oven dried in air at 70°C for 30 min before applying the coating respectively. The coated samples were dried in air at 70°C for 16 hours after applying the coating.

For immersion test, the coated samples edges and backside were covered with a mixture of bees wax and colophony.

-PANI coated glass (used in study of the mechanism of protection) is prepared by spraying PANI solution on one side of the glass substrate followed by drying in air at 70°C for 16 hours

-For XPS and TEM analysis, a spin coating technique was used to prepare different types of coating. PANI solution, sol-gel and PANI/sol-gel coating were diluted ten times to control the thickness of coating to be within 100nm.

-The free standing PANI film was prepared as follows; PANI solution was applied on a Teflon substrate followed by drying at 70 °C over night. The coated sample was then removed from the oven and the free standing film removed from the Teflon substrate using tweezers and a scalpel.

-For XPS analysis, pure (99.999%) aluminium was evaporated under vacuum (10^{-5} torr) on the free standing film forming a layer thickness of 80nm.

-Post-treated samples; the coated sample was immersed in 1% 3-aminipropyl triethoxysilane aqueous solution at 60 °C for 5 min and dried using air stream at room temperature.

REFERENCES

[1] N. Cogger and N. Evans, 2007, "An Introduction to Electrochemical Impedance Measurement," 2007(23 May) .

[2] W. Tait, 1994, "An Introduction to Electrochemical Corrosion Testing for Practicing Engineers and Scientists," Pai Viscor Publications, Raciene, wisconsin, USA, pp. 79--93.

[3] Gamry instruments, 2007, "Electrochemical Impedance Spectroscopy Theory," 2007(23 April) .

[4] G. Kelly, R. Scully, W. Shoesmith and G. Buchheit, 2003, "Electrochemical Techniques in Corrosion Science and Engineering," Marcel Dekker, Inc., 270 Madison Avenue, New York, pp. 426.

[5] R. Akid, and M. Garma, 2004, "Scanning Vibrating Reference Electrode Technique: A Calibration Study to Evaluate the Optimum Operating Parameters for Maximum Signal Detection of Point Source Activity," Electrochimica Acta, 49(17-18) pp. 2871-2879.

[6] R. Sampson, December 2, 1996, "Scanning Electron Microscopy," 2007(25 April) .

[7] P. Goodhew and F. Humphreys, 1988, "Electron microscopy and analysis" Taylor and Francis, Abingdon, Oxfordshire, UK.

[8] M. Ponting, 2004, "The Scanning Electron Microscope and the Archaeologist," Physics Education, 39(2) pp. 166-170.

[9] J. Watts, J. Wolstenholme, 2003, "An Introduction to Surface Analysis by XPS and AES," John Wiley & Sons Ltd, The Atrium, Southern Gate, Chichester, West Sussex PO19 8SQ, England, pp. 212.

[10] J. Fujita, M. Hyland, 2003, "Polyaniline Coatings for Aluminium: Preliminary Study of Bond and Anti-Corrosion," International Journal of Modern Physics, 17(8-9) pp. 1164-1169.

[11] C. Sherman Hsu, 1997, "Handbook of instrumental techniques for analytical chemistry" Prentic-Hall international, Uk, London, pp. 247-277.

[12] K. Birdi, 2003, "Handbook of Surface and Colloid Chemistry," CRC Press LLC, 2000 N.W. Corporate Blvd., Boca Raton, Florida 33431, pp. 67-118, Chap. 3.

[13] M. Reading and D. Hourston, 2006, "Modulated Temperature Differential Scanning Calorimetry Theoretical and Practical Applications in Polymer Characterisation," Springer, P.O. Box 17, 3300 AA Dordrecht, Netherlands, pp. 329.

[14] A. Tracton, 2006, "Coatings Technology Handbook," CRC Press Taylor & Francis Group, USA .

[15] Y. Geng, J. Li, Z. Sun, 1998, "Polymerization of Aniline in an Aqueous System Containing Organic Solvents," Synthetic Metals, 96(1) pp. 1-6.

CHAPTER 4

RESULTS

This chapter consists of three main parts; corrosion performance, fitting of impedance data, mechanical properties and characterization, notably chemical composition and interfacial interaction between metal substrate and coating.

-The corrosion performance of the coatings were based upon EIS measurements and salt spray tests for different coating systems. Furthermore, impedance tests were carried out for bare and coated samples in 3.5% NaCl solutions of different pH value. These results include the effects of different combination of sol-gel and polyaniline. Furthermore, the self healing property was studied using Scanning Vibrating Electrode Technique (SVET).

-Fitting Electrochemical Impedance Spectroscope data was investigated in the second part of this chapter in order to help understand the corrosion mechanism.

-Mechanical properties, in particular the adhesion of the coating to the metal substrate, are presented in this chapter.

-Finally, the chemical characteristics of the coatings were evaluated using XPS while TEM was used to asses the interfacial interaction of the coating and metal substrate

4.1 PART ONE; CORROSION PERFORMANCE

In this part, polarisation, EIS measurements and SST for both bare and coated AA2024 samples are presented. During these tests, the samples were coated on one side only then dried and the edges of the coated samples were waxed to avoid any edge effects.

4.1.1 Polarisation Results

As a preliminary investigation the corrosion properties of bare and PANI coated AA2024 was conducted using a polarisation technique in 3.5% NaCl solution. Anodic and cathodic branches were measured separately. As shown from Figure 4-1 the bare sample has a corrosion current of about $6x10^{-6}$ A/cm^2. The anodic branch of the uncoated sample shows continuous active dissolution of the metal while the cathodic branch exhibits diffusion control. In comparison, the corrosion current of the PANI coated sample is one and half orders of magnitude lower than that of bare sample being $7x10^{-8}$ A/cm^2. The polarisation curve of PANI/sol-gel coated sample, shown in Figure 4-1, exhibits a corrosion current that is approximately equal to that PANI coated sample.

The corrosion potential of the bare sample was measured at -610mV (SCE), while, the PANI coated and PANI/sol-gel coated samples were -640 and -725 mV (SCE) respectively.

Both coated samples showed passive behaviour at potential above the OCP with a breakdown potential for the PANI/sol-gel coating measured at -600mV (SCE) and PANI coated sample at -500mV (SCE). The polarisation data are summarised in Table 4-1.

Table 4-1 Polarisation data

Sample	E_{corr} [mV] (vs SCE)	I_{corr} [A/cm^2]
Bare 2024	-610±30	$6x10^{-6}$
PANI coated AA2024	-640±30	$7x10^{-8}$
PANI/sol-gel coated AA2024	-725±30	$8x10^{-8}$
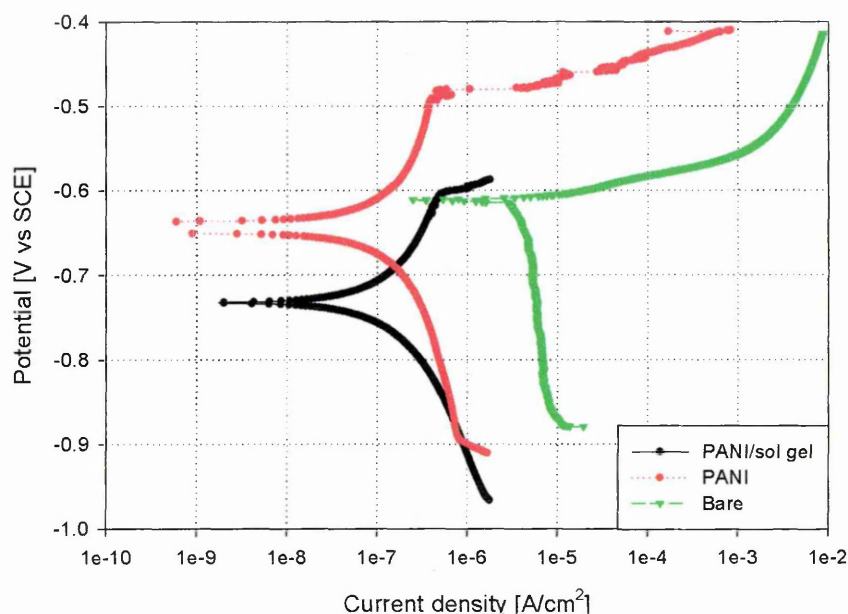
Figure 4-1 Polarisation curves for bare, PANI and PANI/sol-gel coated AA2024 in 3.5% NaCl solution.

4.1.2 Electrochemical Impedance Results

Electrochemical impedance spectroscopy is more appropriate than polarisation for use with non-conductive coatings since sol-gel and PANI (EB) are insulators. The results of bare and coated samples with different coating systems were investigated in this section. Changes in surface morphology, before and after impedance testing were also recorded.

4.1.2.1 Bare sample

SEM analysis of surface morphology of the bare sample was carried out prior to exposure to the corrosive media. Figure 4-2 shows typical features of the bare sample surface. This sample was subjected to the cleaning procedure mentioned in chapter 3. Before immersion in solution, the bare AA2024 sample revealed signs of pitting related to the action of the cleaning process at the IMP sites
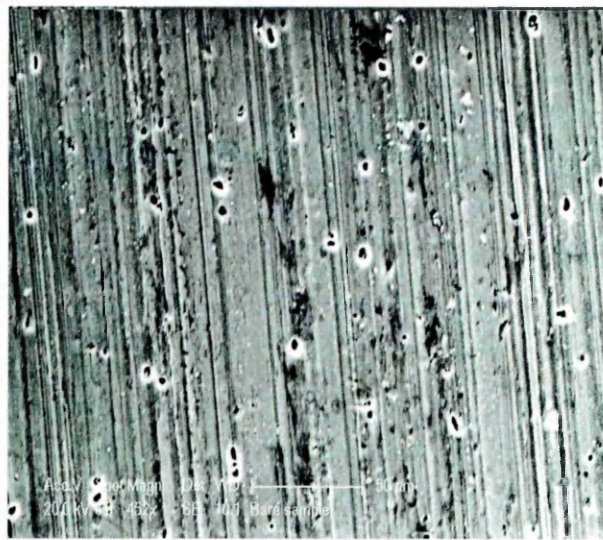
Figure 4-2 SEM image of bare AA2024 sample before immersion

EDX mapping was used to study the elemental features of the surface shown in Figure 4-3. EDX mapping revealed the aluminium matrix and the intermetallic particles found in the alloy (copper, magnesium, manganese).
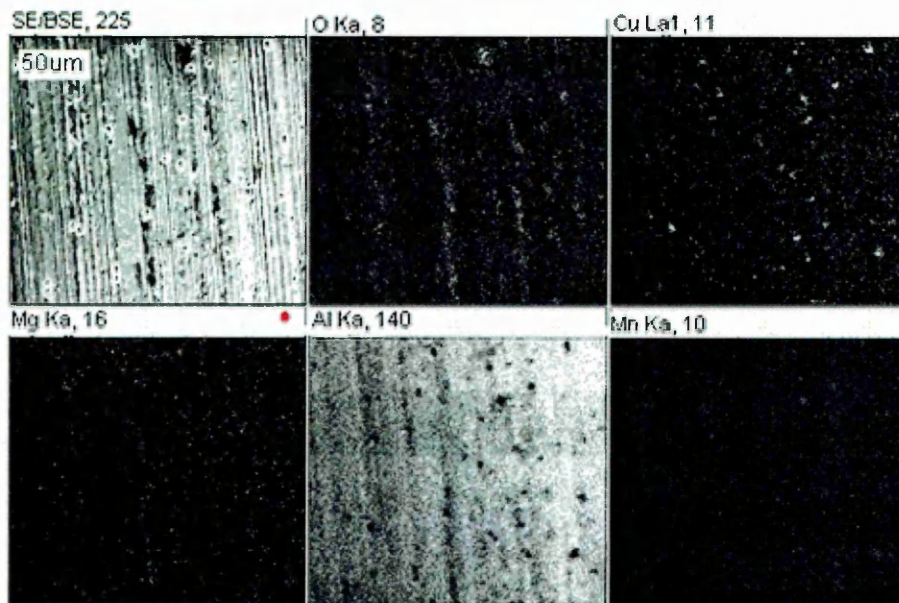
Figure 4-3 Elemental EDX maps for a bare AA2024 sample

Impedance data for the bare metal substrate, see Figure 4-4, showed low impedance, 30 Ohm.cm^2, at high frequencies,(10^5-10^3 Hz) after 1 hrs of immersion, however, it slightly increased to about 40 Ohm.cm^2 after 7 days of immersion. At low frequency range 0.01 Hz, the impedance decreased gradually with immersion time. Moreover the phase angle, Figure 4-5, shows one time constant after one hour of immersion (at 10 Hz), however, a new time

95

constant appeared at 1.0 Hz after 24hrs. After 7 days of immersion, only the second time constant, at 1.0 Hz, remained. This behaviour was accompanied by the appearance of a white gelatinous material covering the entire surface of the bare sample after 3 days of immersion. Examination of the surface revealed heavy corrosion over the entire metal surface with individual pitting being observed, Figure 4- 6.
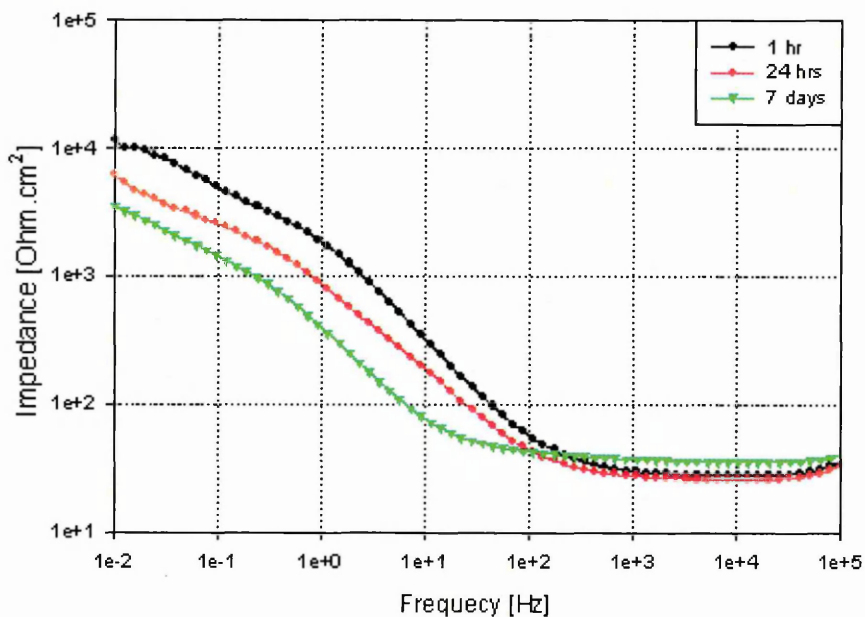
Figure 4-4 Impedance behaviour of bare AA2024 in 3.5%NaCl
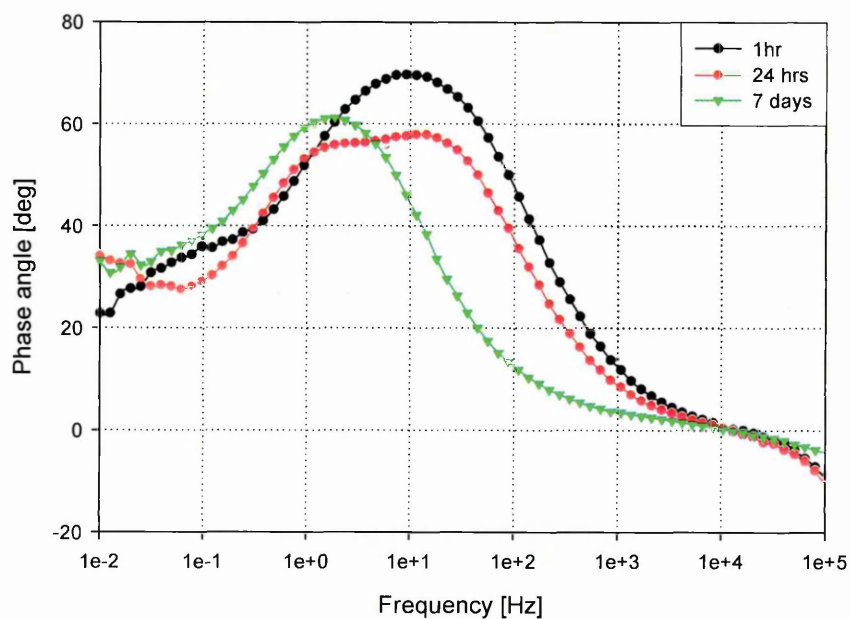
Figure 4-5 Phase angle response of bare AA2024 in 3.5% NaCl solution
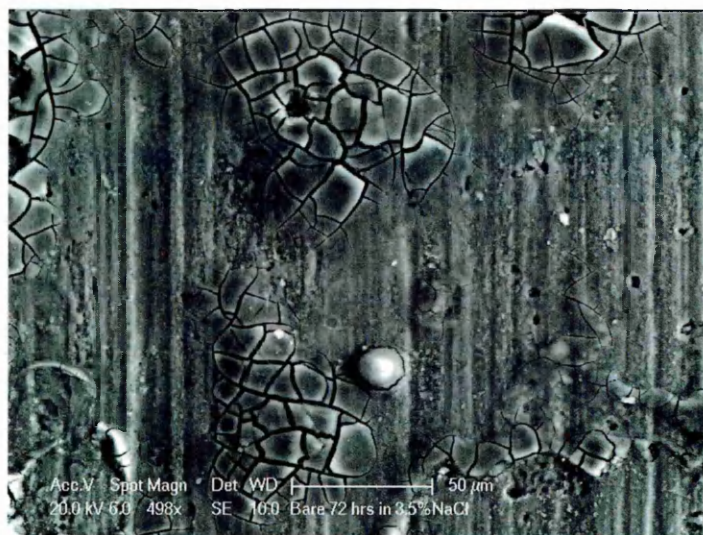
**Figure 4- 6 SEM image of bare AA2024 sample after immersion
for 72 hrs in 3.5% NaCl solution.**

4.1.2.2 Polyaniline coated AA2024

Polyaniline was prepared as the emeraldine base and then dissolved in N-methyl pyrrolidinone (NMP) to form a 3.5% solution. The solution was applied to the bare aluminium substrate and then dried at 70 °C for 24 hours.

The PANI coated sample was then subjected to immersion in 3.5 %NaCl solution and then compared to the PANI/sol-gel coated sample.

An SEM image of the PANI coated sample before immersion is shown in Figure 4-7.

Figure 4-7 SEM image of PANI coated AA sample before immersion
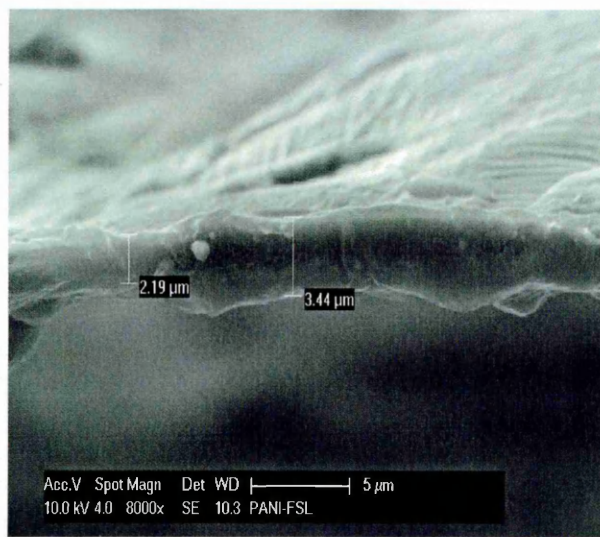
Figure 4-8 SEM image of free standing PANI coating.

The PANI coating thickness was measured at 2-4μm, as shown in Figure 4-8. The sample was then immersed in 3.5% NaCl solution.
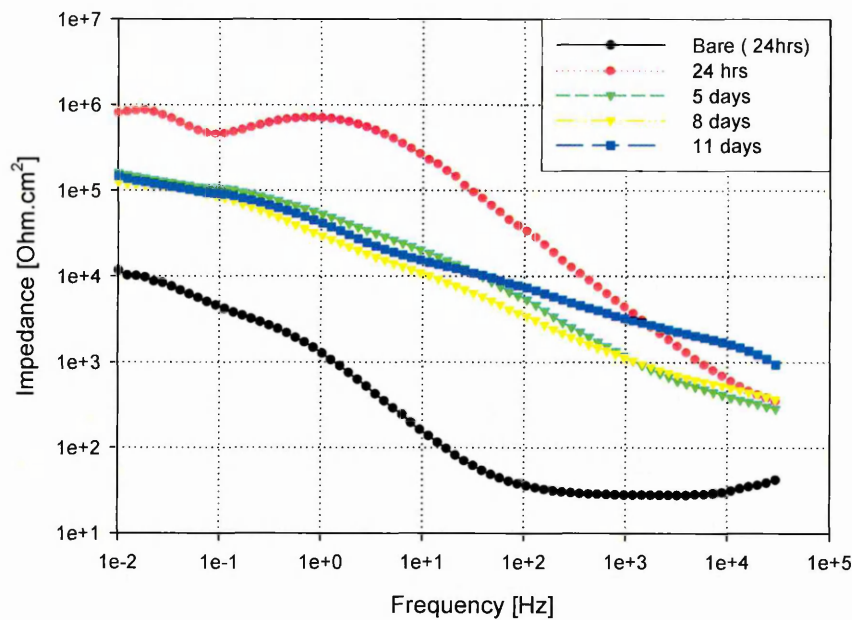
Figure 4-9 Impedance of PANI coated AA2024 in 3.5 %NaCl solution

Figure 4-9, shows the impedance behaviour of the PANI coated sample. The coated sample has an impedance that is one order of magnitude greater than the bare substrate after 11 days exposure. The coating showed a high initial impedance (1×10^6 Ohm/cm^2) in the first day of immersion but then lost about one order of magnitude during the following 5 days. The impedance then remained stable at 1.5×10^5 Ohm/cm^2 for the rest of immersion test (11 days).

98

Figure 4-9, showed that after one day of immersion an inductive effect appeared between 1.0 and 0.01 Hz, however, it completely disappeared after that which may related to the instability of the redox form of PANI [1].

Optical inspection showed that this coating has poor adhesion properties to the metal substrate; although it did exhibit good flexibility being easily bent several times. After 5 days of immersion, the PANI coat completely delaminated from the metal substrate, as shown in Figure 4-10.
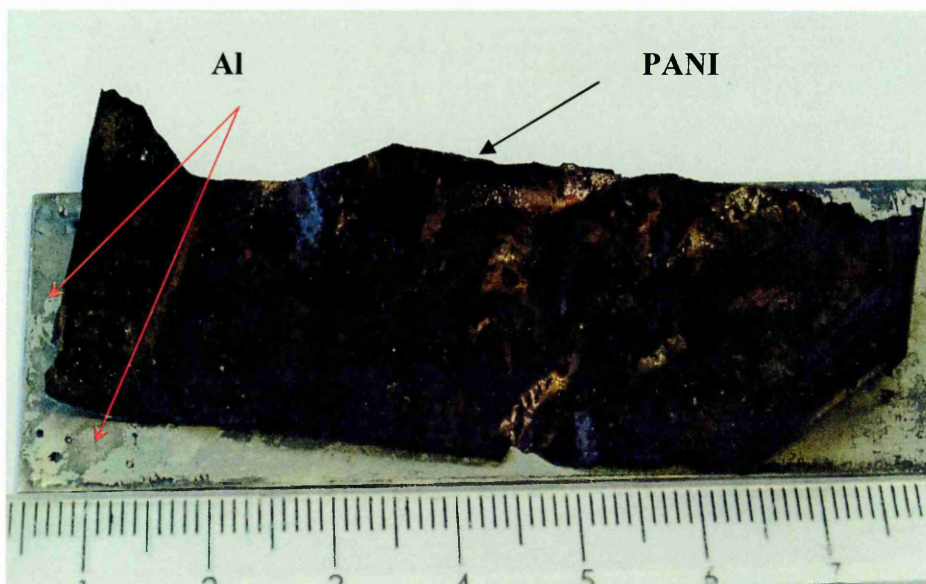
Figure 4-10 Image of PANI film after peeling from aluminium substrate

Examination of the metal substrate showed a dark surface after delamination of PANI coating, which is due the reaction of the PANI with the original surface as shown in Figure 4-11
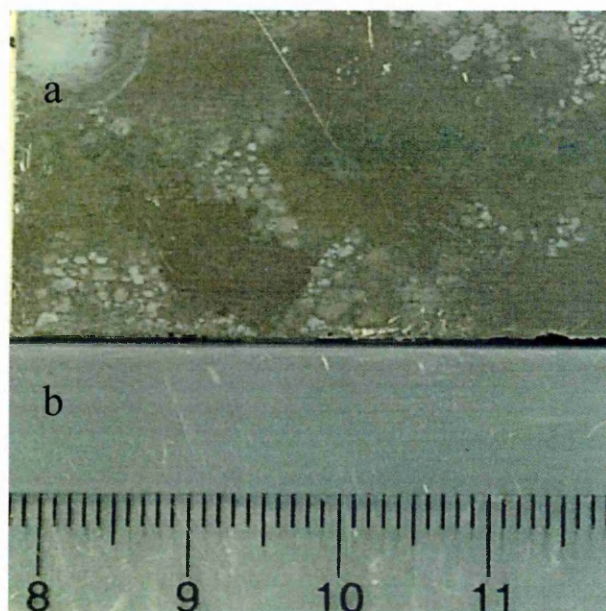
Figure 4-11 Image of substrates (a) surface following delamination of PANI coating and (b) bare sample

To study the nature of reaction layer, impedance measurements were carried out on the sample, from which the PANI was removed, and a bare sample prior to coating. Samples were cleaned with NMP to (1) remove any traces of PANI and (b) subject the bare sample to the same solvent used in applying the PANI coating. The samples were then left to dry at 70°C for 4 hours before being immersed in a 1% NaCl solution for 24 hours. EIS tests were conducted on both samples, the results being shown in Figure 4-12.
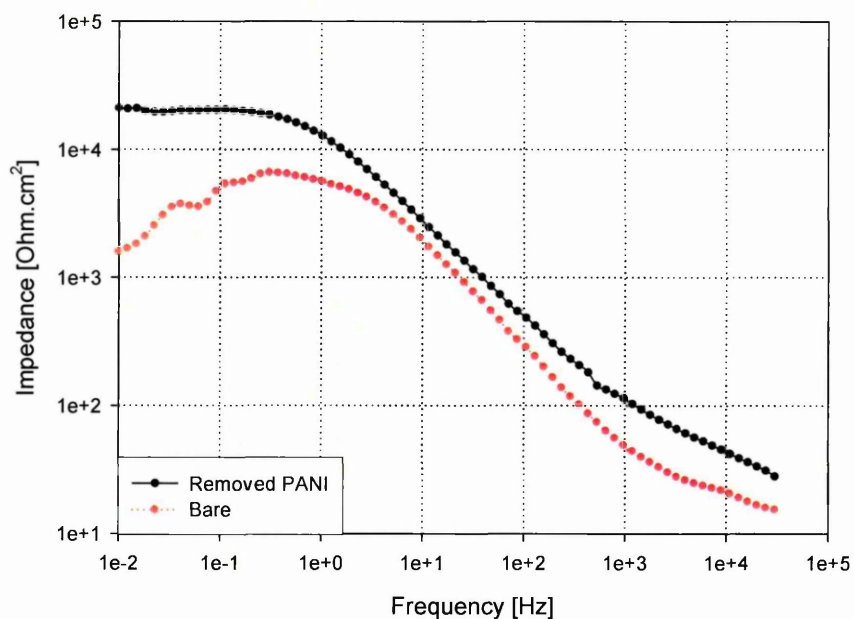
Figure 4-12 Impedance of bare and PANI coated AA2024 surface following delamination of PANI coating samples after 24 hrs in 1 %NaCl solution.
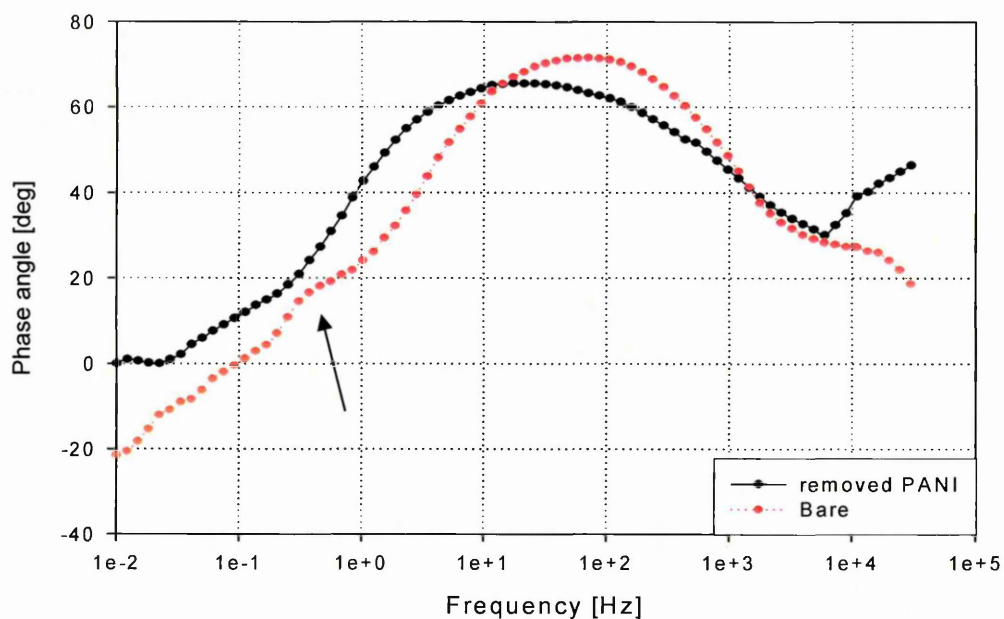
Figure 4-13 Phase angle of bare and PANI coated AA2024 surface following delamination of PANI coating samples after 24 hrs in 1 %NaCl solution.

The impedance value for the PANI delamination sample ($2.2 \times 10^4 Ohm.cm^2$) is one order of magnitude higher than that of bare sample ($1.5 \times 10^3 Ohm.cm^2$). Moreover, the phase angle curve showed a single time constant for the PANI

101

delamination sample at about 10 Hz. However, it showed two time constants for the bare substrate; at 80 Hz and at 0.6 Hz (arrow), the latter may refer to the formation of corrosion products.

These results suggest that the PANI reaction layer offers corrosion protection of AA2024; however, the PANI coating has poor adhesion properties to the metal substrate.

4.1.2.3 Sol-gel coated AA2024

Before studying the corrosion performance of the sol-gel coated AA2024, SEM was used to investigate sol-gel surface morphology. The SEM image of the sol-gel coated sample, Figure 4-14, shows that the surface of the coating was free from cracks and appeared to be uniform.
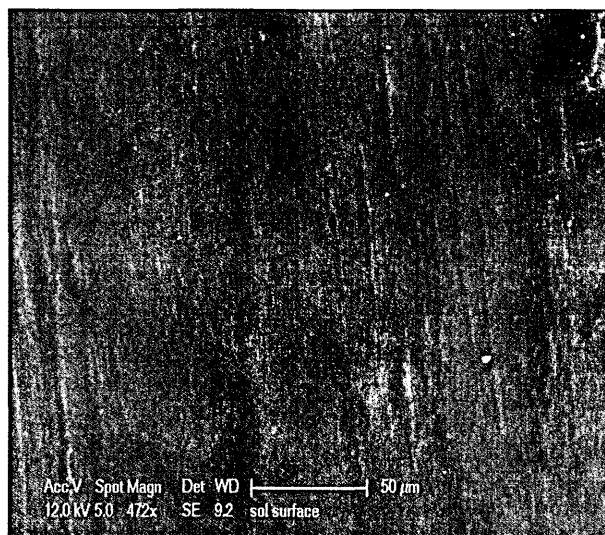
Figure 4-14 SEM image of surface of the sol-gel coated AA2024 sample.

An SEM image of the cross section of the sol-gel coated AA2024 sample, Figure 4-15, showed the coating to have a thickness of 14-16 μm.
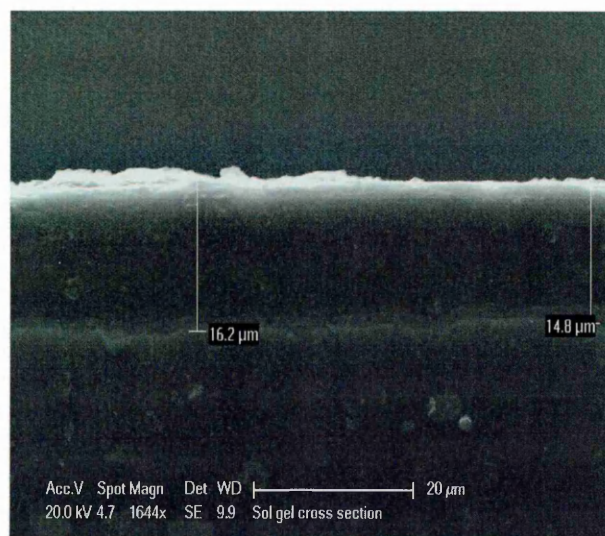
Figure 4-15 SEM image of cross section of sol-gel coated AA2024 sample.

The corrosion properties of the sol-gel coated sample were investigated using EIS in the same electrolyte namely 3.5% NaCl. Figure 4-16 shows that the impedance is initially high (over 10^6 Ohm.cm^2). However, with prolonged immersion, the impedance value decreases by about one order of magnitude within 16 days.
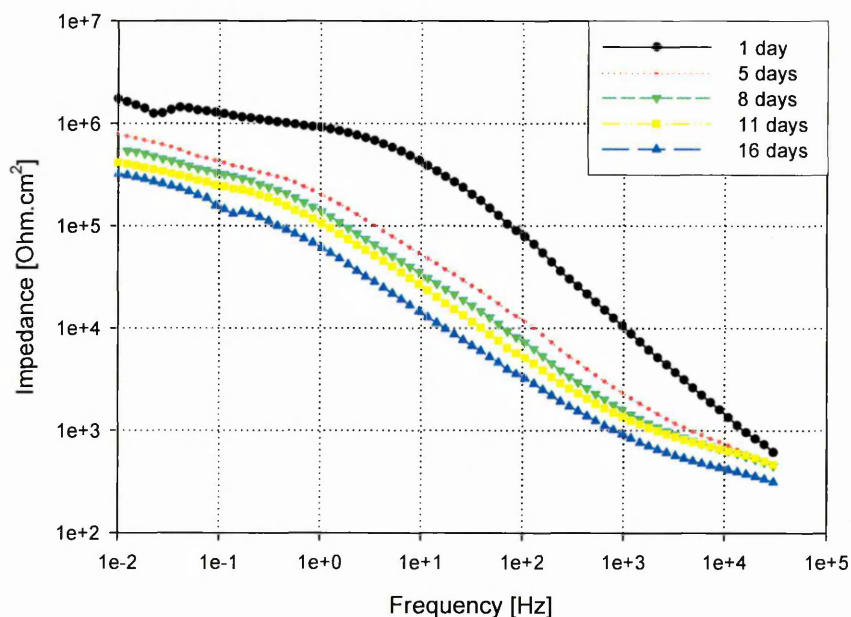

Figure 4-16 Impedance of sol-gel coated AA2024 in 3.5 %NaCl solution
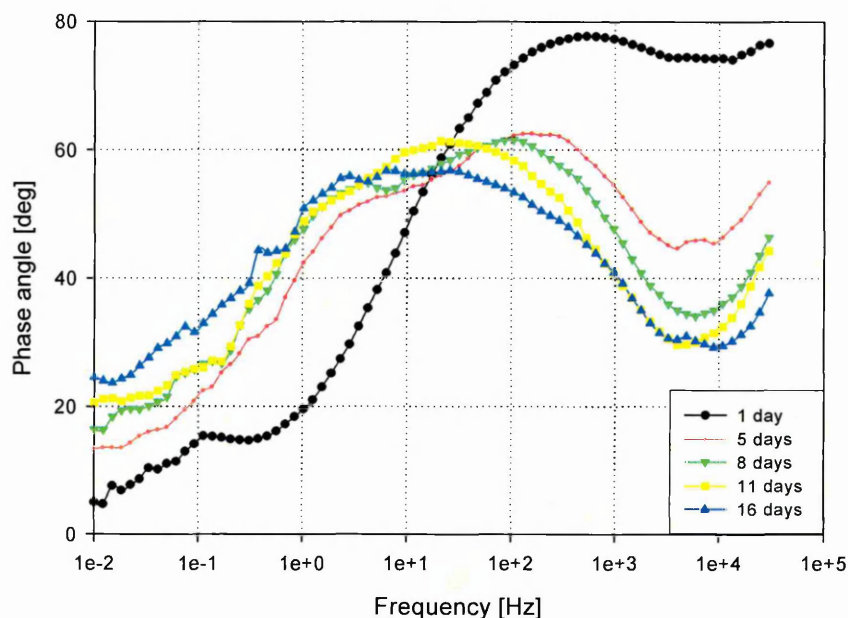
Figure 4-17 Phase diagram of sol-gel coated AA2024 sample in 3.5 %NaCl solution

The phase angle curve, Figure 4-17, showed two time constants; at 3×10^4 Hz and at 10^3 Hz after 24 hrs of immersion. The former showed a decreasing capacitive behaviour which may be related to the hydrophobic property of sol-gel [2]. This hydrophobic property diminished with increasing immersion time as seen in the decrease in phase angle at high frequency. The latter time constant peak, at 10^2 Hz, shifted towards lower frequency, from 10^3 to 1.0 Hz, by prolonged immersion inferring diffusion of electrolyte through the coating [3]. Furthermore, the magnitude of the time constant increased with time of immersion suggesting an increase in the area of the substrate exposed to the electrolyte [4]. This behaviour appeared as a decrease in both capacitive and resistive region in the impedance curve as a sign of break down of the sol-gel coating. This behaviour was accompanied by the appearance of pits (arrowed in Figure 4-18) after 5 days of immersion in the electrolyte. The colour of the pits changed from white, after five days, to dark brown after 16 days.

104
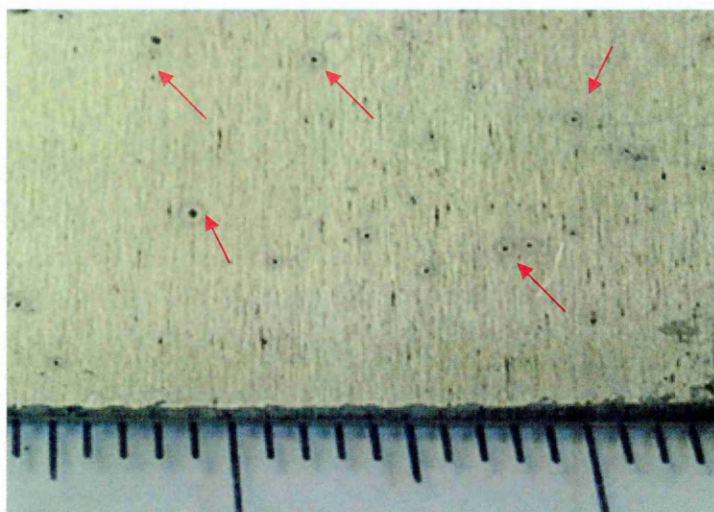
Figure 4-18 Sol-gel coated AA2024 sample after 16 days of immersion in 3.5 %NaCl solution

Figure 4-19-a shows a magnified view of the pitting on the surface of the sol-gel coated sample. Figure 4-19-b showed a magnified pit where another small pit (arrow) was appeared beside the first one. Moreover, numerous pits were initiated on the surface of the sol-gel coated AA2024.
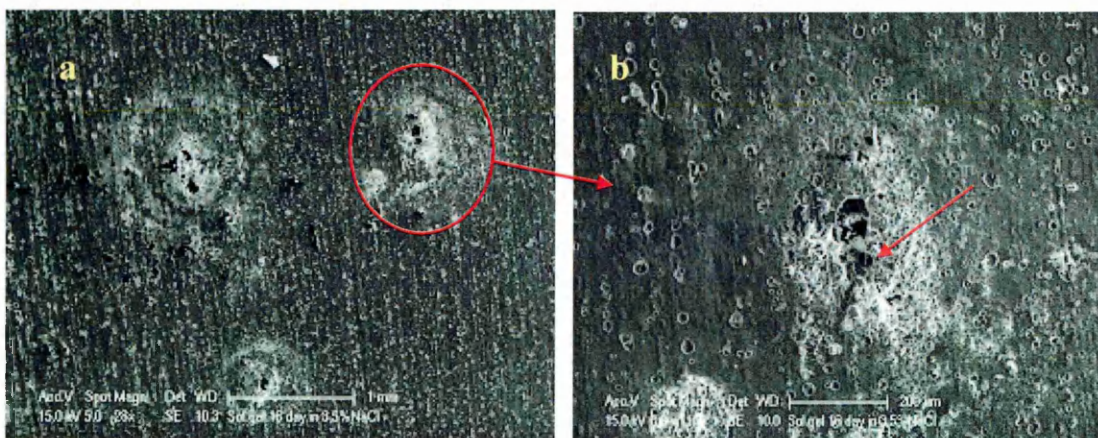
Figure 4-19 SEM image of sol-gel coated AA2024 sample after immersion for 16 days in 3.5% NaCl solution.

These results suggest that the silica sol-gel coating alone has limited corrosion protection for the AA2024.

4.1.2.4 PANI/sol-gel combination coatings

The following combinations of PANI and sol-gel were applied to the AA;

1) PANI primer and sol-gel topcoat, 2) sol-gel primer and PANI top coat (see footnote) and 3) mixtures of PANI and sol-gel.

The impedance curve for the PANI primer and sol-gel topcoat sample is shown in Figure 4-20.
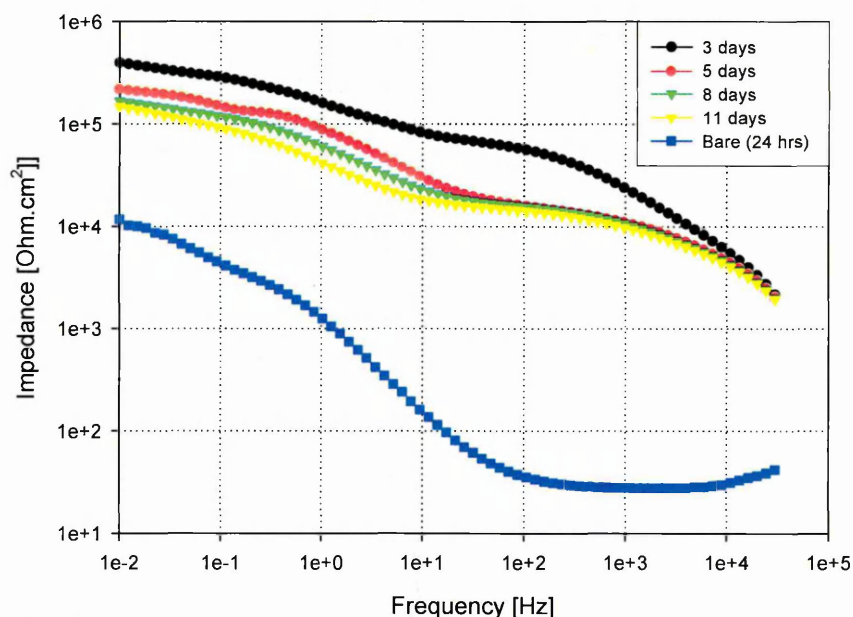
Figure 4-20 Impedance of PANI (primer) and sol-gel topcoat sample in 3.5 % NaCl solution.

The PANI primer and sol-gel topcoat coated 2024 sample showed different behaviour than that of PANI coated sample (Figure 4-9) due to presence of a top coat. The impedance decreased with the immersion time decreasing half an order of magnitude during the 11 days of immersion. Visual inspection showed small cracks in the coating after 3 days and complete delaminated from the metal surface after 11 days.

PANI/sol-gel mixtures were prepared at different relative concentrations. The corrosion performance of these coatings is discussed in the following section.

Note: Preparation of sol-gel primer and PANI top coat could not be performed due to the hydrophobic property of sol-gel which does not allow applying PANI coating to uniformly cover all i.e. it seemed like islands of PANI over sol-gel surface.

4.1.2.5 PANI/sol-gel mixture

Different concentrations of PANI (EB)/sol-gel mixture were prepared as described in chapter 3.

The following relative PANI/sol-gel volume concentrations were prepared; 1:1, 1:4, 1:8, 1:12 and 1:16. These combinations were named as PANI/sol1, PANI/sol4, PANI/sol8, PANI/sol12 and PANI/sol16 respectively. Three coated samples of each ratio were prepared. All the coated samples were dried in air for 16 hours at 70 ºC.

Bode and phase angle plots for PANI/sol16 are shown in Figure 4-21 and Figure 4- 22 respectively. As seen from Figure 4-21, the impedance decreases sharply, in all frequency ranges, with immersion time
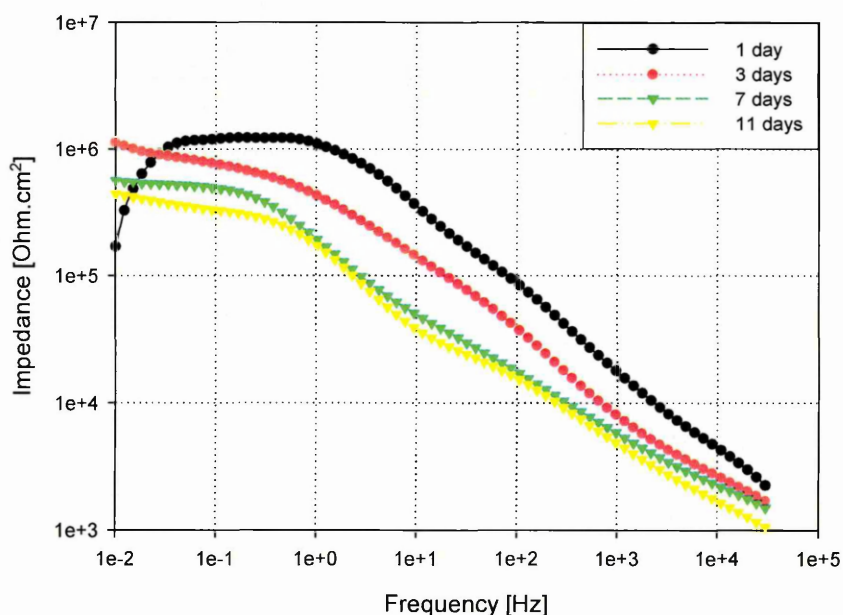
Figure 4-21 Impedance plots of PANI/sol16 coated AA2024 in 3.5% NaCl solution
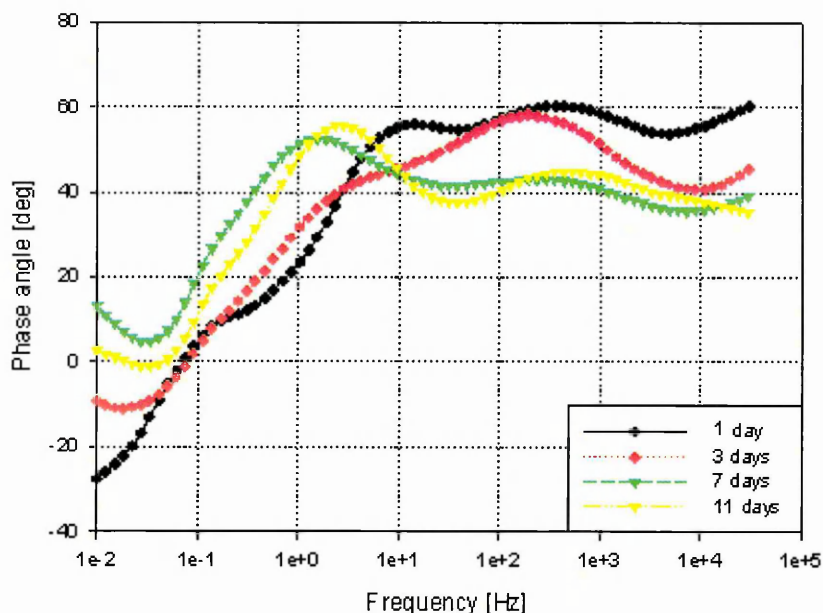
Figure 4- 22 Phase angle plots of PANI/sol16 coated AA2024 in 3.5% NaCl solution

An inductive peak in the impedance curve was observed for the first day of immersion; however, this completely disappeared before the 3 days measurement. The phase angle curve showed three time constants at 10^4, 10^2 and 0.1 Hz. The former peak decreased with the immersion time, while, the latter increases. This is accompanied by the appearance of pitting as shown in Figure 4-23. Visual inspection showed that the number of pits in this sample was less than that of the sol-gel sample.
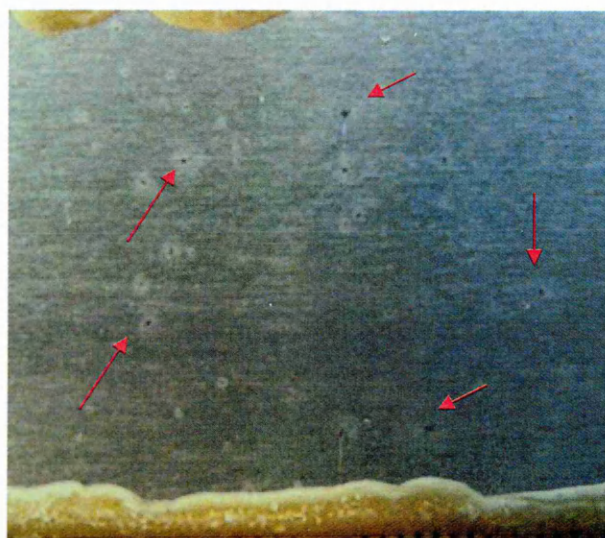
Figure 4-23 Image of PANI/sol16 coated AA2024 after 11 days immersion in 3.5% NaCl solution

An SEM image of the PANI/sol16 after 11 days of immersion, Figure 4-24, reveals pitting, although the depth of pitting is less than that observed for the sol-gel coated sample. However, some cracks are also observed in the coating along with pitting.
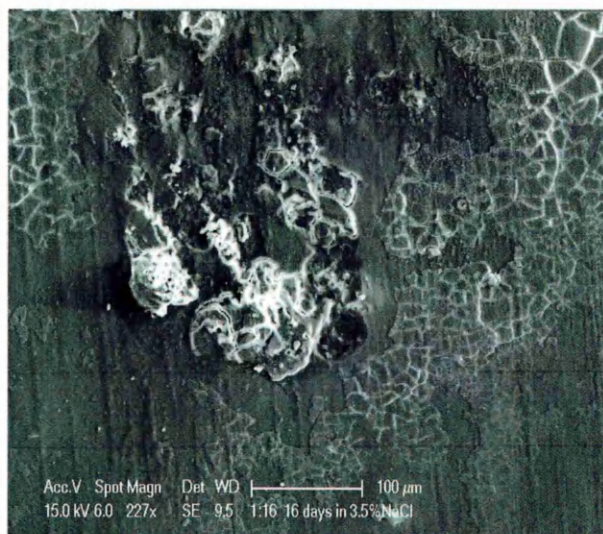
Figure 4-24 SEM image of PANI/sol16 coated AA2024 sample after immersion for 11 days in 3.5% NaCl solution.

Similar results were obtained with the PANI/sol12 (Appendix A), however, it was noted that there were fewer pits, being smaller in size, than the PANI/sol16 formula.

When the relative concentration of PANI: sol-gel is increased to 1:8, i.e. PANI/sol8 the impedance of the coated AA2024 substrate became stable, as shown in Figure 4-25, over a four weeks period.

Figure 4-25 shows a small change in low frequency impedance during 4 weeks of immersion in 3.5% NaCl solution, notably a small increase in the impedance after two weeks of immersion. After 4 weeks of immersion, the impedance dropped and finally became stable (see Figure 4-35 latter). The phase angle curve, Figure 4-26, shows that there are two time constants at about 10^4 and 1.0 Hz. The former displays a slightly decrease after four weeks of immersion, however, the latter increased by prolonged immersion, whilst at the same time, moving towards low frequency region.
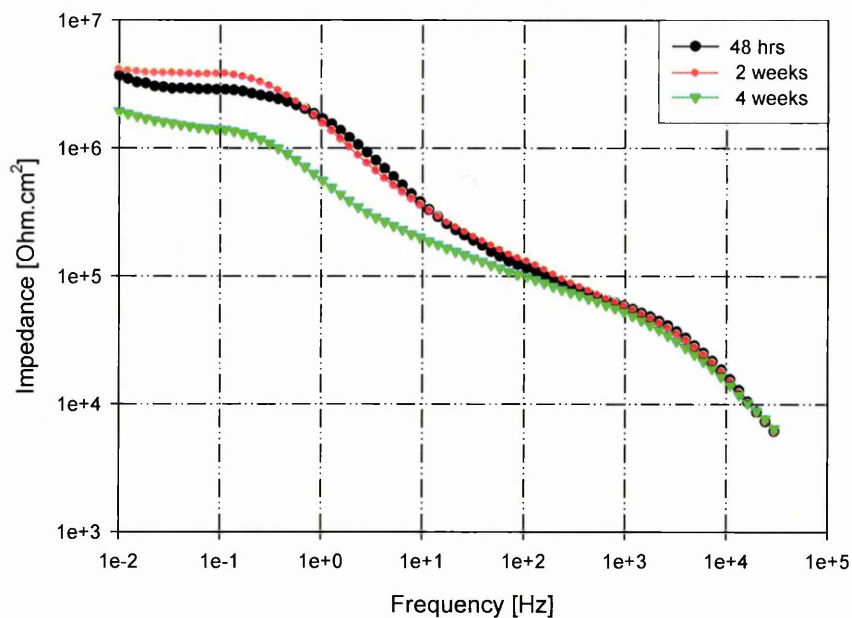
Figure 4-25 Impedance of PANI/sol8 coated AA2024 in 3.5% NaCl solution
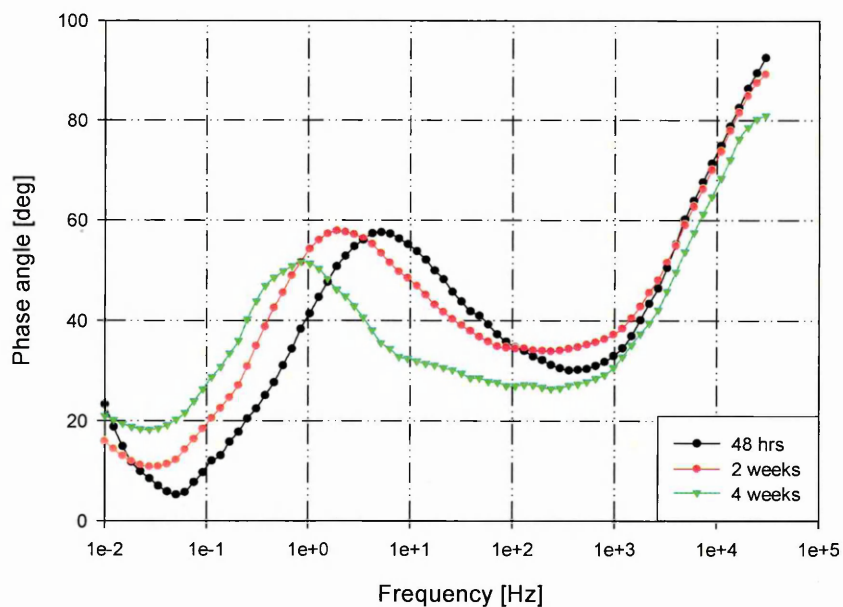
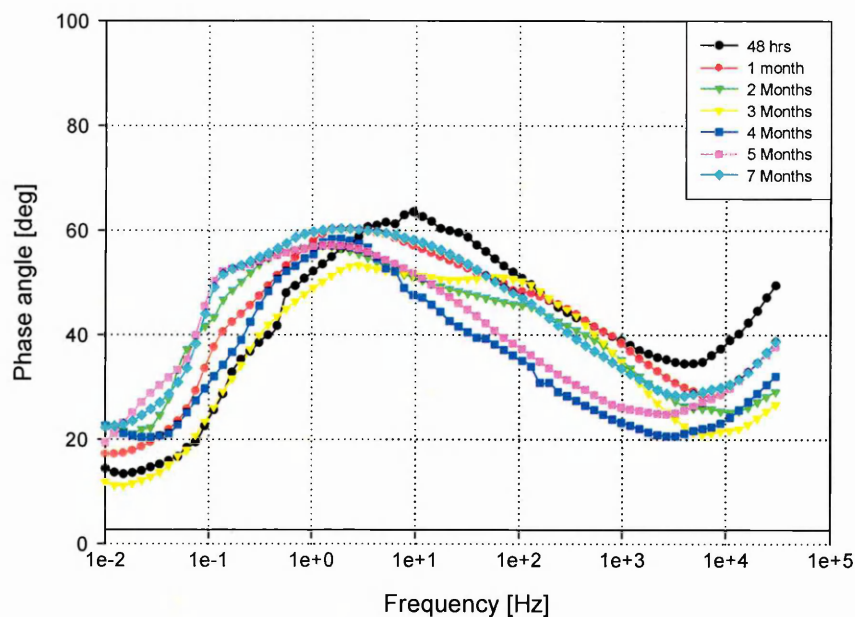**Figure 4-26 Phase diagram of PANI/sol8 coated AA2024 in 3.5% NaCl solution.**

Physical observation of the coating indicated a lack of pitting or delamination, as shown in Figure 4-27. Some dark spots were observed on the surface, these were identified as an accumulation of PANI which did not affect the corrosion performance.

110
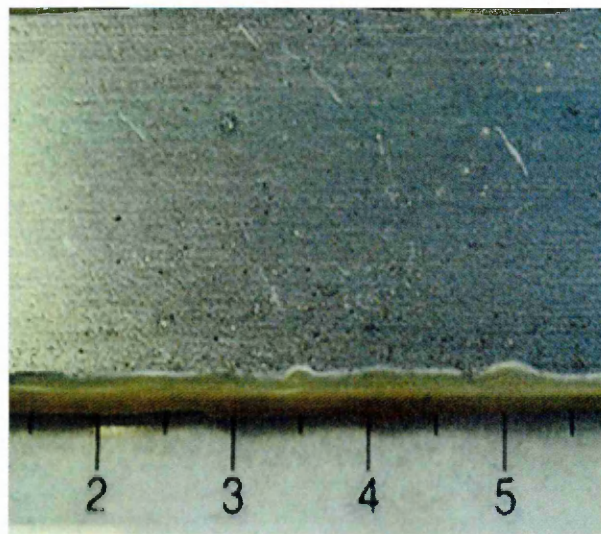
Figure 4-27 Image of PANI/sol8 after 4 weeks immersion in 3.5%NaCl solution

Both PANI/sol4 and PANI/sol1 showed similar behaviour to that of the PANI/sol8 as shown in Figures Figure 4-28 to Figure 4-31.

Both Impedance curves Figure 4-28 and, showed stable values of impedance during the 4 weeks of immersion in the corrosive solution, however, impedance at high frequency decrease in their values with immersion time. Moreover, both phase angle curves, Figure 4-29 and Figure 4-31, showed two time constants at about 10^4 and 1.0 Hz. The latter time constant slightly increased and shifted towards lower frequency with immersion time. This shift accompanied with a decrease of former time constant, at 10^4 Hz.

111
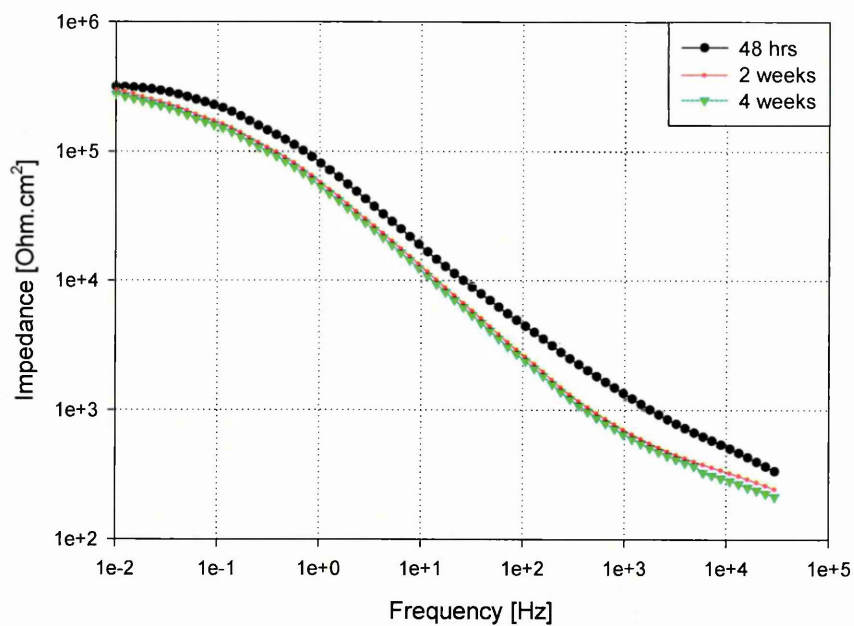
Figure 4-28 Impedance of PANI/sol4 coated AA2024 in 3.5% NaCl solution
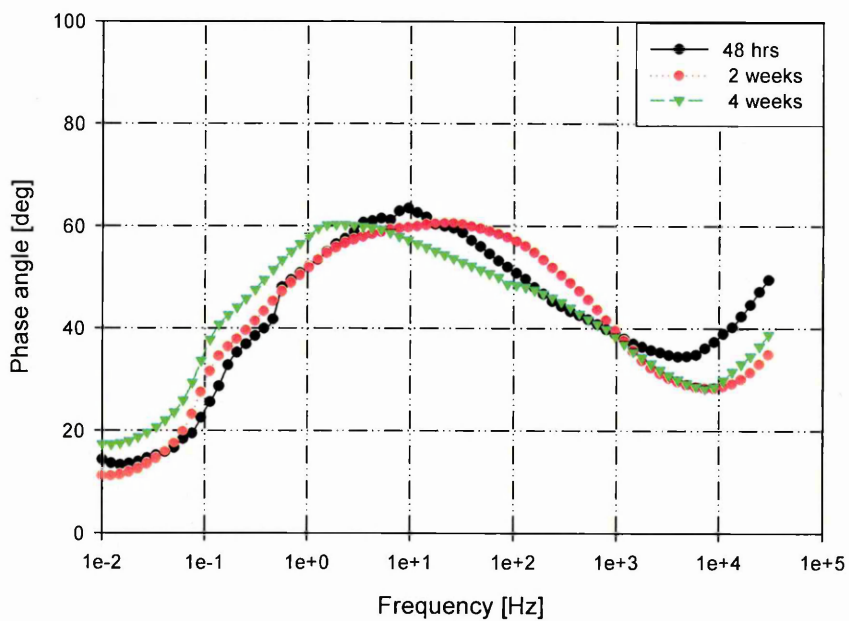
Figure 4-29 Phase diagram of PANI/sol4 coated AA2024 in 3.5% NaCl solution

112
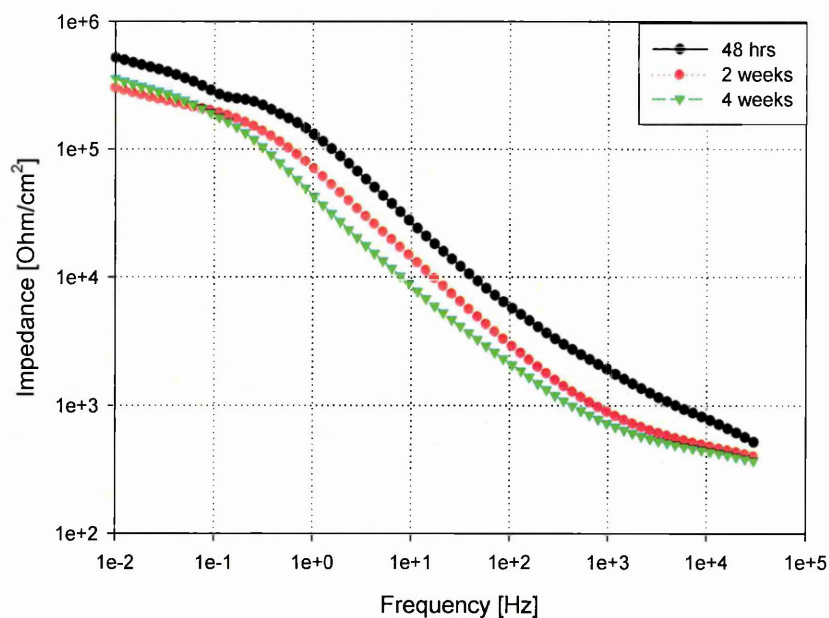
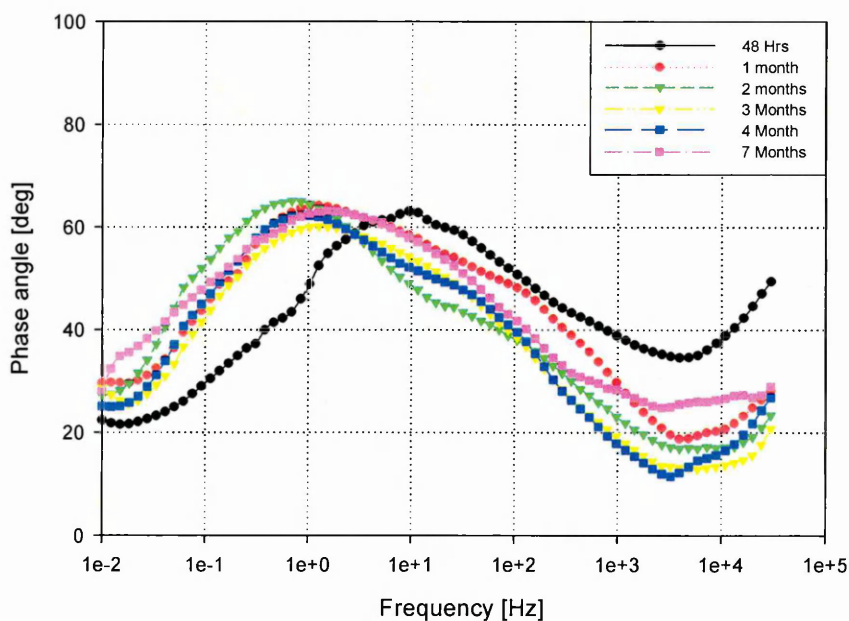**Figure 4-30 Impedance of PANI/sol1 coated AA2024 in 3.5% NaCl solution**
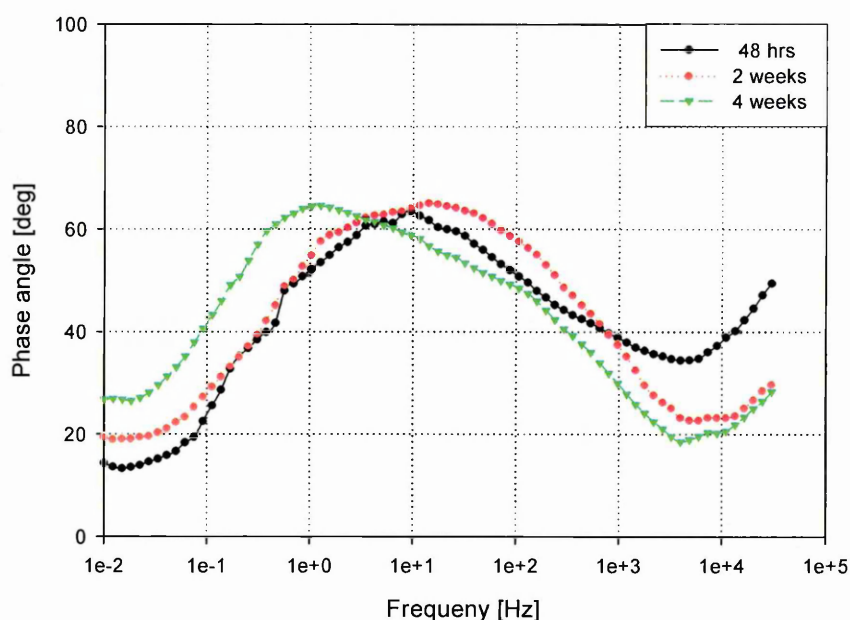
Figure 4-31 Phase diagram of PANI/sol1 coated AA2024 in 3.5% NaCl solution

The three samples had the same corrosion behaviour in 3.5%NaCl solution; they had two time constants at about 10^4 and 1.0 Hz. The high frequency time constant slightly decreased while the low frequency time constant increased and shifted towards lower frequency with immersion time. The low frequency

113

time constant, at 1.0 Hz, was approximately the same value in the three samples.

However, the impedance of PANI/sol8, over 4 weeks period, was greater than that of both PANI/sol4 and PANI/sol1 at all frequency ranges. In addition, PANI/sol8 showed higher phase angle at high frequency range, 10^4 Hz, with respect to PANI/sol4 and PANI/sol1.

4.1.2.6 PANI/sol-gel mixture (prolonged immersion)

For prolonged immersion PANI/sol8, 4 and 1 coated samples were tested in 3.5% NaCl solution for over 7 months. However, before presenting the results of prolonged immersion, the surface morphology of these three samples, before immersion, were investigated. Figure 4-32 provides details of the surface morphology and cross section of all three samples. It can be seen that the surface of PANI/sol8 was uniform and there are some wave like features which may be a result of shrinkage during curing. Some other surface features appeared on increasing the amount of PANI in the sol-gel matrix (discussed later) as shown in Figure 4-32.
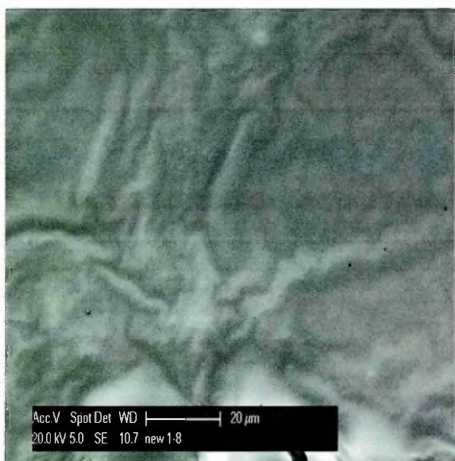
PANI/sol8
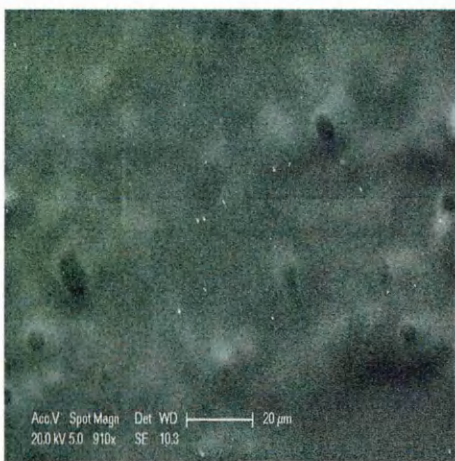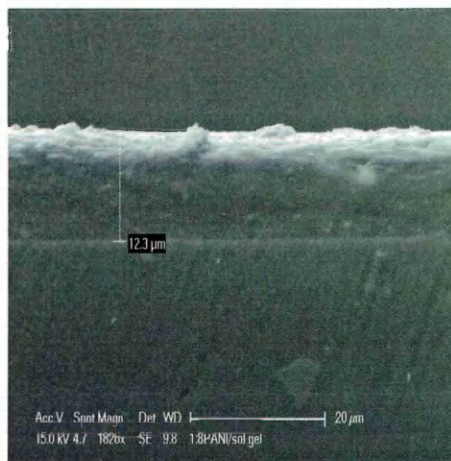
PANI/sol4
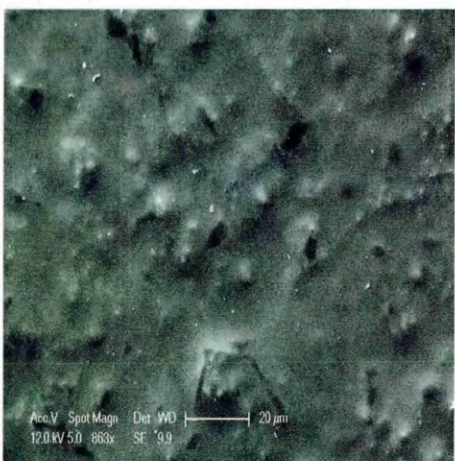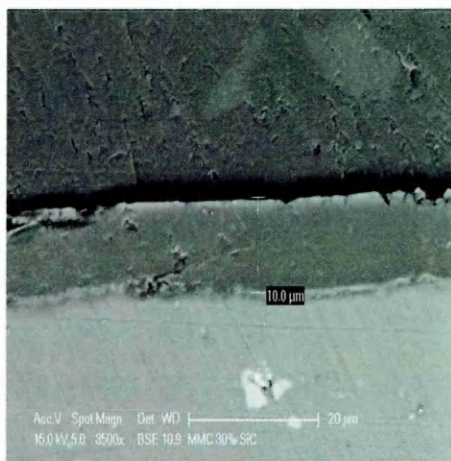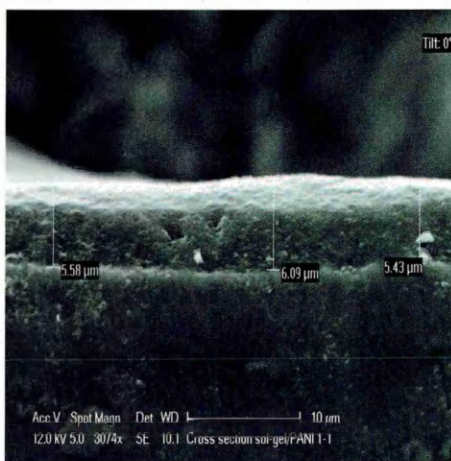
PANI/sol1

Figure 4-32 Surface morphology and cross section of different PANI/sol-gel coatings
before immersion

Moreover, the thickness of the PANI/sol-gel coatings decreases with increasing PANI content; typically 12-13 μm, 9-10 μm and 5-6 μm for the PANI/sol8, PANI/sol4 and PANI/sol1 respectively.

The features appearing in PANI/sol1 were further investigated using EDX mapping, as shown in Figure 4-33.
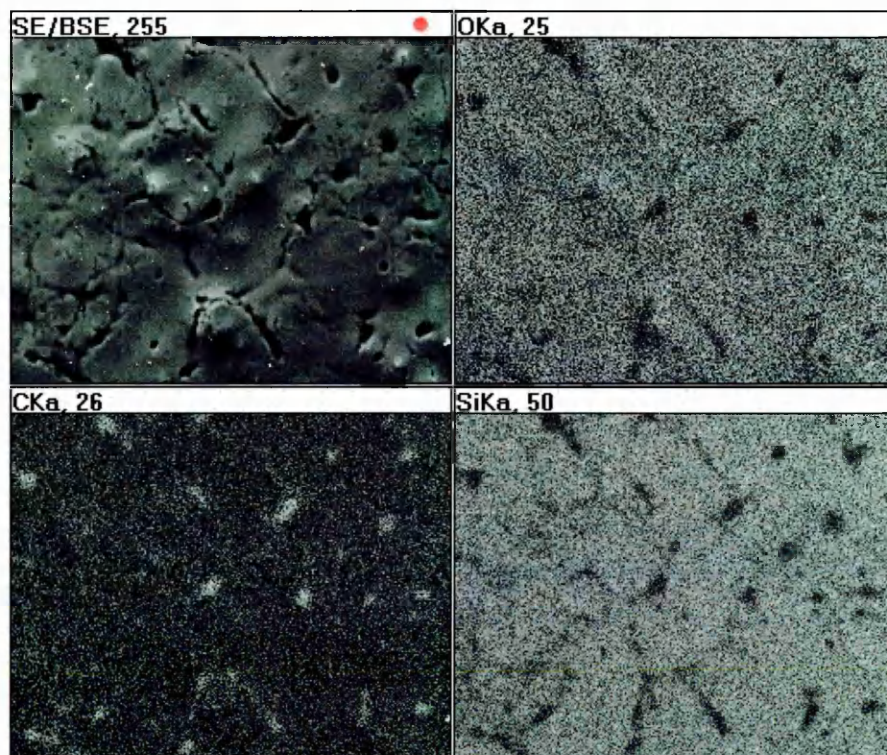
Figure 4-33 EDX mapping of PANI/sol1 sample

From the results of EDX mapping, it can be seen that, these features consisted of mainly carbon, where the carbon represents both polymer and the hybrid silica sol-gel. Comparison of the C and Si maps in Figure 4-33 shows that the dark area in the back scatter image consist of C and represents poor dispersion of the PANI.

Furthermore, by increasing the PANI content in the PANI/sol-gel coating the surface of the coated sample became less uniform and took on the appearance of a porous coating, as shown in Figure 4-34. Such features may affect both the corrosion and mechanical performance of the coating.
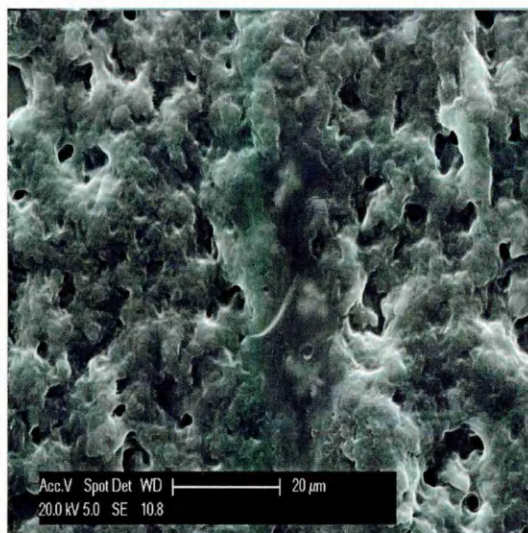
Figure 4-34 SEM image of PAN/sol0.25

The investigation of corrosion performance of PANI/sol8 sample was continued using EIS in 3.5 NaCl solution for up to 24 months. Figure 4-35 shows the coating maintains a stable impedance over this 24 month period of immersion. At the low frequency range (0.01 Hz) the impedance decreased from 4×10^6 to 0.9×10^6 Ohm.cm^2 after 2 months of immersion. However, it remained stable for the remaining 24 months, at about 1×10^6 Ohm.cm^2

The phase angle curve shown in Figure 4-37, highlights a dramatic decrease in phase angle at high frequency (1000-5000 Hz) in the first three months. After this period, it became stable for the remaining 24 months. The curve shows two time constants at 10^4 and 8 Hz. The latter moves from 8 to 0.5 Hz after one month of immersion, moreover, the maximum of this time constant peak was stable during the immersion period.

Figure 4-37 presents two samples of PANI/sol8 after 24 months of immersion in 3.5% NaCl solution. The samples did not show any delamination during this period of testing, however, 2 pits (arrows) has developed on one sample, after 21 months, no pitting was observed on the second sample. The dark spots observed on the sample are the accumulation of PANI in the sol-gel matrix which was originally present in the coating in Figure 4-27.

117
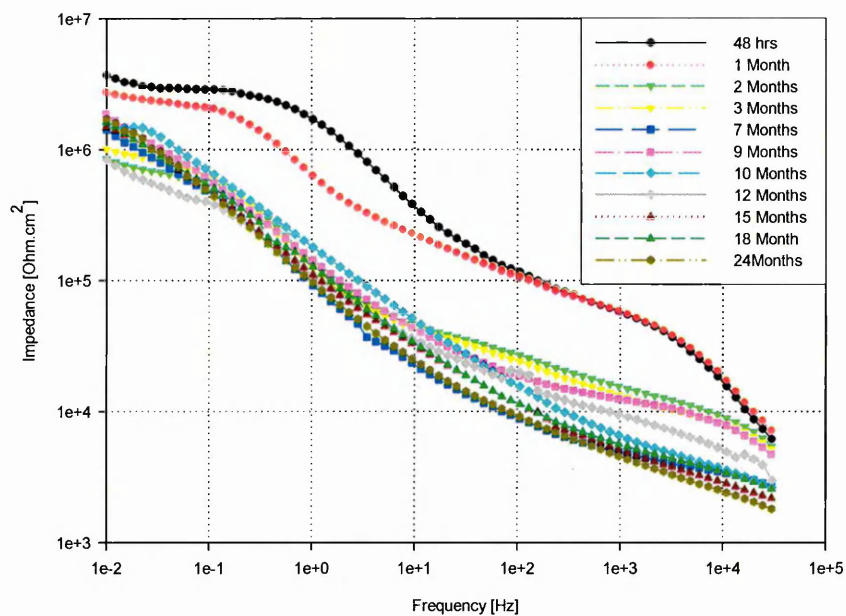
Figure 4-35 Impedance of PANI/sol8 coated AA2024 in 3.5% NaCl solution up to 24 months.
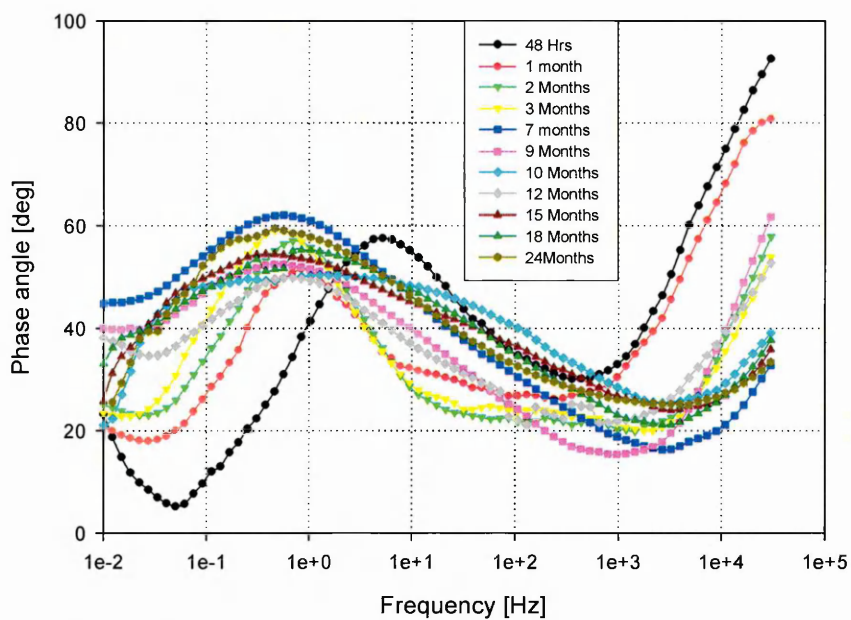
Figure 4-36 Phase diagram of PANI/sol8 coated AA2024 in 3.5% NaCl solution up to 24 months.

118

Figure 4-37 Image of PANI/sol8 coated AA2024 in 3.5% NaCl solution up to 24 months

Stable impedance behaviour was exhibited by the PANI/sol4 sample during 7 months of immersion in 3.5% NaCl solution as shown in Figure 4-38. Moreover, the phase angle, Figure 4-39, showed two time constants at 10^4 and 5 Hz. The latter shifted from 5 to 0.4 Hz after a month of immersion, becoming stable around this frequency. Furthermore, the phase angle at this frequency remained stable over the 7 months period.
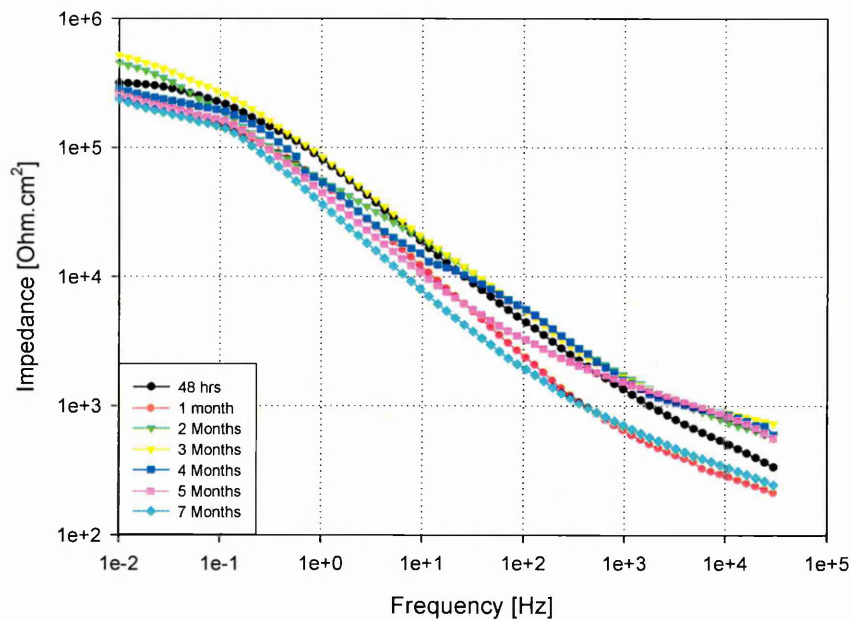
Figure 4-38 Impedance of PANI/sol4 coated AA2024 in 3.5% NaCl solution up to 7 months.

Figure 4-39 Phase diagram of PANI/sol4 coated AA2024 in 3.5% NaCl solution up to 7 months.

The final PANI/sol-gel combination having a ratio of 1:1 exhibited a stable impedance value, at about 5×10^5 Ohm.cm^2, over the 7 months immersion period. Figure 4-40 shows an initial inductive peak at 0.1 Hz after 2 days of immersion which disappeared with immersion time. The phase angle showed

120

two time constants at 10^4 and 10 Hz after 48 hrs immersion period. The latter moved from 10 to 1.0 Hz after one month of immersion remaining stable around this frequency.
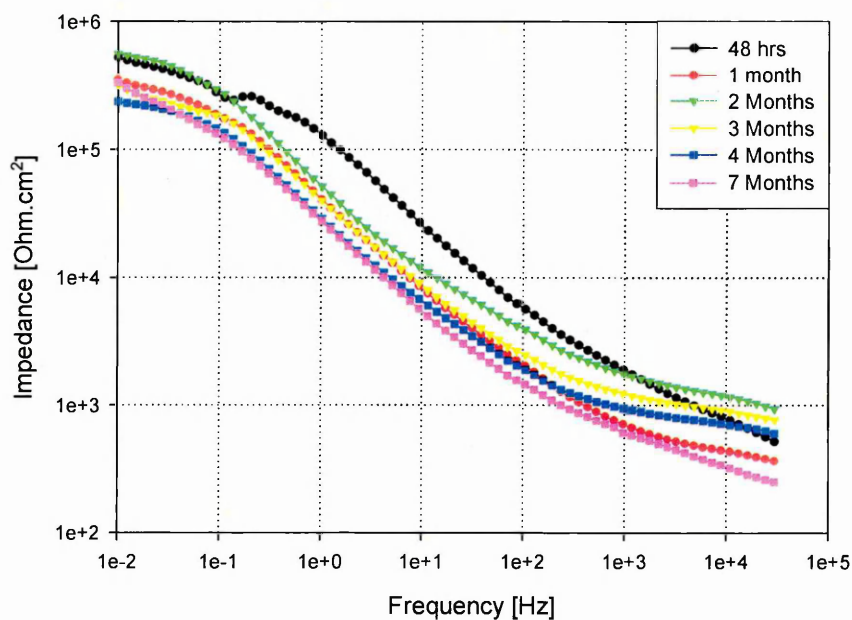
Figure 4-40 Impedance of PANI/sol1 coated AA2024 in 3.5% NaCl solution up to 7 months

Figure 4-41 Phase diagram of PANI/sol1 coated AA2024 in 3.5% NaCl solution up to 7 months

The above results showed that PANI/sol8, PANI/sol4 and PANI/sol1 had the same behaviour in 3.5%NaCl solution with some changes; PANI/sol8 sample has the highest overall impedance with respect to PANI/sol4 and PANI/sol1 samples. At the same time, it has the highest phase angle at high frequency, 10^4 Hz. This behaviour remained stable with the time of immersion, even though all combinations' phase angles decrease with time at that frequency. Moreover, it can be seen that the phase angle position remained at approximately the same position, 1.0Hz, however, its value increased slightly with increasing PANI content from $\approx$ 50 to $\approx$55 then to $\approx$60 deg for PANI/sol8, PANI/sol4 and PANI/sol1 respectively.

PANI/sol8 showed the highest impedance in 3.5% NaCl solution (pH=6.8), therefore, it was used during studying the corrosion performance of PANI/sol-gel coated AA2024 in other different tests.

4.1.3 Immersion in Acidic Solution

The corrosion performance of PANI/sol-gel coated AA2024 was investigated in acidic sodium chloride solution. Figure 4-42 presents the impedance of PANI/sol8 in 3.5% NaCl (pH=3.5) solution along with the impedance of a bare sample for comparison. The impedance of the coated sample (10^5 Ohm/cm^2) is one and half orders of magnitude higher that that of bare sample (3.5×10^5 Ohm/cm^2).

The impedance drops by half of an order of magnitude after the first three days of immersion and then it remained stable, at about 1×10^5 Ohm/cm^2, during the remaining 2 months of immersion.

The phase angle, Figure 4-43, showed two time constants for the coated sample one at about 5×10^3 Hz and the other at about 3.0 Hz, however, the bare sample showed one time constant at about 10 Hz. The high frequency time constant of the coated sample decreased with the time of immersion, moreover, this time constant has shifted towards the low frequency. However, the second time constant seemed to have gradually increased with immersion.

It can be seen that, the overall impedance of coated sample in acidic solution is lower than that of an equivalent coated sample in neutral solution (Figure 4-35).
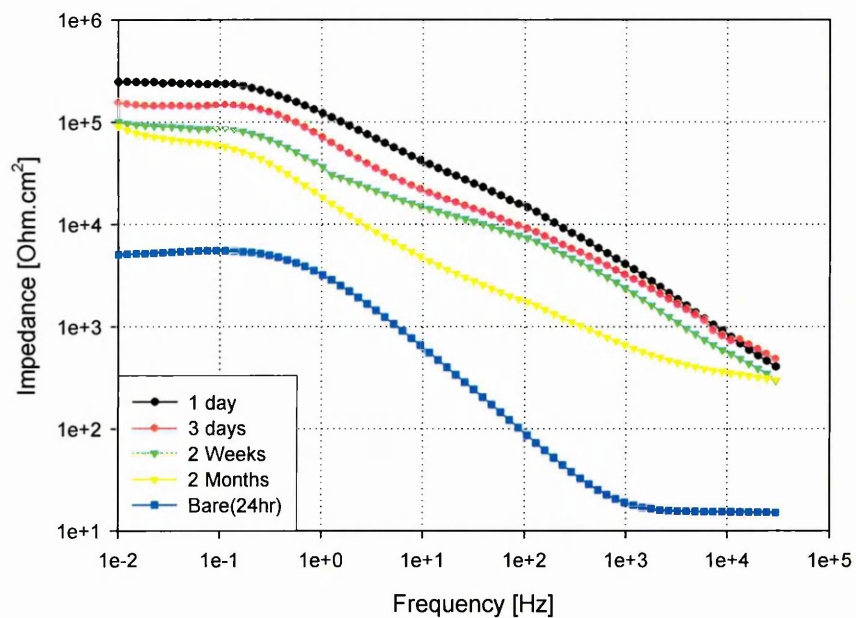
Figure 4-42 Impedance of bare and PANI/sol8 coated AA2024 in 3.5% NaCl (pH=3.5) solution.
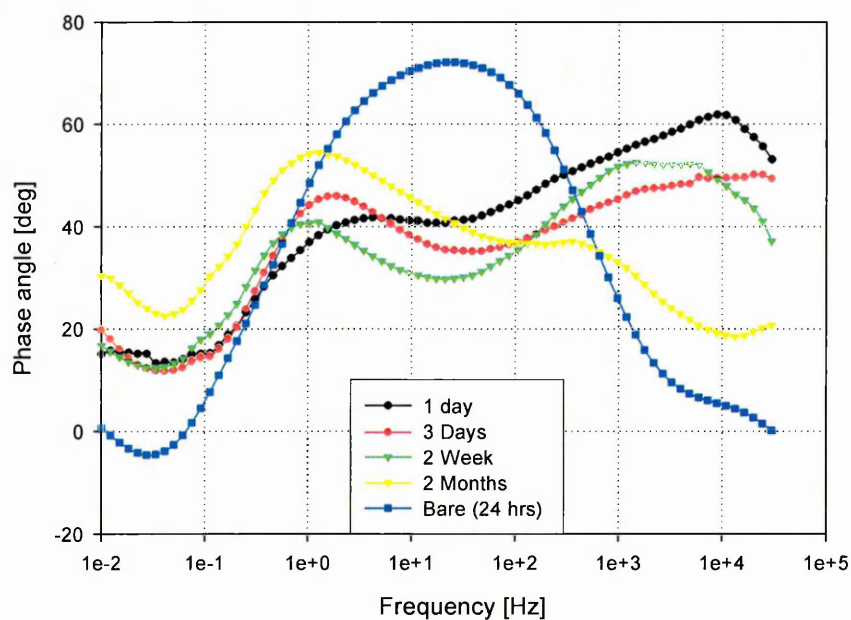
Figure 4-43 Phase angle of bare and PANI/sol8 coated AA2024 in 3.5% NaCl (pH=3.5) solution.

123

4.1.4 Immersion in Alkaline Solution

The EIS coating performance of PANI/sol8 samples were evaluated in 3.5% NaCl at a pH value of 9.2. The impedance and phase angle curves are shown in Figure 4-44 and Figure 4-45 respectively.
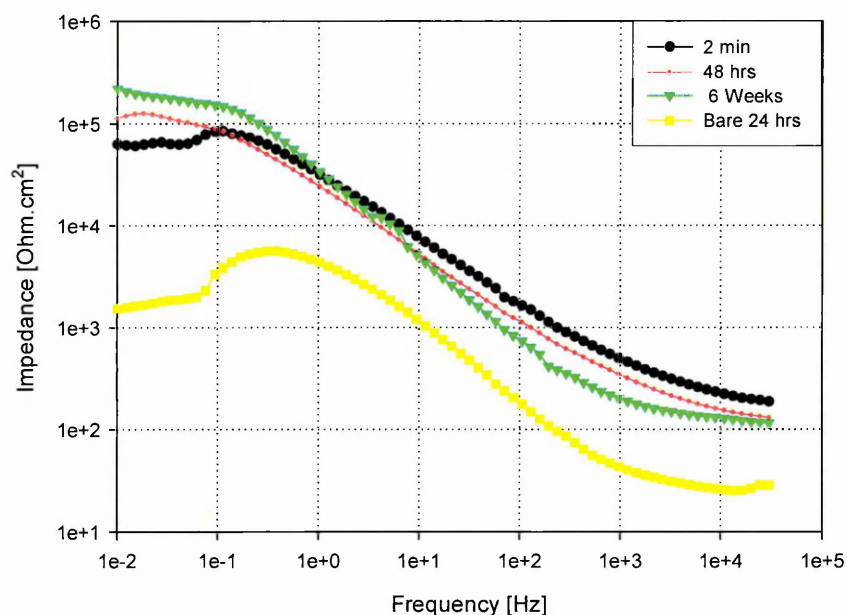
Figure 4-44 Impedance of PANI/sol8 coated AA2024 in 3.5% NaCl (pH=9.2) solution.
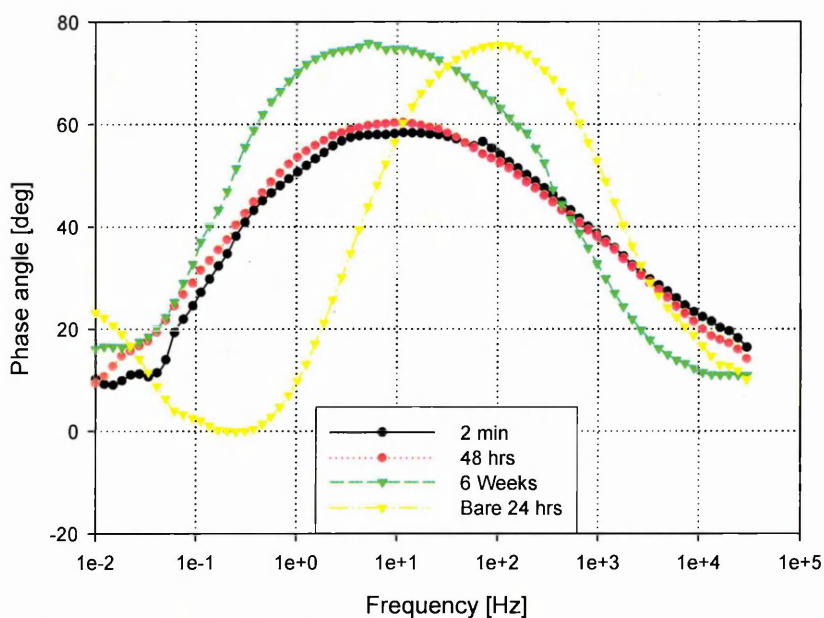
Figure 4-45 Phase angle of PANI/sol8 coated AA2024 in 3.5% NaCl (pH=9.2) solution.

The impedance curve, Figure 4-44, showed that the coated sample is one and a half orders of magnitude greater than that of the bare sample. Interestingly, the impedance of the coated sample increased with increasing time of immersion. Initially, the impedance showed an inductive peak after 2 min of immersion, which decreased with respect to that of 2 hrs, after 48hrs. The high frequency impedance, at 10^4 Hz, showed smaller values, $\approx$180 Ohm.cm^2, with respect to that of both equivalent coated samples in neutral and acidic media in the same period of immersion, Figure 4-36 and Figure 4-42 respectively.

The phase angle, Figure 4-45, showed a single time constant for both bare and coated samples. The phase angle maximum increased with immersion time; however, remaining constant at the same frequency. This behaviour combined with an increase in impedance. Pitting was observed on the bare sample after 2 days of immersion.

The behaviour of PANI/sol8 was improved by adding 0.5%TiO_2 (particle size 30 nm) to the coating mixture (1 volume PANI+ 8 volumes sol-gel) as shown in Figure 4-46. In this case the impedance increased by one order of magnitude, at all frequency ranges when compared to the coating without TiO_2. The impedance decreased initially by about a half of an order of magnitude (after 24 hrs) but then remained stable during the following 2 months of immersion in the alkaline solution.

The phase angle, Figure 4-47, of TiO_2 doped coating increased by at least 30 deg, in high frequency range, compared to coating without TiO_2. Moreover, it showed two time constants at 10^4 and 10 Hz. The high frequency time constant decreased with increasing time of immersion, however, the low frequency time constant increased and shifted towards lower frequency.

Adding 0.5% TiO_2 changed the thickness of the PANI/sol8 by less than 1µm as shown in the SEM image in Figure 4-48.
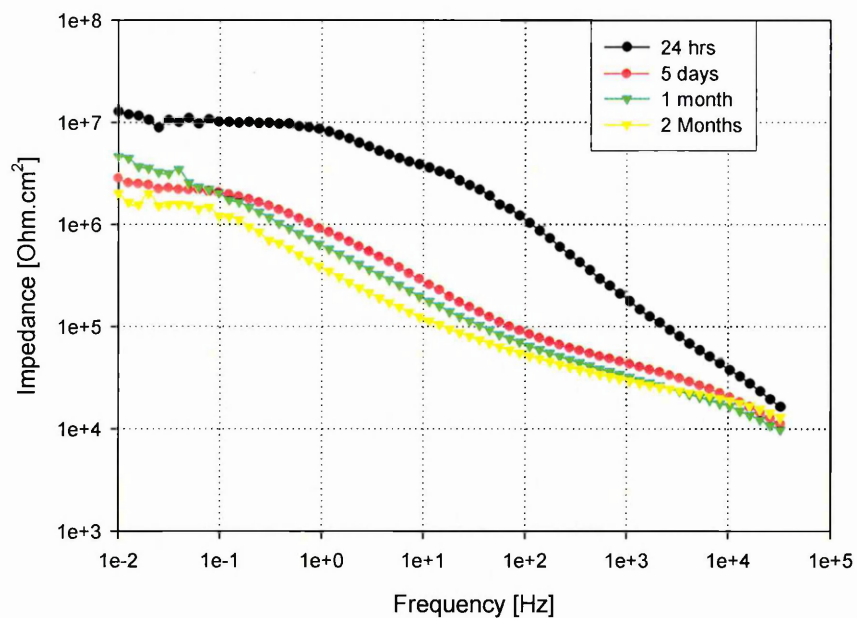
Figure 4-46 Impedance of PANI/sol8 +0.5% TiO$_2$ coated AA2024 in 3.5% NaCl (pH=9.2) solution.
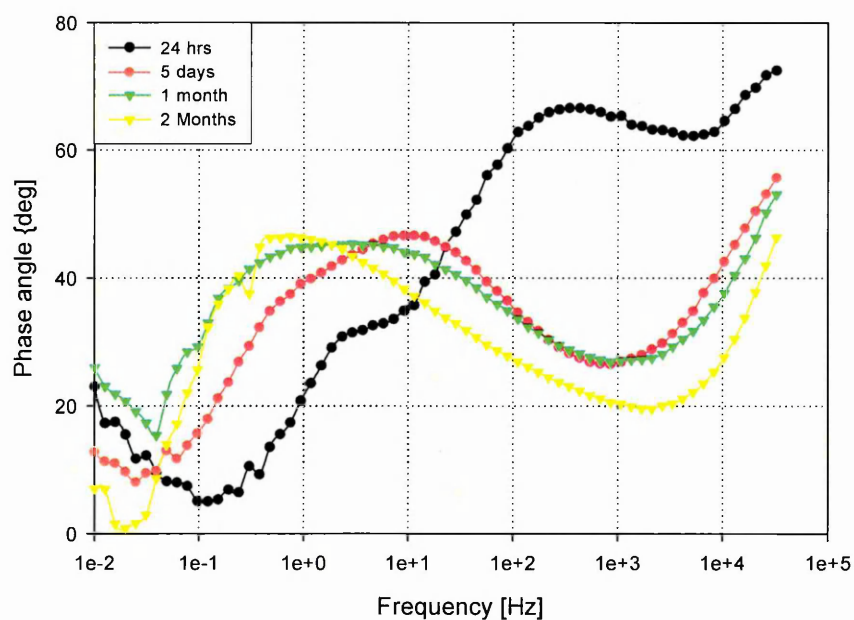
Figure 4-47 Phase angle of PANI/sol8 +0.5% TiO$_2$ coated AA2024 in 3.5% NaCl (pH=9.2) solution

Acc.V Spot Magn Det WD
20.0 kV 4.7 3288x SE 9.9

14.1 μm

10 μm
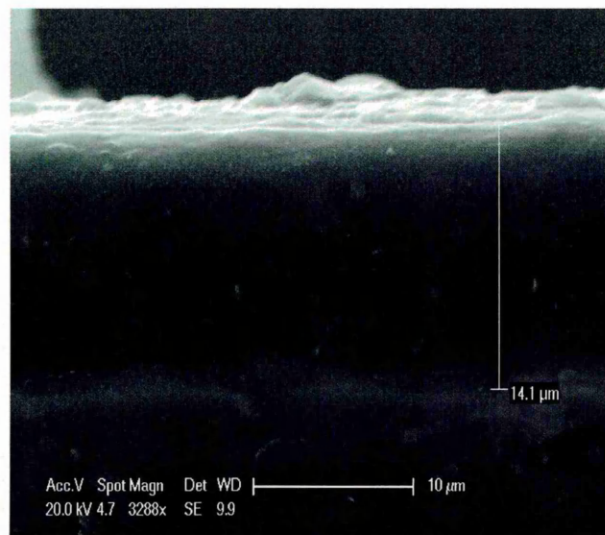
Figure 4-48 SEM image of PANI/sol8 +0.5%TiO$_2$

4.1.5 Salt Spray Test

This test was conducted to evaluate the effectiveness of the PANI/sol-gel coatings as a protective coating for AA2024 material for long term exposure.

In this standard test, all samples were subjected to 500 hours of salt-fog of 5% NaCl in 100% humidity at 40°C. At least 4 samples of each system were subjected to SST; two of the samples were scratched as was the bare samples.

4.1.5.1 Bare and sol-gel coated samples

Figure 4-49 shows the image of bare sample after 72 hrs salt spray testing. It can be seen that a white substance has covered the entire surface of bare sample; moreover, pitting can be seen by the naked eye. An SEM image of the bare sample, after 72hrs in SST, is showing in Figure 4-50, where pits of different sizes are distributed on the surface. These results highlight the aggressiveness of the salt fog environment to the bare metal.

127
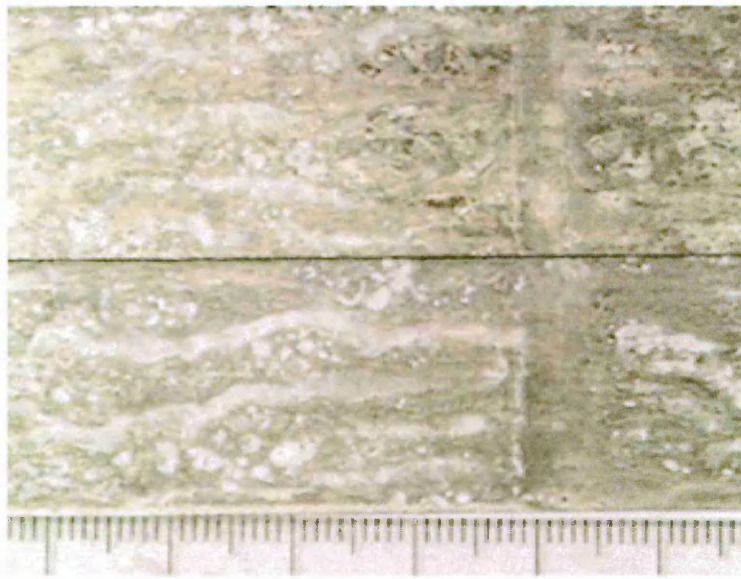
Figure 4-49 Image of bare AA2024 after 72 hrs in salt spray test.
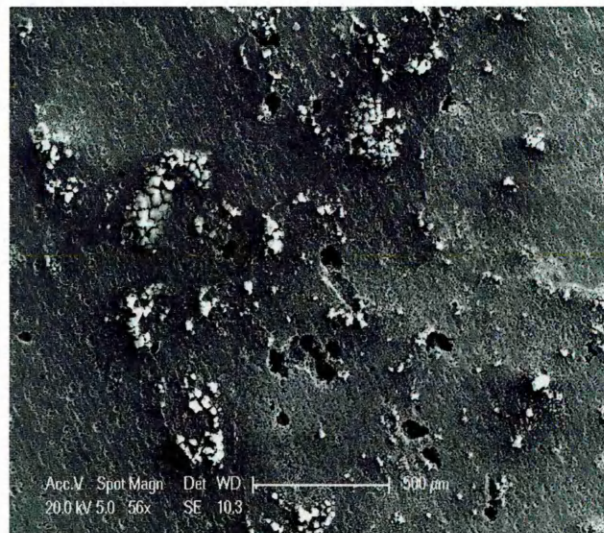
Figure 4-50 SEM image of bare AA2024 after 72hrs in SST

Sol-gel coated samples were also subjected to the salt spray test as shown in Figure 4-51. This figure shows that the sol-gel coated sample has many pits (white spots) after 168 hrs within the SST environment. Numerous pits within and outside of the scratched area appeared after 48 hrs. In addition, the sol-gel coating delaminated at several points along the scratch after 250 hrs. SEM analysis, Figure 4-52, shows pitting at the scratch along with and delamination of the coating (arrowed). EDX mapping was used to identify the degree of delamination of the coating, Figure 4-53.

128
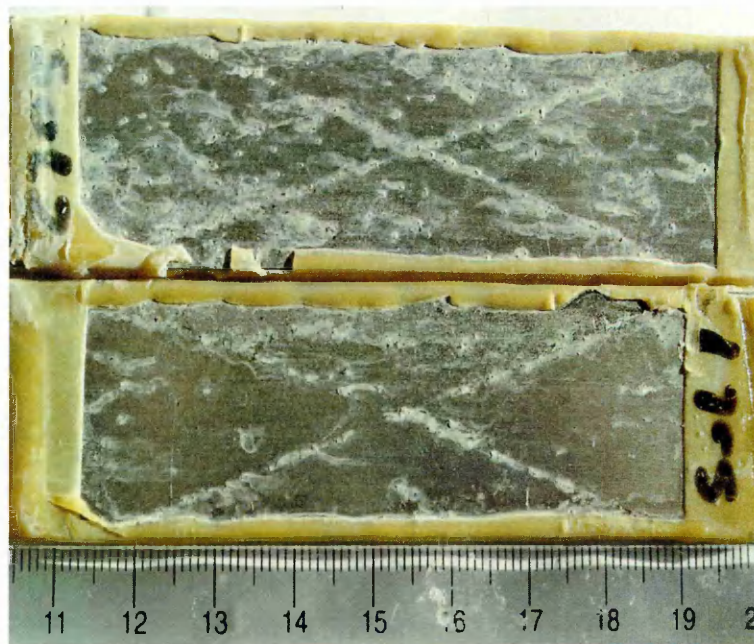
Figure 4-51 Image of sol-gel coated AA2024 after 168 hrs in salt spray test.
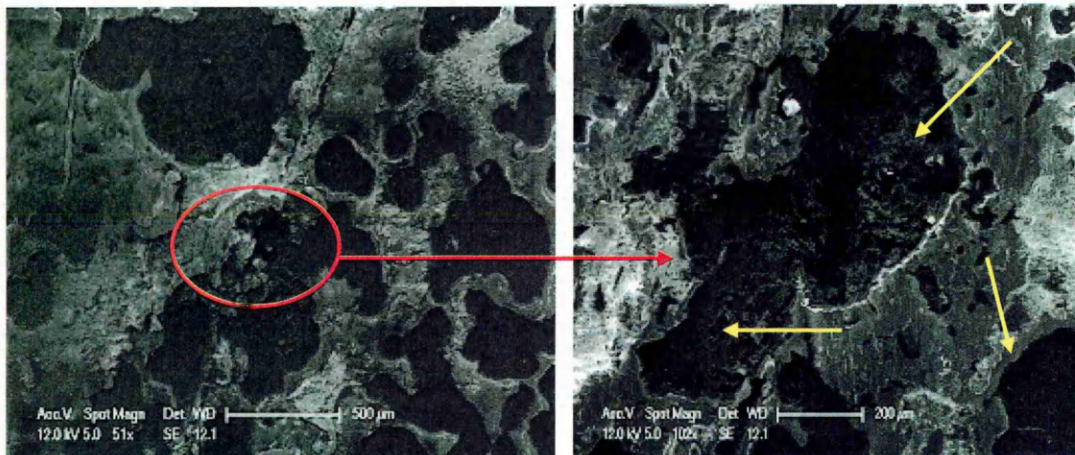
Figure 4-52 SEM image of sol-gel coated AA2024 after 250 hrs in salt spray test.

From Figure 4-53, it can be seen that silicon is absent inside and around the pit; moreover, it shows that copper and chloride along with aluminium is present within the pit. Furthermore, aluminium chloride and oxide cover the delaminated area. These results suggest that the sol-gel coating alone is not suitable for protecting AA2024 from corrosion.

129
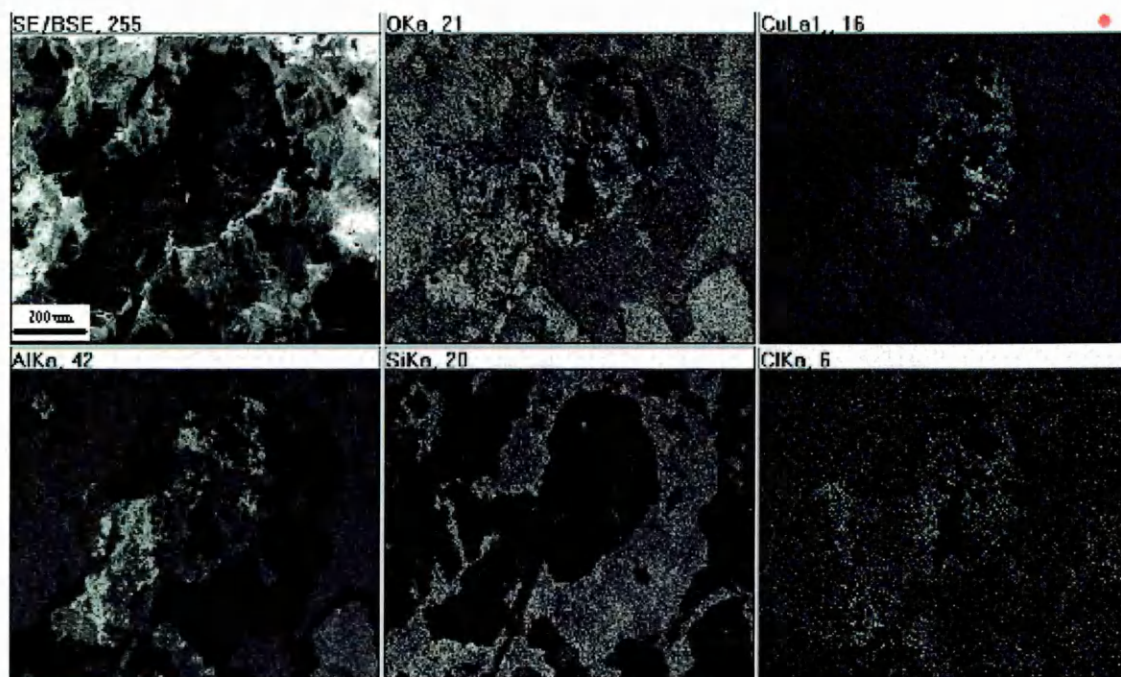
Figure 4-53 EDX maps of a pit in the sol-gel coated AA2024 after 250 hrs in SST

4.1.5.2 PANI/sol-gel coated samples

The PANI/sol8 coated AA2024 samples shown in Figure 4-54 represent 72 hrs in salt spray test. An improvement in the protection can be seen that with limited pitting in the scratch and no pitting away from the scratch. The unscratched samples, Figure 4-55, did not show any sign of pitting or delamination of the coating after 72 hrs of SST.
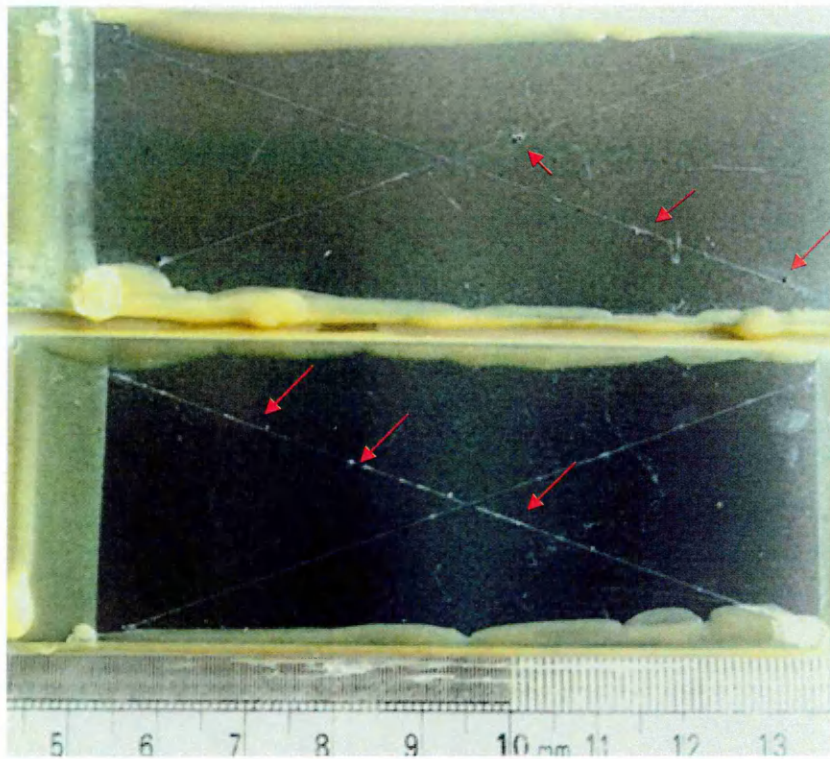
Figure 4-54 Image of PANI/sol8 coated AA2024 after 72 hrs in salt spray test.
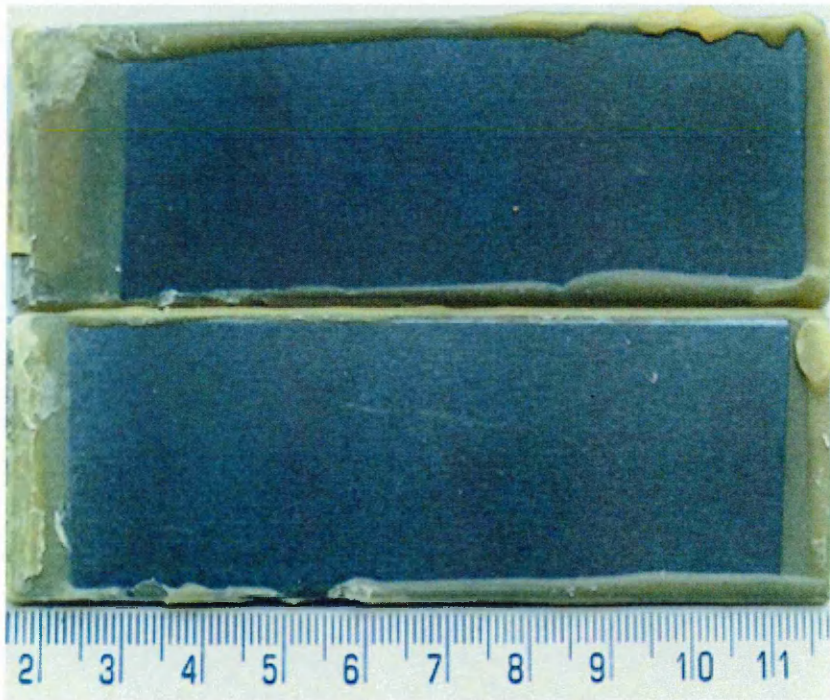
Figure 4-55 image of PANI/sol8 coated AA2024 (non-scratched)
after 72 hrs in salt spray test.

After 300 hrs SST, Figure 4-56, pitting was observed in the scratch. Again no damage was observed for the unscratched samples after 300 hrs, Figure 4-57.

131
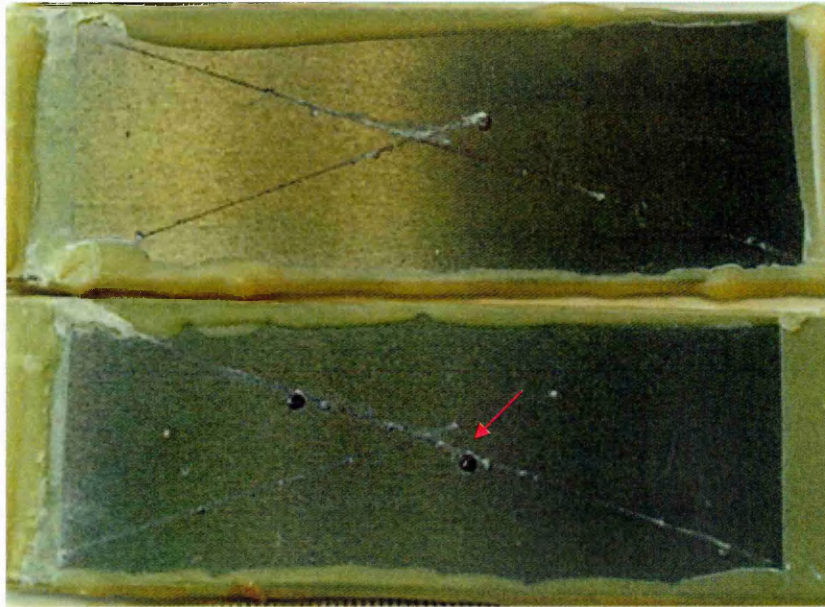
Figure 4-56 Image of PANI/sol8 coated AA2024 after 300 hrs in salt spray test.
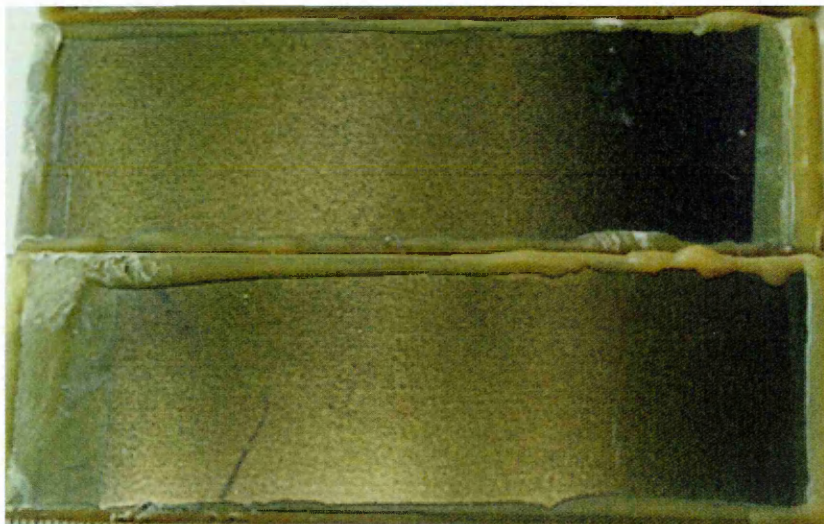
**Figure 4-57 Image of PANI/sol8 coated AA2024 (non-scratched)
after 300 hrs in salt spray test.**

Figure 4-58 represents the scratched PANI/sol8 samples at the end of 500 hrs of SST, no more pitting appeared along the scratch. Moreover, the size of pits seems to be stable and there is no delamination or undercut along or around the scratch. The figure shows that the samples were shiny and there is no crystallisation of sodium chloride on the surface of the sample. The unscratched

132

samples, Figure 4-59, showed a slight reduction in gloss after 500 hrs, although no delamination or pitting appeared during the course of the test.
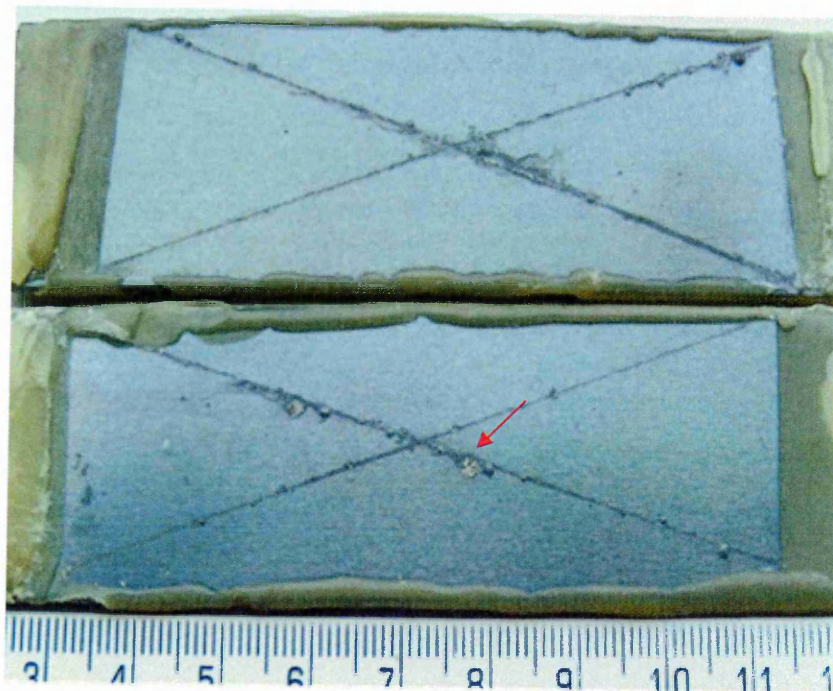
Figure 4-58 Image of PANI/sol8 coated AA2024 after 500 hrs in salt spray test.
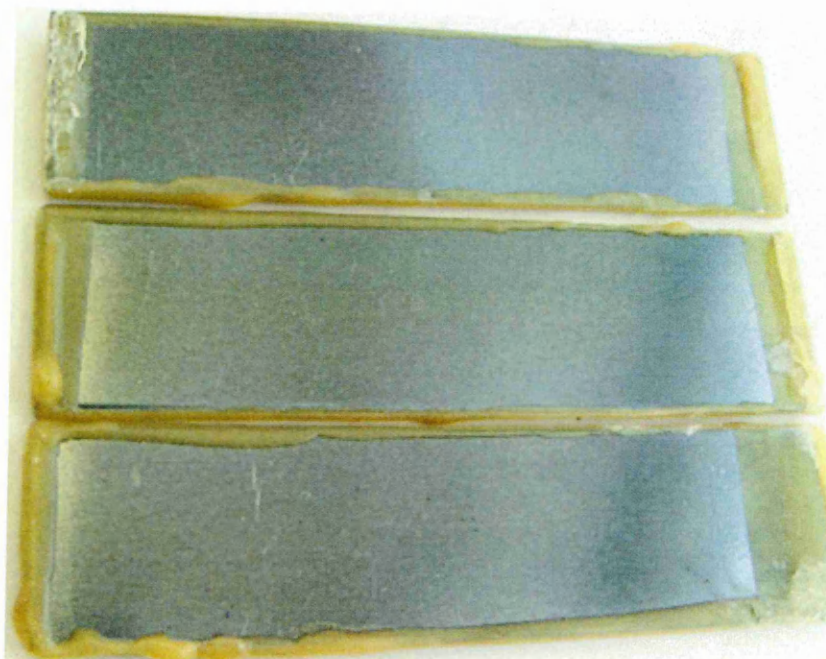
Figure 4-59 Image of PANI/sol8 coated AA2024 (non-scratched) after 500 hrs in salt spray test.

133

4.1.5.3 Post-treated PANI/sol-gel coated samples

"Post treated" PANI/sol8 samples were prepared as described in chapter 3. This post treatment was applied to improve the corrosion performance of "damaged" i.e. scratched samples during SST. In this section only the results for scratched samples are presented.

Post-treated samples were scratched and then subjected to the standard SST for up to 500 hrs. Figure 4-60 shows the post treated sample after 250 hrs in SST. No signs of corrosion, undercutting, or delamination in or away of the scratch was observed. The performance of the coating did not change during the 500 hrs of SST as shown in Figure 4-61.
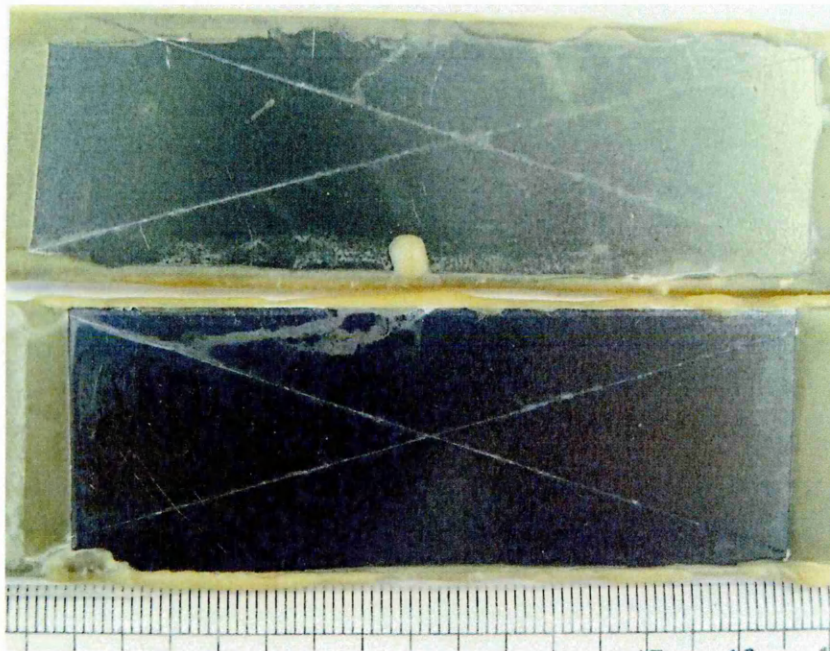
Figure 4-60 Image of post-treated PANI/sol8 coated AA2024 after 250 hrs in salt spray test.
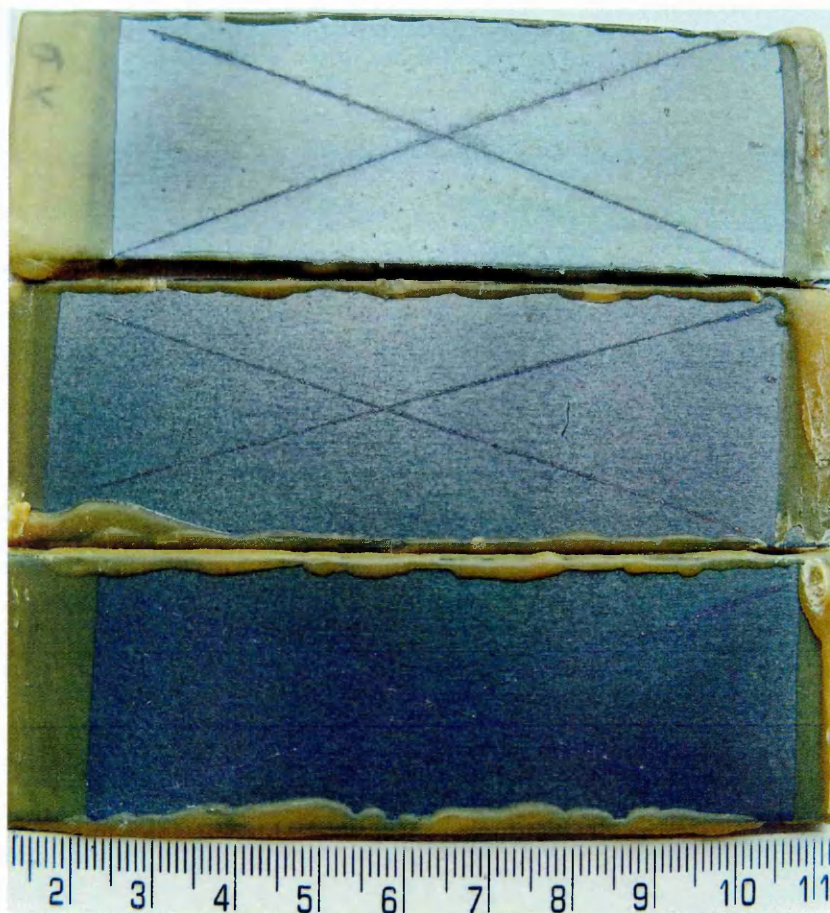
**Figure 4-61 Image of post-treated PANI/sol8 coated AA2024 samples
after 500 hrs in salt spray test.**

Following, the 500 hrs of SST, the sample was then subject to a sellotape pull off (adhesion) test for 20 times. No delamination or undercutting was observed after the test.

After 500 hrs in SST, the pre-scratched sample was washed with deionsed water and then immersed in 3.5%NaCl solution for an hour before conducting EIS.measurements. The results shown in Figure 4-62 indicate an overall impedance is 1.6×10^5 Ohm.cm^2. The high frequency, 10^4 Hz, impedance showed a smaller value, 100 Ohm.cm^2, which may relate to the scratched area was directly exposed to the electrolyte.

The phase angle plot shows two time constants , at 10^3 and 0.8 Hz. Where the latter seems to have the same value and position as an untreated PANI/sol8 coated sample in the same solution. Furthermore, the phase angle showed a small value (10 deg) at high frequency, $>10^4$ Hz, with respect to unscratched sample Figure 4-26.

135
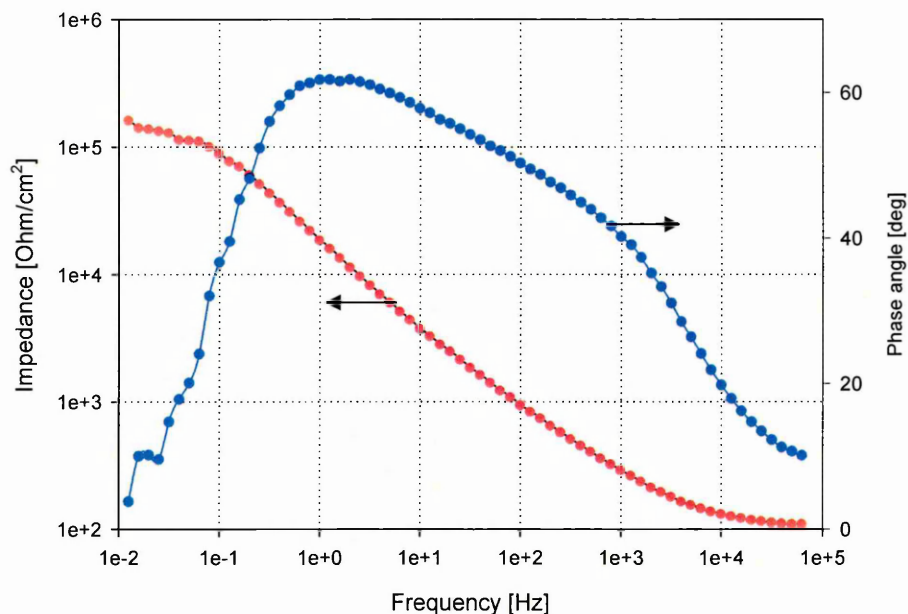
Figure 4-62 Bode plot of post treated scratched PANI/sol8 coated AA2024 after 500 hrs SST.

To investigate whether or not the post-treatment did affect the corrosion behaviour of the PANI/sol-gel coating; EIS was carried out for the post treated sample. The Impedance curve of the post-treated sample, Figure 4-63, showed that the impedance at high frequency, 10^4 Hz, has a capacitive behaviour and this behaviour was stable with time of immersion. Moreover, the impedance behaviour seems to be the same as PANI/sol8 in the low frequency range, however, the post treated sample showed higher low frequency impedance (8×10^7 Ohm.cm^2) compared to that of untreated PANI/sol8 (2×10^6 Ohm.cm^2).

The phase diagram, Figure 4-64, shows capacitive behaviour (85 deg) at the high frequency range during four weeks of immersion.

At lower frequencies, the coating response is similar to a normal PANI/sol-gel sample, where there was a time constant that shifts towards the low frequency. This did not however appear to affect the impedance which remained almost constant with time of immersion, at about 8×10^7 Ohm.cm^2.

The post treatment increased the cross section thickness of the coating by about 3-4µm as shown in Figure 4-65.

These results showed that post treatment improved the corrosion performance in both constant immersion and salt spray tests.

136
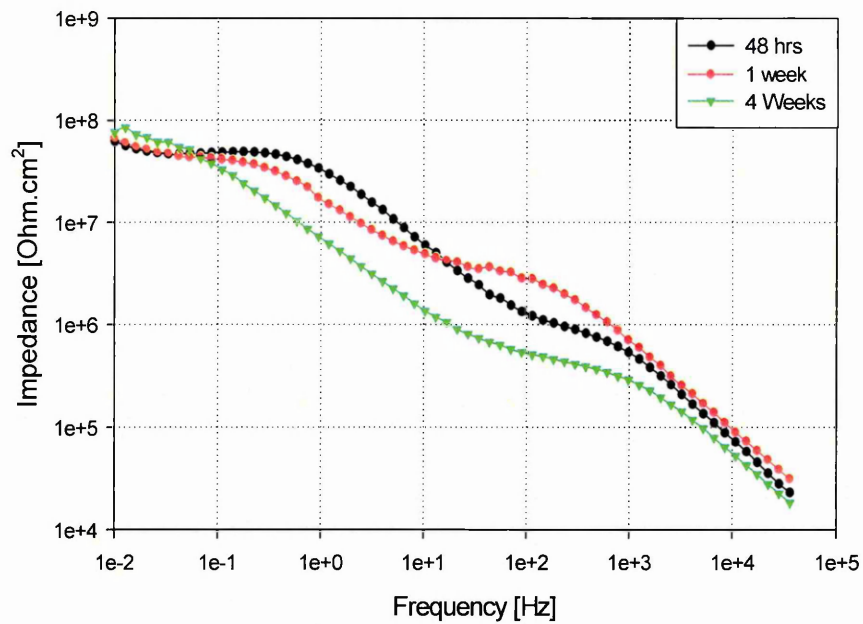
Figure 4-63 Impedance curve of post-treated PANI/sol8 coated AA2024 in 3.5% NaCl solution.
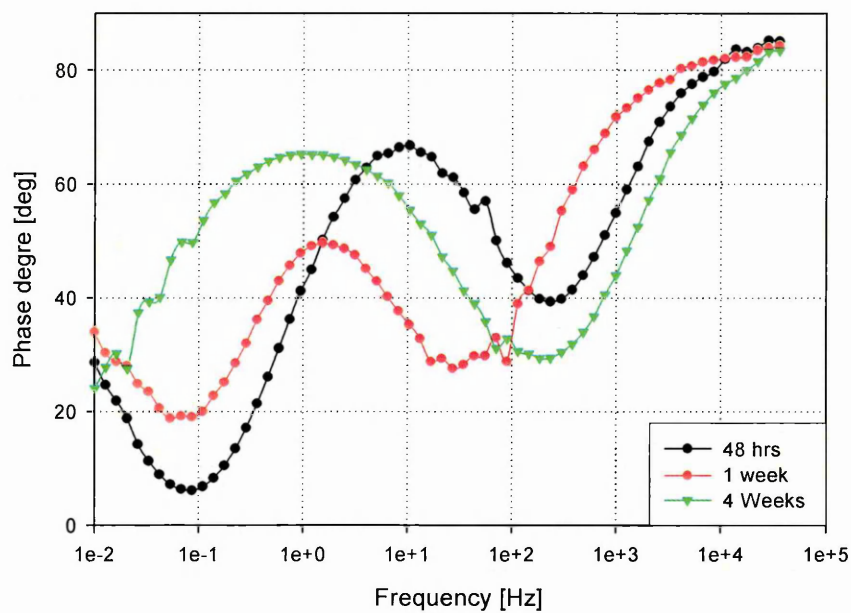
Figure 4-64 Phase diagram of post-treated PANI/sol8 coated AA2024 in 3.5% NaCl solution.

137
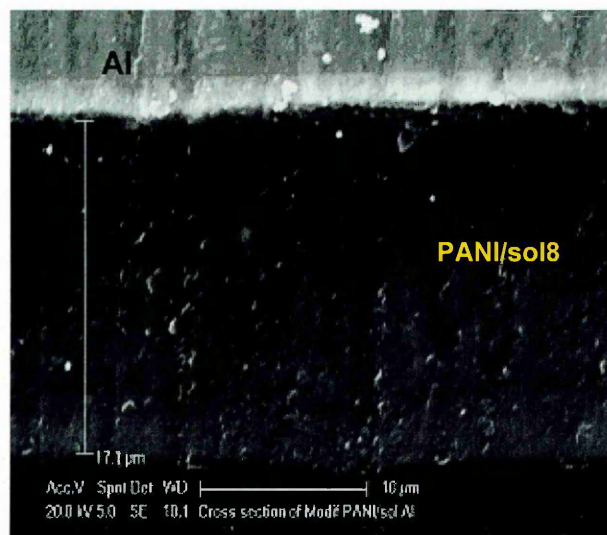
Figure 4-65 SEM image of post treated PANI/sol8

4.1.6 Scratch Test

An investigation of the "self healing" property of the PANI/sol-gel coating was carried out from EIS measurements of samples before and after scratching in 3.5%NaCl solution.

The impedance curve, Figure 4-66, shows that the sample decreases in impedance by about one and an half orders of magnitude directly after scratching at both high and low frequency. Continued immersion showed that this lost of impedance was recovered with time.

138
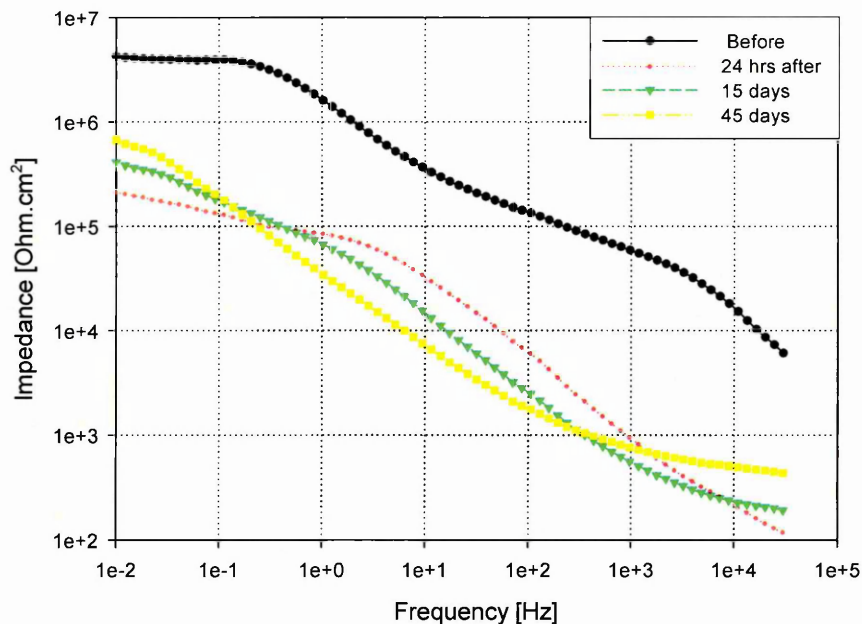
Figure 4-66 Impedance of PANI/sol8 coated AA2024 in 3.5 %NaCl solution, before and after scratching.

The phase angle plot shown in Figure 4-67 identified the sample as having two time constants at about 10^4 and 1.0 Hz before scratching, however, they shifted to 2×10^2 and 1×10^{-1} Hz respectively after scratching. These time constants may relate to the coating and metal/coating interface respectively. The high frequency time constant of the scratched sample shifted towards lower frequency with immersion time and its peak decreased with immersion time. The low frequency time constant peak increased with the immersion time which suggests an increase in capacitance of the interface. This was combined with an increase in impedance in the same frequency region. Moreover, the capacitive behaviour was clearly defined with immersion time; such behaviour is not seen with inert barrier coatings. SEM analysis of the scratched PANI/sol8 sample, Figure 4-68, showed that the scratch is typically 140-180 µm wide. Moreover, it can be seen that there is no delamination or undercutting or pitting within the scratched area. EDX maps of the scratched sample, Figure 4-69, indicated that the scratch penetrated through the coating to the metal substrate as both aluminium and copper could be detected. Furthermore, there was no sign of corrosion products in the scratched area after 7 days of immersion in 3.5% NaCl solution. PANI/sol-gel alone coated samples showed neither

139

undercutting or blistering, rather there was an accumulation of white aluminium oxide (arrows) at the scratch line following five months of immersion in 3.5 %NaCl solution as shown from the image, Figure 4-70.
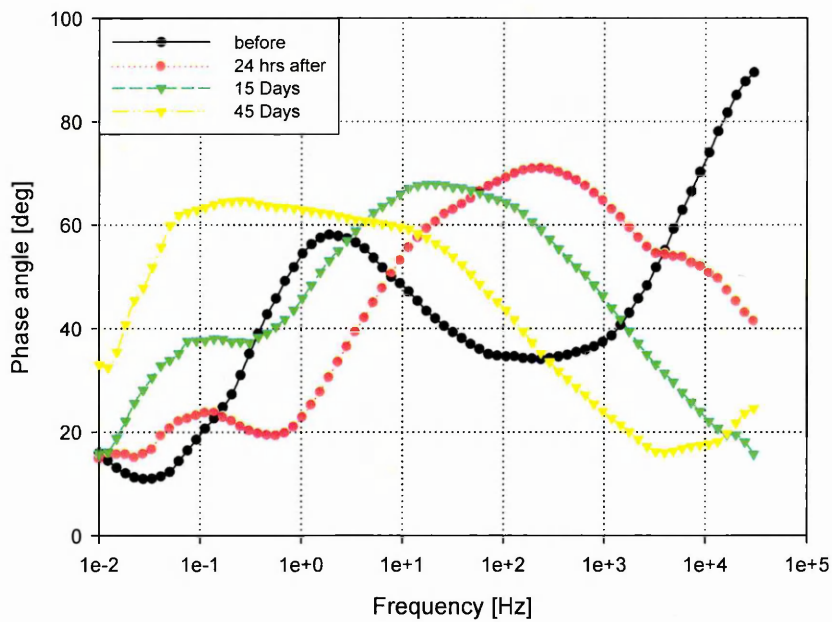
Figure 4-67 Phase angle of PANI/sol8 coated AA2024 in 3.5 %NaCl solution, before and after scratching.
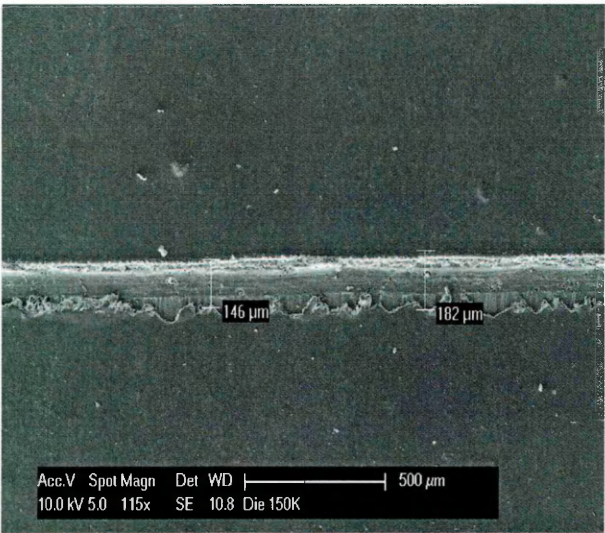
Figure 4-68 SEM image of the scratched PANI/sol8 sample after 7 days of immersion in 3.5% NaCl solution.

140
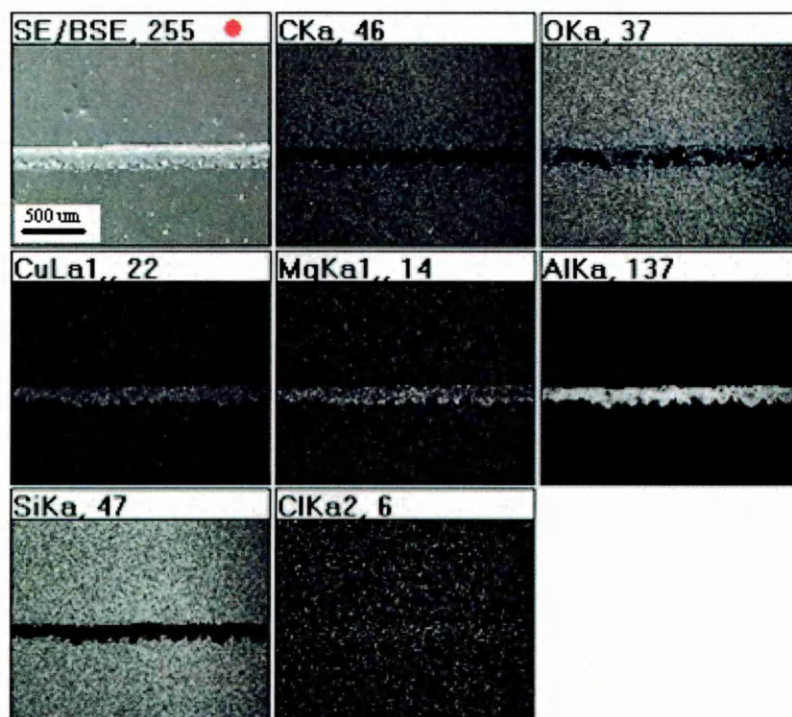
Figure 4-69 EDX analysis of scratched PANI/sol8 coated sample after 7 days in 3.5% NaCl solution
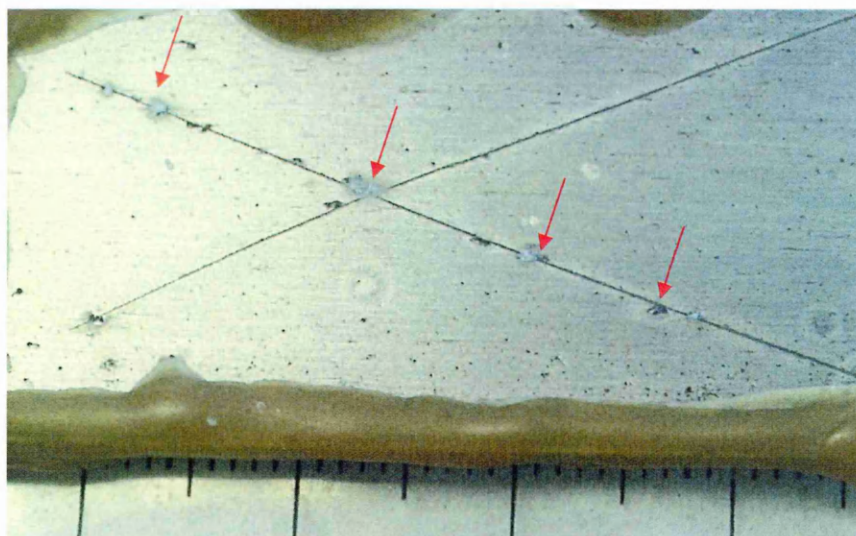
Figure 4-70 Image of scratched PANI/sol8 coated AA2024 after 5 months in 3.5%NaCl solution

4.1.7 SVET Tests

SVET was used to study the self healing process of the PANI/sol-gel coating. PANI/sol8 sample, pre-immersed in 3.5%NACL solution for 5 days, was

scratched and then a SVET line scan (across the scratch) of SVET was carried out in 0.35% NaCl solution. Figure 4-71 shows the change of current density with both immersion time and distance from the scratch. Here it can be seen that the current density of the scratched area initially decreases at the beginning of scan, then increases over the next 4 hrs of immersion. Finally the current density decreases to the value of unscratched area. No further activity is found at the scratch site.

These results suggest that a PANI/sol-gel coating exhibits a "self healing" type behaviour to AA2024 substrate.
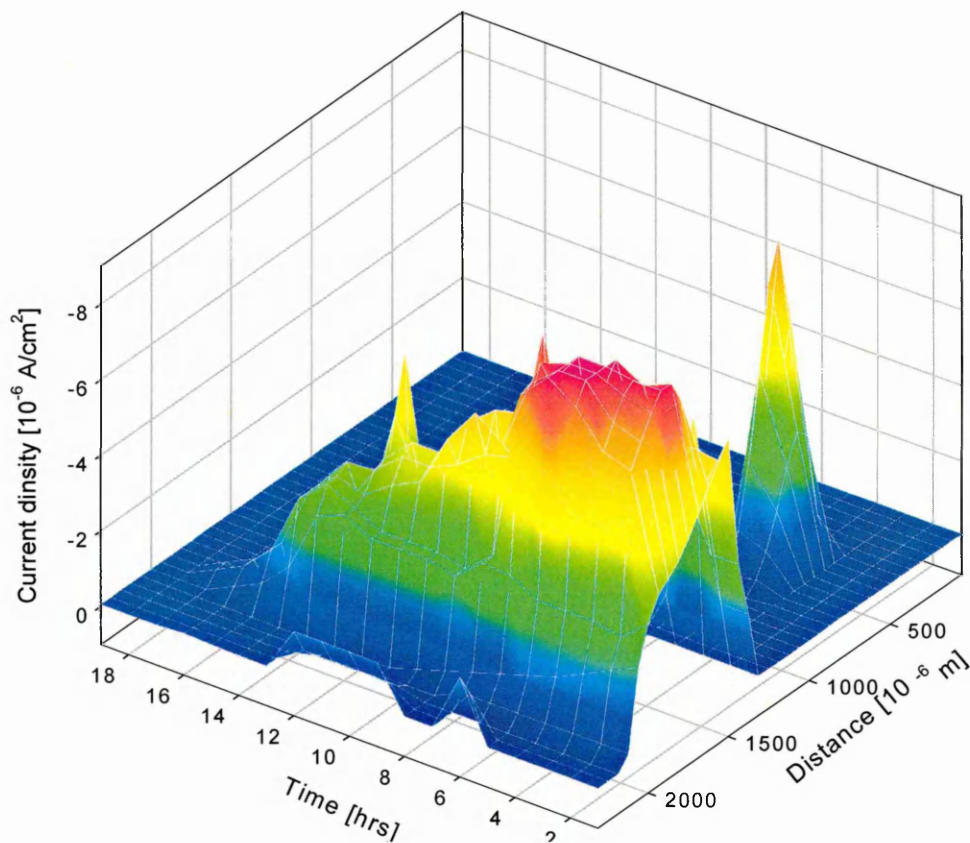
Figure 4-71 SVET time-lapse line scan of scratched PANI/sol8 coated AA2024 sample in 0.35% NaCl solution

4.2 PART II: MECHANICAL TESTING

A coating will fail to provide anti-corrosion protection when it delaminates or fractures due to mechanical action. The tests used to investigate the mechanical behaviour of the coating systems were; adhesion, micro-hardness, hardness and bend test. The results of these tests are given below;

4.2.1 Adhesion Test

Without sufficient adhesion, a coating of otherwise excellent barrier properties to weather, chemicals, scratches, or impact properties would be worthless. The adhesion of the coated samples was tested using two techniques namely; Pull off and Cross-Cut Test.

4.2.1.1 Pull off Test

The results of the test are given in Figure 4-72 and all raw data is given in appendix B.

Figure 4-72 shows that the sol-gel, PANI/sol8 and post-treated samples had better adhesion than that of the adhesive with the bare sample. The adhesion properties significantly decreased with increasing PANI content. The silica sol-gel had the highest value while PANI/sol1, had the lowest adhesion value. PANI alone showed higher adhesion value (4.2 MPa) than that of PANI/sol1 (3.1 MPa). This value may relate to the diffusion of glue through the PANI layer since PANI layer was 3 μm thick.
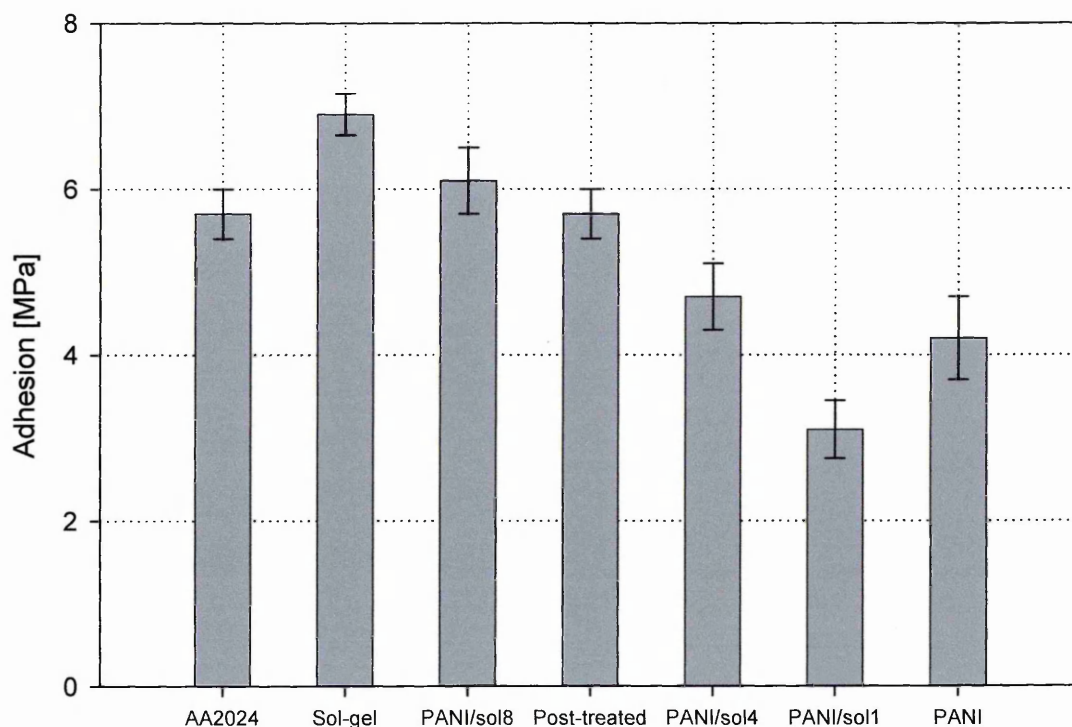
Figure 4-72 Pull Off adhesion test of different coating systems.

Figure 4-73 presents the surface of samples after the Pull off test along with their corresponding dollies. The photo shows that as the PANI content increases the percent of coatings delamination increases. Furthermore, the sol-gel coating, Figure 4-73-a, did not show any signs of coating delamination rather adhesion failure occurred. In contrast with the sol-gel coating, PANI/sol1 coating was completely removed from its dolly surface (see Figure 4-73-f). These results suggest that PANI content decreases the adhesion strength of the coating.
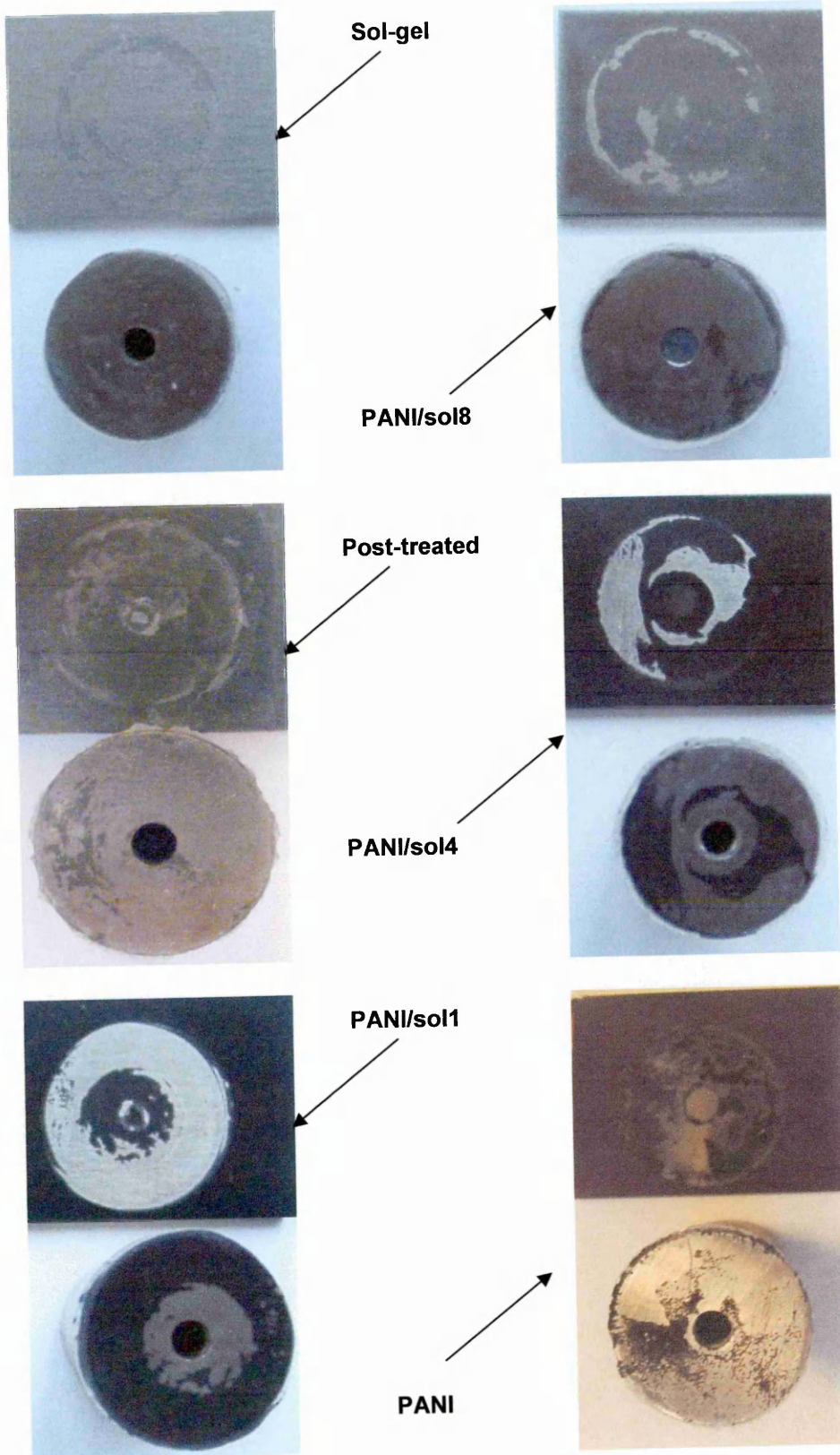
Figure 4-73 Images of Pull Off test samples with their dollies

4.2.1.2 Cross Cut Test

The cross cut test was applied for coated samples in support of the results of the Pull Off test. Moreover, this test can be applied to wet samples in which water may affect the adhesion properties of coatings. The test was applied for different coated samples and the results are shown in the following table;

Table 4-2 Cross cut adhesion test results

Sample name	Percent area removed
Sol-gel	0%
PANI/sol8	0%
Post-treated	0%
PANI/sol4	<5%
PANI/sol1	<5%
PANI only	0%

As Table 4-2 shows, the sol-gel, PANI/sol8, post-treated and PANI coated samples showed good adhesion while PANI/sol4 and PANI/sol1 coated samples exhibited failure of the coating at the scratch lines (arrows), images of different samples showed in Figure 4-74. Moreover, delamination of the PANI/sol1 coating was greater, both in size and number, than that of the PANI/sol4. These results support the Pull Off test results; notably as the PANI content increases the adhesion properties decrease.

146
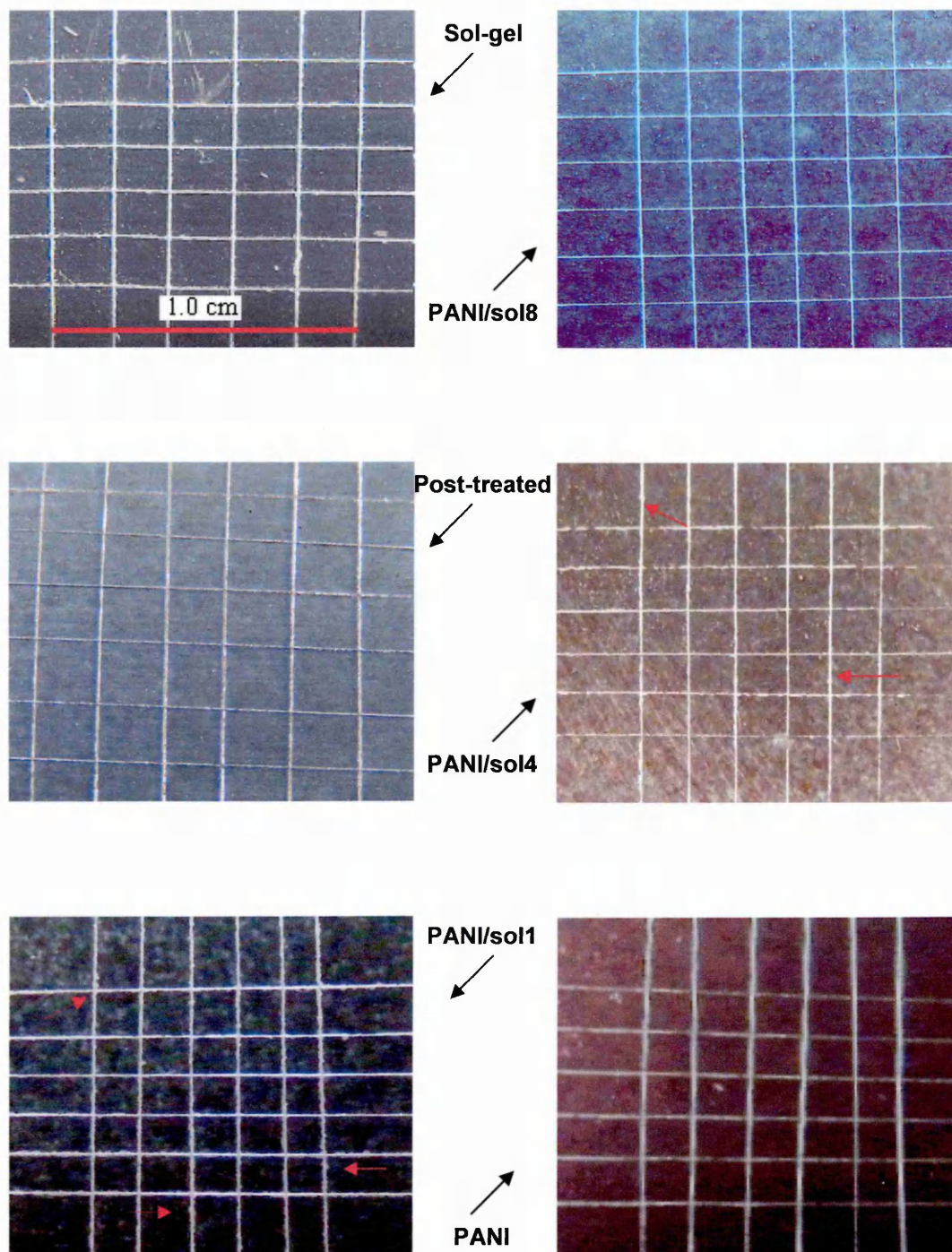
Figure 4-74 Images of Cross Cut test of different coating systems

Further assessment of the adhesion properties of coatings was carried out using samples that had been immersed in 3.5% NaCl solution for 24 hrs and dried using an air stream. Samples were scratched and subjected to the test; these results are shown in Table 4-3

Table 4-3 Cross Cut adhesion test results of coated samples after immersion in 3.5%NaCl solution for 24hrs.

Sample name	Percent area removed
Sol-gel	0%
PANI/sol8	0%
Post-treated	0%
PANI/sol4	<5%
PANI/sol1	5-15%
PANI only	100%

PANI-only coating showed a dramatic change in the adhesion to the metal substrate that PANI coating completely removed from the metal substrate even before applying the test, Figure 4-75. The PANI/sol1 coating showed a significant change in the adhesion behaviour due to immersion with failure of the coating, at the scratch lines, (arrows) increasing. Images of the coated substrate, after immersion, are shown in Figure 4-75. Moreover, sol-gel, PANI/sol8 and post-treated coated samples did not show any change in adhesion as a results of immersion in 3.5% NaCl solution for 24 hrs.

148
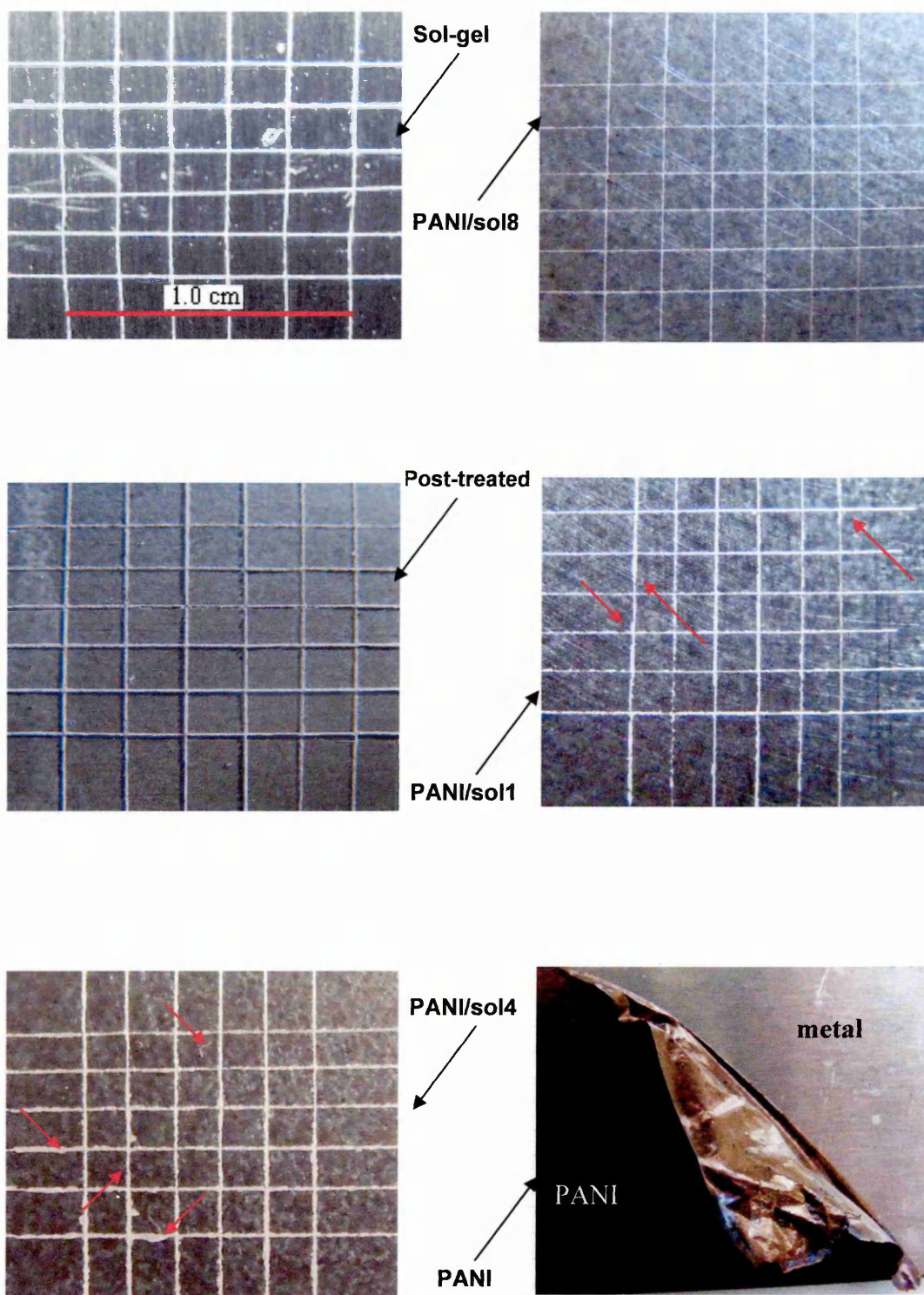
Figure 4-75 Images of Cross Cut test of different coating systems after immersion in 3.5%NaCl solution for 24hrs.

4.2.2 Micro-Hardness

The micro-hardness of the different coatings was measured, in addition to that of the bare AA2024 substrate. The hardness of the PANI only coated sample could not be measured since the maximum coating thickness was typically 8 µm and was insufficient to avoid the influence of the substrate during measurement. Micro-hardness test results, Table 4-4, showed that sol-gel had the highest micro-hardness value (21.0). As the PANI content increased, the micro-hardness decreased. Moreover, the post-treated sample exhibited lower value than that of PANI/sol-8 due to the post-treatment forming a thin outer layer on the coating.

Table 4-4 Micro-hardness test results

Sample name	Results HV
AA2024	161.83
Sol-gel	21.02
PANI/sol8	17.22
Post-treated	14.12
PANI/sol4	10.37
PANI/sol1	9.632

4.2.3 Pencil hardness test

A pencil hardness test was applied to further support the results of the micro-hardness test. This test can be applied for thinner coatings and has the advantage that it allows all coating systems, including PANI, to be compared, as shown in Table 4-4

Table 4- 5 Pencil hardness index of different coating system

Sample name	Pencil index
Sol-gel	5H
PANI/sol8	4H
Post-treated	3H
PANI/sol4	2H
PANI/sol1	2H
PANI only	HB

The results of the Pencil test were consistent with those of the micro-hardness test, where the sol-gel coating is the hardest coating and as the PANI content increase as the hardness decreases.

4.2.4 Bend test

This test was carried out to measure both adhesion and elongation of the coating systems. Test samples were strips having a size that covered the whole of the mandrel. Following bending, each strip was checked separately using a magnifying lens.

Optical inspection of the coated samples showed no cracking of the sol-gel, PANI/sol8, post-treated and PANI/sol4 samples. The PANI/sol1coating resisted cracking up to a mandrel diameter of 1.3cm where upon horizontal cracks appeared in the coating layer. In comparison, the PANI coating showed cracking at a mandrel diameter of 1.5 cm.

4.3 PART III: COATING CHARACTERISATION

In this part of the chapter characterisation of the coatings was carried out in an attempt to understand how the PANI/sol-gel coating offers protection to the AA2024.

4.3.1 PANI Characterisation

PANI was chemically prepared, as described in chapter 3; acetone was added to the water to improve the solubility of PANI within the sol-gel matrix. The prepared dark blue powder, typically emeraldine base, was characterised using FTIR and XPS.
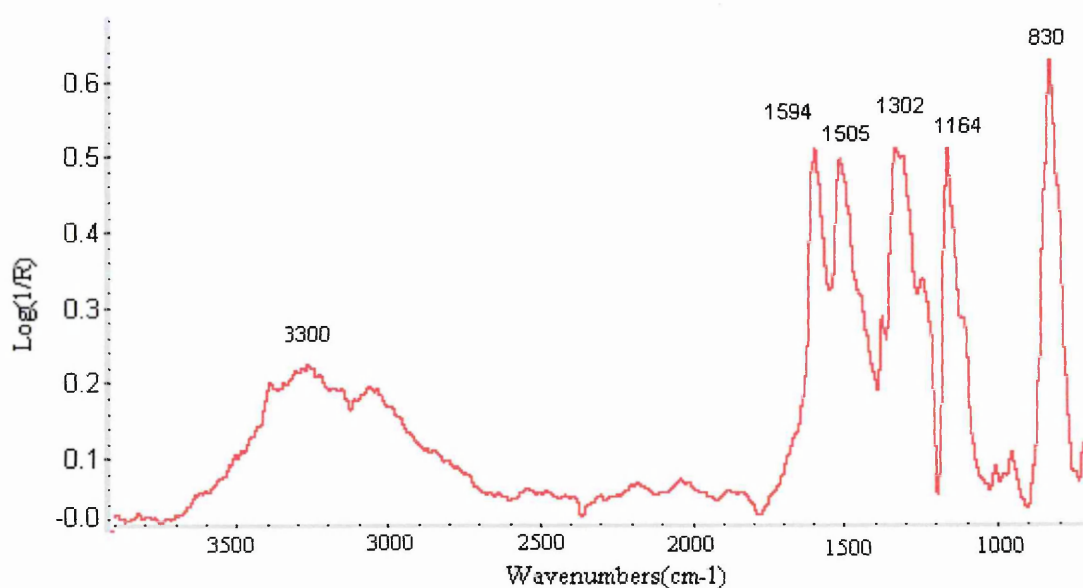
Figure 4-76 FTIR of Polyaniline powder

Figure 4-76 shows the FTIR spectrum of the prepared polyaniline. The spectrum consisted of six main peaks at 830, 1164, 1302, 1505, 1594 and a broad peak at 3300cm^{-1}. These peaks represent bending vibration of C-H on the aromatic rings, vibration of N=Q=N ring, stretching vibration of C-N, stretching vibration of N-B-N ring, stretching vibration of N=Q=N rings and stretching of H bond of N-H, respectively. Where: Q is quinone ring and B is benzene ring. This result agrees with previous FTIR analysis of PANI [5] [6] [7] [8]. The spectrum showed that the peaks at 1594 and 1505 have comparable intensity which suggests that this material is emeraldine base.

152

Name	Pos.	At%
O 1s	532.7	1.62
C 1s	284.7	85.42
N 1s	399	12.89
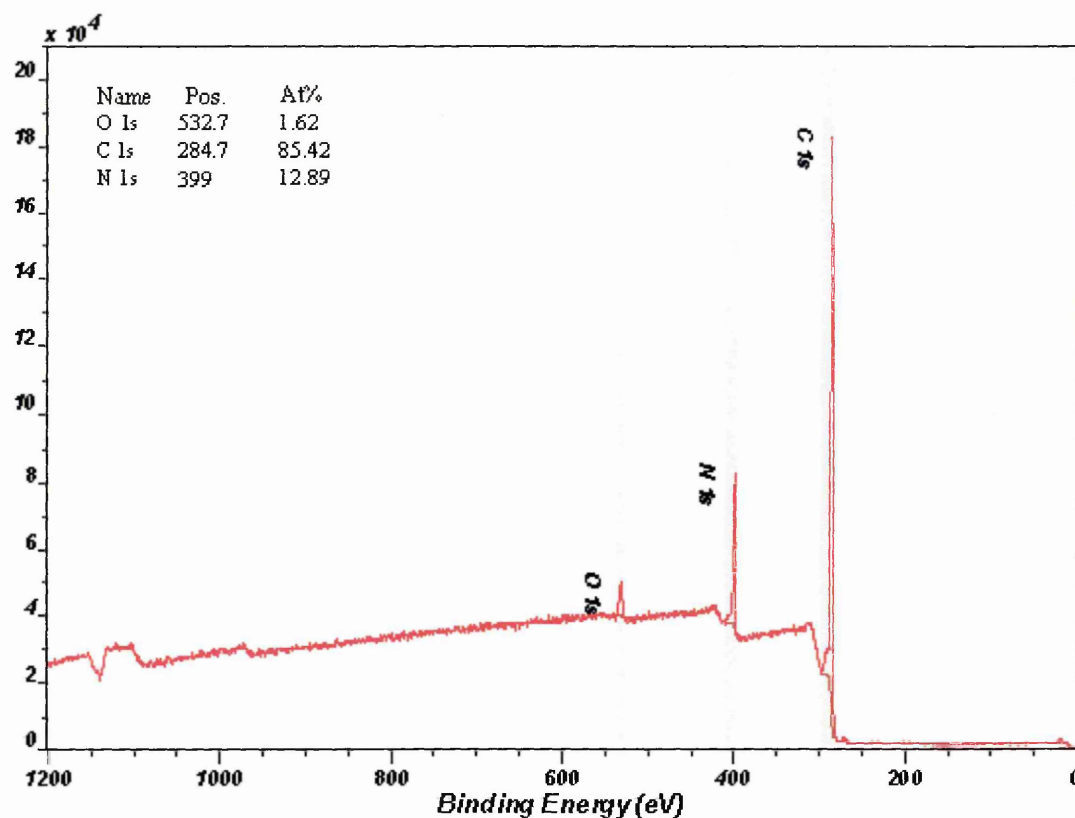
Figure 4-77 XPS survey of polyaniline powder

Figure 4-77, shows the C_{1s} N_{1s}, and O_{1s} peaks found from XPS analysis. The theoretical relative concentration ratio of carbon to hydrogen is 6:1; however, the XPS analysis implies that their relative concentration is 6.9:1 which agrees with that found by Fujita et al [9] and Lim et al [10]. This additional carbon may arise from hydrocarbon surface contamination. The analysis also detects some oxygen in the as-prepared powder which is common in polyaniline (emeraldine base) [9] [11].
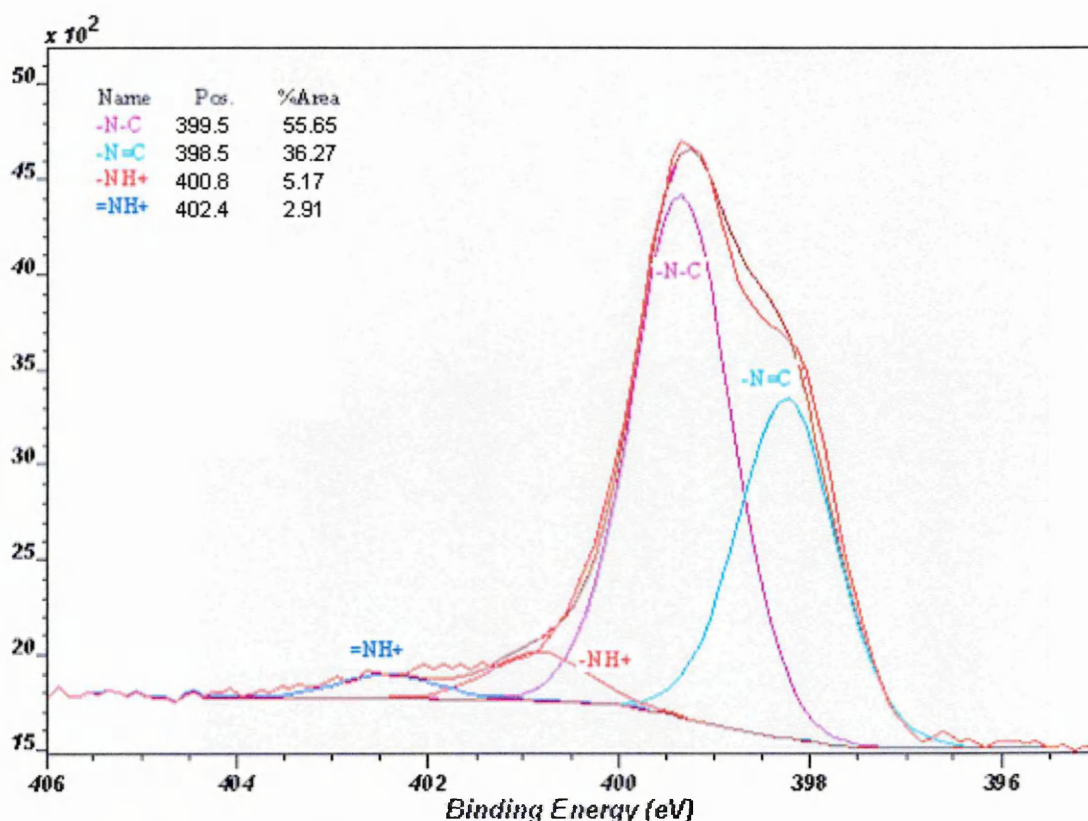
Figure 4-78 High resolution XPS N s1 core level spectra of PANI (EB) powder

According to the reported results of polyaniline [5] [9] [11] [12] these peaks are attributed to nitrogen bonds, as shown in the following table:

Table 4-6 XPS analysis of Nitrogen atom components

Bonding Energy [eV]	Type of N atom	Percent of total area [%]
398.5	-N=C-	36.27
399.5	-NH-C	55.56
400.7	-N$^+$H-	5.17
402.5	=N$^+$H-	2.90

The intensities of the protonated forms, peaks at 400.7 and 402.5 eV, are small with respect to the other bonds indicating that the concentrations of positively charged nitrogen atoms are very low in PANI. Furthermore, the relative concentration of non-protonated N, [-N=C-]/[-NH-C]=0.69, this value being in agreement with Li et al[13].

The above XPS and FTIR results are proof that the prepared material is polyaniline in its emeraldine base (EB) form.

154

Although, PANI (EB) was prepared as PANI (EB) powder, the powder was dissolved in NMP during preparation of both PANI and PANI/sol-gel coatings. For more understanding of PANI coatings, PANI (EB) solution was dissolved and applied to a glass slide and the coating was then dried at 70°C for 16 hrs before analysis by FTIR and XPS techniques.

Figure 4-79 shows the FTIR spectra of PANI after being dissolved in NMP and dried onto a glass slide. The spectra showed a new peak at 1662 which is related to C=O from the NMP which forms a hydrogen bond with the amine group of the PANI i.e. C=O·····HN [14].
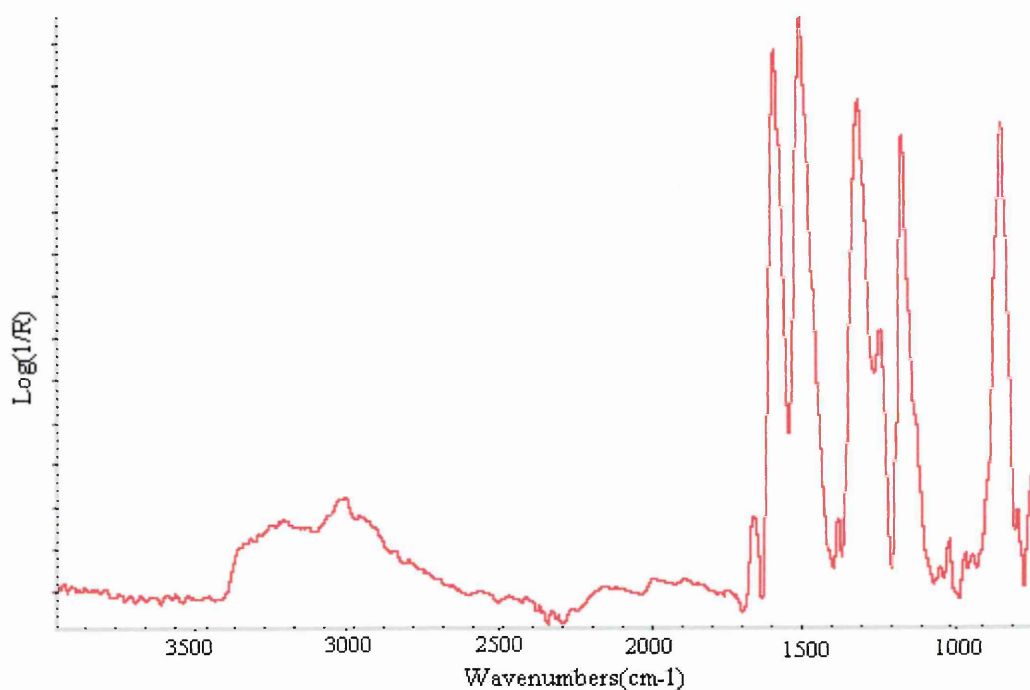
Figure 4-79 FTIR of Polyaniline dissolved in NMP then dried

The high resolution XPS N 1s core level showed the same species of powder sample, however, some changes in the relative concentration was took place as showed in Figure 4-80

Name	Pos.	%Area
-N-C	399.5	55.16
-N=C	398.5	32.58
-NH+	400.8	9.39
=NH+	402.413	2.86
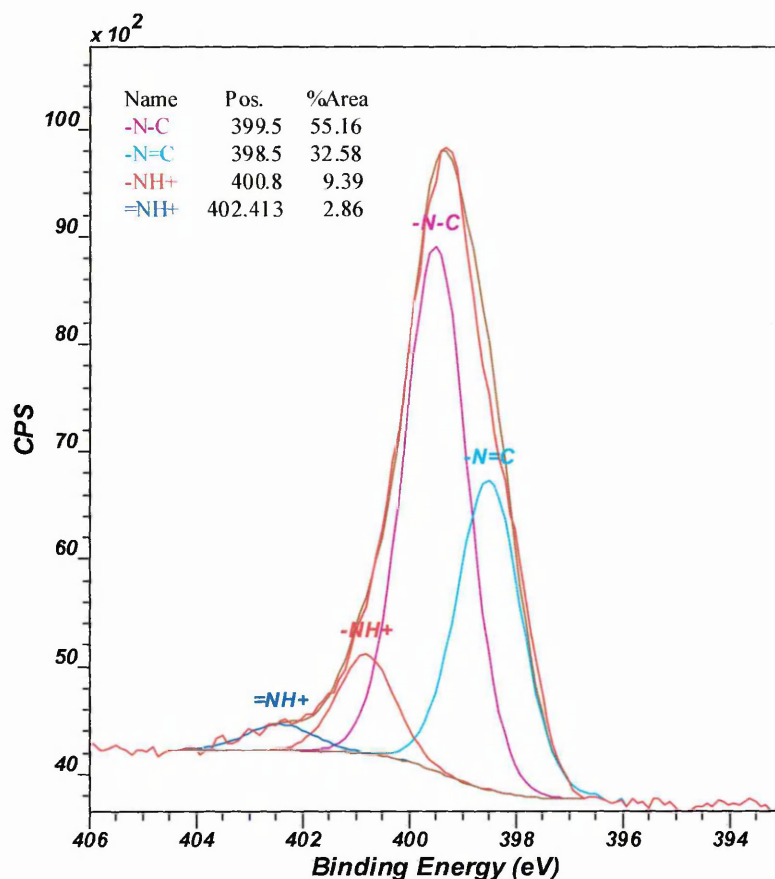
Figure 4-80 High resolution XPS N s1 core level spectra of PANI/NMP film

4.3.2 PANI Interaction with Sol-Gel

The interaction of PANI with the sol-gel was investigated using XPS technique; sol-gel only and PANI/sol-gel coatings were analysed separately. Both coatings were separately on applied to a Teflon sheet and then dried at 70°C for 16 hrs. The coatings were removed from the Teflon sheet as a free standing film, or powder, before subjecting to the XPS analysis.

156
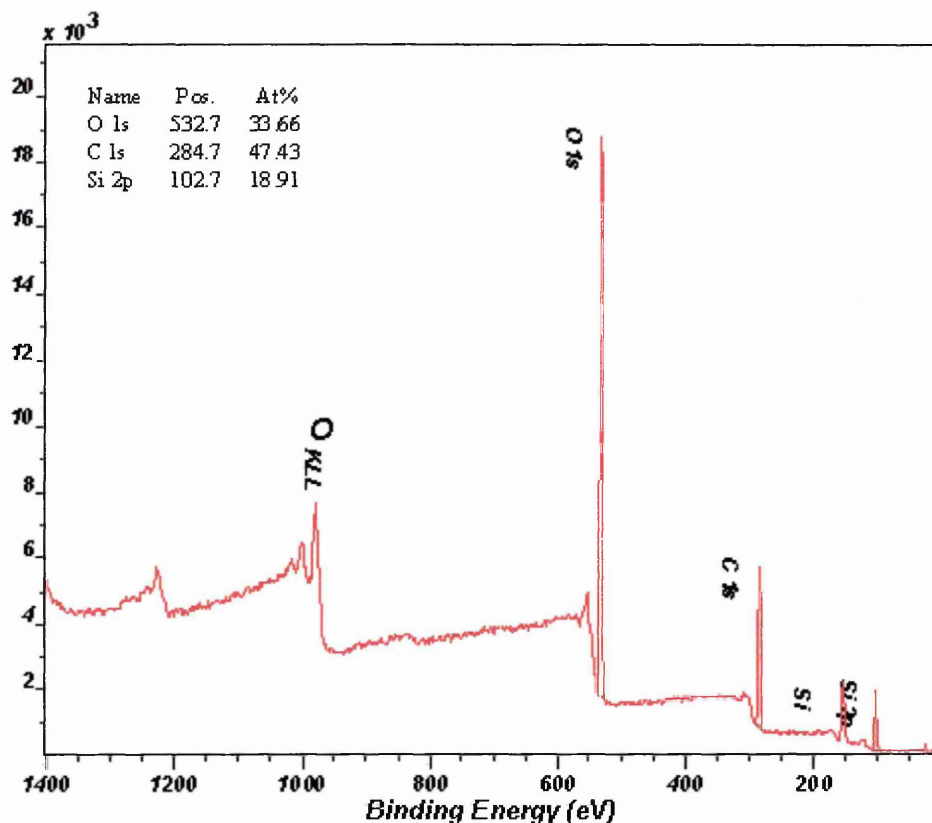
Figure 4-81 XPS analysis of silica sol-gel

XPS analysis as shown in Figure 4-81 identified the presence of three elements in the sol-gel coating namely; silicon, carbon and oxygen.

High resolution XPS analysis of Si 2p peak of the sol-gel only and PANI/sol-gel coatings are shown in Figure 4-82 and Figure 4-83 respectively. It can be seen that there is no shift or broadening of the Si 2p peak occurs after adding PANI to the sol-gel. Typically, two peaks appeared at 103.3±0.1eV and 101.8±0.1eV representing Si-O-Si and C-Si-O respectively [15]. The high resolution, N 1s core level, (see Figure 4-84) showed the same components of PANI/NMP with a decrease the percentage of N=C and increase of NH+. This change may be related to the protonation of N=C by the acid catalyst used within the silica sol-gel.

157
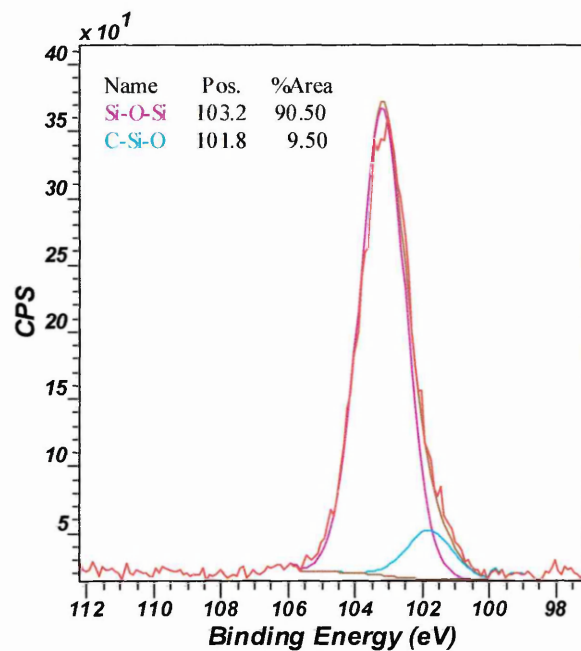
Figure 4-82 High resolution XPS Si 2p core level spectra of sol-gel coating.
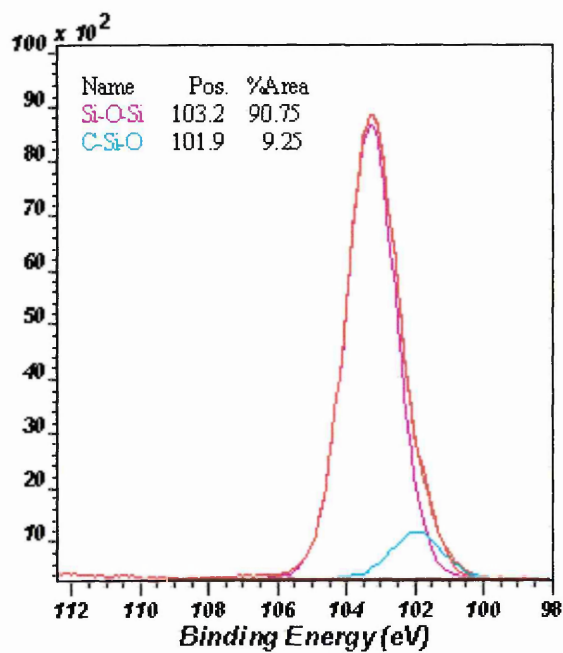
Figure 4-83 High resolution XPS Si 2p core level spectra of PANI/sol-gel coating

158
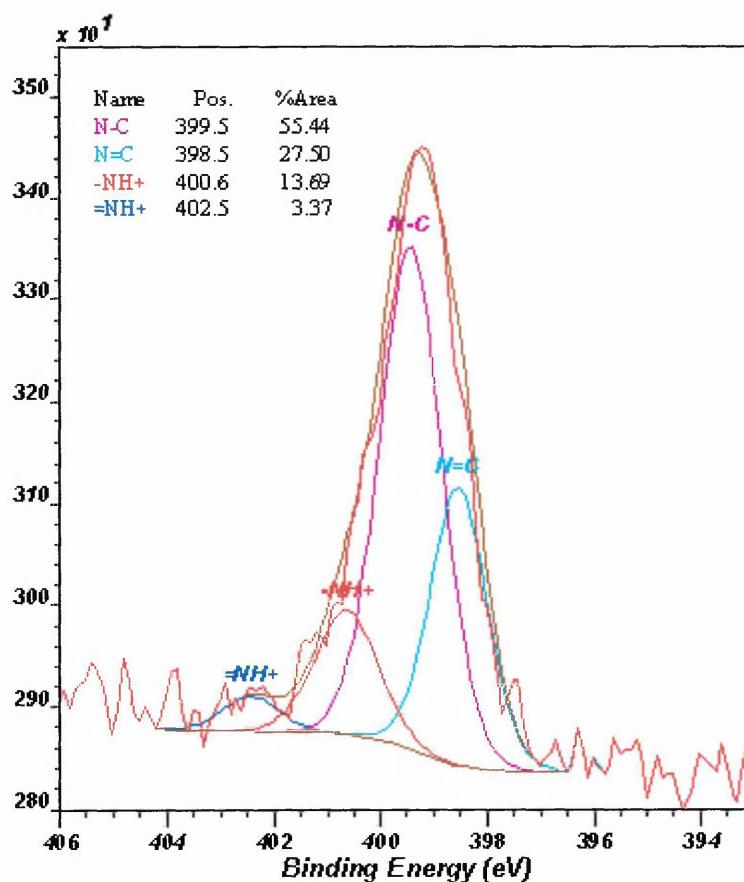
Figure 4-84 High resolution XPS N 1s core level spectra of PANI/sol-gel coating

Observation of PANI/sol-gel solution showed that the PANI content was not chemically bound to the sol-gel, but rather the PANI was suspended in the sol-gel matrix and this suspension seems to take place without interaction between PANI and sol-gel, Figure 4-85.
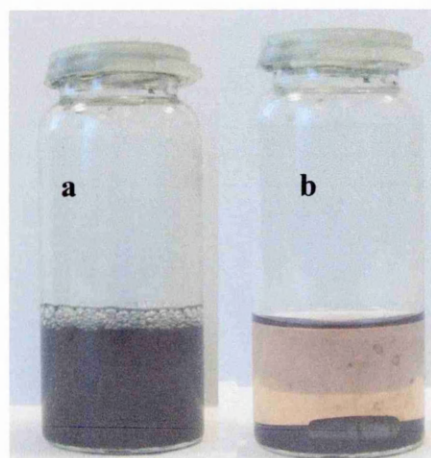
Figure 4-85 PANI/sol-gel a) directly after preparation b) two weeks on shelf.

159

4.3.2 Interaction of PANI with Aluminium

XPS analysis of bare substrate, Figure 4-86, showed that the alloy contains; aluminium, copper, magnesium, carbon, silicon and oxygen. Carbon is also found, being due to the contamination by handling and the atmosphere.
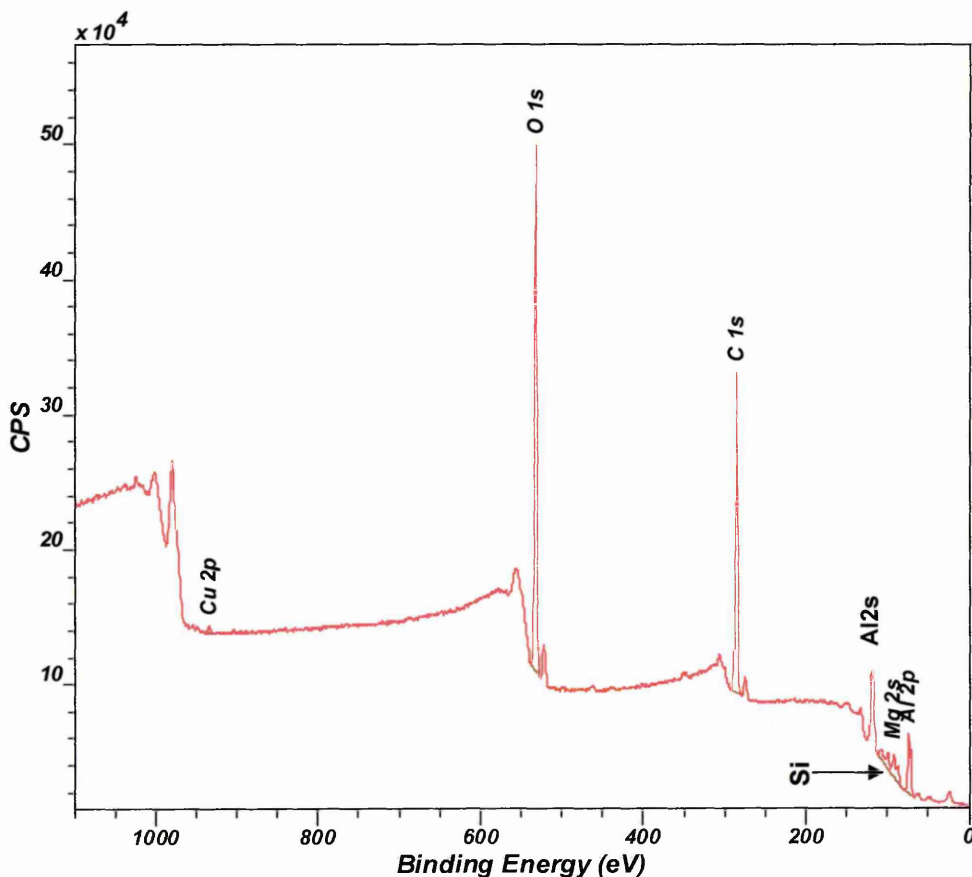
Figure 4-86 XPS survey of bare AA2024

The high resolution XPS of Al 2p core level (Figure 4-87) showed that aluminium has two main species at 72.8±0.1 and 75.6±0.1 eV which relate to the aluminium metal and native aluminium oxide respectively [16]. The oxide content is around three times that of the metal. The oxygen/aluminium oxide atomic concentration is about 2:1 which is more that the theoretical value (1.5:1).

160
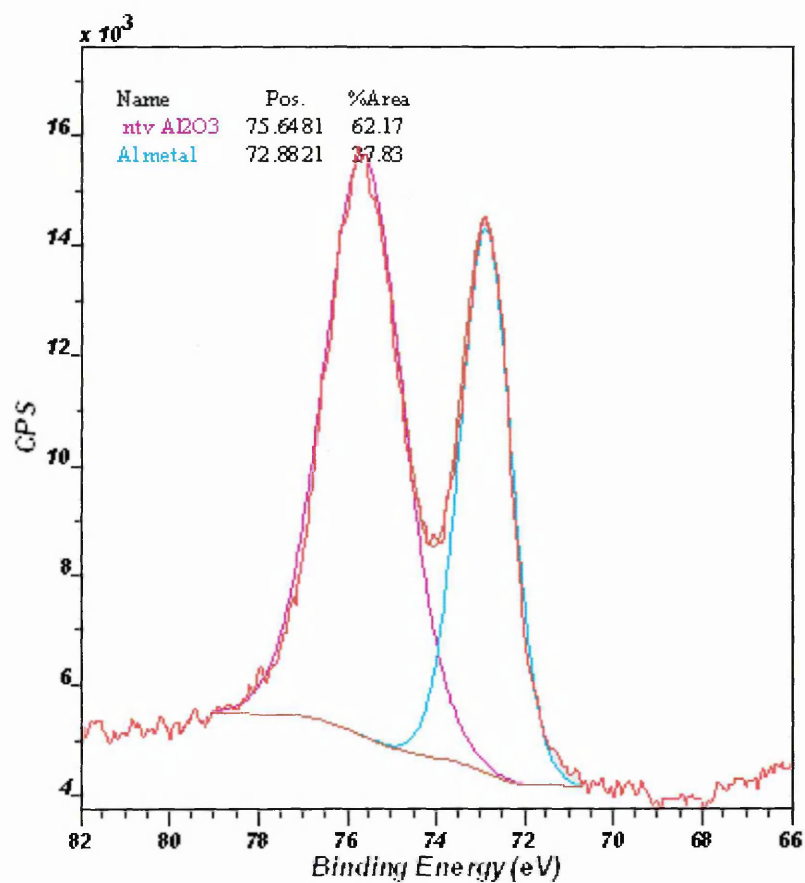
Figure 4-87 High resolution XPS Al 2p core level spectra of bare AA2024.

Wide XPS scan of the thin film PANI coated bare substrate; is shown in Figure 4-88, revealing only Al, C, O and N in the spectrum where the nitrogen peak represents PANI. The high resolution Al 2p core level, Figure 4-89, did not show any peak shifts for the Al metal and native oxide.
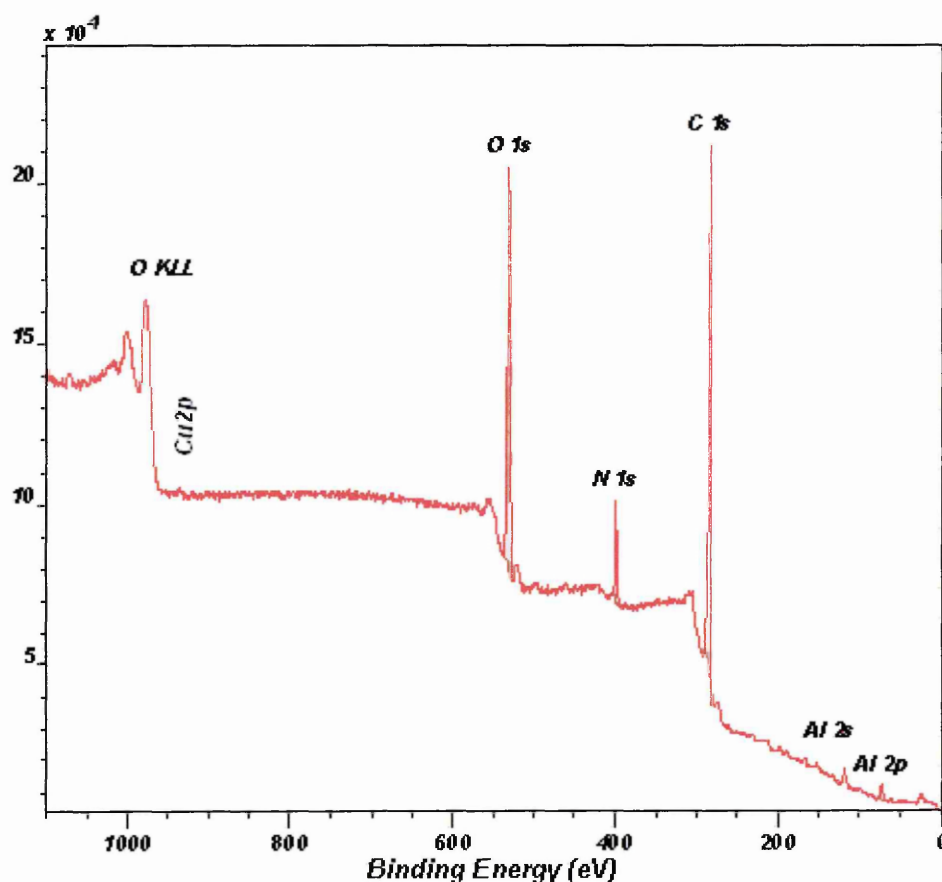
Figure 4-88 XPS survey of PANI coated AA2024

Name	Pos.	%Area
Al Oxide	75.6354	85.23
Al metal	72.78.11	14.77
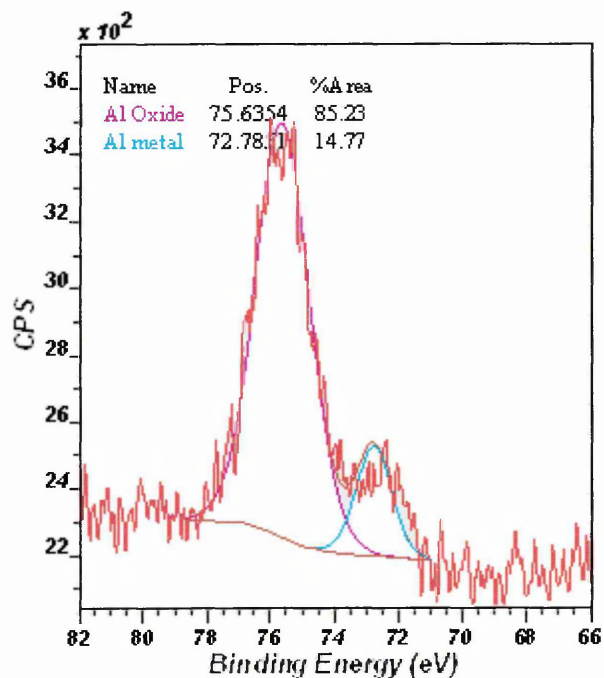
Figure 4-89 High resolution XPS Al 2p core level spectra of PANI coated AA2024

The high resolution N1s core level of PANI coated AA2024 showed some changes with respect to that of PANI/NMP film as shown in Figure 4-90.

162

Name	Pos.	%Area
N-C	399.6	59.14
N=C	398.4	24.10
-NH+	400.8	14.07
=NH+	402.6	2.69
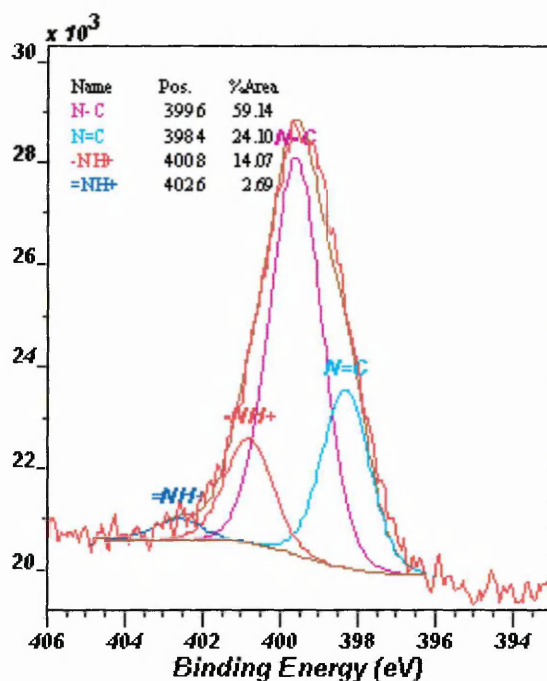
Figure 4-90 High resolution XPS N 1s core level spectra of PANI coated AA2024.

Here the N=C component decreases from 32% to 24 %, while the N-C component increases from 55% to 59%. Moreover =NH$^+$- increased from 9 to 14%. This reflects a decrease in the N-Q-N bonding of the polyaniline which represents the oxidised form in the PANI chain. At the same time there is an increase in the N-B-N bonding of the polyaniline (reduced form of PANI (EB) chain). The relative concentrations of the oxidised and reduced forms of PANI (EB) present an understanding of the changes taking place when PANI is applied to the metal substrate. The relative concentration of oxidised to reduced forms was decreased from 0.58 to 0.45 in PANI/NMP film and PANI coated AA2024 respectively i.e. the PANI is reduced when applied to the substrate.

The interaction of PANI and the substrate was further investigated using FTIR. Figure 4-91 shows the FTIR region of interest, 1000-2000 cm^{-1}, for the PANI/NMP film and PANI coated AA. The relative concentration of oxidised and reduced forms can be measured from the relative peak heights at 1594 (N=Q=N) and 1505 (N-B-N) respectively. The spectrum representing PANI applied to the Al substrate showed that the height of 1594 peak is slightly decreased with respect to 1505 peak.

163
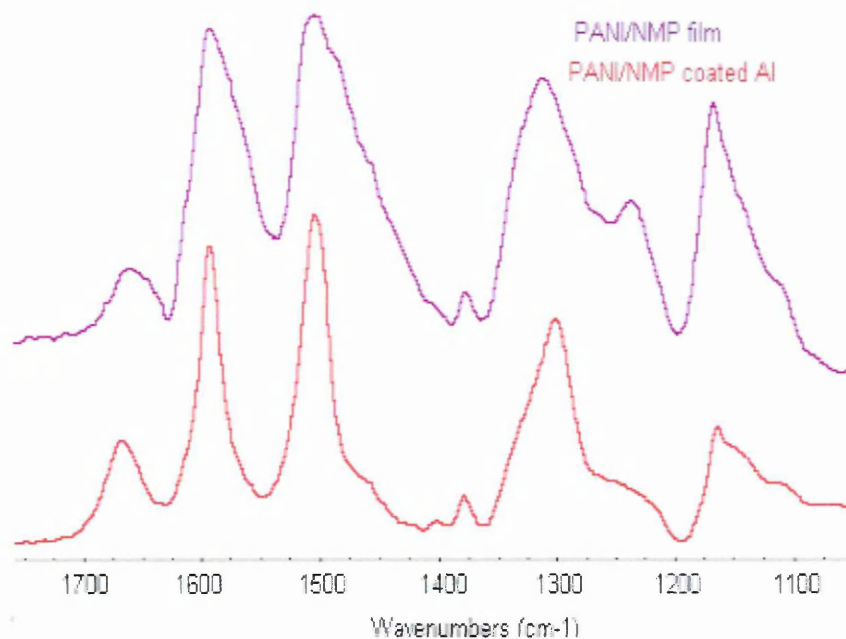
Figure 4-91 FTIR spectrum of PANI/NMP film and PANI coated AA2024

The FTIR and XPS results suggest that PANI may be reduced when applied to the Al substrate. This postulation is not valid unless the Al substrate or other species, in the PANI coating system, is oxidised to complete the electrochemical reaction.

To study the Al substrate underneath the PANI coating, XPS depth profiling was used. Pure aluminium (99.99) was used to avoid any other interaction between the PANI and the substrate alloying elements. Aluminium was evaporated under vacuum (10^{-5} torr) on a free standing film of PANI (EB) at 60±5°C. The evaporating chamber was left under vacuum for one hour before evaporation to remove surface gases. The evaporated aluminium thickness was adjusted to ≈50 nm and the XPS depth profile was carried out from the aluminium side to polymer.

The XPS wide scan survey, Figure 4-92, showed that four elements are present notably; oxygen, carbon, nitrogen and aluminium. The sputtering time between each scan is approximately 15 sec with the exception of the first and the last scan where a 60 sec interval was used. In this figure the arrow shows the sputtering direction. The highlighted region appears to be the PANI/Al interface where, Al begins to disappear and carbon appeared. Furthermore, the oxygen

164

content gradually decreases from the outer aluminium layer to the interface. It then begins to increase again at the interface.
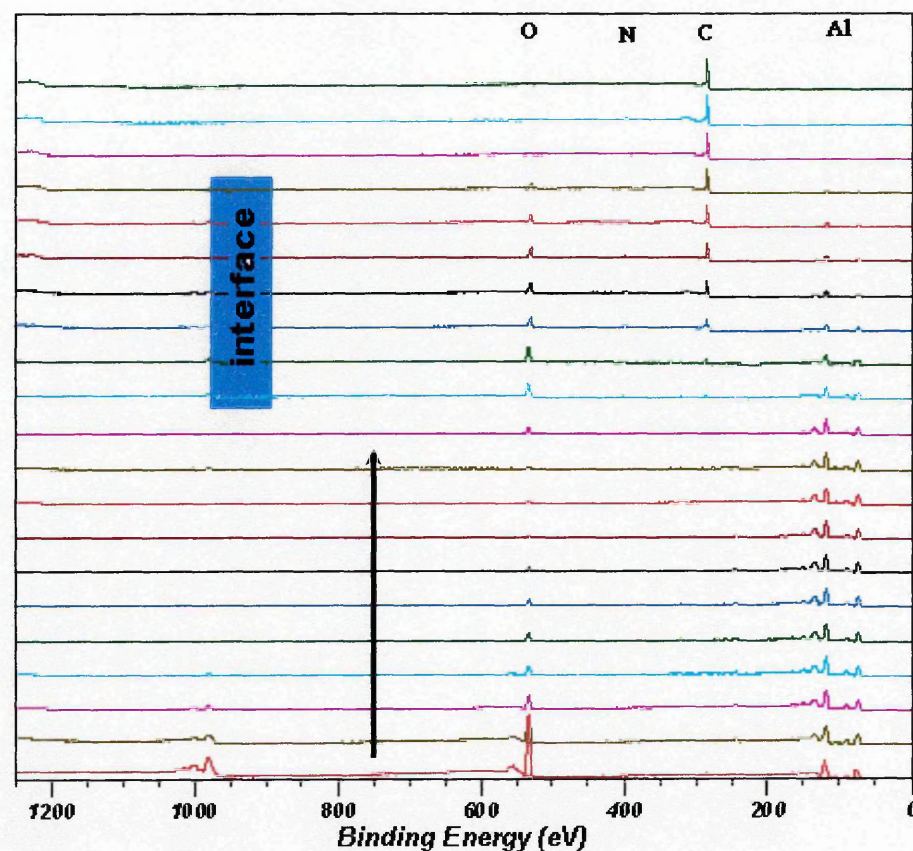


Figure 4-92 XPS depth profile survey of PANI/Al

The elemental atomic percentage is shown in Figure 4-93, where it can be seen that carbon appears on the surface of the aluminium before sputtering, however, it completely vanishes after first sputtering. This carbon content appears to be due to atmospheric contamination.

The oxygen content gradually decreases from the surface to PANI/Al interface region where it increases sharply and then decreases to a near zero value in the depth of the polymer at the end of sputtering. The aluminium content decreases gradually at the interface region while, the carbon and nitrogen content gradually increases from the interface up to the end of the sputtering process, where the sum of their content was over 99%.
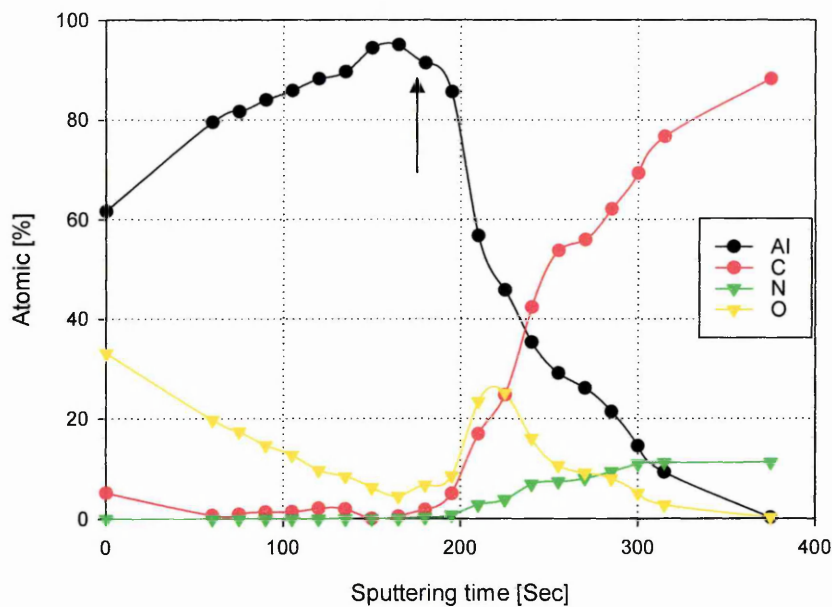
Figure 4-93 Change of elemental atomic percent with XPS sputtering time

The relative atomic ratio of carbon to nitrogen, Figure 4-94, was relatively stable around a value of 6.5:1 which is near the theoretical value (6:1). The ratio is observed to reach 8:1 at the beginning of the PANI/Al interface which may relate to contamination of the PANI film before evaporation of aluminium.
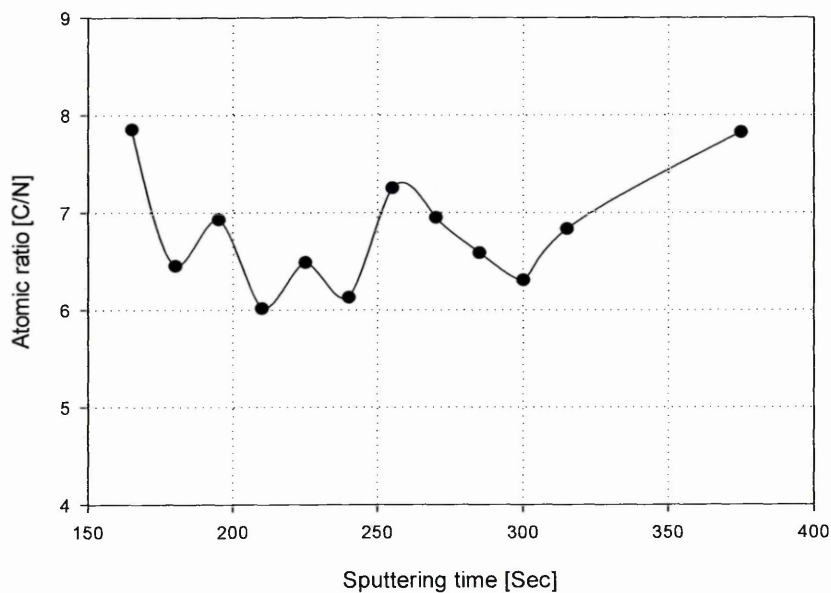

Figure 4-94 Change in carbon/nitrogen atomic ratio with sputtering time.

166

The change of the Al 2p core level with sputtering time is shown in Figure 4-95. Where two peaks at 72.8±0.15eV and 75.6±0.15eV are observed. The first peak, 72.8eV, remained at the same position until the end of sputtering, however, the peak at 75.6±0.1eV gradually decreased up to the interface and then increased again as sputtering continued. The peak broadened and shifted to 75eV as showed in Figure 4-95.
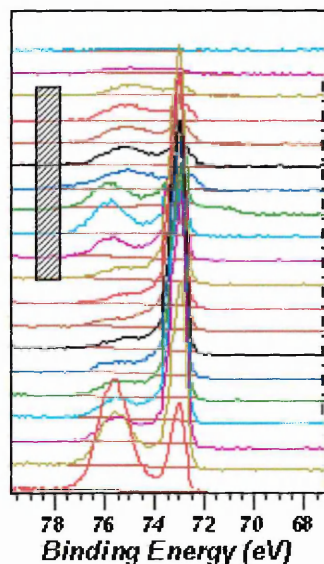
Figure 4-95 XPS high resolution Al 2p core level with all sputtering time

Details of individual XPS high resolution Al 2p core level spectra are showed in Figure 4-96. It can be seen that a new component at 74.5±0.15eV, was required for a perfect fit with the two peaks at 72.8 and 75.6eV of Al within the PANI/Al interface region. The percentage of this component, denoted "Al-X", increased with sputtering time i.e. towards the PANI direction within the interface region.
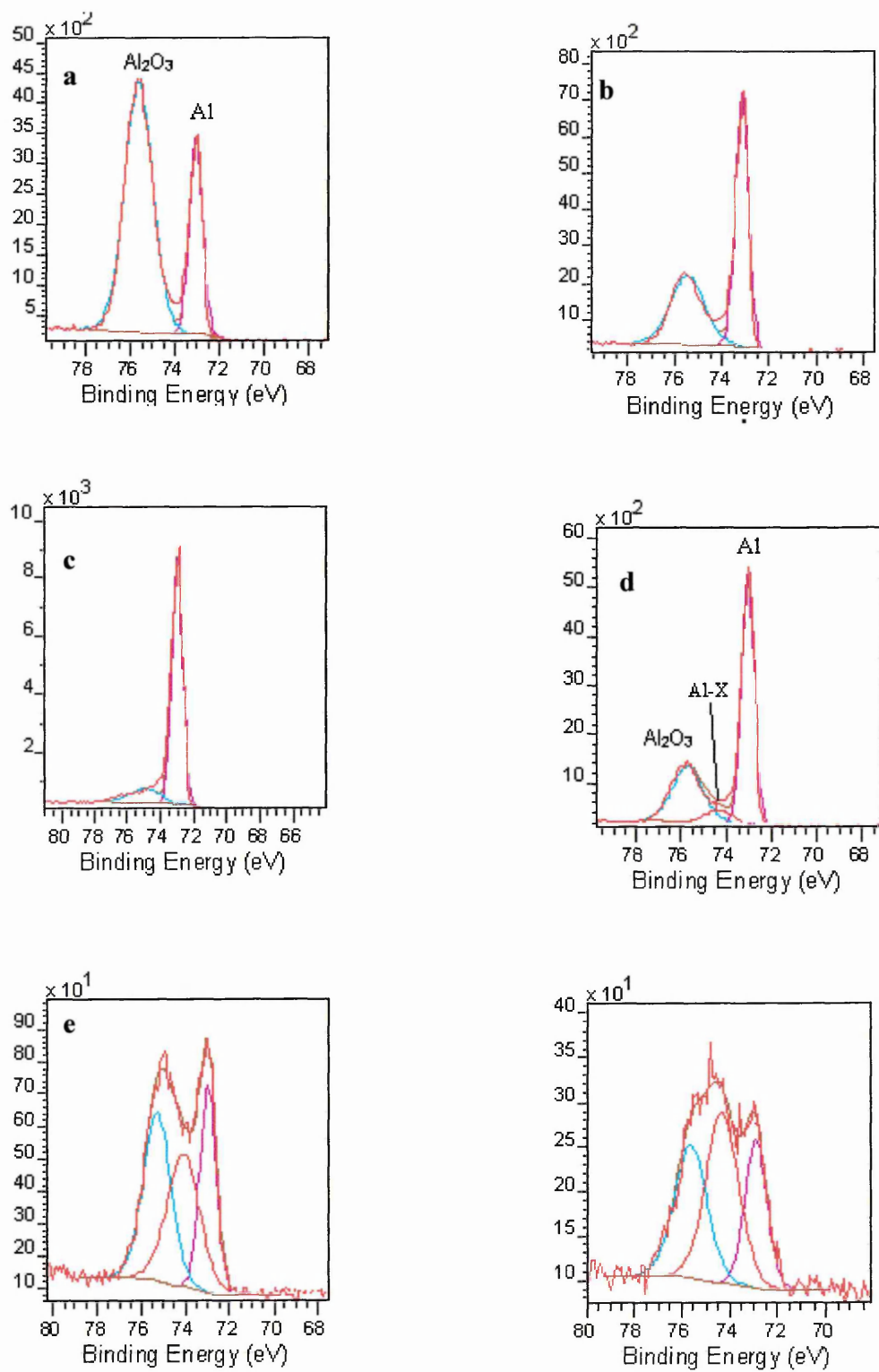
Figure 4-96 Change of Al components with sputtering time a) before sputtering b) 60 sec c) 165 sec d) 195 sec e) 270 sec and f) 315 sec

168
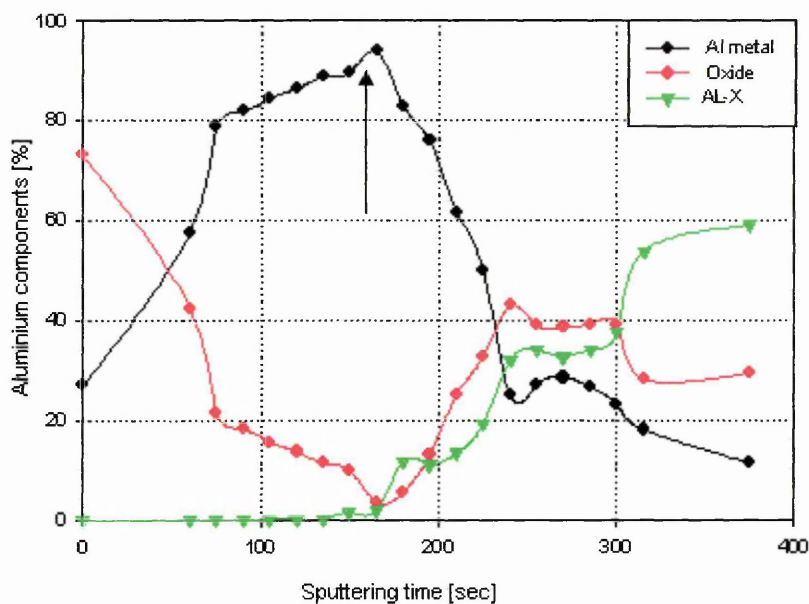
Figure 4-97 Percentage change of Al components with depth profile.

The percentage change of these Al species with sputtering time is shown in Figure 4-97. The Al-X begins to appear at the interface, at a sputtering time of 180 sec, and increases with sputtering time, towards the direction of PANI. At the same time, the aluminium oxide decreases from the outer layer of the aluminium surface until at the interface region; it begins to increase again. Over the same period, the Al metal increased up to the PANI/Al interface and then subsequently decreased.

The relative atomic ratio of aluminium oxide (Al 2p) and the whole oxygen (O1s) with sputtering time is shown Figure 4-98. From the plot it can be seen that following an initial increase at the outer surface of the Al, the relative atomic ratio was stable at about 0.72, which is near the theoretical value (0.66). At the interface region, the ratio decreases sharply i.e., the oxygen content increases beyond the theoretical value (O:Al = 3:2).

This result suggests that there is an evidence of a new anonymous, Al-X, which is rich in oxygen, e.g. Al-O-X or Al-O_z.

169
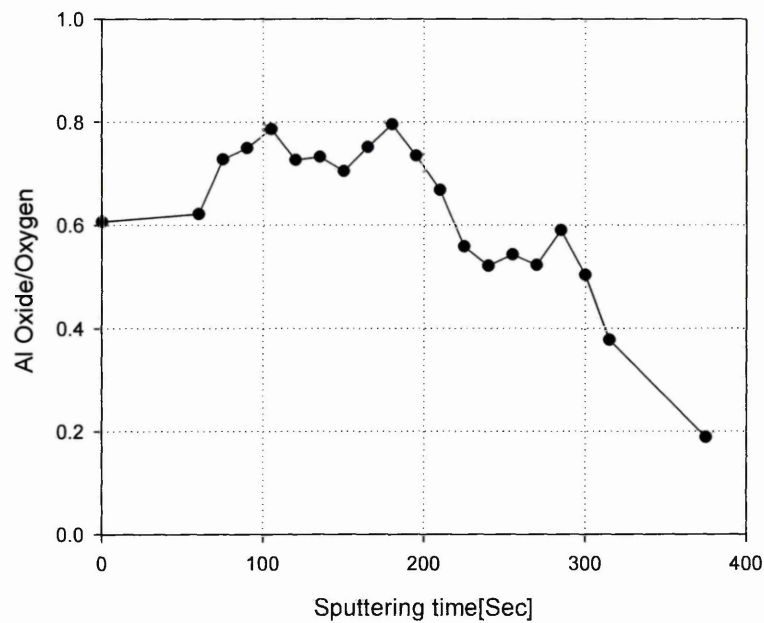
Figure 4-98 the relative atomic concentration of Al oxide to oxygen.

XPS high resolution N 1s core level scans, Figure 4-99, revealed that the N 1s peak shifted from 399.5eV to a lower binding energy at 398.8 which may be related to increase the percentage of the low binding energy component of N 1s with sputtering time.
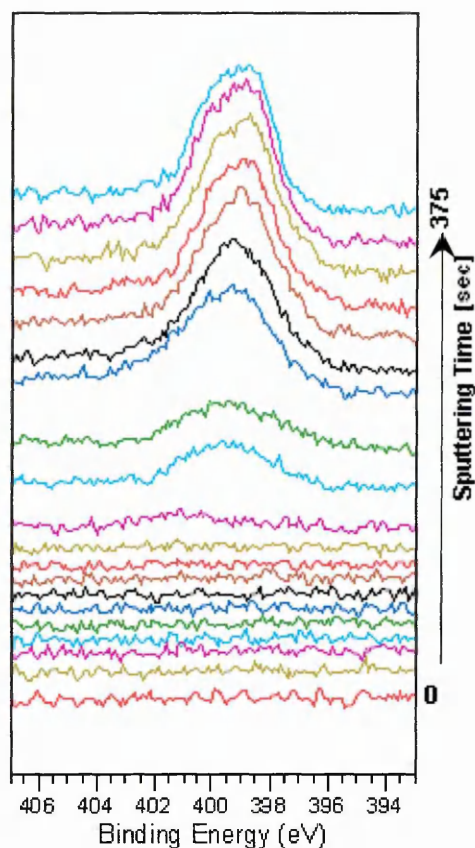
**Figure 4-99 High resolution N1s core level with sputtering time**

It can be seen that the four species, at 398.4±0.15, 399.5±0.15, 400.7±0.15 and 402.5±0.15eV, fit under one XPS band. The first spectrum, figure4-100(a) exhibited a low signal: noise ratio, however, the signal to noise gradually increased in figures b to f. From these figures, it seems to be the case that, the =N-C- peak increases with the sputtering time with respect to the N-C peak. Figure 4-101 shows the relative concentration of these four species as a function of sputtering time. It can be seen that the concentration of -N=C increased with sputtering time while, the -N-C concentration decreased over the same sputtering period. Moreover, the concentration of doped species,-NH+ and =NH+, appeared stable during sputtering. The relation between the ratio of N=C and N-C is further illustrated in Figure 4-102 where it is clear that the ratio of   [-N=C/-N-C] increases towards the direction of PANI.

171
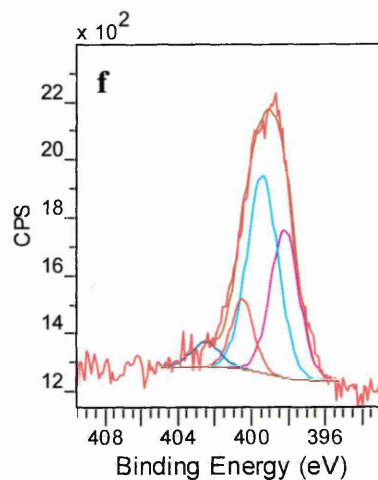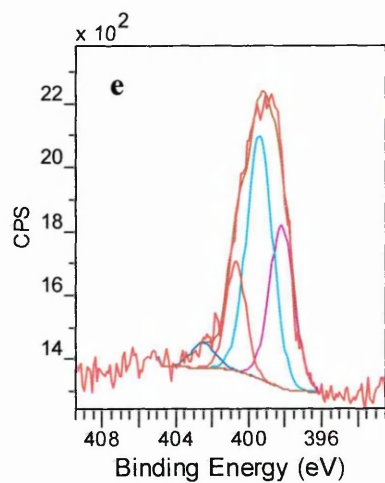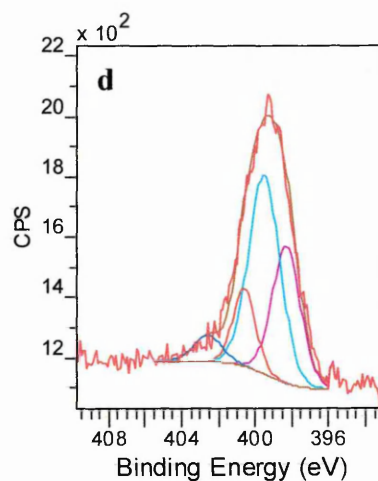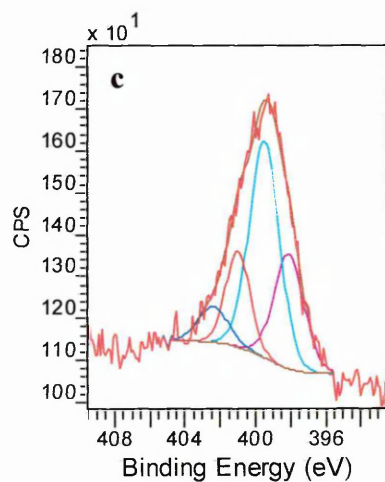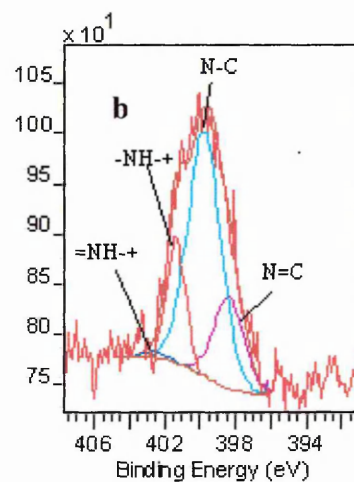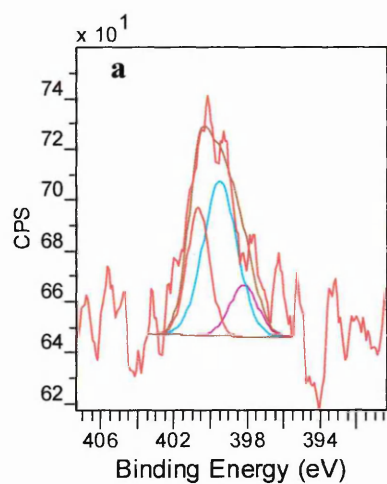
Figure 4-100 Change of N components with sputtering time a) 195sec b) 210 sec c) 240 sec d) 270 sec e) 300 sec and f) 375 sec
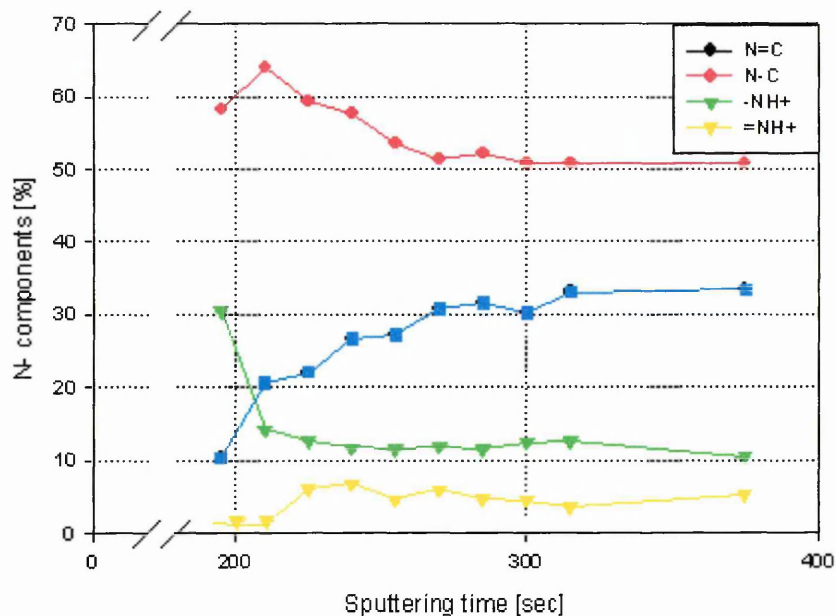
Figure 4-101 Relative percentage of N 1s components with sputtering time
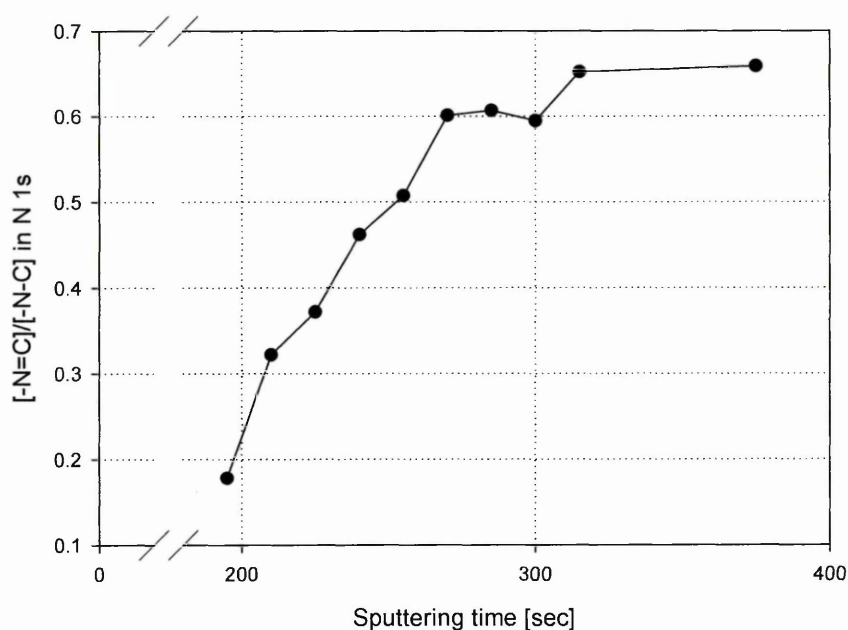
Figure 4-102 Relative concentration of [-N=C]/ [-N-C] from N 1s components with sputtering time

In support of the previous results, carbon, C1s, peaks were plotted as a function of sputtering time, see Figure 4-103 a-f. The XPS spectra showed four species that fitted in the C 1s envelope at 284.8, 285.5, 286.2 and 287.7eV representing C-C (and C-H) C-N, C=N [14] and C=O [16] respectively.
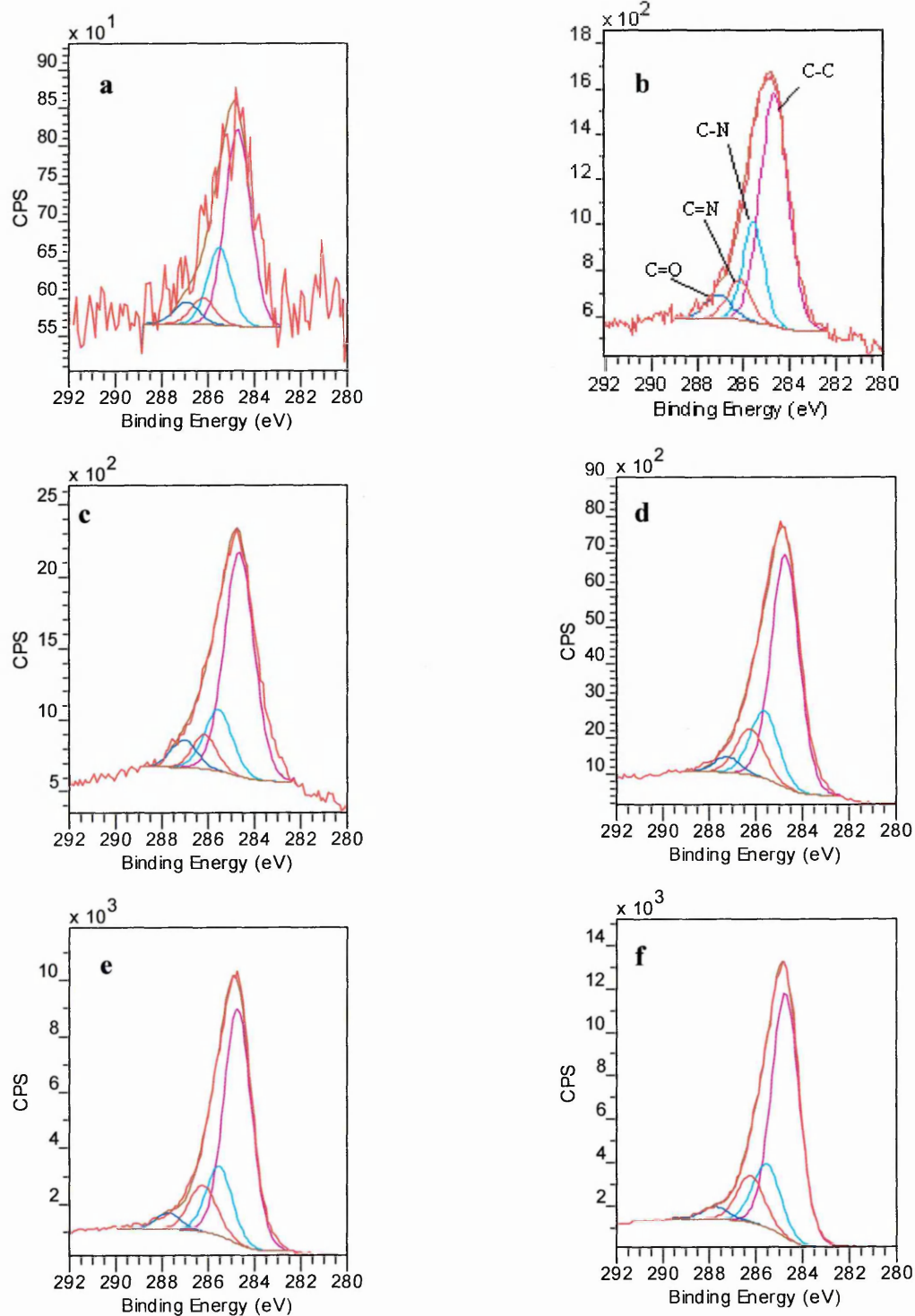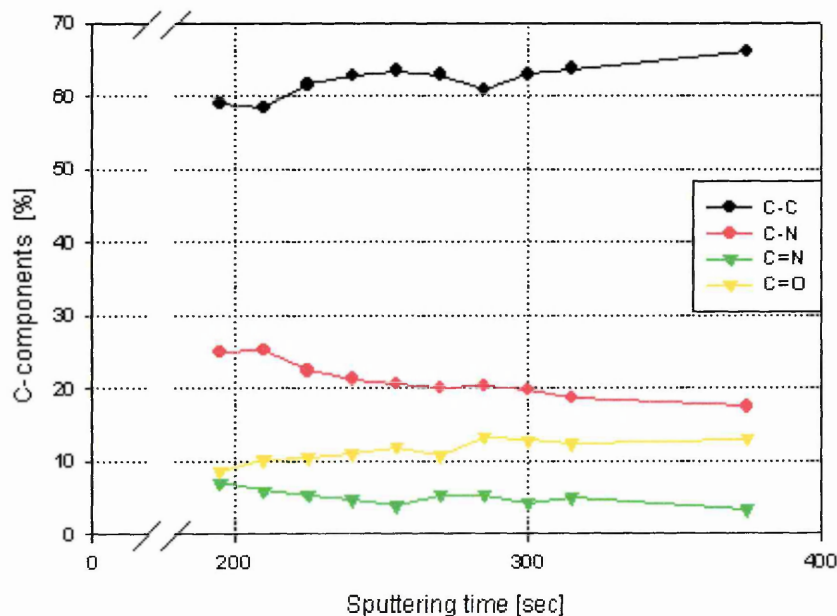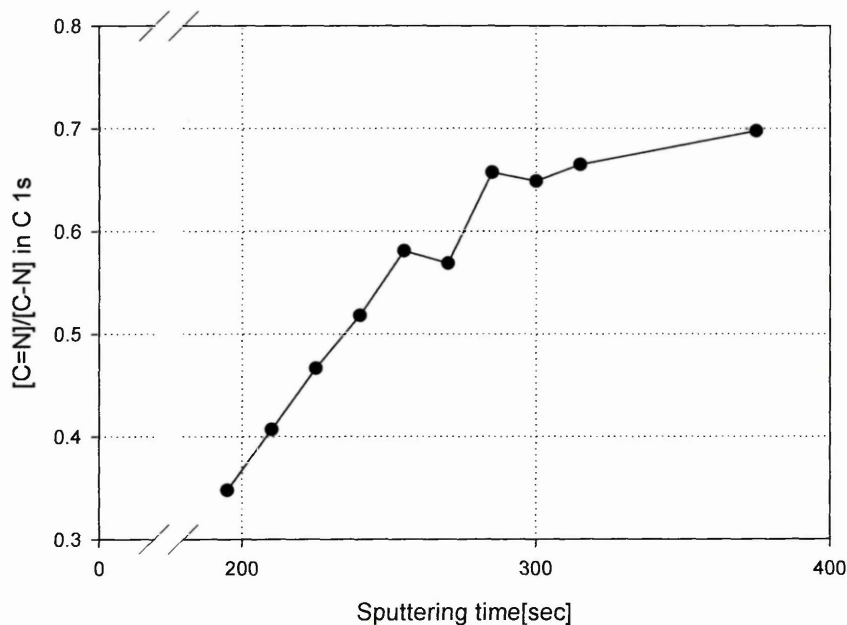
Figure 4-103 Change of C 1s components with sputtering time a) 195sec b) 210 sec c) 240 sec d) 270 sec e) 300 sec and f) 375 sec

Figure 4-103 shows the C=N peak at 286.2 increasing with sputtering time (in the direction of the PANI). The C=O peak, at 287.7 Figure 4-103-a, seemed to

174

be higher (at the edge of interface), however, it became smaller and stable after that. This may relate to contamination of the free standing PANI surface. The relative concentrations of these four species are shown in Figure 4-104. It can be seen that C=N increasing with sputter in the direction of the PAN, however, C-N decreased over the same region. The ratio of [C=N]/[C-N] are plotted Figure 4-105 where it can be seen that, the ratio gradually increases with sputtering time and becoming stable at about 0.7. This figure showed a similar trend to that of the ratio of [N=C]/[N-C] in Figure 4-102 which supporting the postulation that PANI is oxidised as sputtering in the PANI direction.

Figure 4-104 Relative percentage of C 1s components with sputtering time

175

Figure 4-105 Relative concentration of [-N=C]/ [-N-C] from C 1s components with sputtering time

The above results were obtained using a sample prepared by the evaporation of pure Al, 99.99%, onto the surface of a free standing PANI film under high vacuum conditions, 10^{-5} torr, this preparation method may have an influence on the XPS results and does not reflect the actual conditions of a normal coating procedure under normal pressure and temperature.

The following section describes an XPS study carried out for a thin PANI film coated on AA2024, prepared under normal conditions of pressure and temperature.

The XPS profiling was carried out from the PANI direction towards the AA2024 substrate. Furthermore, this study concentrated on the change of Al 2p and N1s in order to support the results obtained in the previous section. It should be noted that, the alloying elements of 2024, such as Cu and Mg, were not taken into consideration.

As it can be seen from Figure 4-106, there is small amount of oxygen on the surface of PANI; however, this completely disappears with sputtering. Oxygen is then observed on the edge of PANI/Al interface.

The atomic ratio of C: N is shown in Figure 4-107. The ratio shows an initial high value around, 8.7 which becomes stable around 7 up to the edge of

176

interface (arrowed). This value then increased to 9.3, at the edge of PANI/aluminium interface, returning back to 7, before showing unstable values beyond the interface. The erratic behaviour of the C: N ratio appears to relate to contamination of the surface.
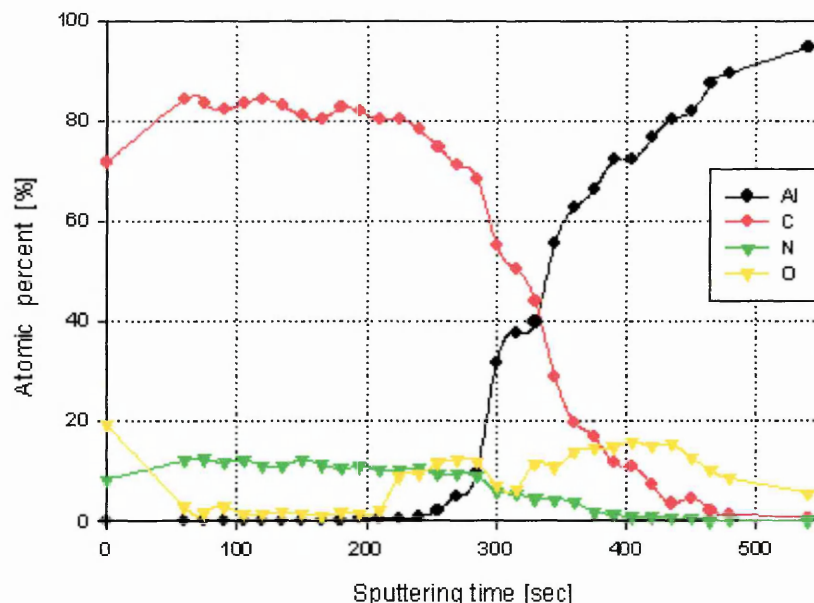
Figure 4-106 Change of elemental atomic percent of elements with XPS sputtering time
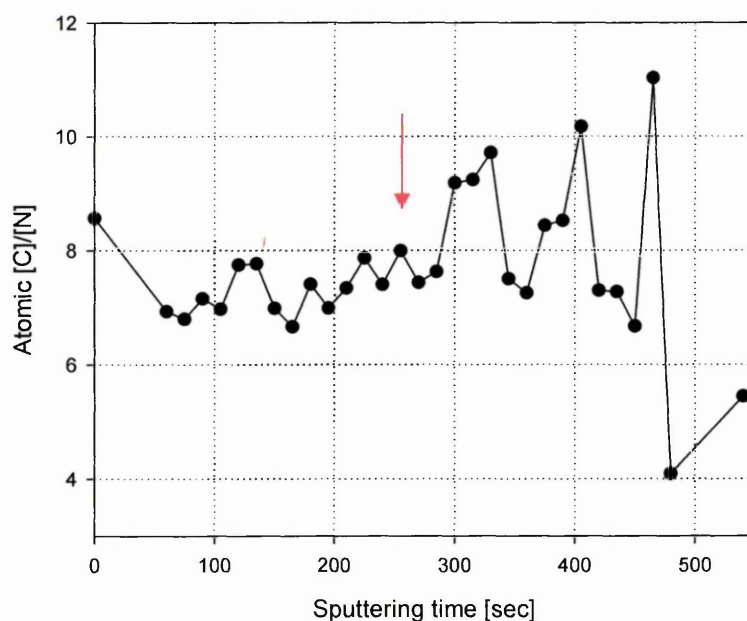
Figure 4-107 Relative atomic concentration of carbon to nitrogen with sputtering time.

High resolution XPS N 1s core level spectra are shown in Figure 4-108 (a-f). Here the N=C peak at 298.4±0.15 eV decreased with sputtering time i.e. towards the Al. Furthermore, the relative concentration of [N=C]/[N-C] in N1s

spectrum gradually decreased with sputtering towards Al as shown in Figure 4-109.
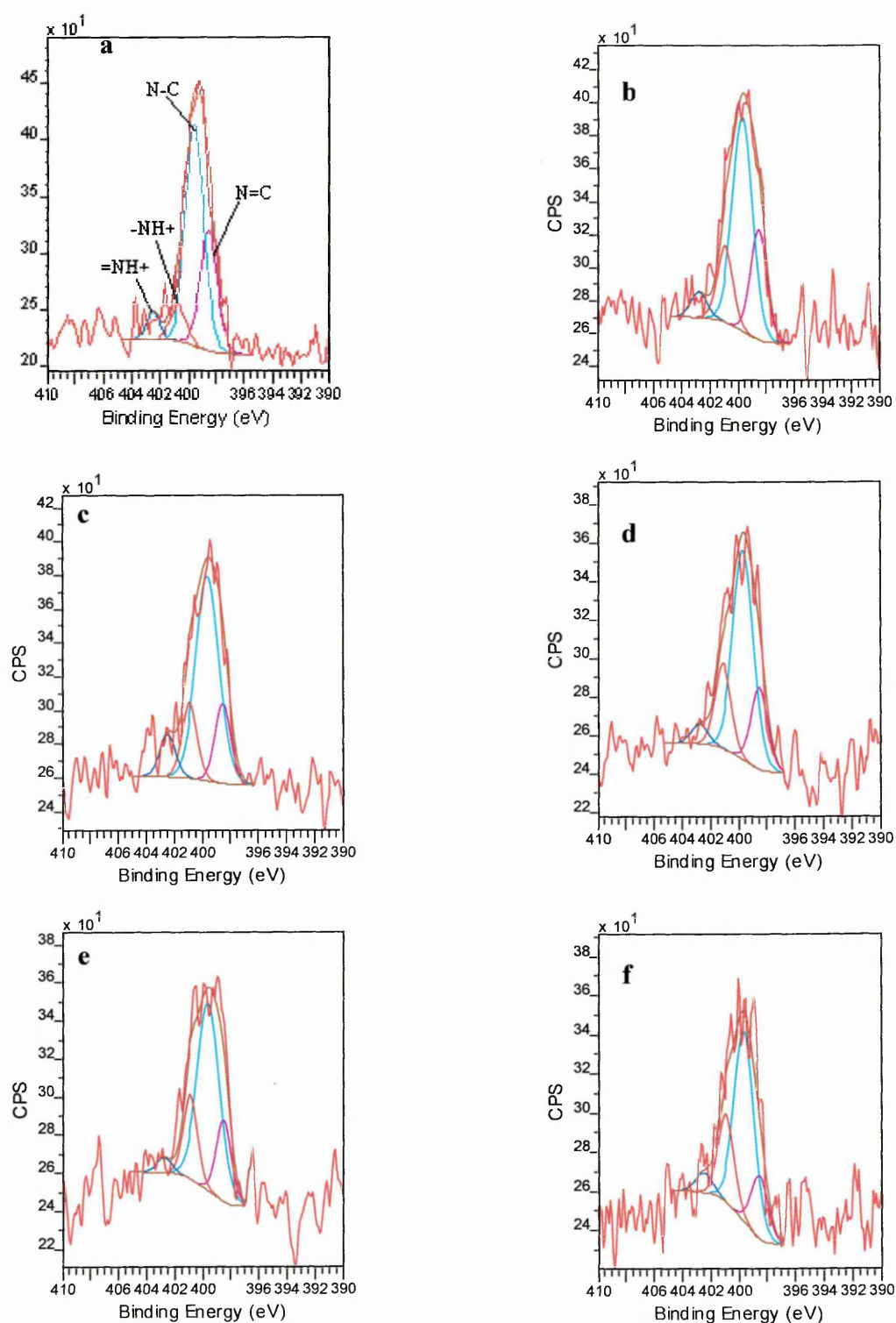
Figure 4-108 Change of N 1s components with sputtering time a) 195 sec b) 225 sec c) 330 sec d) 375 sec e) 435 sec and f) 450 sec

178
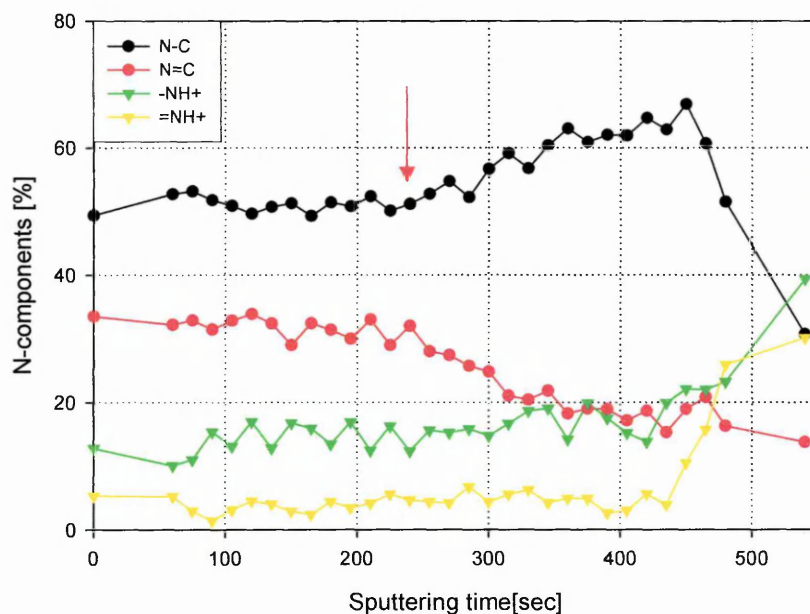
Figure 4-109 Relative percentage of N 1s components with sputtering time.

High resolution (Al 2p) XPS analysis is shown in Figure 4-110, where three species are identified at $72.8\pm0.1eV$, $74.5\pm0.15eV$, and $75.6\pm0.15eV$ representing metallic Al, Al-X and aluminium oxide. The Al-X component appeared at the interface region and decreased with sputtering time i.e. moving towards the Al. The relative percentages of these three components are shown in Figure 4-111. It is clear from the figure that the Al-X decreases sharply with sputtering time, moreover, aluminium oxide gradually decreases with sputtering time (towards the Al).
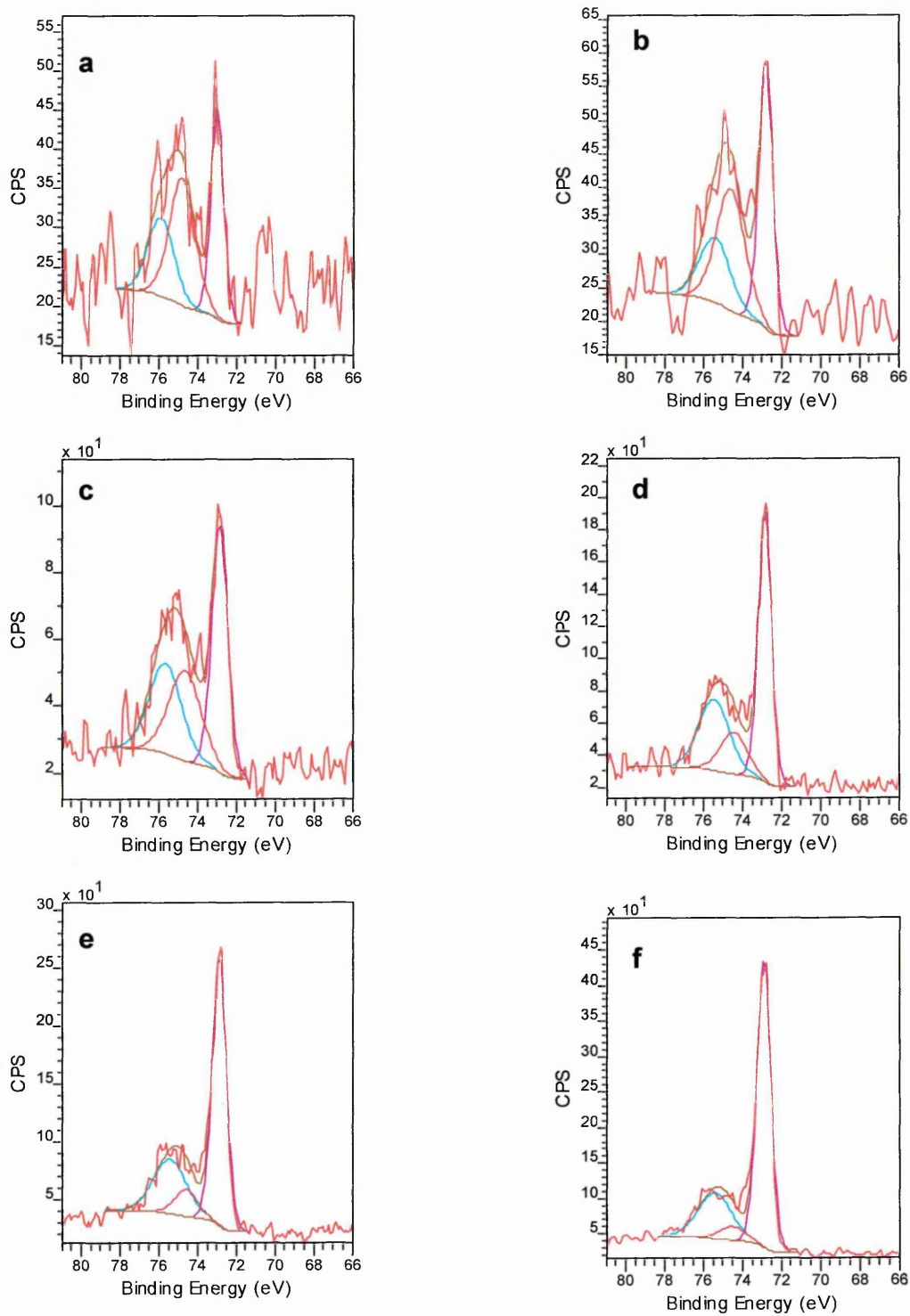
Figure 4-110 Change of Al 2p components with sputtering time a) 225 sec b) 270 sec c) 330 sec d) 375 sec e) 405 sec and f) 480 sec
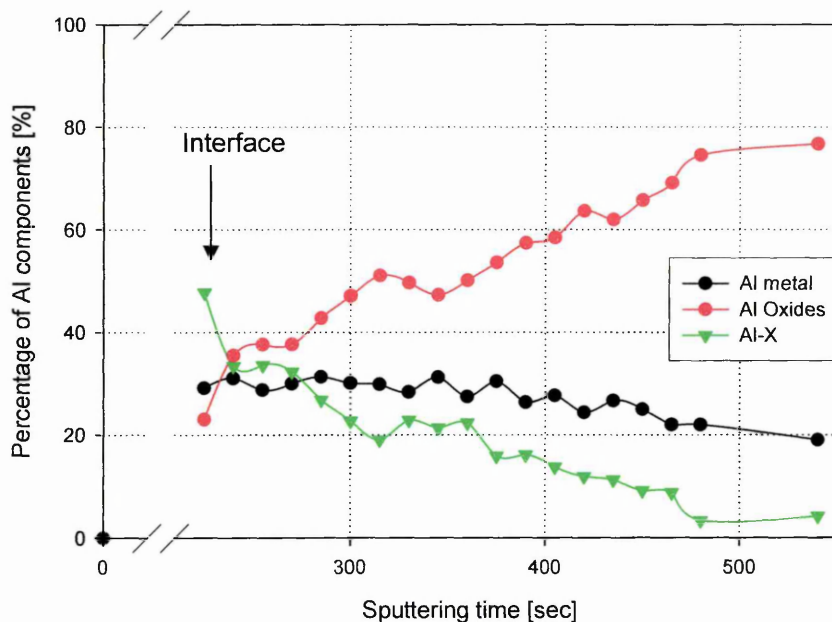
180

Figure 4-111 Change of Al 2p components with sputtering time

These results appear to be in agreement with those obtained from XPS depth profiling of the previous sample (Al evaporated over a PANI film).

4.3.3 TEM study

Investigation of the PANI/Al interface was also conducted using a TEM technique. The PANI coating thickness was 1.3 μm as seen in Figure 4- 112 which showing an SEM image of an FIB sectioned sample. It can be seen that there is a platinum cover on the surface of PANI which used to stabilise the sample during handling.

181
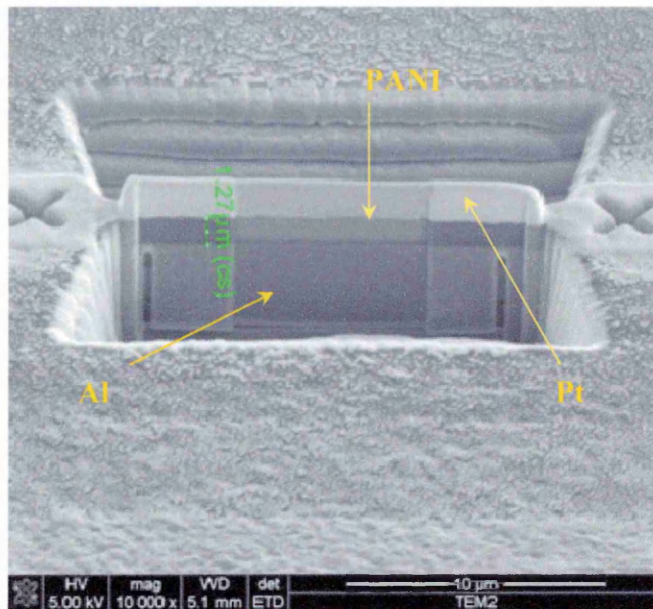
Figure 4- 112PANI coated AA2024 TEM sample

The TEM image of the PANI/Al interface, Figure 4-113, shows that the interface is about 30nm thick. The parallel lines on the Al side are representative of the alloy structure of AA2024.
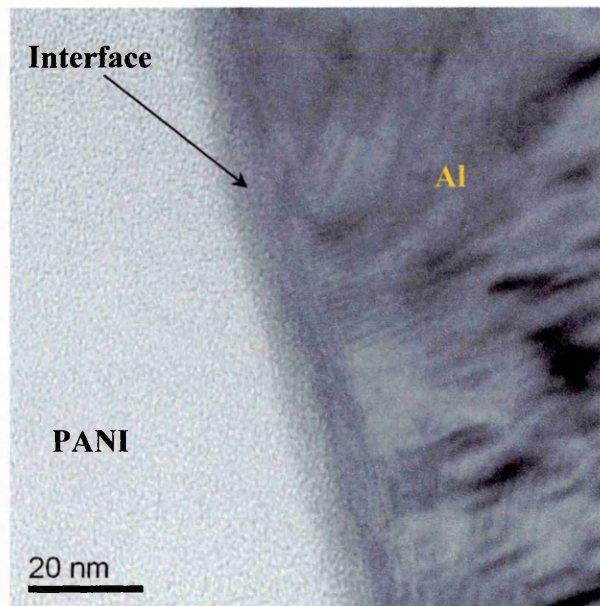
Figure 4-113 TEM image of PANI/AA2024 interface

EDX elemental analysis was used to study the interface region at different location across the interface as shown in Figure 4-114. The circles represent EDX analysis positions. Since the EDX resolution was around 6nm, the

distance between each circle was chosen to be more than 6 nm. Two EDX lines annotated as 1 to 6 and 7 to 12 were chosen to include two points in the Al, two points at the interface and two points in the PANI side, as shown in Figure 4-114.
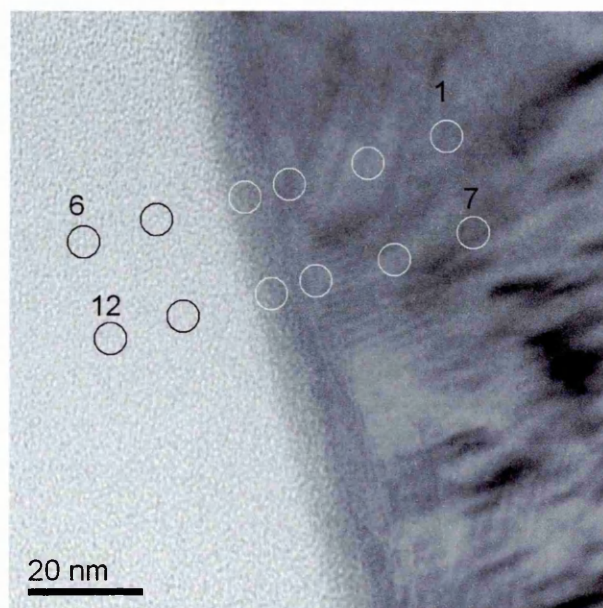
Figure 4-114 EDX point analysis of the PANI/AA2024 interface

Figure 4-115 shows representative EDX spectra from each of these locations. The EDX spectra show platinum and copper along the EDX line analysis. The platinum and copper seem to be stable in all spectra which may be due to contamination of the sample from the standard holder of the TEM. Carbon appears in aluminium side being smaller than that found at the interface and polymer sides. Carbon in the aluminium side may exist due to contamination of the sample from handling, whereas, the high carbon content at the interface and PANI is mainly due to carbon from the polymer.

Figure 4-116 shows the elemental change across the interface. In this estimation, the carbon content on the Al side is assumed to represent a background value for all other points. It can be seen that oxygen content has a peak in the interface region; moreover, Al and Mn percentage, in the PANI region, were very small (<1%) which may refer to the interference of these elements.
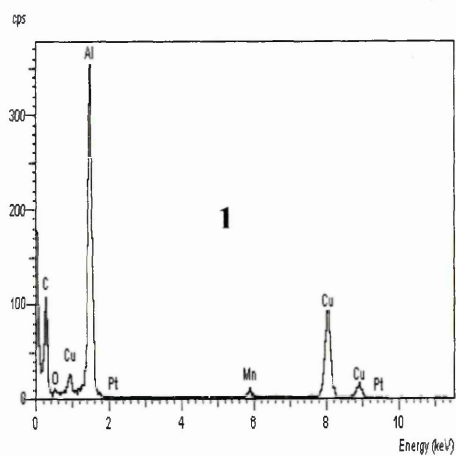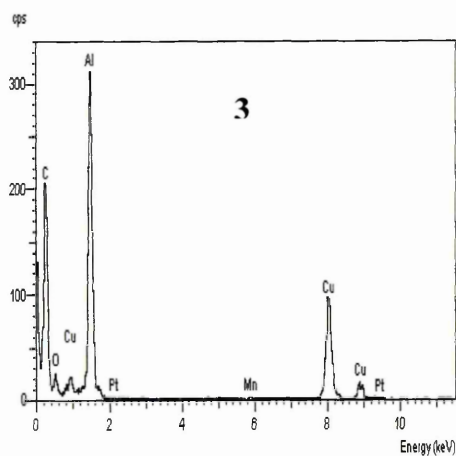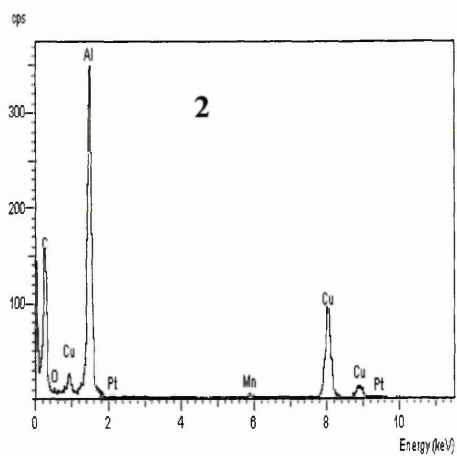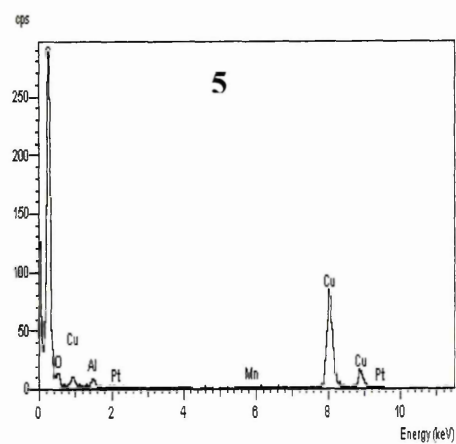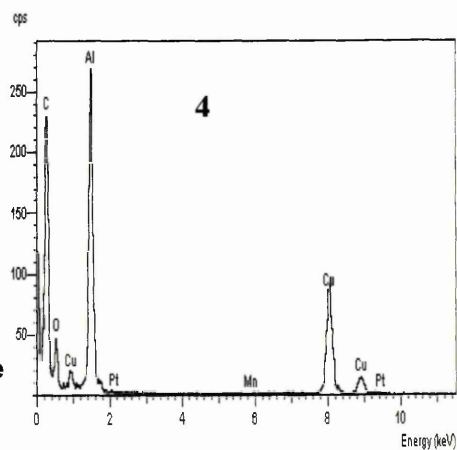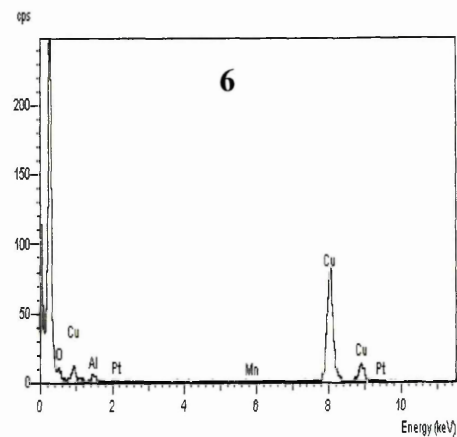
Figure 4-115 EDX line spectrum of the PANI/Al interface.
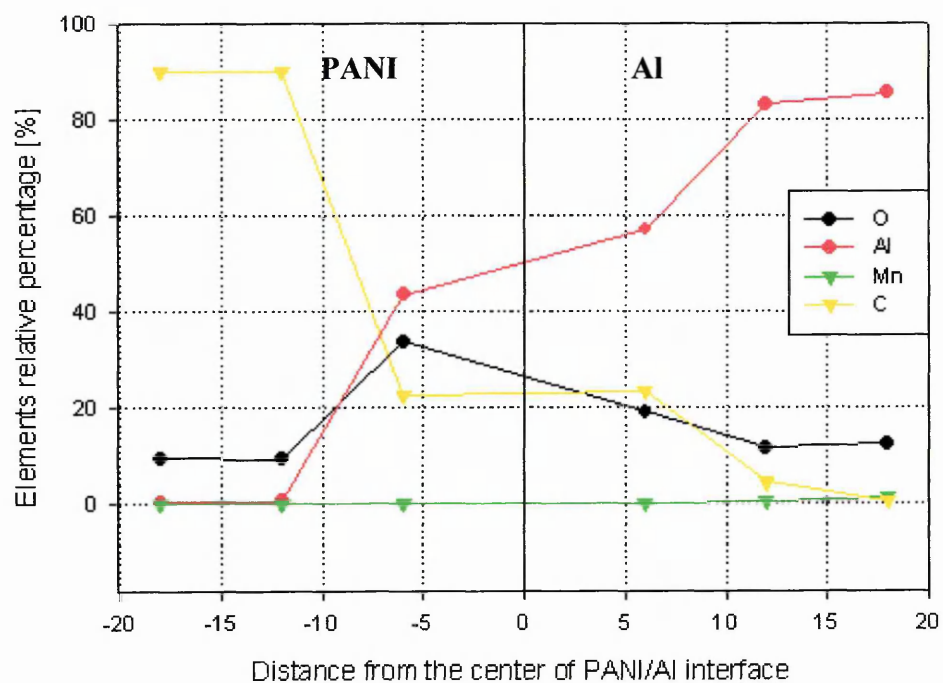
Figure 4-116 Change of elemental content across the PANI/Al interface
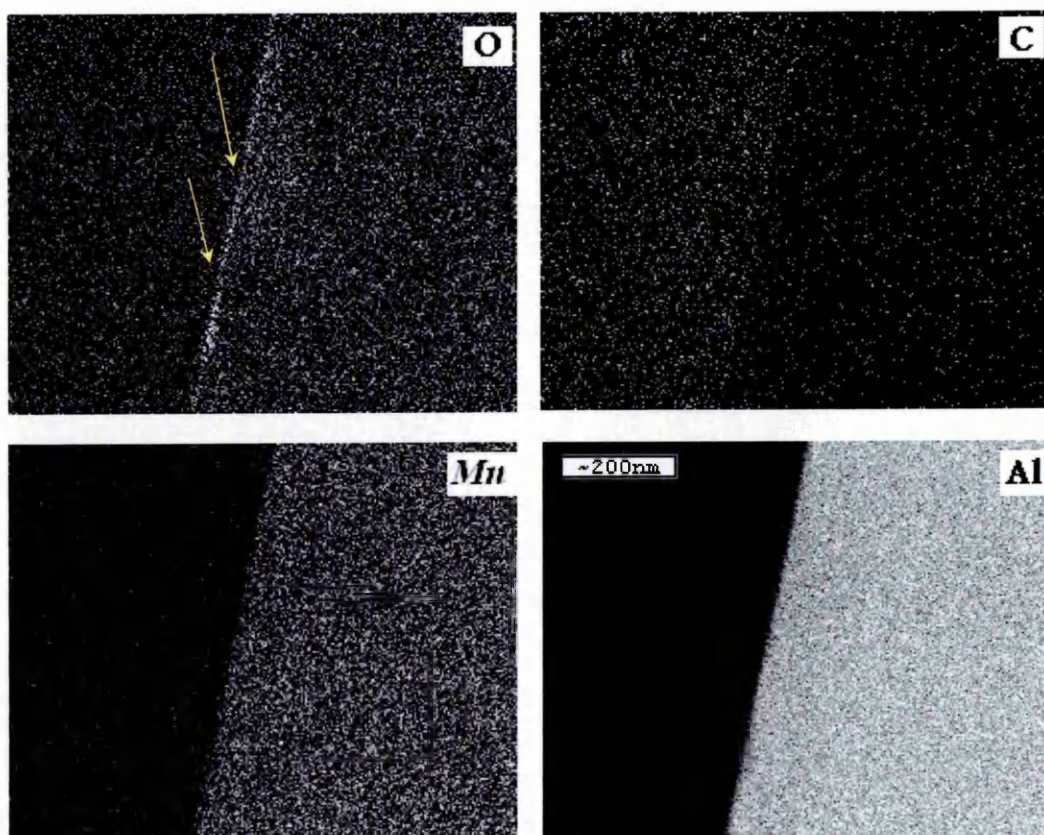
Figure 4-117 EDX mapping of PANI/Al interface

EDX mapping was conducting at the PANI/Al interface as shown in Figure 4-117. It is clear from EDX mapping that there is an increase in oxygen content at the interface (arrows), however, it could not be distinguish at which side of the interface the oxygen was favoured.

The TEM results also appear to be in agreement with the XPS results in that there was an increase in the amount of oxygen at the PANI/Al interface.

REFERENCES

[1] E. Hür, G. Bereket, and Y. Şahin, 2006/10/2, "Corrosion Inhibition of Stainless Steel by Polyaniline, Poly(2-Chloroaniline), and Poly(Aniline-Co-2-Chloroaniline) in HCl," Progress in Organic Coatings, 57(2) pp. 149-158.

[2] W. Daoud, J. Xin, X. Tao "Superhydrophobic Silica Nanocomposite Coating By A Low-Temperature Process" Journal Of The American Ceramics Society 2004;87(9), pp1782-1784..

[3] B. Szczygieł, And M. Kołodziej, 2005, "Composite Ni/Al$_2$O$_3$ Coatings And Their Corrosion Resistance," Electrochimica Acta, 50(20) pp. 4188-4195.

[4] L. Jianguo, G. Gaoping, And Y. Chuanwei, 2005, "EIS Study Of Corrosion Behaviour Of Organic Coating/Dacromet Composite Systems," Electrochimica Acta, 50(16-17) pp. 3320-3332.

[5] X. Zeng, And T. Ko, 1998, "Structures And Properties Of Chemically Reduced Polyanilines," Polymer, 39(5) pp. 1187-1195.

[6] P. Rodrigues, M. Cantão, P. Janissek, 2002/11, "Polyaniline/Lignin Blends: Ftir, Mev And Electrochemical Characterization," European Polymer Journal, 38(11) pp. 2213-2217.

[7] W. Stockton And M. Rubner, 1997, "Molecular-Level Processing Of Conjugated Polymers. 4. Layer-By-Layer Manipulation of Polyaniline via Hydrogen-Bonding Interactions," Macromolecules, 30(9) pp. 2717-2725.

[8] R. Mathur, D. Sharma, S. VaderaR, 2001, "Doping Of Emeraldine Base With The Monovalent Bridging Iron Oxalate Ions And Their Transformation Into Nanostructured Conducting Polymer Composites," Acta Materialia, 49(1) pp. 181-187.

[9] J. Fujita, H. Margaret, 2003, "Polyaniline Coatings For Aluminium: Preliminary Study Of Bond And Anti-Corrosion," International Journal Of Modern Physics, 17(8-9) pp. 1164-1169.

[10] S. Lim, K. Tan, And E. Kang, 1998, "Interactions Of Evaporated Aluminium Atoms With Polyaniline Films Effects of Dopant Anion And Adsorbed Oxygen," Synthetic Metals, 92(3) pp. 213-222.

[11] A. Monkman, G. Stevens And D. Bloor, 1991, "X-Ray Photoelectron Spectroscopic Investigations Of The Chain Structure And doping

187

Mechanisms In Polyaniline," Journal Of Physics D :Applied Physics, 24 pp. 738-749.

[12] S. Kumar, F. Gaillard, G. Bouyssoux, 1990, "High-Resolution XPS Studies Of Electrochemically Synthesized Conducting Polyaniline Films," Synthetic Metals, 36(1) pp. 111-127.

[13] Z. Li, E. Kang, K. Neoh, 1997, "Effect Of Thermal Processing Conditions On The Intrinsic Oxidation States And Mechanical Properties Of Polyaniline Films," Synthetic Metals, 87(1) pp. 45-52.

[14] Y. Lee, J. Kim, J. Kang, 2000, "Annealing Effects Of Dilute Polyaniline/NMP Solution," Macromolecules, 33(20) pp. 7431-7439.

[15] M. Ferrara, L. Mirenghi, A. Mevoli And L. Tapfer, 2008, "Synthesis And Characterization Of Sol–Gel Silica Films Doped With Size-Selected Gold Nanoparticles," Nanotechnology, 19(36) pp. 365706.

[16] B. Vincent Christ, "Handbook Of The Elements And Native Oxides," XPS International, USA, 1999.

CHAPTER 5

DISCUSSION

In this chapter, the results obtained from the experimental work are discussed; moreover, the processing condition of PANI/sol-gel coatings is also discussed. The discussion, in Chapter 5, mainly consists of four parts; processing conditions, corrosion performance, mechanical properties and finally corrosion mechanism.

5.1 PREPARATION CONDITION OF PANI/SOL-GEL COATINGS

PANI sol-gel coatings were prepared using a silica base sol-gel and 3.5% PANI (EB) solution. The coatings were applied onto AA 2024 and cured at 70°C for 16 hrs in an air oven prior to testing.

According to Tzou et al [1] [2] PANI/NMP solutions (>5%) are unstable and rapidly form gels at room temperature, therefore during this study PANI/NMP solution was kept at 3.5% to avoid the formation of a gel prior to application to the substrate. The DSC curves in Figure 5-1 generally showed two endothermic processes (1) from 35°C to 110°C and (2) between 120 and180°C and one exothermic process occurred after 250°C. The first endothermic process occurred with the sol-gel (free of PANI), whereas, the second process did not. The second process increased with increasing PANI content as shown from the figure. The exothermic process occurred in all sol-gel containing samples, but not in the PANI sample. It can be concluded that endothermic processes at 35-110°C and the process commencing at 230°C are related to the sol-gel, while, the endothermic process at 120-180°C is related to the PANI. Between 35-110°C evaporation of solvents (water and ethanol) from the sol-gel and NMP from PANI, and condensation of sol-gel takes place. From 210-380°C it appears that degradation of the organic component in the sol-gel takes place. Note: TG

189

analysis of free standing sol-gel showed a weight loss of 8% between 220 and 390°C.
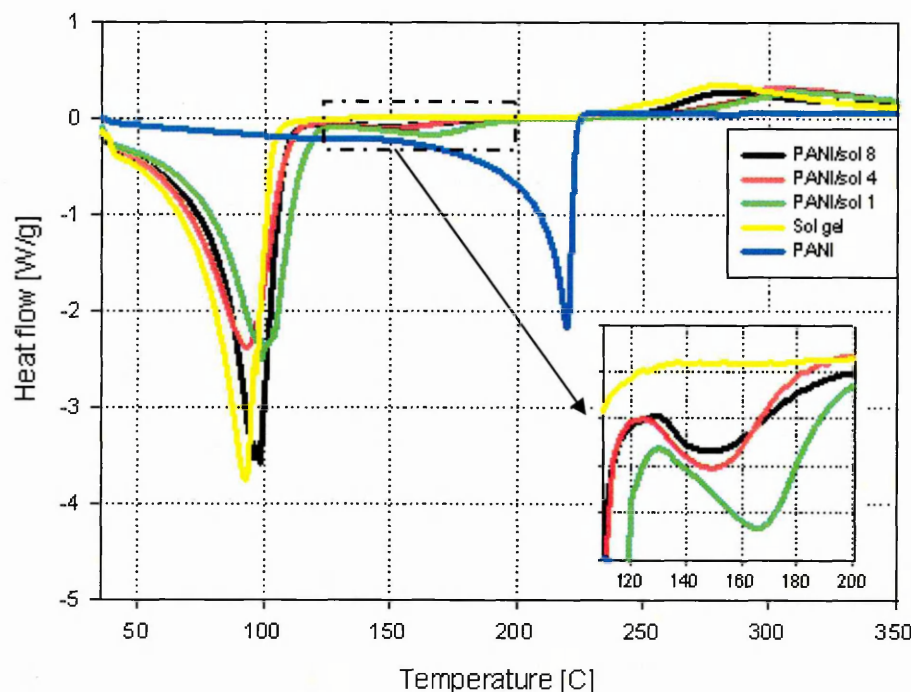
Figure 5-1 DSC of PANI/ sol-gel coating and PANI/NMP 3.5% solution

The second process is related to the PANI. When PANI is dissolved in NMP, hydrogen bonds form between the PANI and part of NMP [3]. The PANI/NMP DSC curve showed continuous evaporation of free NMP (no H-bonding) from 35 to 142 °C after when PANI begins to form a cross-linked structure [4] which is irreversible [5]. Moreover, at ≈180°C the hydrogen bond of PANI/NMP breaks down and evaporation of NMP takes place.

However, the sharp endothermic peak of break down of the PANI/NMP' hydrogen bond disappeared in the PANI/sol-gel coatings. This may be related to the break down of the H-bond between PANI and NMP when mixed with sol-gel. The silica based sol-gel is catalysed with nitric acid which would dope PANI and break any hydrogen bonds [3]. These results suggest that the second endothermic of PANI/sol-gel coating (120-180°C) was mainly related to PANI cross-linking and continuous evaporation of NMP.

According to Lee et al [5] PANI cross-linking begins to form from 100°C, this result suggests the end limit for the curing of PANI/ sol-gel coatings should be below 100°C.

The PANI/sol-gel coating showed some phase separation during curing at 90±5°C as showed in Figure 5-2. This can be explained by the difference in solubility in solvents and/or surface tension of sol-gel and PANI [6]. At high temperature, 90-100 °C the rapid evaporation of sol-gel solvents (water and ethanol) may lead to rapid condensation of the sol-gel; meanwhile, PANI is still soluble in NMP. In such a case, the PANI solution would be expelled from the sol-gel matrix leading to phase separation.
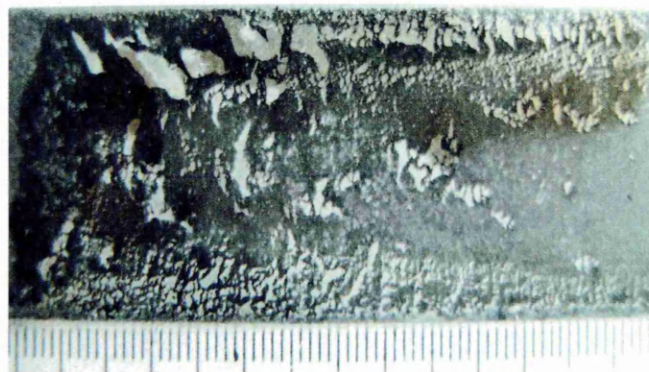
Figure 5-2 PANI/sol1 cured at 90±5°C for 16 hrs

At 70°C, the coating did not show any phase separation, however, it was necessary to investigate "how long sol-gel coating takes at that temperature to complete the curing reaction"

Another DSC study was conducted where (1) sol-gel and PANI/sol1 samples were separately heated from 35 to 70°C and then kept at that temperature for 5 hrs and then cooled to room temperature. (2) Each sample from 1 was subsequently heated from 35°C to 350°C to check if there is any decomposition process that did not take place at 70°C. this procedure was carried out to investigate whether the curing reaction was complete after 5 hrs.

Figure 5- 3 shows the sol-gel and PANI/sol1 samples DSC curves before and after heating at 70°C for 5 hrs.

It is clear from the DSC curves that the samples were completely cured after 5 hrs at 70°C. Moreover, sol-gel and PANI/sol1 coated AA2024 samples were cured at 70°C and their hardness were measured every hour for 7 hrs using

191

pencil hardness test. Pencil index of the coated samples showed stable values after curing for 5 hrs. These results support the thermal analysis results in that curing of sol-gel and PANI/sol-gel samples at 70 °C for 16 hrs was sufficient.
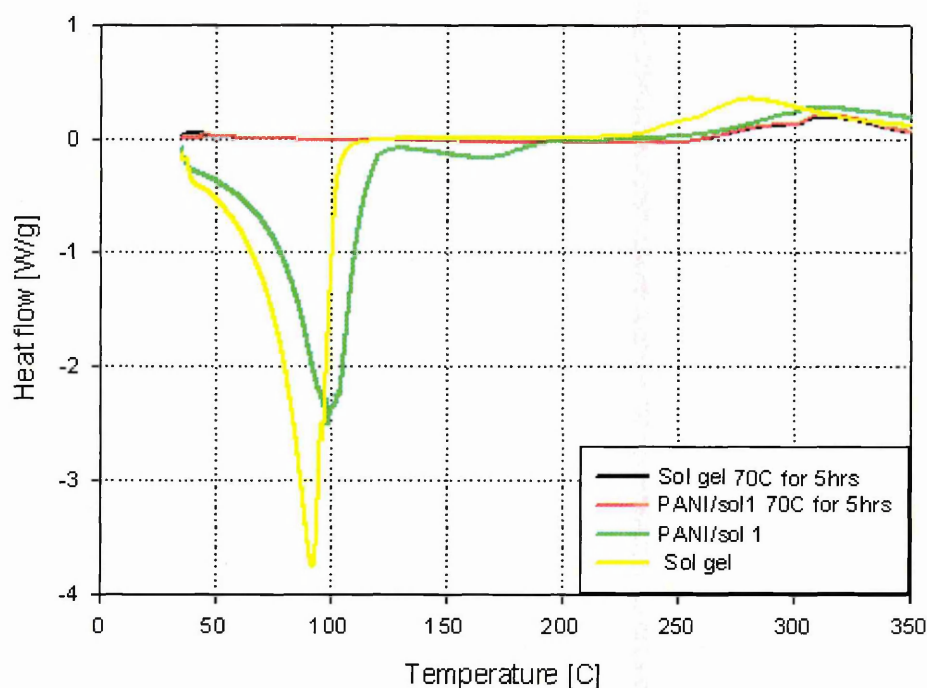
Figure 5- 3 Sol-gel curing at 70°C for 5 hrs

5.2 CORROSION PERFORMANCE

5.2.1 Bare AA2024

EIS data for bare AA 2024 immersed in 3.5% NaCl (prior to 24 hrs, see Figure 4-5) showed a single time constant, which, ideally, may be modelled using the circuit presented in Figure 5-4. The circuit consists of a solution resistance (R_s), charge transfer resistance (R_{ct}) parallel to a capacitance element representing the double layer capacitance (C_{dl}) forms at the metal/electrolyte interface.
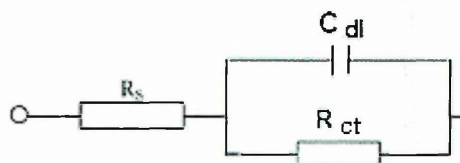
Figure 5-4 Equivalent circuits used for numerical fitting of the EIS data of bare sample before 24 hrs

After 24 hrs, a second time constant appears in the low frequency range (0.1 Hz) which corresponds to 'general' corrosion; observation of the surface showed widespread pitting over the entire surface after 72 hrs of immersion. This behaviour was accompanied with the formation of white gelatinous material followed by changing the colour of some spots to a brown colour on the surface. The white gelatinous material was mainly $Al(OH)_3$ which usually forms on the Al surface as a corrosion product [7]. However, the brown colour relates to the severe dealloying of Al_2CuMg particles which is followed by removal and distribution of copper across the sample surface after exposure to sodium chloride solution [6] [8].

These features suggested the break down of the bare sample in 3.5%NaCl solution within 24 hrs.

5.2.2 PANI coating

The polarization results, Figure 4-1, of PANI coated AA2024 showed that the PANI coated sample has lower corrosion potential than that of bare sample which may be due to the reactivity of the PANI. This result may indicate that the corrosion protection properties of PANI are not due to a simple galvanic coupling process, by which the polymer has a lower oxidation potential than the metal it is protecting, as assumed by Ahmad et al [9].

The impedance results of the PANI coated AA, Figure 4-9, showed an inductive peak on the first day of immersion in sodium chloride solution, which may be related to the instability of the redox form of PANI [10]. A part of PANI (EB) seems to change its oxidation state to the conductive form (ES) due to interaction with water molecules leading to an increase in its conductivity [11] [12] or due to protonation by Cl^- ions.

The PANI coated sample exhibited a stable impedance value for a thin film coating (3µm). Furthermore, the coated surface following delamination of the PANI coating showed higher impedance (1.5×10^6 Ohm.cm^2) than that of bare sample (1.0×10^4 Ohm.cm^2). Indeed these results indicated that the protection was neither related to barrier properties nor due to a shifting of the electrochemical reaction interface from the metal/solution interface to the polymer/solution interface [13]. This may relate to the formation of (1) an oxide

layer or (2) an inert or insulating interface. All these possible mechanisms will be discussed later in this chapter.

5.2.3 Sol-gel coating

The impedance results of the sol-gel coating, Figure 4-17, showed two time constants; one at high frequency (10^{-4} Hz) and the other at low frequency (0.1 Hz). The former represents the outer layer of coating which decreased with immersion time. However, the later, represents the corrosion products, increased with immersion time, this combined with a decrease in impedance values together with a change in the appearance of pits from white to reddish brown colour (Cu deposition).

Fitting the EIS data in an electrical circuit allows understanding the corrosion process within this silica sol-gel coating. The EIS equivalent circuit shown in Figure 5-5 is typically for organic barrier coating, and is applicable to this coating. This circuit contains the following components;

(1) An electrolyte resistance (R_s); (2) pore sol–gel layer resistance (R_p); (3) sol-gel coating capacitance (Q_c) (4) double layer capacitance (Q_{dl}) and (5) charge transfer resistance (R_{ct}). Moreover, constant phase elements were used instead of pure capacitors.
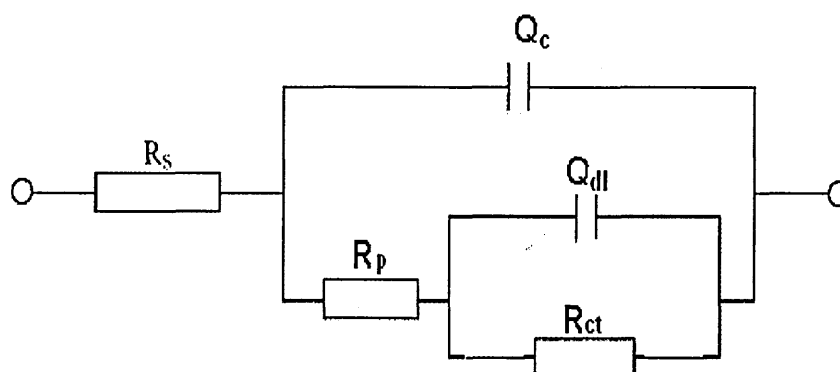
Figure 5-5 Equivalent circuits used for numerical fitting of the EIS data for a sol-gel coated AA2024 in 3.5%NaCl solution

(Appendix C) contains the parametric changes for the equivalent circuit during 16 days of immersion.
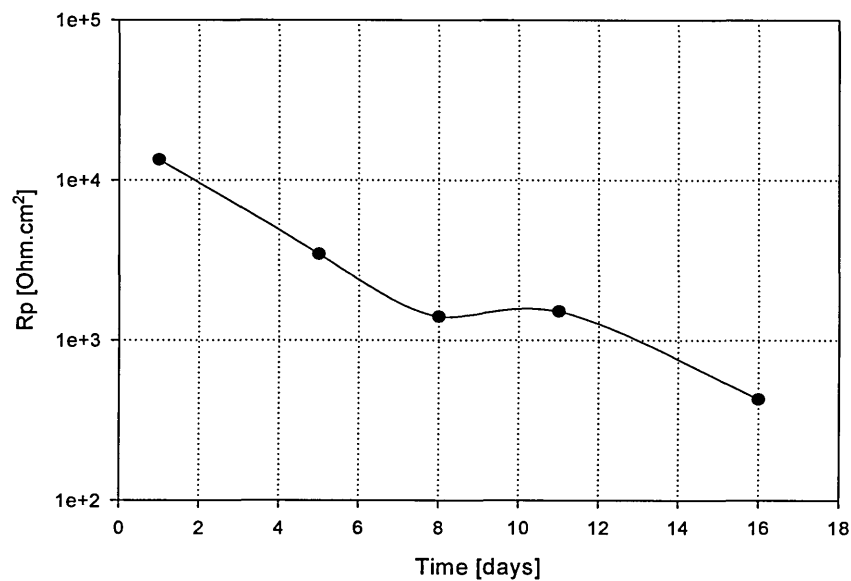
Figure 5-6 Change in sol-gel pore resistance with immersion time.

Figure 5-6 show the change of sol-gel pore resistance during 16 days of immersion in 3.5% NaCl solution. It can be seen that the pore resistance decreases dramatically during the first 8 days of immersion. A period of stability between 8-11 days was noted. This stability coincided with the change of surface colour from white to brown (pitting). These corrosion products may act to fill the sol-gel pores and temporary stabilise the pore resistance.
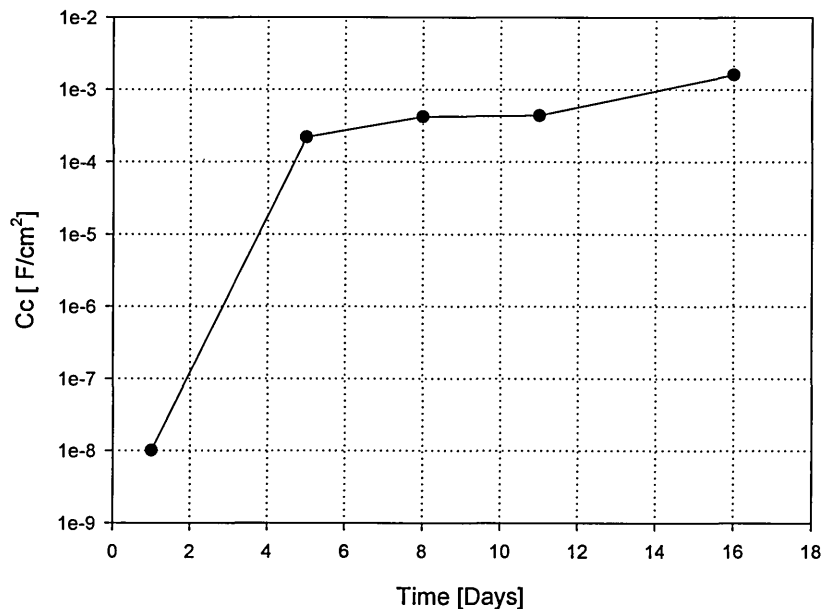
Figure 5-7 Change of sol-gel coating capacitance of sol-gel coated AA2024 in 3.5%NaCl solution with immersion time.

The sol-gel coating capacitance showed a continuous increase during the 16 days period of immersion, see Figure 5-7. The rapid decrease of pore resistance and increase of coating capacitance may be attributed to electrolyte ingress within the coating.

The charge transfer resistance decreases continuously with immersion time as shown in Figure 5-8. At the same time, the double layer capacitance (C_{ld}) increases sharply with immersion time as shown in Figure 5-9. These results indicate a rapid break down of the sol-gel coating in 3.5% NaCl solution within a few days of immersion.

Visual inspection of the samples suggests that changes in the low frequency time constant relate to the development of corrosion products. These corrosion products resulted from electrolyte penetrating the sol-gel causing a breakdown of the coating.
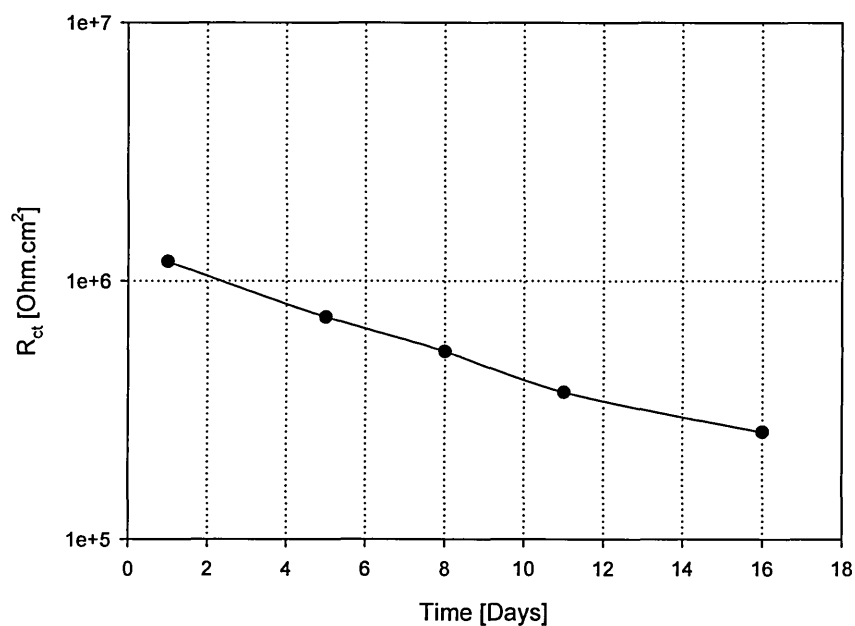
Figure 5-8 Change of charge transfer resistance of sol-gel coated AA2024 in 3.5%NaCl solution with immersion time.
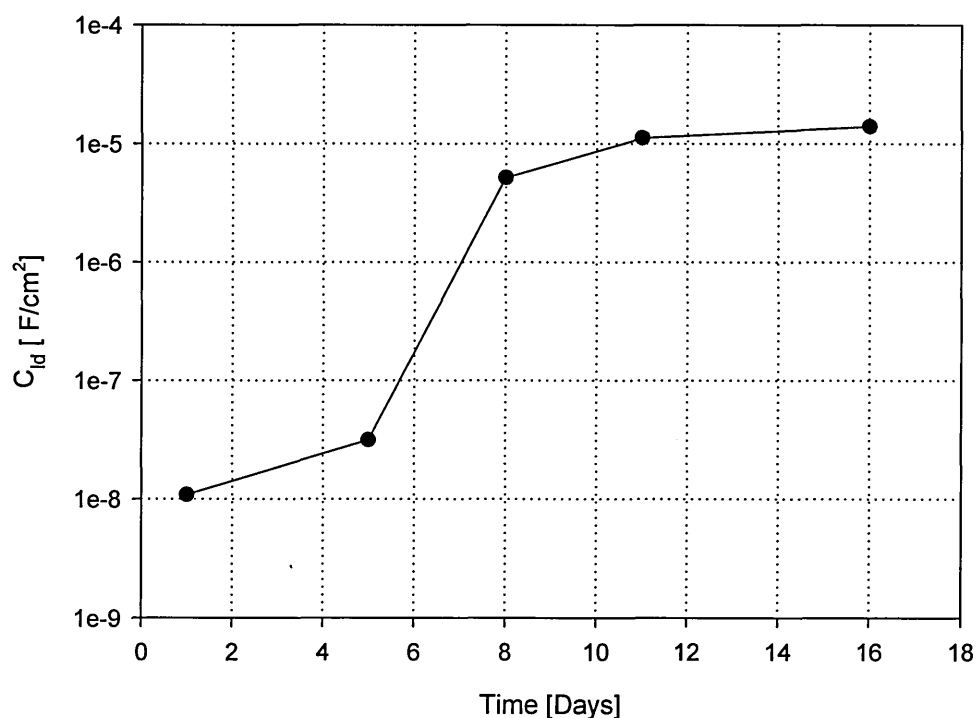
Figure 5-9 Change of double layer capacitance of sol-gel coated AA2024 in 3.5%NaCl solution with immersion time.

The sol-gel did not demonstrate any long-term protection under salt spray testing and pits appeared on the entire surface after 72 hrs followed by delamination of the coating as well as undercutting near the scratched area.

These results indicate that sol-gel coating may act as an inactive barrier coating for AA2024; moreover, this silica based sol-gel coating alone has limited corrosion protection properties to AA2024.

5.2.4 PANI/sol-gel coating.

PANI/sol-gel coatings showed that there is a minimum concentration of PANI notably 1:8 PANI: sol-gel, required to offer corrosion protection. Adding a small concentration of PANI provides some protection, as shown with PANI/sol16 and PANI/sol12 (see Figure 4-23 and appendix A), in which the degree of pitting, number and pit size, were less than that of a sol-gel coating.

Increasing the PANI content to be greater than the sol-gel concentration (PANI/sol 0.25), produced a coating that exhibited a porous surface which

affected the mechanical properties of the coating. This aspect will be discussed later in this chapter.

PANI/sol8, 4 and 1 showed superior corrosion protection for AA2024 up to 7 months of immersion in 3.5%NaCl solution (see section 4.1.2.6).

To understand the corrosion behaviour of these PANI/sol-gel coatings, EIS data of PANI sol-gel coatings were fitted into two equivalent circuits as shown in Figure 5-10. These circuits contained two embedded RC circuits representing the coating/electrolyte and coating/metal interfaces respectively. The high frequency circuit was ascribed to a coating capacitance (C_c) and pore resistance (R_p) of the sol-gel polymer coating, while, the low frequency represented the double layer capacitance (C_{dl}) and charge transfer resistance (R_{ct}) of the under lying metal as shown in Figure 5-10-a. Two constant phase elements (Q_c and Q_{dl}) were used instead of pure capacitances (C_c and C_{dl} respectively) for both frequencies. The equivalent circuit, Figure 5-10-b, contains a Warburg element for semi-finite diffusion i.e. diffusion in the coating layer.

(Appendix D) contains the parametric changes for the equivalent circuit during the course of immersion.
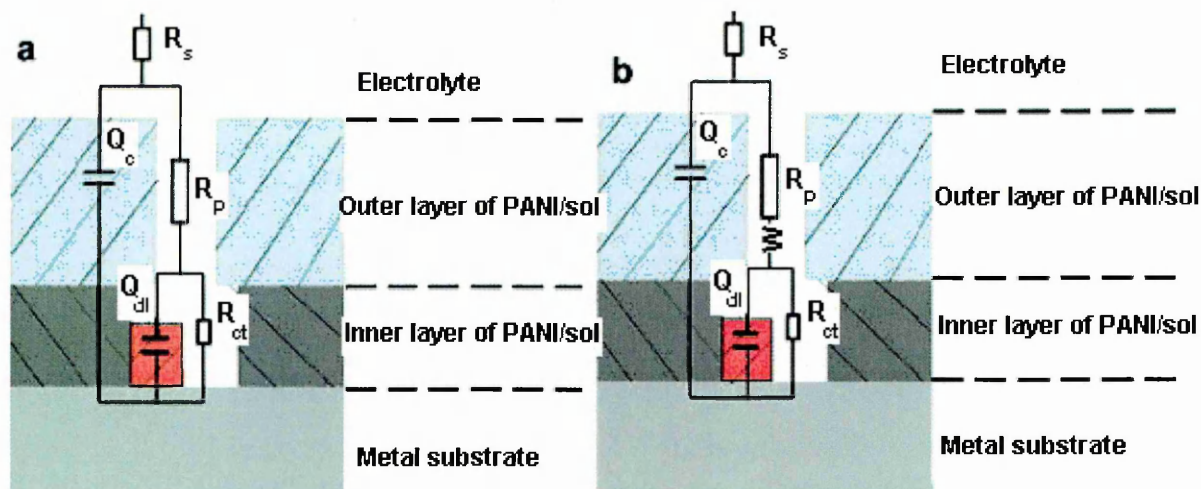
Figure 5-10 Equivalent circuits used for numerical fitting of the EIS data PANI/sol8, PANI/sol4 and PANI/sol1 (a) before 14 days and (b) after 14 days (not to scale)

The outer circuit, R_p and Q_c, represent the interaction at the coating/electrolyte interface. Figure 5-11 shows the change of pore resistance with the time of immersion for PANI/sol coatings (PANI/sol8, PANI/sol4 and PANI/sol1). The

198

pore resistance values decreased with increasing PANI content i.e. PANI/sol8>PANI/sol4>PANI/sol1. PANI/sol-gel coatings show a similar trend, notably decrease in R_p during the first month of immersion, however, after this initial period, the values of pore resistance and coating capacitance reach a plateau and remain almost unchanged for up to 7 months of immersion. The initial sharp decrease may be related to the protonation of the PANI by the electrolyte within the sol-gel matrix and/or the uptake of water over the first few days, which can also be seen as an increase in the coating capacitance as shown in Figure 5-12. This behaviour explains the decrease of impedance at high frequency, 10^4 Hz, (see Figures 4-25, 4-28 and 4-30) and shifting of the time constant towards lower frequency at the beginning of immersion (see Figures 4-26, 4-29 and 4-31). Diffusion of water through the coating depends upon the porosity and hydrophobicity of the coating. Based upon equivalent circuit fitting this process appears to take around two weeks.

After 210 days the PANI/sol4 and 1 samples were damaged. This damage was not due to the exposure or corrosion rather a potentiostat failure; therefore, it was not possible to acquire long-term data from these specimens. The PANI/sol8 sample did survive and the data provided after the 210 days point is shown in the insets of figures 5-11 to 5-14.
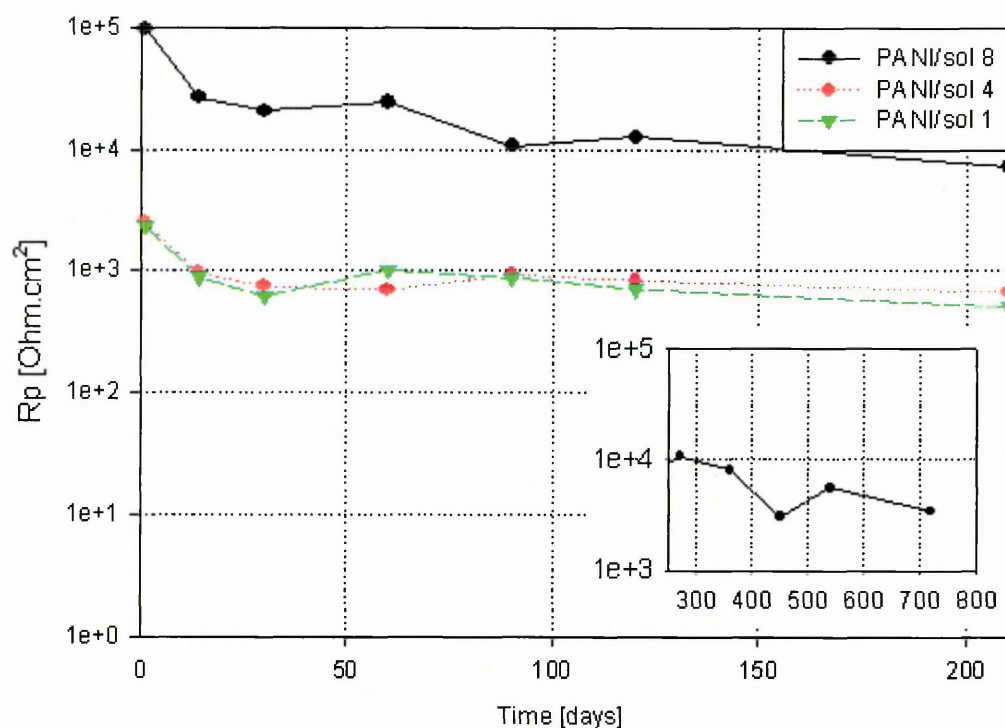
Figure 5-11 Change of pore resistance of PANI/sol-gel coated AA2024 in 3.5% NaCl solution with immersion time. Inset-behaviour for PANI/sol8 sample from 250-720 days.
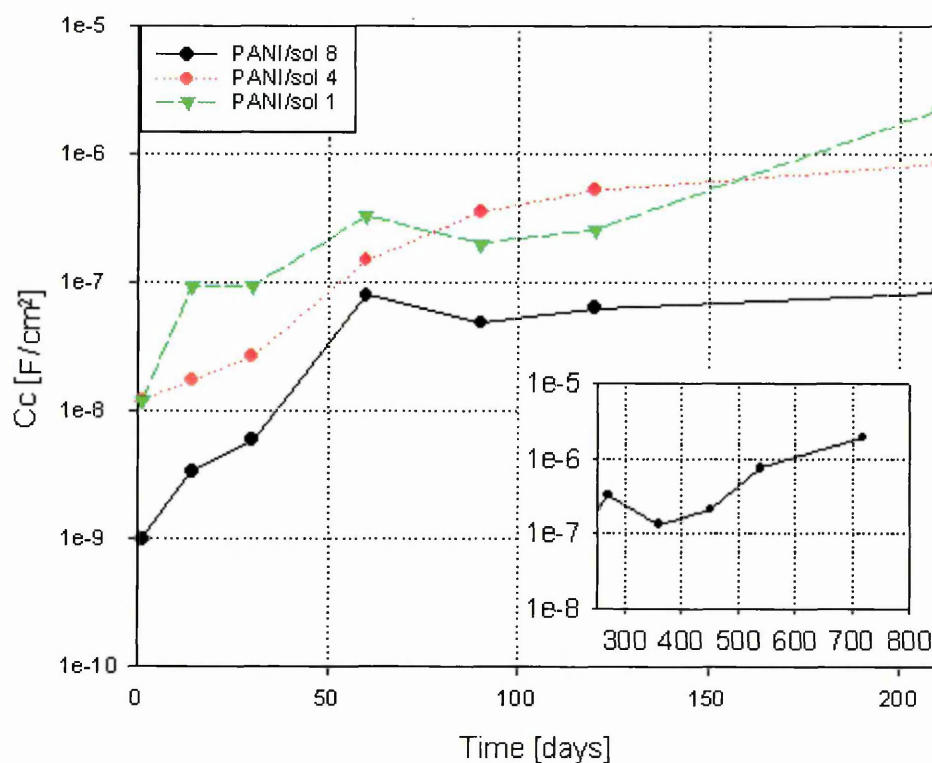
Figure 5-12 Change of coating capacitance of PANI/sol-gel coated AA2024 in 3.5% NaCl solution with immersion time. Inset-behaviour for PANI/sol8 sample from 250-720 days.

200

Figure 5-13 presents the change in charge transfer resistance as a function of immersion time for all three coatings. Here it can be seen that the R_{ct} values for these coatings become stable after one month of immersion within the same order of magnitude (10^5-10^6 Ohm.cm^2).

R_{ct} values reflect processes occurring at the coating/metal interface; PANI can be protonated by the ingress of the electrolyte and this would increase the conductivity of the coating, with the magnitude of change being related to the PANI content. PANI/sol4 and PANI/sol1 have a higher percentage of PANI above that of PANI/sol8 and appear to be affected more by the protonation of PANI.

In addition, PANI may interact with the substrate forming a passive layer that prevents the corrosion process at the substrate. PANI protonation and interaction with the metal substrate seems to take two weeks to complete, as shown in Figure 5-13.
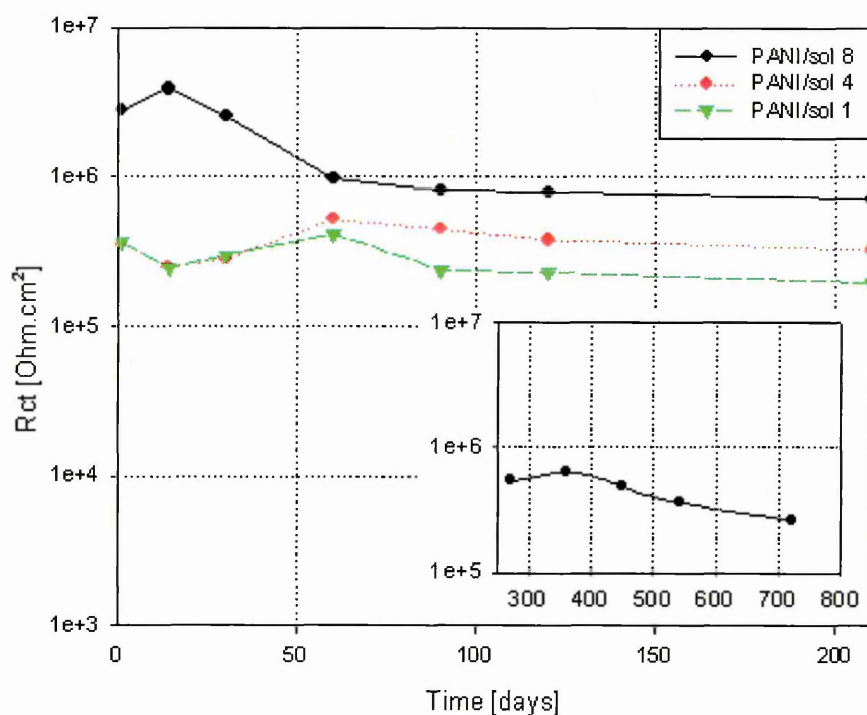
Figure 5-13 Change of charge transfer resistance of PANI/sol-gel coated AA2024 in 3.5% NaCl solution with immersion time. Inset-behaviour for PANI/sol8 sample from 250-720 days.

The EIS phase angle for the three PANI/sol-gel coating systems, chapter 4, exhibited shifts in the time constant peak from high to low frequency. This shift occurred after one month of immersion and was followed by stability in both

201

value and position up to the end of the test. This behaviour is related to the ingress and/or uptake of electrolyte through the coating and appears as an initial increase in the double layer capacitance, as shown in Figure 5-14. After 1-2 months the C_{dl} values becomes stable; this behaviour may be due to the formation of a passive layer at the interface region. Additionally the three PANI/sol-gel coatings have the same trend in behaviour with the difference in values being related to the difference in porosity, hydrophobicity, PANI content and coating thickness.
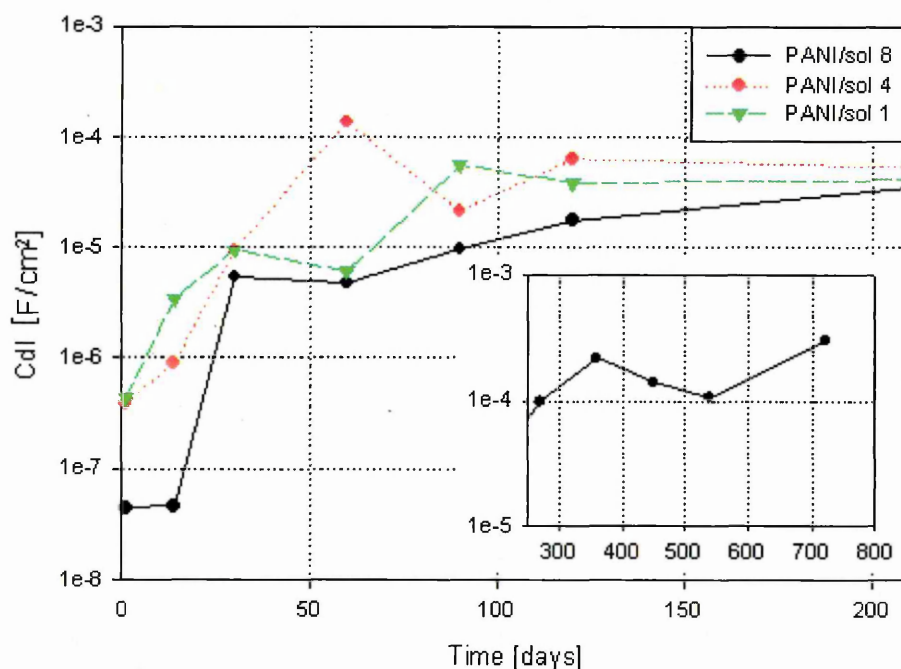
Figure 5-14 Change of double layer capacitance of PANI/sol-gel coated AA2024 in 3.5% NaCl solution with immersion time. Inset-behaviour for PANI/sol8 sample from 250-720 days.

Although, the impedance results of the PANI/sol8, 4 and 1 coatings showed similar behaviour, the impedance values increased with decreasing PANI content at all frequency regions. This behaviour related to the thickness of the coating. The cross section study of PANI/sol-gel coating showed that PANI/sol8 had a thicker coating ($\approx$13µm) being greater than that of both PANI/sol4 (10µm) and approximate double that of PANI/sol1 ($\approx$7µm), this may explain the difference in impedance between the three coatings in all frequency regions. Higher sol-gel contents were reflected in higher phase angles at high frequency, 10^4 Hz. This behaviour may be related to the hydrophobic property of the sol-

202

gel [14]. The contact angles of different coating system were measured with immersion time in 3.5% NaCl solution as shown in Figure 5-15. It was seen that the contact angle increased with increase in the sol-gel content i.e. increasing hydrophobicity. Moreover, the sol-gel coating measurements finished after 21 days of immersion due to spreading of pits over the whole of the coating surface. Moreover, the increase of PANI content seems to increase the porosity of PANI/sol-gel coatings as shown in the SEM images of different PANI/sol-gel coatings (Figures 4-32 and 4-34). This result suggests that the difference in the EIS phase angle for different coatings, in the high frequency range, is attributed to the hydrophobicity of the coating.
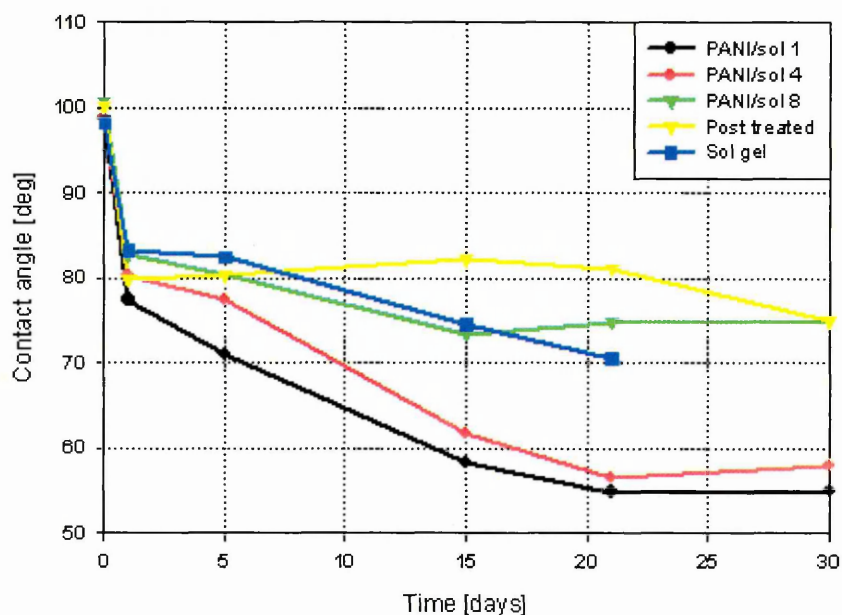
Figure 5-15 Contact angle of different coating systems with immersed

in 3.5%NaCl solution

5.2.5 Corrosion performance in acidic medium

EIS data for the PANI/sol8 coating, immersed in 3.5%NaCl solution pH=3.5, was fitted to two equivalent circuits, as shown in Figure 5-16.

The circuit containing two embedded RC circuits represents the coating/electrolyte and coating/metal interfaces respectively. The high frequency circuit consists of a coating capacitance (C_c) and pore resistance (R_p) of the coating, while, the low frequency circuit represents the double layer capacitance (C_{dl}) and charge transfer resistance (R_{ct}) of the under layer metal. Two constant phase elements (Q_c and Q_{dl}) were used instead of pure

capacitances (C_c and C_{dl} respectively) for all frequencies. The equivalent circuit components contains a Warburg element of diffusion i.e. diffusion in the inner layer.
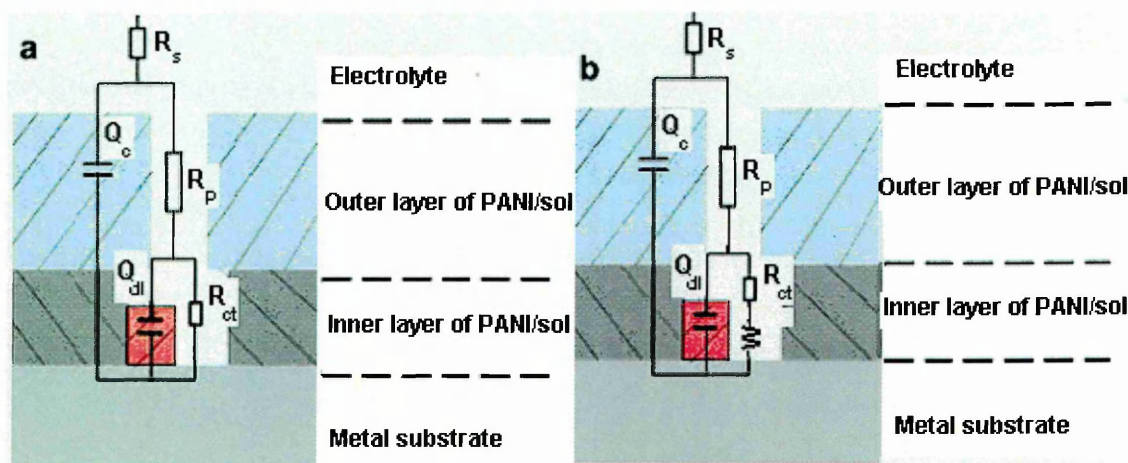
Figure 5-16 Equivalent circuits used for numerical fitting of the EIS data PANI/sol8

(a) before 30 days and (b) after 30 days of immersion in

3.5% NaCl (pH=3.5) solution (not to scale)

The pore resistance value, Figure 5-17, gradually decreases around one order of magnitude, however, the coating capacitance showed an increase with the immersion time in 3.5% NaCl (pH=3.5) solution. This behaviour may be attributed to the uptake of electrolyte through the coating layer which gradually increases the conductivity of PANI content [15].
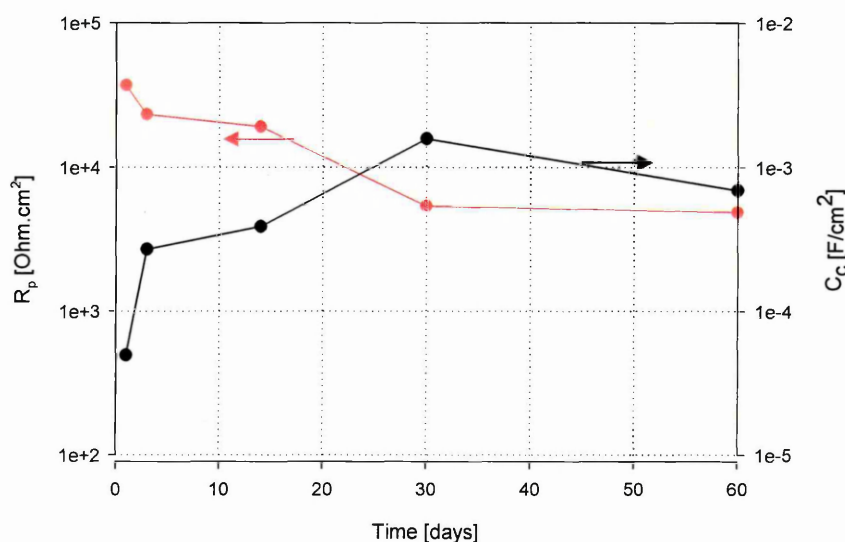
Figure 5-17 Change of pore resistance and coating capacitance of PANI/sol8 coated AA2024 in 3.5% NaCl (pH=3.5) solution with immersion time.

The change of charge transfer resistance and the double layer capacitance with the immersion time for PANI/sol8 is shown in Figure 5-18. The charge transfer resistance initially decreases, however, after two weeks of immersion, it reached to a stable value for the remaining two months. Similarly, the double layer capacitance showed stable values within a half order of magnitude during the course of the test. This stable behaviour is attributed to the inner layer of the PANI/sol8 coating which forms a passive layer at the coating/metal interface.
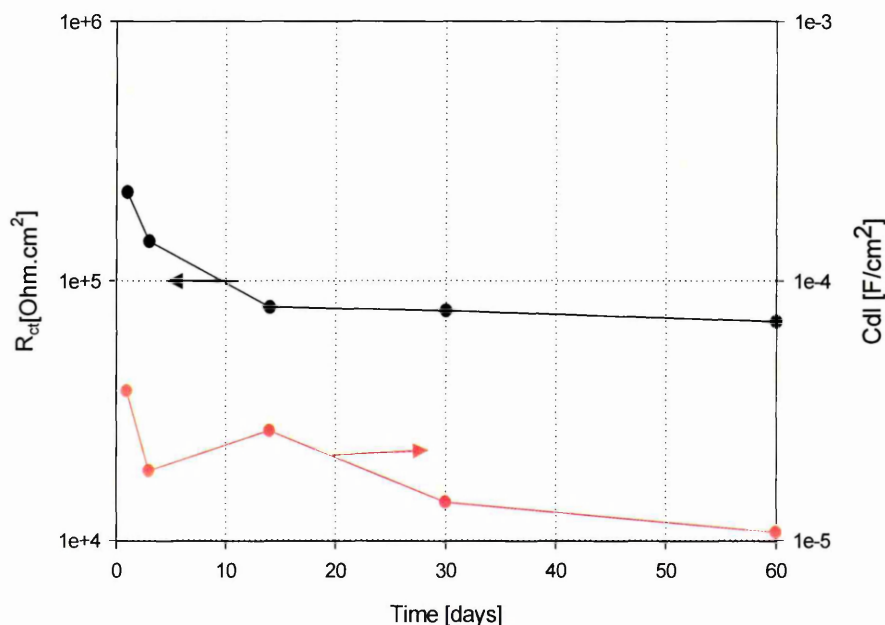
Figure 5-18 Change of charge transfer resistance and double layer capacitance of PANI/sol8 coated AA2024 in 3.5% NaCl (pH=3.5) solution with immersion time

PANI/sol8 showed different performance in acidic medium (Figure 5-18) compared to that in a neutral medium, Figures 5-13, as the impedance in an acidic is lower value than that in a neutral solution.

When the PANI/sol8 coating was immersed in an acidic solution, the PANI oxidation state changed to the emeraldine salt (ES) which is the conductive form of PANI. Consequently, the total PANI/sol8 resistance decreased and finally the overall impedance value decreased. It seems that the emeraldine base within the matrix of PANI/sol8 takes about 5 days for complete transformation to emeraldine salt (see section 2.4). After 14 days of immersion, the overall impedance seems to be stable. This change may be related to the formation of a passive or inert layer at the coating/metal interface since visual

inspection detected neither corrosion products nor pitting during the 2 months of immersion in 3.5%NaCl (pH=3.5).

5.2.6 Corrosion performance in alkaline medium

The silicon-oxygen bond, e.g. silicate and glass, is unstable in alkaline solutions (pH>9) [16], however, PANI/sol8 showed good stability and protection ability for AA2024 in pH=9.2 solution. PANI/sol-gel coating seems to have a different behaviour in an alkaline solution than that in neutral and acidic solutions. The coating offered good barrier properties to AA2024 since only one time constant could be observed from the inspection of the phase angle spectra which represents the barrier characteristics of the coating [17]. The high frequency (10^4 Hz) phase angle showed lower value (20 deg) than that of similar coating in neutral medium (80deg) during the same time of immersion (compare Figures 4-45 and 4-26). This may be attributed to the rapid penetration of electrolyte into the coating. The impedance of the coating gradually increased with time which is mainly due to a gradual change of PANI to its emeraldine base form which is a good insulator (conductivity $\approx 10^{-9}$ S cm^{-1}) [15].

By adding titanium dioxide (particle size 30nm) to the coating system (PANI/sol8), a new capacitive time constant appeared at high frequencies, 10^4 Hz, which decreased with immersion time (see Figures 4-46 and 4-47). Moreover, the low frequency time constant shifted towards lower frequencies, increasing to a maximum during the first month, after which it decreased. This increase in the low frequency time constant is related to the complete transformation of PANI to EB.

The enhancement in the corrosion performance is related to improved barrier properties that prevent transport of species through the PANI/sol-gel coating by adding TiO$_2$ [18].

The above results suggest that PANI has a different mechanism of protection depending upon the pH of the corrosive media.

5.2.7 Post treated PANI/sol8

Previous examination of the PANI/sol8 revealed pitting in the scratched area during salt spray testing (see Figure 4-54). However, no pits appeared away from the scratched area. Images of SST of PANI/sol8 samples (figures 4-54, 4-

56 and 4-58) and visual inspection noted that the pits initiated in the first few hrs (before 72hrs) then propagated at these positions as time elapsed without the development of undercutting or delamination. Importantly, no new pits appeared after 72hrs.

These results suggest the coating has one or more of the following properties:

1) PANI/sol-gel coating has a cathodic potential with respect to AA2024.
2) PANI/sol-gel coating acts as a barrier coating.
3) The assumed passive or inert film was not completely formed before being subject to SST.

If the PANI/ sol-gel coating is cathodic to the substrate or has barrier properties, pitting, general corrosion, undercut and delamination would appear at the scratch as a result of the SST however, none of these phenomena occurred. Moreover, scratch test results, figures 4-66 and 4-67, showed that PANI/sol-gel coating exhibits "self healing" behaviour.

The third property suggested above seems to be the most plausible. To investigate this hypothesis, a SST was conducted as follow: PANI/sol8 sample was pre-immersed in 3.5% NaCl solution for 5 day then scratched before exposure to SST for 72 hrs, Figure 5-19. It is clear from this figure that the pre-immersed sample did not experience any pitting or undercutting up to 72 hrs in SST.
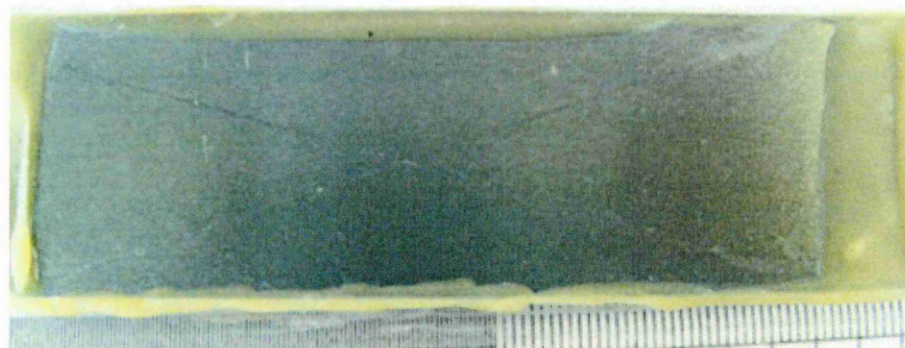
Figure 5-19 Image of pre-immersed sample after 72 hrs SST

This result combined with the immersion test results, Figure 5-11 to Figure 5-14, suggest that PANI/sol-gel coatings require a few days of immersion in a solution to be "activated" that is to form a protective layer at the coating/metal interface. Similar results were observed by Tallman et at [19] where, after ten days of

207

immersion of doped PANI (ES) with epoxy top coat in dilute Harrison's solution, the impedance began to increase. The authors suggest that this behaviour occurs when sufficient electrolyte is present at the metal/polymer interface.

The post-treated procedure, mentioned in chapter 3, was carried out to "activate" PANI before samples were subject to SST.

The post- treatment procedure appears to have two advantages:

1) It heals any defects that are produced during the spray deposition of the PANI/sol8 coating by forming a homogeneous thin film ($\approx$3µm) as shown in Figure 4-65.

2) It activates the PANI in the PANI/sol8 coating.

Visual inspection of the post-treated sample noted a change in the sample colour from blue (EB) to greenish blue (ES) after the post-treatment process. This change in colour may due to a change in oxidation state of PANI from the base form to the doped form of PANI [20]

Furthermore, the electrical conductivity of PANI after immersion in deionised water at 60°C for 5 min was significantly improved, 10^{-6} S.cm^{-1} with respect to that before immersion (10^{-9} S.cm^{-1}). A similar value of conductivity was obtained when a free standing film of PANI was immersed in 1 % NaCl solution for 3 days. XPS analysis of the free standing film of PANI, after immersion in 1% NaCl for 3 days (see Figure 5-20), identified that the change in electrical conductivity was mainly due to an increase of doped species (-NH^{+}) at the expense of N=C species i.e.[-NH^{+}]/[N=C] changes from 0.3 to 2.7.

Name	Pos.	%Area
N=C	398.56	9.27
N-C	399.61	50.81
-NH+	400.71	24.76
=NH+	402.46	15.16
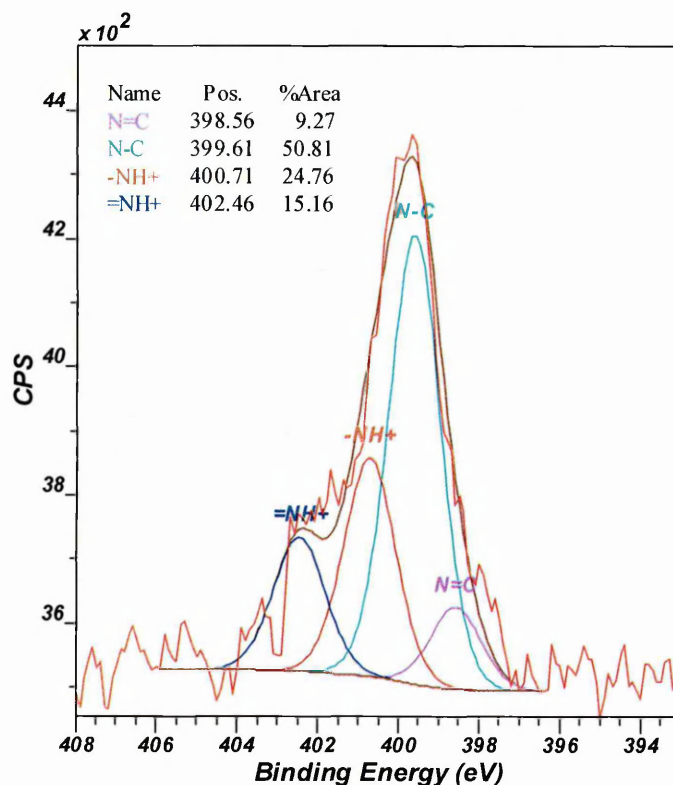
**Figure 5-20 High resolution N 1s of PANI after immersion
in 1% NaCl solution for 3 days.**

These results suggest that the post-treatment process applied to the coating enhances both electrical conductivity and barrier properties of PANI/sol-gel coatings.

5.3 MECHANICAL PROPERTIES OF COATINGS

The mechanical testing of different coating systems, Figure 4-72 to 4-75, showed that as the PANI content increased, adhesion with the metal substrate decreased. This may be explained by the fact that PANI has poor adhesion to the metal substrate [21] [22] [23] [24]. Due to time limitation of this study, the poor adhesion of PANI to the metal substrate will be investigated in the future work. To improve the adhesion performance of PANI, a PANI combined sol-gel coating system was developed. The SEM and TEM cross sections of sol-gel coated AA2024 showed that there was good adhesion between the sol-gel and the substrate, Figure 4-15, and that silica particles was present at the interface, Figure 5-21(red arrows), indicating these particles are bonded with the metal substrate.

209
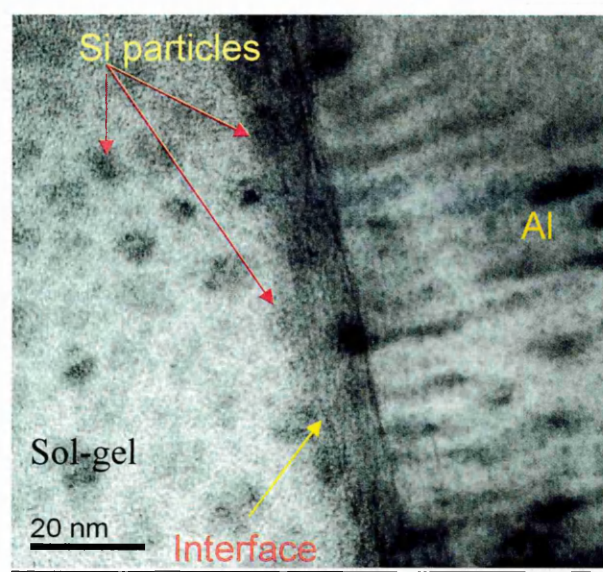
Figure 5-21 TEM image of sol-gel/Al interface

Glow Discharge Optical Emission Spectroscopy (GDOES) results obtained from the same sample, see Figure 5-22, show that the interface of sol-gel/AA does not have a sharp edge between silicon and aluminium but rather a gradual transition of the Al and sol-gel coating which supports the TEM results in that the sol-gel forms a strong bond to AA2024.

These results coupled with the mechanical property results, chapter 4, explain that the adhesion between sol-gel and aluminium substrate is attributed to the formation of a stable covalent Al–O–Si bond at the interface [25].
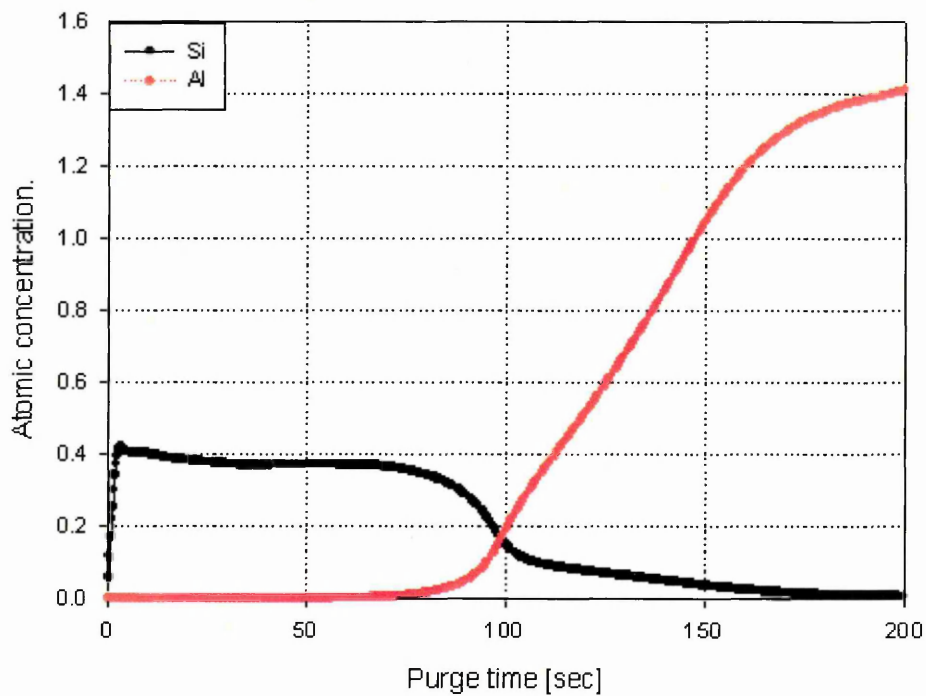
Figure 5-22 GDOES profile of sol-gel coated AA2024

210

5.4 MECHANISM OF PROTECTION

A review of the literature, presented in chapter1, offered several corrosion protection mechanisms for PANI coated onto different aluminium alloys notably;

1) A "barrier" action of PANI was suggested by [26] [27] [28] [29] since PANI (ES) is reduced to PANI (LB) which has low ion permeability.

2) Cogan et al [26] suggested that residual solvent and/or oligomers and/or monomers from the polymerization process act as inhibitors

3) Epstein [30] suggested that PANI (EB) reduces the surface copper content in AA2024 thereby decreasing the galvanic coupling within the alloy microstructure.

4) Growth of Al_2O_3 layer at the coating metal interface was assumed by numerous authors [19] [31] [32] [33], however, Racicot [34] related corrosion protection to the formation of an oxide-like interfacial layer between the polymer and the metal surface.

All the above suggestions may or may not lead to protection of AA2024 from corrosion in 3.5% NaCl solution. The above findings are addressed in the light of this current research work and the following comments are given. The first suggestion would not lead to a coating that offers self healing properties as found in this study.

The second assumption seems to have little relevance to this study as the prepared PANI was washed many times with deionised water and acetone, moreover, PANI showed a change in its oxidation state [26] [27].

A reduction of the surface content (Epstein [30]) of copper may only be feasible if the coating was very porous and thin to allow copper ions to diffused though it to the solution. However, in this study the coating thickness was typically 12 μm, and therefore any dissolution of copper would be observed around the interface or within the coating. This was not observed by XPS analysis.

The final suggestion relating to the formation of oxide or oxide-like layer at the interface required further investigation to understand the whole mechanism of protection.

Chapter 4 results showed that PANI/sol-gel coating can offer corrosion protection for AA2024 for long period (up to two years) of immersion in 3.5%NaCl solution however; a similar sol-gel formulation coating only can not

protect same substrate for more than a 5 day period. These results clearly suggest that the corrosion protection is related to the presence of PANI.

The impedance results correlate with an electrical circuit which incorporates a resistive pathway at the coating/metal interface. Therefore in order to understand the mechanism of protection it is necessary to determine the nature of the compound(s) that form at the PANI/Al interface. The remaining section of the discussion is devoted to addressing this.

Part 1:

PANI is directly coated onto a glass substrate followed by drying at 70°C for 16hrs. When the coated glass substrate is immersed in 1.0 %NaCl solution in direct contact with bare AA2024 sample for 3 days, the PANI colour changes from blue to transparent green, as shown in Figure 5-23-a. However, after drying in air for 2 weeks, the PANI colour changed back to its original blue colour.
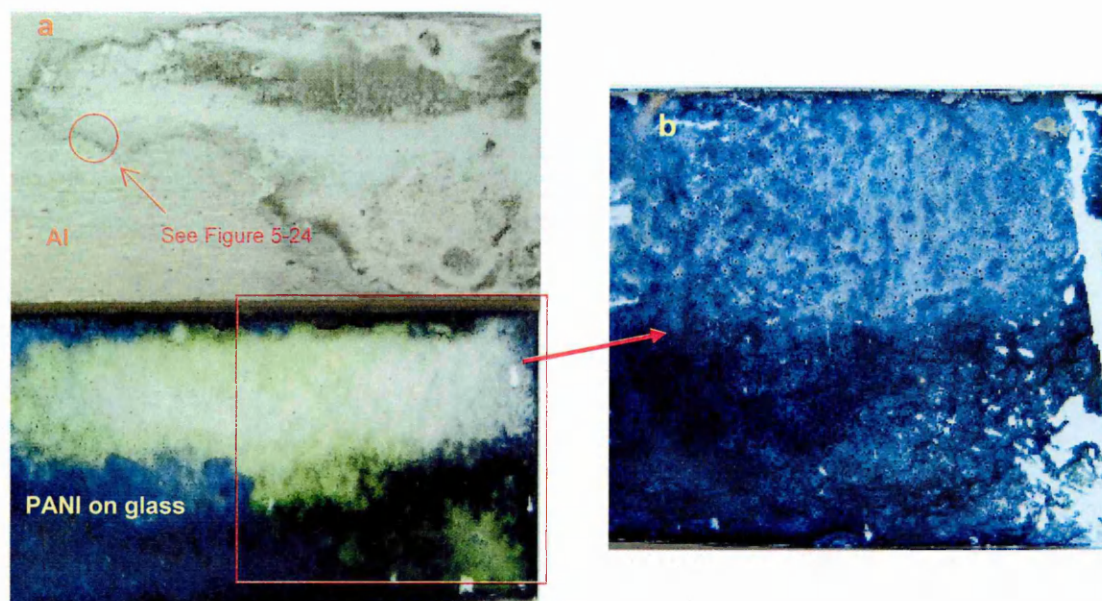
Figure 5-23 a) PANI coated glass in contact with AA2024 in 1.0 %NaCl solution for 3 days b) same PANI coated glass sample after drying for 2 weeks in air.

The SEM image in Figure 5-24 shows the edge of the contact area (between PANI and AA) and non- contact area. It is clear from the image that the area in contact with the PANI(a in Figure 5-24) did not show sign of corrosion, however, the area represented by b in Figure 5-24, showed some corrosion products,

moreover, selective corrosion has taken place at the intermetallic particles (red arrows).
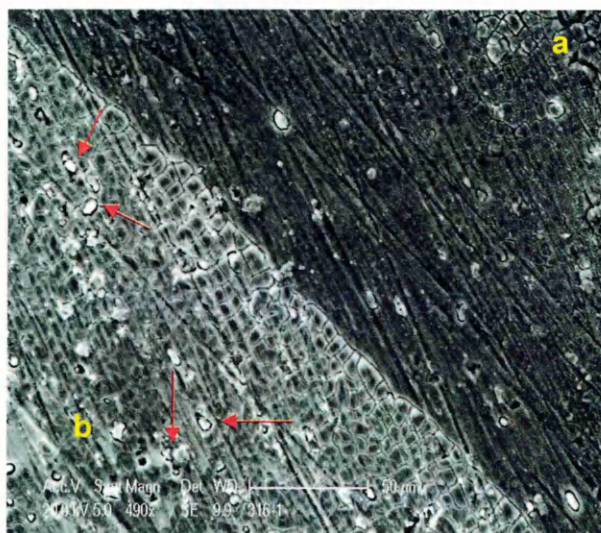
Figure 5-24 SEM image of AA2024 after 3 days immersion in 1.0% NaCl solution
a) area of contact between PANI and AA b) area on non contact

XPS analysis of the contact area showed traces of nitrogen which may have come from traces of PANI or from a compound that has been created from the interaction of Al with PANI. High resolution of Al 2p showed two components at binding energies of 74.55 and 75.5 eV which are attributed to Al-X and Al_2O_3 respectively as shown from Figure 5-25. It can be seen that the amount of Al-X was greater than that of Al_2O_3. Moreover, Al-X seems to be stable in air if the time interval between preparation and analysis of the sample (one week) is taken into consideration.

The impedance results of a similar sample, notably a PANI film removed from the AA surface, in 1% NaCl solution, see Figure 4-1, shows that PANI forms an interface offering significant corrosion protection.
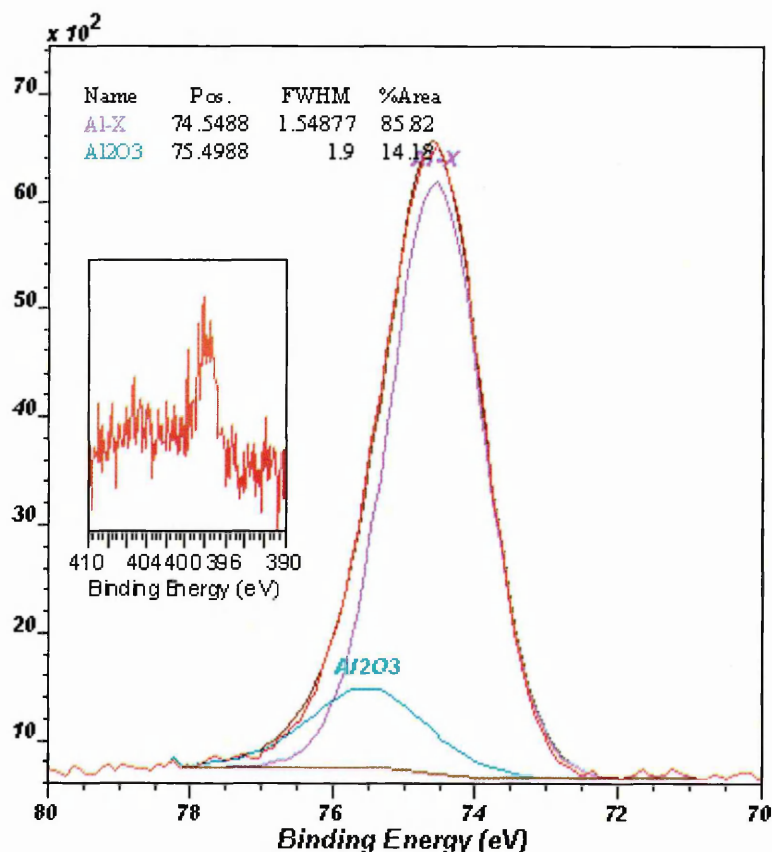
Figure 5-25 High resolution Al 2p of the contacted area, inset high resolution N 1s

These results suggest that PANI reacts with Al forming a compound that can protect AA2024 in NaCl solution.

Part 2

FTIR analyses of PANI coated aluminium before and after immersion in 3.5% NaCl, were compared as a function of immersion time. Comparison was also made with the same sample immersed, followed by air drying for one week. The results of this analysis are given in Figure 5-26. Here the relationship (ratio) of the reduced (A): oxidised (B) forms was measured for the 4 different samples. This ratio, shown in Figure 5-27, reflects the oxidised state of the surface and can be correlated with the corrosion behaviour of the system.

214

Wave no.	Structure
1167	N=Q=N
1314, 1379	C-N (aromatic)
1512	N-B-N
1595	N=Q=N
1667	C=O of NMP
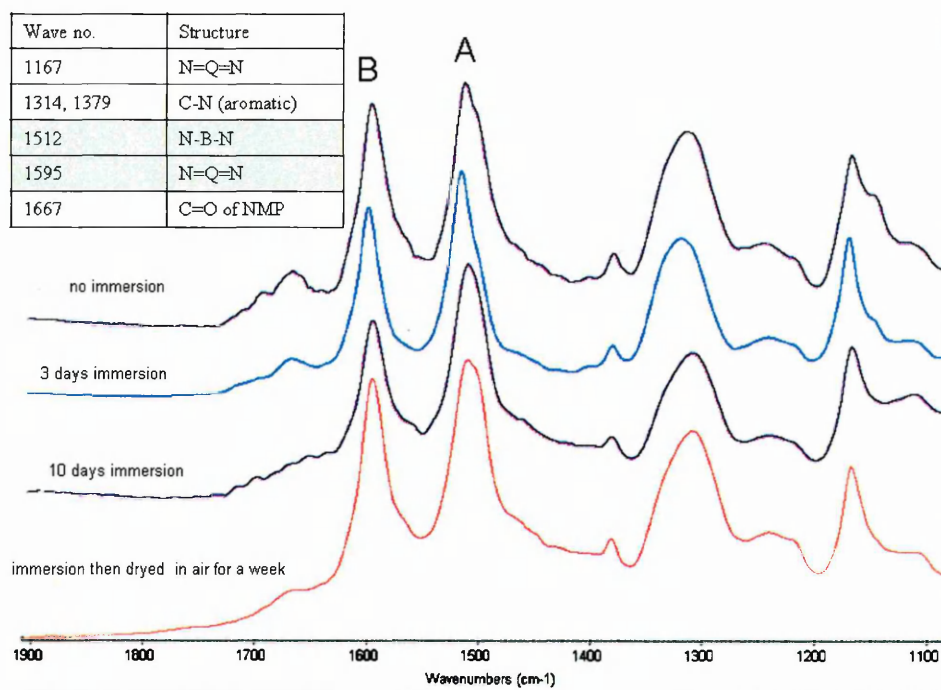
Figure 5-26 FTIR spectra of PANI coated AA2024 before and after immersion in 3.5%NaCl solution
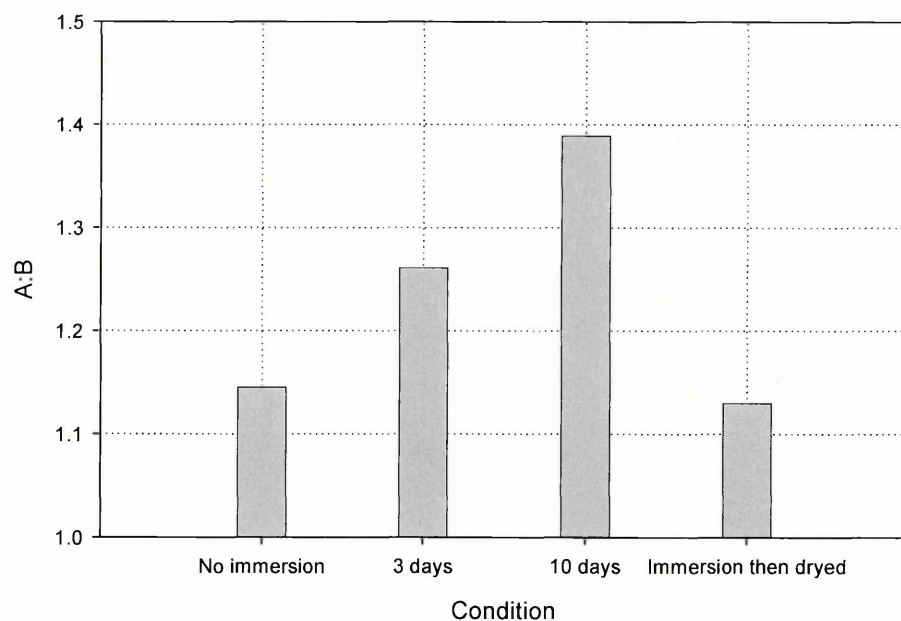
Figure 5-27 A:B ratio at different conditions

According to the results in Figure 5-26 and Figure 5-27, when the EB form of PANI was immersed in NaCl solution the ratio A:B increased. Visual inspection of the sample noted that the colour before immersion was dark blue which changed to pale green after immersion. The colour change reversed after drying

215

in air. The pale green colour of PANI may be a result from a mixture of the blue colour of PANI (EB) and the transparent yellow colour of PANI (lecomeraldime). This can take place in one of the following two ways;

1) The oxidised form (B) is converted to the reduced from (A) by the following reaction

$$PANI(B) + e^- \Rightarrow PANI(A) \qquad (5-1)$$
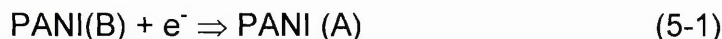
In this case the supply of electrons is provided by the oxidation of Al to aluminium ions.

$$Al \Rightarrow Al^{3+} + 3e^- \qquad (5-2)$$
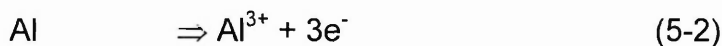
In this case Al will continue to corrode but at a higher corrosion rate than without PANI coating. This did not happen.

Alternatively,(2) the oxidised form (B) undergoes a cross-linking reaction, as shown in Figure 5-28
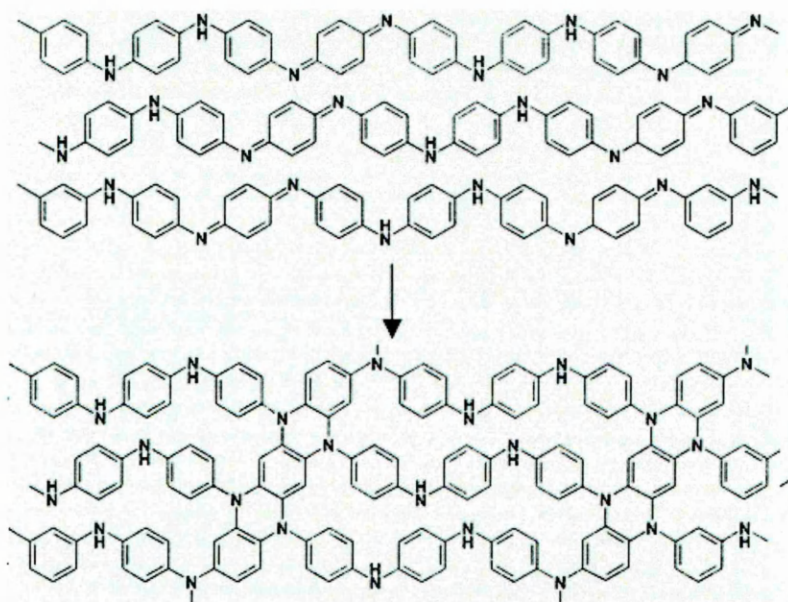
Figure 5-28 Proposed cross-linking scheme of PANI (EB) [5].

According to Lee [5] PANI forms cross linked molecules above 100°C, moreover, the cross linked molecule can not be re-oxidised [5]. From Figure 5-26, it can be seen that the ratio of A:B decreased following drying in air after 1 week which suggest the cross linking mechanism proposed above does not occur. In addition all coatings were cured below 100°C, notably 70°C/16 hrs

An alternative mechanism is suggested, notably

216

3) Reaction of the oxidised form (B) with the Al substrate to form an Al-PANI compound would lead to the loss of the blue colour of PANI (EB). This is supported by the theoretical study by Calderone [35] who concluded that the oxidised form of PANI is significantly more reactive with metal atoms than the reduced form of PANI.

In this case reaction of the Al and PANI would lead to the formation of a complex that can act as a protective layer causing stability of the impedance value. In addition, the reduced form of PANI was found to be oxidised in air at room temperature and this reversible reaction can take place up to 10^4 times [32].

Part 3:

XPS results for the PANI coated pure and 2024 aluminium alloy, shown in chapter 4, identified three components of aluminium. Two of these components, notably Al metal and aluminium oxide, were detected at all stages of depth profile. However, a new component (Al-X) was detected only at the PANI/Al interface; at a binding energy of 74.6±0.15eV fwhm=1.5±0.1. Furthermore, the concentration of Al-X appears to increase as the depth profile progress from the Al towards the PANI. Given the comments from part1 and part 2 above it is feasible that the compound formed at the PANI/Al interface is in part responsible for corrosion protection.

A review of the literature suggests the binding energy of 74.6±0.15eV may relate to one or more of the following;

1) Al_2O_3 [36]
2) Chemisorbed oxygen on Al surface [37].
3) Substoichiometric aluminum oxide due to ion bombardment [38].
4) AlOOH [39]
5) Al-O-C [40] [38]
6) Al-O-N complex [41] [42] [43]

Based on XPS results, it is possible that one or more of the above compounds can exist at the PANI/Al interface.

Whilst considering which of these compounds might exist at the PANI/metal interface, the premise that the PANI/sol-gel coatings offer self healing behaviour needs to be taken in account.

Al_2O_3 is not considered to be responsible for the peak at 74.6 eV as Al_2O_3 already exists in the XPS 2p core level of Al having a fwhm= 2±0.1eV [39]. In order to fit only two components (Al metal and Al_2O_3) in the Al 2p envelope, the Al_2O_3 position would need to be 75 eV with a fwhm value equal to 2.5eV, which is not applicable. Furthermore, Al_2O_3 does not protect AA2024 in such an aggressive solution, 3.5% NaCl. These results suggest therefore that the Al-X is not Al_2O_3.

The assumption that oxygen is chemisorbed on Al surface should lead to a level of corrosion protection without PANI. This does not occur.

The third assumption, substoichiometric aluminum oxide (O:Al<1.5) is obtained due to Ar ion bombardment during XPS analysis. This compound is only produced in the XPS chamber and would not occur under normal coating conditions. In this case, corrosion protection was due to Al_2O_3 which was discussed above; therefore, Al-X is not this substoichiometric aluminum oxide.

AlOOH (Boehmite) can protect Al in neutral pH solutions that do not contain Cl$^-$ ions [44]. However, protection was afforded by Al-X in 3.5% NaCl solution at pH= 6.8 and acidic pH=3.5 as shown in chapter 4. On this basis, it is suggested that Al-X is not AlOOH.

The fifth assumption, Al-O-C, was suggested [40] for the interaction between PANI in its emeraldine salt and Al, moreover, this interaction would not affect the oxidation state of PANI i.e. there would be no change of colour of PANI due to this interaction. Furthermore, the depth profile XPS high resolution of C 1s of PANI/Al interface did not show any new compound related to Al-O interaction with carbon. These results suggest that the Al-X is not Al-O-C.

PANI (EB) consists of two group; an oxidised group (containing N=C) and a reduced group (containing N-C), the oxidised group is significantly more reactive with metal atoms than the reduced group [35]. Therefore, if there is any interaction between PANI and Al, the oxidised group would be the major or the part to interact with Al.

This is supported by a change of relative concentration of [N=C]/[N-C] across the PANI/Al interface where N-C concentration increased as the depth profile went towards Al, at the expense of N=C.

The imine group, N=C, seems to be reduced to a state equivalent to an amine group, N-C, [41] [43]. The absence of a peak shift or the generation of a new

compound in N 1s indicates that there was weak indirect chemical bonding (ionic or covalent) between nitrogen species and Al atoms [41].

From these results, it may be concluded that, PANI (EB) interacts with Al forming an Al-O-N complex. The oxidised part of PANI (N=C) interacted with Al atoms creating an equivalent state to the amine group. This interaction seems to be enhanced by ionic species that diffused in the PANI/Al interface.

This conclusion could explain the change of PANI colour (part 1) when immersed in contact with AA2024 where the blue colour of EB was changed to transparent colour of leucoemeraldine when the oxidised form, N=C, was reduced to a similar or equivalent state of the reduced form [42].[43] After drying of the PANI film in air, the reduced form (N-C) was oxidised by oxygen in the air creating the oxidised form (N=C) [45].

REFERENCES

[1] K. Tzou, and R. Gregory, 1995, "Improved Solution Stability and Spinnability of Concentrated Polyaniline Solutions using N,N'-Dimethyl Propylene Urea as the Spin Bath Solvent," Synthetic Metals, 69(1-3) pp. 109-112.

[2] K. Tzou, and R. Gregory, 1993, "Mechanically Strong, Flexible Highly Conducting Polyaniline Structures Formed from Polyaniline Gels," Synthetic Metals, 55(2-3) pp. 983-988.

[3] E. Ponzio, R. Echevarria, G. Morales, C. Barbero, 2001, "Removal of N-Methylpyrrolidone Hydrogen-Bonded to Polyaniline Free-Standing Films by Protonation-Deprotonation Cycles Or Thermal Heating," Polymer International, 50(11) pp. 1180-1185.

[4] Z. Li, E. Kang, K. Neoh, 1997, "Effect of Thermal Processing Conditions on the Intrinsic Oxidation States and Mechanical Properties of Polyaniline Films," Synthetic Metals, 87(1) pp. 45-52.

[5] Y. Lee, J. Kim, J. Kang, 2000, "Annealing Effects of Dilute Polyaniline/NMP Solution," Macromolecules, 33(20) pp. 7431-7439.

[6] A. Bernasik, J. Haberko, J. Włodarczyk-Miśkiewicz, 2005, "Influence of Humid Atmosphere on Phase Separation in polyaniline–polystyrene Thin Films," Synthetic Metals, 155(3) pp. 516-522.

[7] C. Vargel, M. Jacques, and D. Schmidt, 2004, "Corrosion of Aluminium," Elsevier, Amsterdam, pp. 81-109.

[8] R. Buchheit, R. Grant, P. Hlava, B. Mckenzie, G. Zender, 1997, "Local Dissolution Phenomena Associated with S Phase (Al2CuMg) Particles in Aluminum Alloy 2024-T3," Journal of the Electrochemical Society, 144, pp. 2621-2628.

[9] N. Ahmad, and A. MacDiarmid, 1996, "Inhibition of Corrosion of Steels with the Exploitation of Conducting Polymers," Synthetic Metals, 78(2) pp103-110.

[10] E. Hür, G. Bereket, and Y. Şahin, 2006, "Corrosion Inhibition of Stainless Steel by Polyaniline, Poly(2-Chloroaniline), and Poly(Aniline-Co-2-Chloroaniline) in HCl," Progress in Organic Coatings, 57(2) pp. 149-158.

[11] A. Alix, V. Lemoine, M. Nechtschein, 1989, "Water Absorption Study in Polyaniline," Synthetic Metals, 29(1) pp. 457-462.

[12]   L. Shacklette, 1994, "Dipole and Hydrogen-Bonding Interactions in Polyaniline: A Mechanism for Conductivity Enhancement," Synthetic Metals, 65(2-3) pp. 123-130.

[13]   J. Lacroix, J. Camalet, S. Aeiyach, K. Chane-Ching, J. Petitjean, E. Chauveau, P. Lacaze, 2000, "Aniline Electropolymerization on Mild Steel and Zinc in a Two-Step Process," Journal Of Electroanalytical Chemistry, 481(1) pp. 76-81.

[14] W. Daoud, J. Xin, X. Tao, 2004; "Superhydrophobic silica nanocomposite coating by a low-temperature process". Journal of the American Ceramics Society 87(9):1782-1784.

[15] S. Freund and B. Deore, 2007, "Self-Doped Conducting Polymers," John Wiley & Sons Ltd, The Atrium, Southern Gate, Chichester, West Sussex PO19 8SQ, England, pp. 326.

[16] T. El-Shamy and C. Pantano, 1977, "Decomposition of Silicate Glasses in Alkaline Solutions," Nature, 266 pp. 704-706.

[17]   M. Vecino, I. Gonzalez , M. Munoz, A. Santamaria, E. Ochoteco, JA. Pomposo, 2004, "Synthesis of Polyaniline and Application in the Design of Formulations of Conductive Paints," Polymers For Advanced Technologies, 15(9) pp. 560--563.

[18] S. Radhakrishnan, C. Siju, D. Mahanta, 2009, "Conducting polyaniline– nano-TiO2 Composites for Smart Corrosion Resistant Coatings," Electrochimica Acta, 54(4) pp. 1249-1254.

[19] D. Tallman, Y. Pae, GP. Bierwagen, 2000, "Conducting Polymers and Corrosion: Part 2 - Polyaniline on Aluminium Alloys " Corrosion, 56(4) pp. 401-410.

[20]   D. Sarno, S. Manohar, and A. MacDiarmid, 2005, "Controlled Interconversion of Semiconducting and Metallic Forms of Polyaniline Nanofibers," Synthetic Metals, 148(3) pp. 237-243.

[21]   W. Araujo, I. Margarit., M. Ferreira, 2001, "Undoped Polyaniline Anticorrosive Properties," Electrochimica Acta, 46(9) pp. 1307-1312.

[22] W. Li, D. Hooks, P. Chiarelli, 2003, "Fabrication and Characterization of Optically Active Multilayer Thin Films Based on Polyaniline Colloids," Langmuir, 19(11) pp. 4639-4644.

[23] D. Keqiang, J. Zhenbin, M. Wenshi., 2003, "Corrosion Protection of Mild Steel with Polyaniline-Thiokol Rubber Composite Coatings," Zashchita Metallov, 39(1) pp. 78-83.

[24] G. Troch-Nagels, R. Winand, A. Weymeersch, 1992, "Electron Conducting Organic Coating of Mild Steel by Electropolymerization," Journal of Applied Electrochemistry, 22(8) pp. 756-764.

[25] M. Zheludkevich, I. Salvado and M.. Ferreira, 2005, "Sol–gel Coatings for Corrosion Protection of Metals," Material Chemistry, 15pp. 5099- 5111.

[26] S. Cogan, M. Gilbert, G. Holleck, J. Ehrlich and M. Jillson, 2000, "Galvanic Coupling of Doped Poly-Aniline and Aluminium Alloy 2024-T3" Journal Of The Electrochemical Society, 147(6) pp. 2143--2147.

[27] L. Cecchetto, R. Ambat, A. Davenport, 2007/2, "Emeraldine Base as Corrosion Protective Layer on Aluminium Alloy AA5182, Effect of the Surface Microstructure," Corrosion Science, 49(2) pp. 818-829.

[28] K. Wu, C. Chao, C. Liu, 2007, "Characterization and Corrosion Resistance of Organically Modified silicate–NiZn ferrite/polyaniline Hybrid Coatings on Aluminum Alloys," Corrosion Science, 49(7) pp. 3001-3014.

[29] K. Wu, P. Chen, C Yang, 2008, "Infrared Stealth and Anticorrosion Performances of Organically Modified Silicate-NiZn ferrite/polyaniline Hybrid Coatings," Journal of Polymer Science, Part A, Polymer Chemistry, 46(3) pp. 926-935.

[30] A. Epstein, J. Smallfield, H. Guan1999/6, "Corrosion Protection of Aluminum and Aluminum Alloys by Polyanilines: A Potentiodynamic and Photoelectron Spectroscopy Study," Synthetic Metals, 102(1-3) pp. 1374-1376.

[31] J. Seegmiller, J. da Silva, D. Buttry, S. de Torresi, R. Torresi, 2005, "Mechanism of Action of Corrosion Protection Coating for AA2024-T3 Based on Poly(Aniline)-Poly(Methylmethacrylate) Blend " Journal of The Electrochemical Society, 152(2) pp. B45-B53.

[32] S. Yang, R. Brown and J. Sinko, 2005, "Designing Conductive Polymers for Improved Metal Protection , 11 48 (2005)," European Coating Journal, 11pp. 48--54.

[33] S. Sathiyanarayanan, S. Syed Azim, G Venkatachari., 2008, "Performance Studies of Phosphate-Doped Polyaniline Containing Paint Coating for

Corrosion Protection of Aluminium Alloy", Journal of Applied Polymer Science, 107(4) pp. 2224-2230.

[34]   R. Racicot, R. Brown, , and S. Yang, 1997, "Corrosion Protection of Aluminum Alloys by Double-Strand Polyaniline," Synthetic Metals, 85(1-3) pp. 1263-1264.

[35]   A. Calderone, R. Lazzaroni, and J. Brédas, 1994, "Theoretical Studies of the aluminum/emeraldine Interface," Physical Review B, 49(20) pp. 14418-14426.

[36]   K. Arata, M. Hino, 1990, "Solid Catalyst Treated with Anion. XVIII. Benzoylation of Toluene with Benzoyl Chloride and Benzoic Anhydride Catalysed by Solid Superacid of Sulfate-Supported Alumina," Applied Catalysis, 59(1) pp. 197-204.

[37] S. Flodström, C., Martinsson, R. Bachrach, S. Hagström., R. Bauer, 1978, "Ordered Oxygen Overlayer Associated with Chemisorption State on Al(111)," Physical Review Letters, 40(13) pp. 907-910.

[38] M. Vasile and B. Bachman, 1989, "Aluminium Deposition on Polyimides : The Effect of in Situ Ion Bombardment," Journal of Vacuum and Science Technology A, 7(5) pp. 2992-2997.

[39]   B. Vincent Crist, 1999, "Handbook of The Elements and Native Oxides," XPS International, LLC, USA, .

[40]   C. Basavaraja, R. Pierson, T. Vishnuvardhan, 2008, "Characterization and Electrical Behavior of polyaniline–poly-N-Isopropylacrylamide-Co-Acrylic acid/alumina Aqueous Dispersions in the Presence of Dodecyl Benzenesulfonic Acid," European Polymer Journal, 44(5) pp. 1556-1566.

[41]   Y. Liu, M. O'Keefe, A. Beyaz, T. Schuman, 2005, "Synthesis and Characterization of Aluminium-Polyaniline Thin Films and Membranes," Surface and Interface Analysis, 37(10) pp. 782-791.

[42] S. Lim, K., Tanand, E. Kang, 1998, "Interactions of Evaporated Aluminium Atoms with Polyaniline Films Effects of Dopant Anion and Adsorbed Oxygen," Synthetic Metals, 92(3) pp. 213-222.

[43]   S. Lim, K. Tan, E. Kang, 1998, "Interactions of Evaporated Aluminium Atoms with Polyaniline Films: An x-Ray Photoelectron Spectroscopic Study," Journal of Vacuum and Science Technology A, 16(1) pp. 13-20.

[44] Z. Ahmad, 2006, "Principles of Corrosion Engineering and Corrosion Control," Elsevier Science & Technology Books, Oxford, UK, pp. 660.

[45] S. Yang, R. Brown, and J. Sinko, 2005, "The Double Helix: Designing Conductive Polymers for Improved Metal Protection," European Coatings Journal, (11) pp. 48-54.

224

CONCLUSION

This research reports on a new application of using a mixture of silica sol-gel with an organic conductive polymer, polyaniline, as an anti-corrosion coating for an aluminium alloy AA2024. This application was investigated systematically to evaluate the corrosion performance of these coatings in 3.5% sodium chloride solutions at different pH. Electrochemical impedance spectroscopy, salt spray test, scanning vibrating electrode technique, and scanning electron microscopy were used to understand the corrosion performance mechanism of these coatings.

The corrosion performance tests indicated that the protection of AA2024 by these coating may related to the formation of a layer at the coating/ metal interface. This layer was studied by the X-ray photoelectron spectroscopy and Transmission Electron spectroscopy.

The following conclusions can be drawn from the study;

6.1 CORROSION PERFORMANCE

1) Bare AA 2024 can not be used in 3.5% solution.

2) PANI only protects AA 2024 from corrosion in 3.5% NaCl (pH=6.8). The protection property comes from the formation of a PANI/metal interface. However, PANI is easily delaminated from the metal surface after a short period of immersion.

3) Sol-gel without the presence of a corrosion inhibitor had limited corrosion protection on AA 2024 in 3.5% NaCl (pH=6) and pits appeared after 5 days of immersion.

4) PANI/sol-gel does not provide the same protection to AA 2024 in the alkaline NaCl solutions than in the neutral or acidic NaCl solution; however, it can decrease the rate of corrosion. Addition of TiO_2 improved the corrosion protection of PANI/sol-gel coating in an alkaline medium.

5) Salt spray test results showed that non-scratched PANI/sol-gel coated AA2024 samples passed 500 hrs SST with neither pit formation nor delamination.

6) Salt spray tests results of scratched PANI sol-gel coated AA 2024 samples showed some pits in the scratched area after 72 hr; however, no more pits appeared after this period.

7) Salt spray test showed that PANI needs to be activated before salt spray testing in order to pass the 500 hrs test without pitting in the scratched area. This activation mainly improves the conductivity of PANI.

8) The post-treated scratched PANI/sol-gel coated AA 2024 can pass 500 hrs SST without any pit or delamination or undercut inside or outside the scratched area.

9) EIS and SVET studies showed that PANI/sol-gel can offer a "self-healing" effect for the coated AA2024 sample. This was supported by SEM studies.

10) The EIS study showed that the PANI/sol-gel combination successfully protected AA2024 in both acidic and neutral 3.5 % NaCl solutions for long periods up to 2 and 24 months respectively.

6.2 OPTIMUM FORMULATION AND CONDITIONS

1) The best combinations of PANI and sol-gel is produced by mixing the sol-gel with PANI solution in the range of 1:1 to 1:8 PANI/sol volume relative concentrations.

2) Increasing the PANI concentration above 1:8 leads to the formation of a porous coating.

3) Doping of PANI within a sol-gel matrix offers a promising coating system for corrosion prevention.

4) PANI sol-gel coating is completely air cured after 5 hrs at 70 °C.

5) There is a minimum concentration of PANI required to protect AA2024 from corrosion. This minimum concentration depends on the nature of the metal substrate and corrosive medium.

6.3 MECHANICAL PROPERTIES

1) Sol-gel offers good adhesion as observed from Cross Cut and Pull Off adhesion tests even after immersion in the corrosive solution.

2) TEM analysis of sol-gel coated AA 2024 showed that silica particles existed at the sol-gel/ metal interface forming a strong bond between silicon and aluminium atoms (Si-O-Al).

3) The PANI/sol-gel coating showed reduced adhesion to the metal substrate, with respect to sol-gel coating. The adhesion to the metal substrate decreased with increasing PANI content in the coating mixture.

4) PANI sol-gel coating has durable mechanical properties and can be used to protect AA 2024 for long durations (up to 2 years) when immersed in aerated 3.5% sodium chloride solution.

6.4 CORROSION MECHANISM

1) PANI/ sol-gel system takes more than 24 hours to be stable in the corrosive solution. This stabilisation results from a change in the PANI (EB) oxidation state from EB to ES through the interaction with water.

2) The corrosion protection mechanism of PANI/sol-gel coating in neutral and acidic media results from the formation of a protective layer at the coating/metal interface. However, the protection in alkaline medium may also be attributed to the improved barrier properties of PANI (EB) on addition of 0.5% TiO_2.

3) The interaction between PANI and aluminium seems to be activated by immersion in the corrosive electrolyte.

4) TEM and XPS showed that PANI adsorbs oxygen on PANI surface which can not be removed under high vacuum (10^{-5} torr).

5) The XPS depth profile of PANI/Al interface results showed that the PANI was reduced as the depth analysis went towards Al substrate. Moreover, Aluminium showed a new compound rather than Al metal and oxide at the interface. This compound may be responsible for the improved corrosion protection. The analysis showed that the oxidised part of PANI (EB) reacted with Al atoms forming anonymous compound contains Al-O-N group compound. This interaction produced a weak indirect bond between Al and PANI.

Future work

During the course of this study, the following future work was identified:

1. PANI/sol-gel mixture to be further improved to protect AA 2024 in alkaline medium. This might be achieved by changing the oxidation state of the PANI from EB to ES by choosing a suitable dopant.

2. Study the interaction of different oxidation state of PANI with an aluminium substrate in dry and wet conditions.

3. Further understanding the nature of the Al-O-N compound as this may lead to the use this compound directly in the corrosion protection of aluminium alloys.

4. Investigate and understand the poor adhesion properties of PANI.

5. Study the effect of other additives to the PANI/sol-gel coating such as carbon nanotubes and TiO_2 which may allow the concentration of PANI to be increased without affecting the mechanical properties of the coating.

6. Study the different preparation techniques of PANI, such as water base PANI, with this kind of silica base sol-gel or with absolute water based silica sol-gel coating.

7. Assess the possibility of using the PANI/sol-gel coating to other metals such as magnesium and steel alloys.

8. Study other applications to this PANI/sol-gel coating such as electromagnetic impulse shielding.
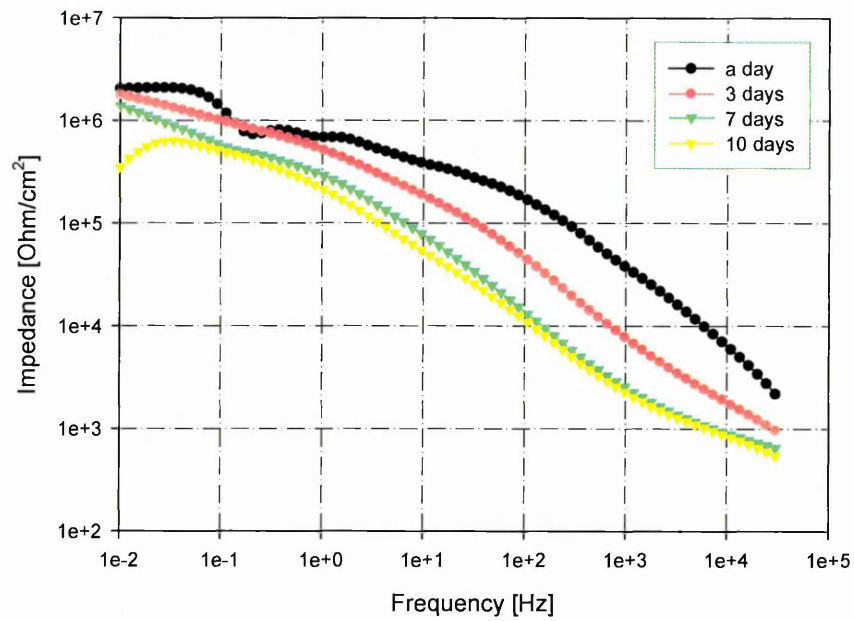
Impedance of PANI/sol12 coated AA 2024 in 3.5% NaCl solution
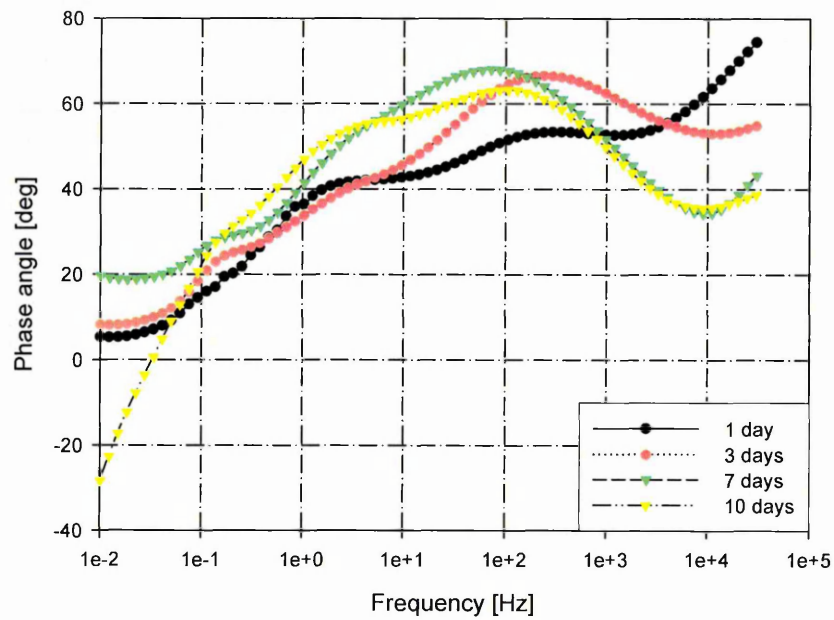
Phase diagram of PANI/sol12 coated AA 2024 in 3.5% NaCl solution
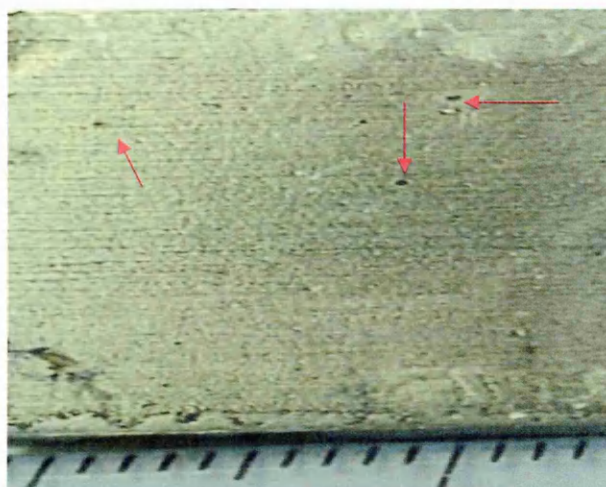
Image of PANI/sol12 coated AA 2024 after 10 days immersion in 3.5% NaCl solution (pitting arrowed)
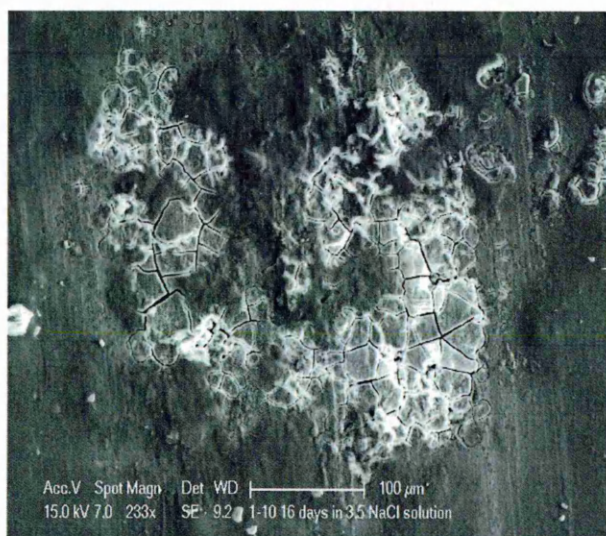
SEM image of PANI/sol12 coated AA 2024 sample after 11 days immersion in 3.5% NaCl solution.

Appendix B

Pull Off adhesion test results of different bare and coating systems

Sample name	Results MPa				Average
AA 2024	5.1	5.3	5.0	5.1	5.1
Sol-gel	7.1	7.0	6.8	6.7	6.9
PANI/sol8	6.1	6.2	6.3	5.9	6.1
Post-treated	5.7	5.5	5.8	5.8	5.7
PANI/sol4	4.5	4.7	4.9	4.6	4.7
PANI/sol1	3.2	3.3	3.0	3.0	3.1
PANI only*	4.3	4.5	4.0	3.9	4.2

*3 μm thickness

Appendix C

Sol-gel fitting data

Time [days]	R_s	Q_c	n	R_p	Q_{dl}	n	R_{ct}
1	40.6	1E-08	1	13410	1.08E-08	1	1189000
5	35.2	1.24E-06	0.62	3447	3.14E-08	1	723900
8	55	1.52E-06	0.58	1401	3.57E-07	0.82	533400
11	51	1.57E-06	0.5789	1512	5.86E-07	0.7945	397700
16	31.2	4.48E-06	0.5221	428.6	8.03E-07	0.7962	484500

Appendix D

PANI/Sol1 fitting data

Time [days]	R_s	Q_c	n	R_p	O	B	Q_{dl}	n	R_{ct}
2	42	1.19E-08	1	2346			4.348E-07	1	1.19E-08
14	36	9.18E-08	1	885			3.481E-06	1	9.18E-08
30	47	9.25E-08	1	623	7.12E-06	1.354	9.492E-06	1	9.25E-08
60	28	2.85E-08	0.86	1014	1.32E-05	1.257	3.655E-08	0.7018	2.85E-08
90	36	1.84E-08	0.866	875.8	2.92E-05	1.501	7.437E-06	0.83	1.84E-08
120	45	2.42E-08	0.86517	706.2	4.48E-05	0.1497	4.358E-06	0.8237	2.42E-08
210	44	2.68E-07	0.8607	503.3	3.92E-05	0.4965	7.324E-07	0.7152	2.68E-07

234

PANI/Sol 4 fitting data

Time [days]	Rs	Qc	n	Rp	O	B	Qdl	n	Rct
2	29.5	1.21E-08	1	2523		3.957E-07	1	356600
14	35	1.72E-08	1	675.5		9.238E-07	1	252300
30	46	2.63E-08	1	610.4	1.1E-05	2.05	9.576E-06	1	526000
60	51	1.14E-08	0.86	724.7	1.5E-05	2.475	3.191E-06	0.7018	284100
90	35	3.56E-08	0.866	946	7.7E-05	5.563	2.434E-06	0.83	450900
120	46	5.54E-08	0.86517	843	1.93E-05	4.732	8.242E-06	0.8237	383800
210	39	8.81E-08	0.8607	676.4	6.01E-05	0.03282	1.091E-06	0.7152	828900

PANI/Sol8 fitting data

Time [days]	Rs	Qc	n	Rp	O	B	Qdl	n	Rct
2	31	9.74E-10	1	97700		4.41E-08	1	2786000
14	51	3.31E-09	1	26600			4.61E-08	1	3897000
30	38	1.75E-09	0.94	20620	1.66E-06	0.07748	5.15E-07	0.8376	25590000
60	42	2.06E-08	0.9244	24250	1.94E-06	0.05641	6.27E-07	0.858	981100
120	42.5	1.34E-08	0.9292	10750	6.6E-06	2.33	1.97E-06	0.8791	810008
210	40.2	6.22E-08	1	12634	7E-06	1.677	1.94E-06	0.8318	784000
270	37	1.2E-08	0.8933	7292	1.95E-06	2.44	3.82E-06	0.8213	714000

236